Ground and Airborne Geophysical Techniques Commonly Used in the Mining Industry in the United States--A Reference for the Bureau of Land Management

Prepared by

Roger A. Haskins

Division of Mining Law and Salable Minerals
Bureau of Land Management
U.S. Department of the Interior
Washington, D.C.

1986

Table of Contents

Appendices

I. Introduction

This reference is designed to acquaint the mineral specialist with the basic geophysical systems, their components and operations in common use in the metallic minerals industry, and with the interpretation of geophysical data. It does not cover all of the geophysical systems now in use.

Geophysical data are valuable in appraising mineral resources on the public land, both for their Geology, Energy, and Mineral (GEM) potential, and for classification of mineral lands under the land disposal and mineral leasing laws.

Individuals who are engaged in projects requiring the review of geophysical data should obtain a copy of Practical Geophysics for the Explorations Geologist (Van Blaricom, 1980). It is the most complete and readable source available for the nongeophysicist on the basic theory, use, and interpretation of geophysical data in the mining industry. Mineral specialists wishing to delve further into the theory, development, interpretation, and operational use of the various available ground and airborne geophysical systems should read these papers: Grant and West (1966), Parasnis (1979), Telford (1976), Van Blaricom (1980), and Skinner (1981).

The Appendices included at the end of this reference contain key articles on the use and interpretation of the most common geophysical systems and units that will be met in the field. Appendix II was written by the author (Haskins); the others are reproduced from the literature. For units not covered, operating and interpretation manuals are normally available from the equipment manufacturer or contractor.

A number of patented and registered systems and units are discussed in this reference. Such discussion is for illustrative purposes only. The Bureau of Land Management does not endorse or imply endorsement of any system or unit discussed herein.

The author thanks the individuals and organizations who have given permission for reproduction of the figures and tables in this reference. These include Geonics, Ltd., S.H. Ward and the Society of Exploration Geophysicists, Northwest Mining Association, Scintrix, Ltd., Drone Geophysics, Ltd., and Geoterrex, Ltd. Special acknowledgment is given to those who have permitted reproduction of copyrighted material and to those authors and journals whose papers are reproduced in the appendices of this reference.

II. General Theory of Electromagnetic (EM) Surveying

All airborne and ground EM systems operate on the same basic principles. An electrically conductive body (a conductor: faults, massive sulfide bodies, shear zones, graphite, swamps, clay, etc.), lying in the ground and in contact with water, will produce an electromagnetic field by electrochemical action. Conductors can be "excited" into producing an EM field by hitting them with a manmade EM field (Figure 1). Naturally occurring EM fields are measured on the ground or in the air by several passive methods. The most common method detects these natural EM fields by the way they interfere with manmade EM fields.

A transmitter (TX) sends out a primary signal whose inphase and quadrature components are tightly controlled. Any conducting body intersected by this primary field becomes "excited" and generates a secondary field of its own. The secondary field is at the same frequency as the transmitted primary field but is be out of phase and quadrature with the primary field. The secondary field is measured by a receiver (RX) and recorded for analysis.

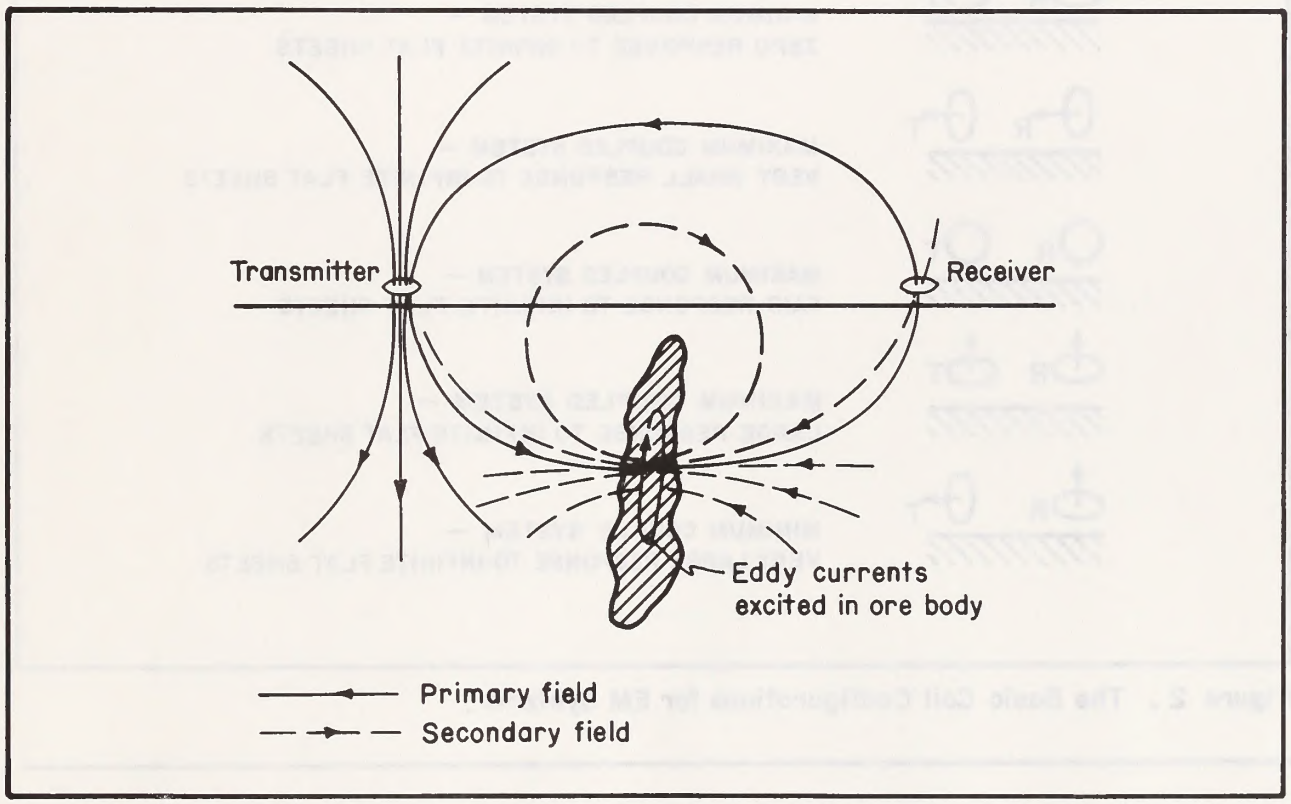

Figure 1. Excitation of an Ore Body by an EM Field.

Geophysical systems employing both a TX and a RX are categorized as either maximum or minimum coupled (Figure 2). Minimum-coupled systems are capable of recording only inphase (dip or tilt angle) information. Maximum-coupled systems record both inphase and quadrature data and provide more quantitative information about the conductivity-thickness product.

The recorded data are analyzed to determine the conductor's strike, dip, depth below the RX, and its conductivity-thickness product. The conductivity-thickness product is the conductor's conductivity multiplied by its thickness (width). Conductivity is the reciprocal of resistivity. Resistivity is expressed in units of standard ohm-meters (SOHM). Conductivity is expressed as the reciprocal of SOHM; as MHOS. The majority of massive sulfide deposits have conductivity-thickness products of 5 to 30 MHOS.

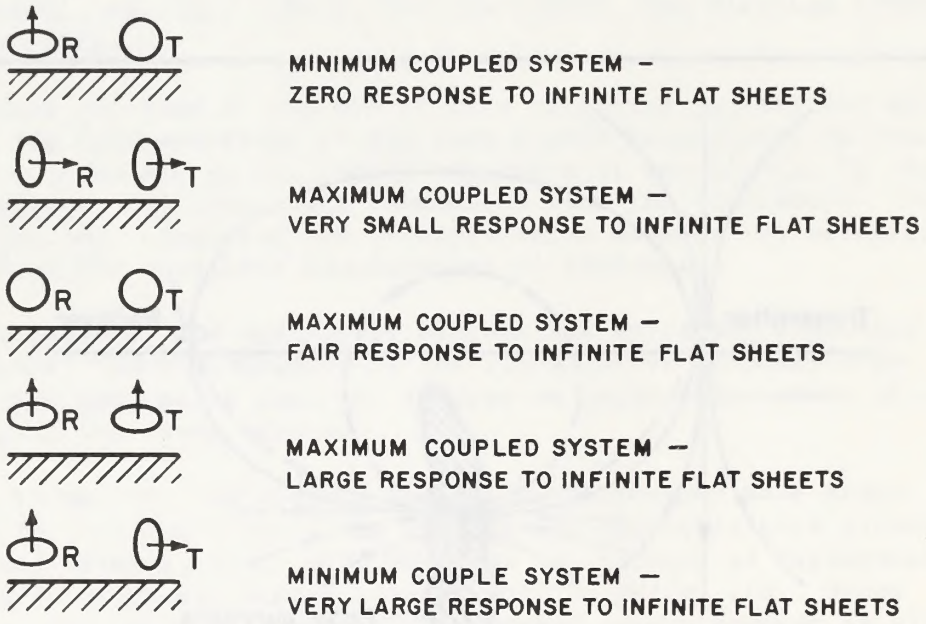

Figure 2. The Basic Coil Configurations for EM Systems.

III. General Airborne Electromagnetic (AEM) Survey Techniques

Fixed-wing aircraft operate at approximately 400 feet above the ground. If a towed RX (a "bird") is used, the aircraft altitude is controlled so that the bird is at approximately 150 feet above the ground. Flight-line spacing for reconnaissance work is normally one-fourth mile (1320 feet). For fill-in surveying, saturation surveys, or target delineation, flight-line spacing is reduced to one eighth mile (660 feet). A twin-engined, propeller-driven aircraft normally is used.

Helicopter-mounted systems operate at 150 feet or less above the ground. If a towed bird is used, the helicopter operates so as to place the bird at tree-top height. Helicopter units are used to fill in gaps in fixed-wing surveys, in steep or hilly terrains where fixed-wing aircraft cannot operate safely, and to pinpoint the location of EM targets located by fixed-wing aircraft. Flight-line spacing for helicopter surveys ranges from one-fourth mile to as few as 100 feet. Helicopter surveys usually cost 30 percent to 75 percent more per line mile than fixed-wing surveys.

IV. The Major Airborne Electromagnetic Systems

Today's exploration toolbox contains six major types of AEM systems. Five types utilize various portions of the EM spectrum and one utilizes gamma-ray radiation produced by the emissions of certain daughter products of uranium and thorium, and by the emissions of potassium 40 (K^{40}). Depending on survey requirements, these systems can be mounted in either fixed-wing aircraft or in helicopters.

The five AEM systems were originally developed in Canada and Sweden in the 1950's and early 1960's. They are updated as technology advances in the electronics and microprocessor industries. The systems were developed to locate massive sulfide bodies or elongated ultramafic bodies. The exploration environment was the structurally disturbed volcano-sedimentary ("greenstone") belts that lie in the shield and cratonic areas of these countries. The AEM systems perform best where the rocks dip more than 30 degrees.

The sixth AEM system is the gamma-ray spectrometer, which was developed in Canada in the early 1970's. It is capable of operating in all geologic environments, including those with flat-lying strata.

V. Systems That Operate on Measuring Changes in Frequency Modulation

The first AEM systems developed and operated were units measuring changes in frequency modulation. Various units became operational in the early 1950's and several modernized units are still operational. They function by measuring the changes in the inphase and quadrature components between a transmitted primary field and a received secondary field at one or more frequencies. The TX is mounted in a fixed-wing aircraft or in a helicopter. The RX is either carried in the aircraft or towed below in a bird. (Figure 3). A proton precession magnetometer is always carried as well. Table 1 lists the major units (and manufacturers of AEM units) now available in North America and gives their operating parameters.

A. Single Frequency Inphase/Quadrature Units (Example: Scintrix HEM 701)

This helicopter-mounted unit has both the TX and RX carried in the machine. The TX and RX are vertically mounted coaxial coils, and are maximum coupled. The operating frequency is 1600 Hz. Figure 4 illustrates the unit's recorder tape with the geophysical response of a conductor upon it. The anomaly is the Sturgeon Lake Mine of Mattagami Mines, Ltd., in southwestern Ontario. The ore body contains 12,400,000 short tons grading 0.91 percent copper, 0.82 percent lead, 7.6 percent zinc, and 3.04 ounces/ton silver. The ore body is 1,800 feet long by 300 feet wide by 600 feet deep.

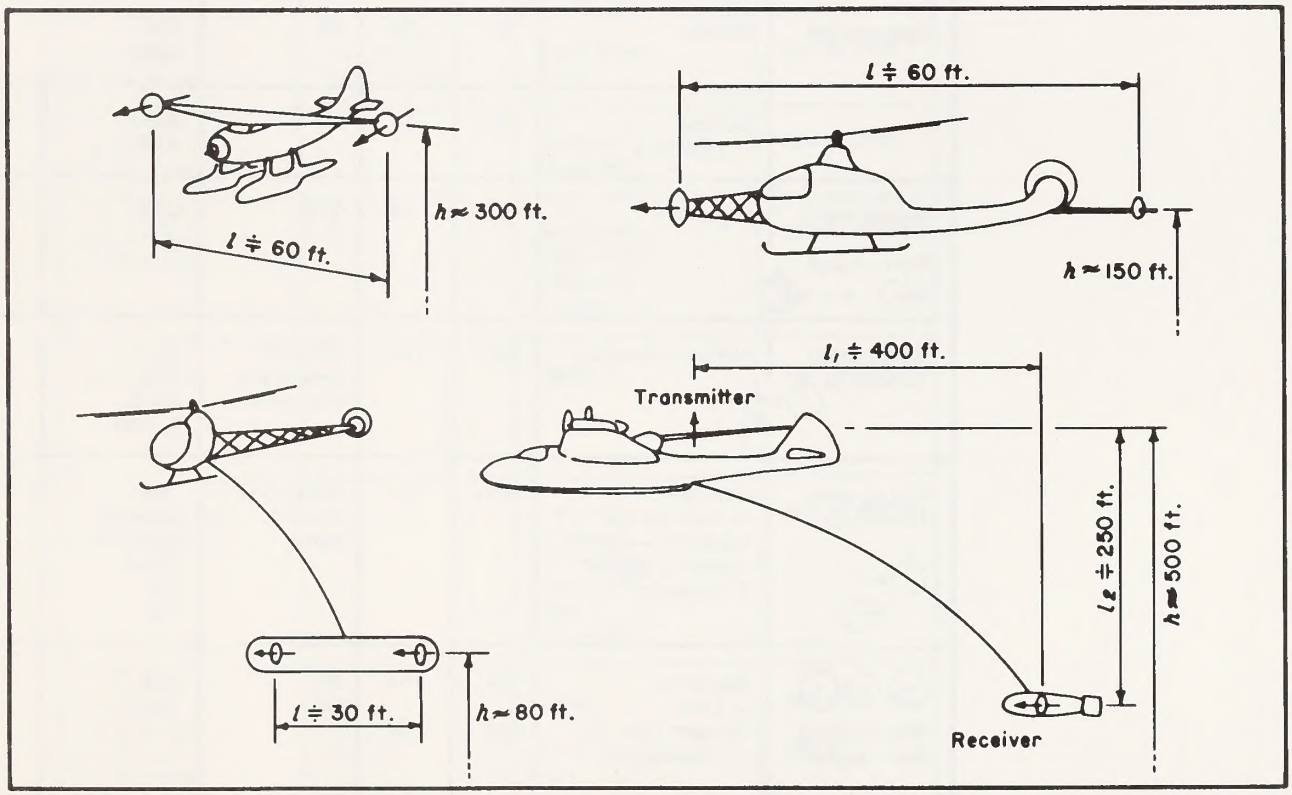

Figure 3. Examples of Airborne EM Installations and Configurations.

EM System Trans. Rec. Tx Rx Flight Dirn	Manufacturer/ contractor — Survey platform H=Helicopter FW=Fixed Wing	Normal Survey height in feet Trans. Tx	Rec. Rx	Tx-Rx separation in feet	Freq. (Hz)
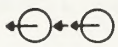	Kenting-Scintrex Tridem — Canso FW	164	164	83	500 2000 8000
	Barringer — Aerodat H	98	98	29.5	900
	Geonics — EM33 H	98	98	20	400-4000 (normally 736)
Vertical coaxial	Northway — LHEM 200 — LHEM 250 H	98 98	98 98	29.5 29.5	4000 1000
Rigid coupled	Sander H	98	98	23	500-4000
	Scintrex — HEM-802 H	98	98	27	735 & 3220
Multicoil boom Rigid coupled 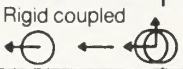	Dighem II H	98	98	27.8	900
Max coupled Towed bird 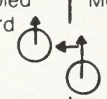	McPhar—Quadrem FW	459	164	885; 295 behind and 295 below	95, 855, 2565, & 7695
Max coupled Towed bird 	Barringer — Mark 6 Input Geoterrex — Canso Questor — Skyvan & Trislander FW	394	164	246 behind and 246 below	286 pulsed ½ sine waves per sec
 Wing mounted Max coupled	Geoterrex — Otter So quem Emal 19 — Cessna L19 FW	164 164	164 164	691 361	320 625

Table 1. Airborne electromagnetic survey systems available for purchase or as a contract service.

	Measure in phase out of phase	Noise level ppm	Response from overburden	Power requirements
	in phase & out of phase	20	Small but increases with freq. to moderate	28V dc 500W
	in phase & out of phase	2	Small	28V dc 340W
	in phase & out of phase at 2 time constants	<0.5	Small at low freqs.	28V dc 225W
	in phase & out of phase	5 5	Moderate Small	28V dc 25W 28V dc 60W
	in phase & out of phase	1 in phase 2 out of phase	Small at low freqs.	28V dc 75W
	in phase & out of phase	1	Small at lower freq.	28V dc 35W
	in phase & out of phase	1	Removed by differencing measured signals	28V dc 370W
	out of phase	500	Medium	28V dc 2000W
	Transient decay at 6 intervals	50	Large on channel 1, decreasing rapidly with higher channels	56V dc 3000W
	in phase & out of phase in phase & out of phase	20 35	Small Small	28V dc 500W 28V dc

EM System Trans. Tx / Rec. Rx Flight Dirn	Manufacturer/ contractor — Survey platform H = Helicopter FW = Fixed Wing	Normal Survey height in feet Trans. Tx	 Rec. Rx	Tx-Rx separation in feet	Freq. (Hz)
Ground loop 	Scintrex — Turair II H	Ground Loop	98	7.9 for Rx coils	200, 400 & 800
	Barringer — E-Phase	N/A	295	infinity	3 simult. freq.
	— Radiophase H or FW	N/A	295	infinity	14-28 KHz
	Geonics — EM 18 H or FW	N/A	98 984	infinity	12.25 KHz
Very low frequency (VLF)	Herz — Totem 1A H or FW	N/A	98 984	infinity	12-25 KHz
	McPhar — Kem H or FW	N/A	98 984	infinity	12-25 KHz
	Scintrex — SE 90 H or FW	N/A	98 984	infinity	12-25 KHz

Table 1. (continued) Airborne electromagnetic survey systems available for purchase or as a contract service.

	Measure in phase out of phase	Noise level ppm	Response from overburden	Power requirements
	Field strength ratio and phase difference	0.1% FSR 0.1° PD	Varies with frequency	28V dc 15W mg for ground coil
	out of phase out of phase	0.01% 0.01%	Variable at different freqs.	28V dc 42W
	in phase & out of phase	0.5%	Large	28V dc 50W
	Total field & vert. quad.	Depends on distance of Tx	Large	28V dc 14W
	Dip angle & amplitude	0.5 μV at sensor coils.	Large	28V dc 10W
	Vertical field vector in in phase & out of phase wrt hori. vector	<1%	Large	28V dc 30W

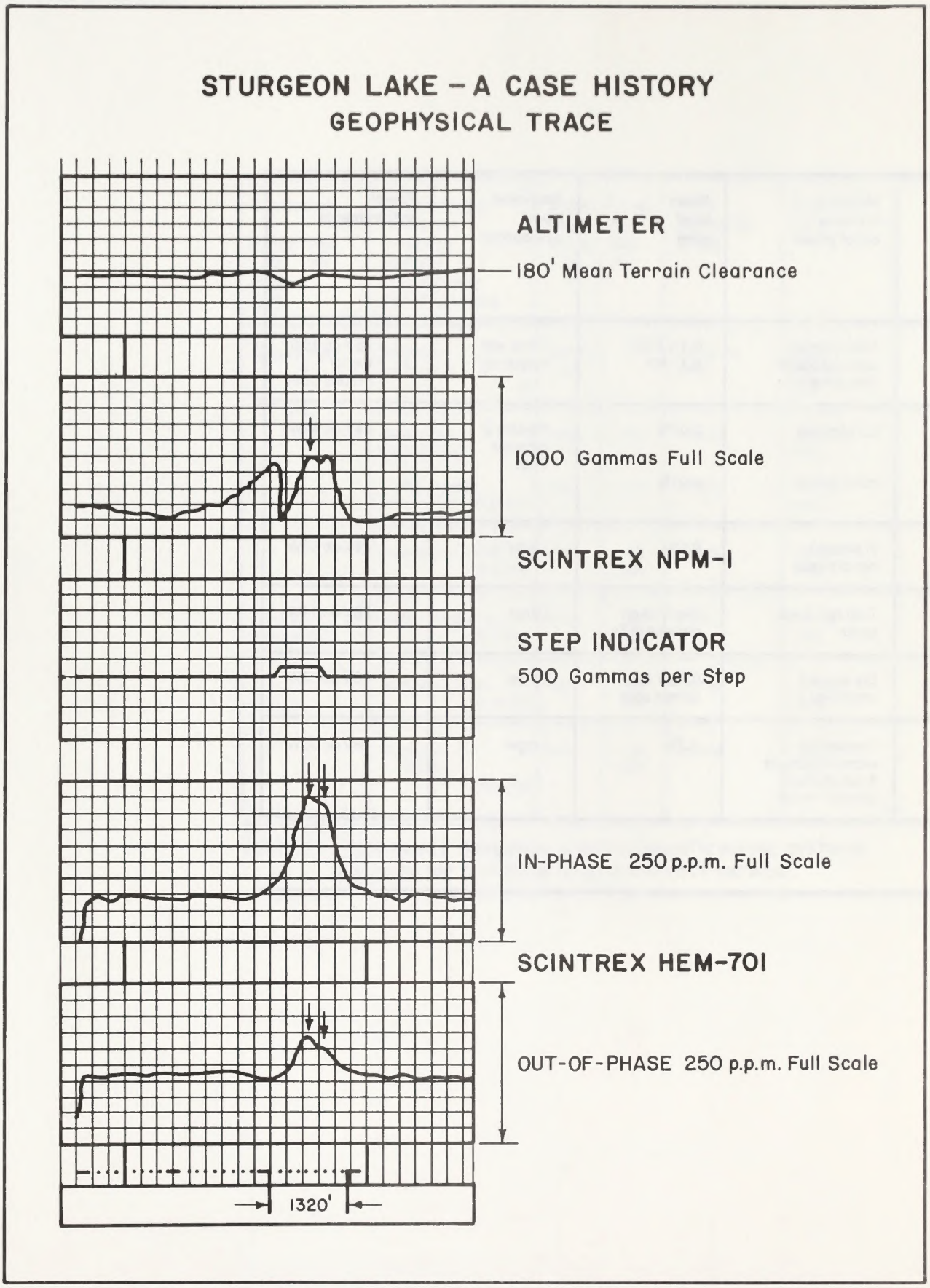

Figure 4. Response of the Sturgeon Lake Deposit to the HEM 701 System.

B. The DIGHEM II and DIGHEM III Systems

The DIGHEM system is a helicopter-mounted, single-frequency unit with TX and RX carried below in a towed bird. The TX is vertical. The RX consists of three orthogonal coils, two vertical and one horizontal, giving the RX a "whale tail", a "fish tail", and a standard vertical RX coil. The coaxially mounted RX coil is maximum coupled with the TX coil, the other two RX coils are minimum coupled. The operating frequency is 918 Hz. Figure 5 is a RX record of the DIGHEM II response to a copper-nickel deposit in Montcalm Township, Ontario.

This system has three unique features. One is the ability to detect conductors lying parallel to the flight line, due to the orientation of the "fish tail" RX coil. The second is a standard software package that allows the system to give a direct readout of the apparent resistivity of the ground below the RX. The third is a built-in anomaly recognition function in the software package that gives the unit the capability to locate weak conductors lying in highly conductive ground or in ground of high magnetic permeability.

A new operational variant of the DIGHEM II/III system has two TX coils mounted orthogonally and operating at 882 Hz and 918 Hz. The use of two frequencies allows for better conductor detection and produces more quantitative data for conductor evaluation. The DIGHEM IV unit is currently in the flight-testing stage. The full operating parameters of the DIGHEM II/III system and its data interpretation are given in Fraser (1972, 1979). The use and interpretation of the airborne resistivity functions for mapping of ground resistivity are discussed in Fraser (1978). Additional material on magnetite mapping with the DIGHEM II is presented in Appendix X of this reference.

C. The TRIDEM System

The TRIDEM system, manufactured by Scintrix, Ltd., is a three frequency, inphase/quadrature system operating three sets of TX-RX coils simultaneously at 520 Hz, 2020 Hz, and 8020 Hz. The TX and RX coils are mounted in the vertical coaxial mode and are maximum coupled. All coils are in the aircraft, and the TX-RX separation is 77 feet. Three widely spaced frequencies allow the detection of conductors under a wide range of ground conductivity conditions. The data recovered from the three frequencies allow quantitative evaluation of the conductor. Figure 6 shows the TRIDEM response to the Magusi ore body, near Noranda, Quebec. The ore body contains more than 4 million short tons grading 1.2 percent copper, 3.55 percent zinc, and recoverable gold and silver. The deposit is 1,500 feet long by 90 feet wide by at least 1,350 feet deep.

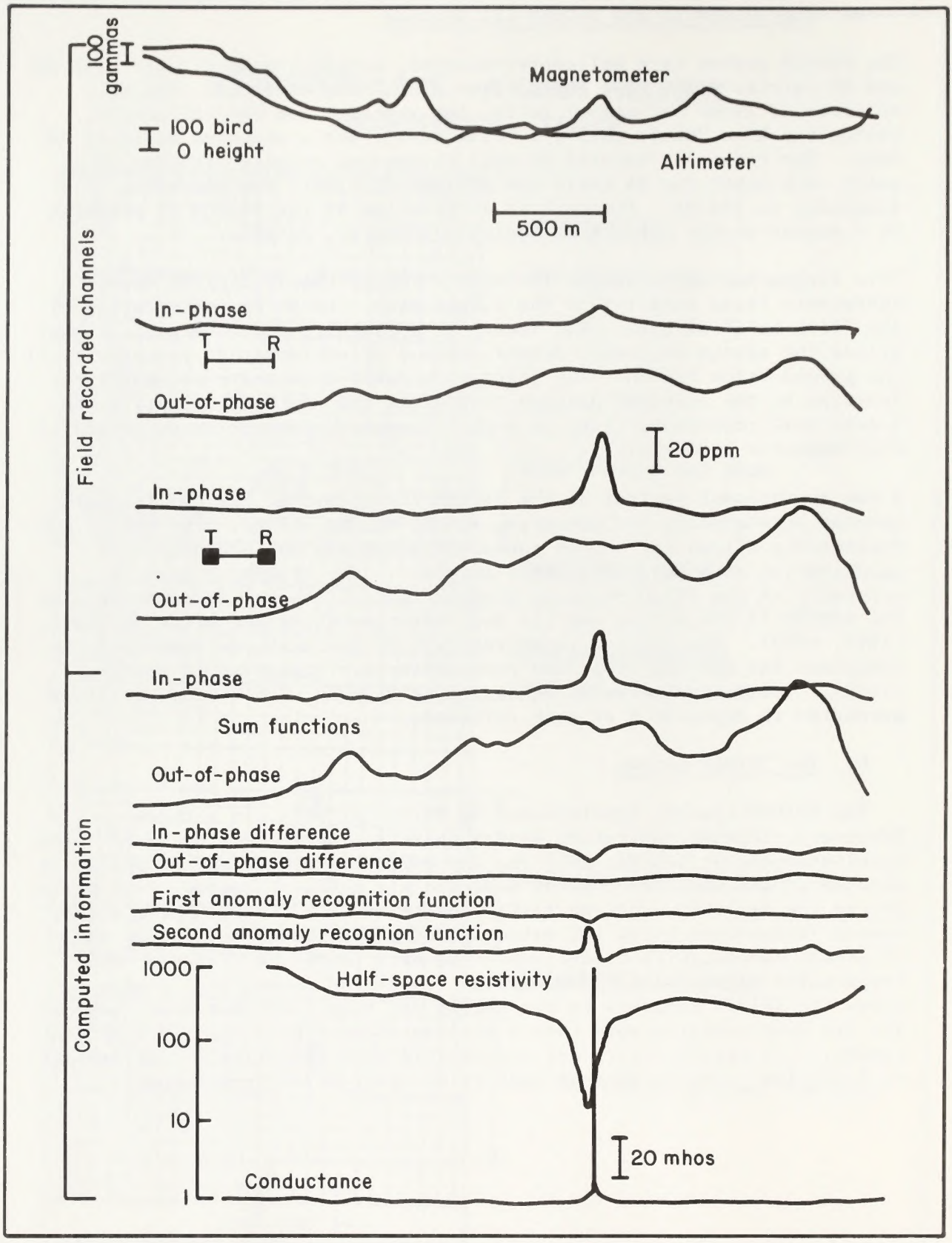

Figure 5. Dighem II recording over the Montcalm Township copper-nickel discovery.

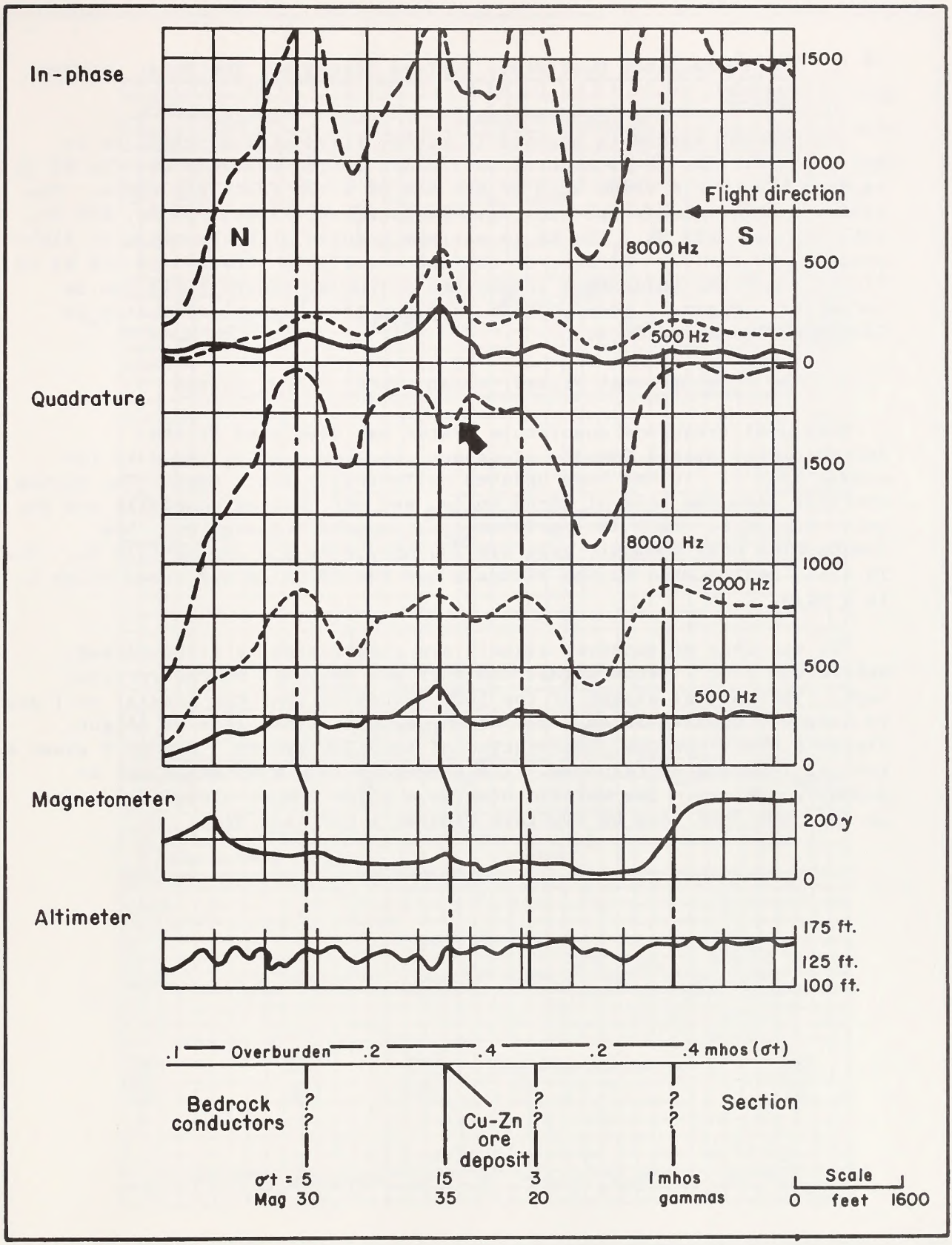

Figure 6. Tridem traverse over the Magusi deposit, Quebec, Canada.

D. Multi-frequency Quadrature Systems (Example: The McFar Quadrem System)

The QUADREM system is mounted in either fixed-wing aircraft or in helicopters. The TX is mounted vertically in the aircraft and the RX is carried below in a towed bird at the end of a 400 foot-long cable. The system simultaneously operates five frequencies, 95 Hz, 285 Hz, 855 Hz, 2565 Hz, and 7695 Hz. The Rx is maximum coupled with the magnetic field produced by the TX. Because of the uncontrollable rotation of the RX in flight, only the quadrature components of the secondary field can be recovered. Figure 7 is a QUADREM response to a conductor located in Cavendish Township, Ontario.

E. The International Nickel Company, Ltd. (INCO) System

This dual-frequency quadrature system was developed by the International Nickel Company of Canada, Ltd. (now INCO, Ltd.) in the middle 1950's. It has been updated periodically since then. The system operates with two sets of TX-RX coils, one set mounted coaxially and the other coplanar. Each set operates at different frequencies. The frequencies most commonly used are 350 Hz-750 Hz and 350 Hz-1250 Hz. The TX coils are mounted in the aircraft and the RX coils are towed below it in a bird.

The two sets of received signals are electronically filtered and subtracted from a datum signal and then are recorded on the receiver tape. The unusual aspect of the INCO system is that the coaxial coil set is oriented upwards at an angle of 45 degrees to the line of flight. Figure 8 shows the coil orientation of the INCO system. Figure 9 shows a typical INCO system response. The target is INCO's Whistle Mine at Sudbury, Ontario. The Whistle Mine is a major copper-nickel producer. It is 1,400 feet long by 100 feet wide by 1,000 feet deep.

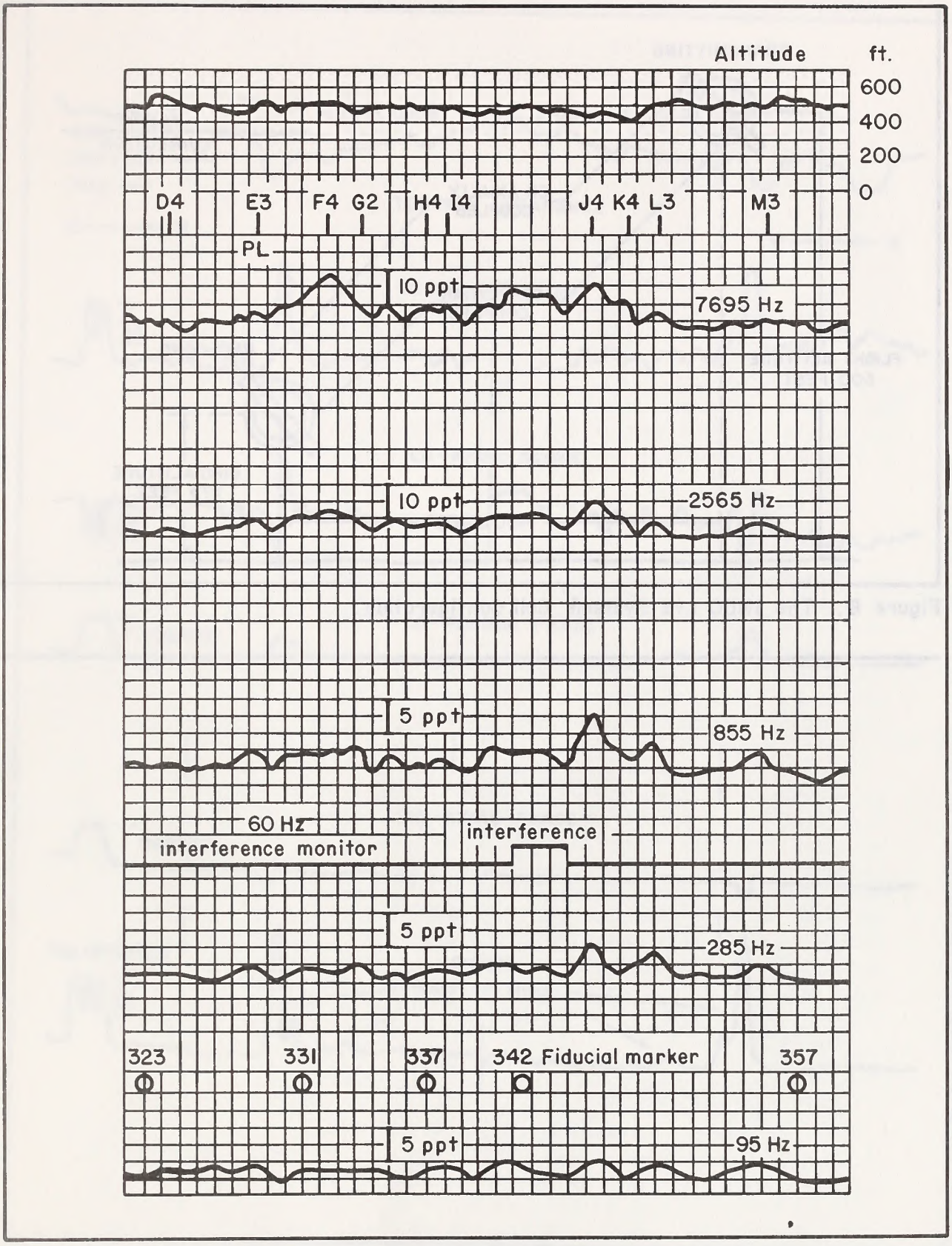

Figure 7. Example of a Quadrem flight record.

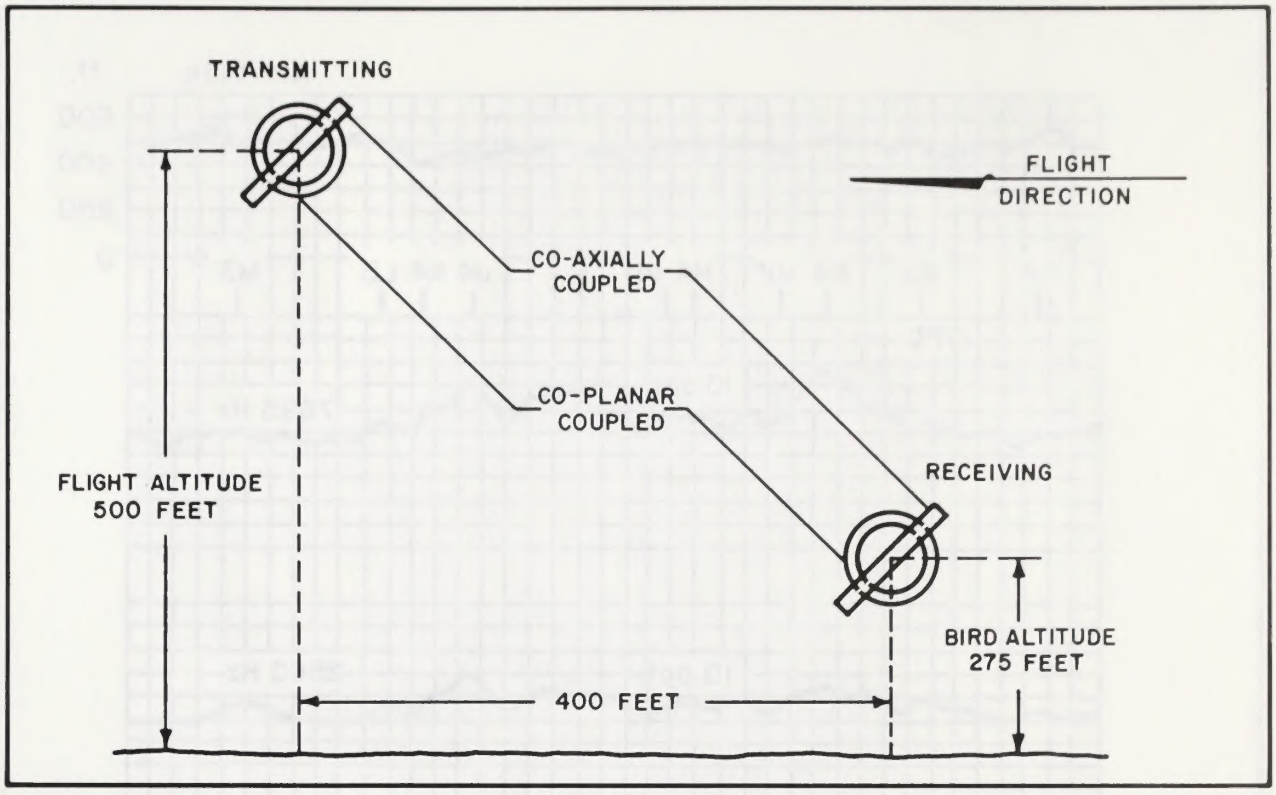

Figure 8. The INCO Ltd System's Coil Configuration.

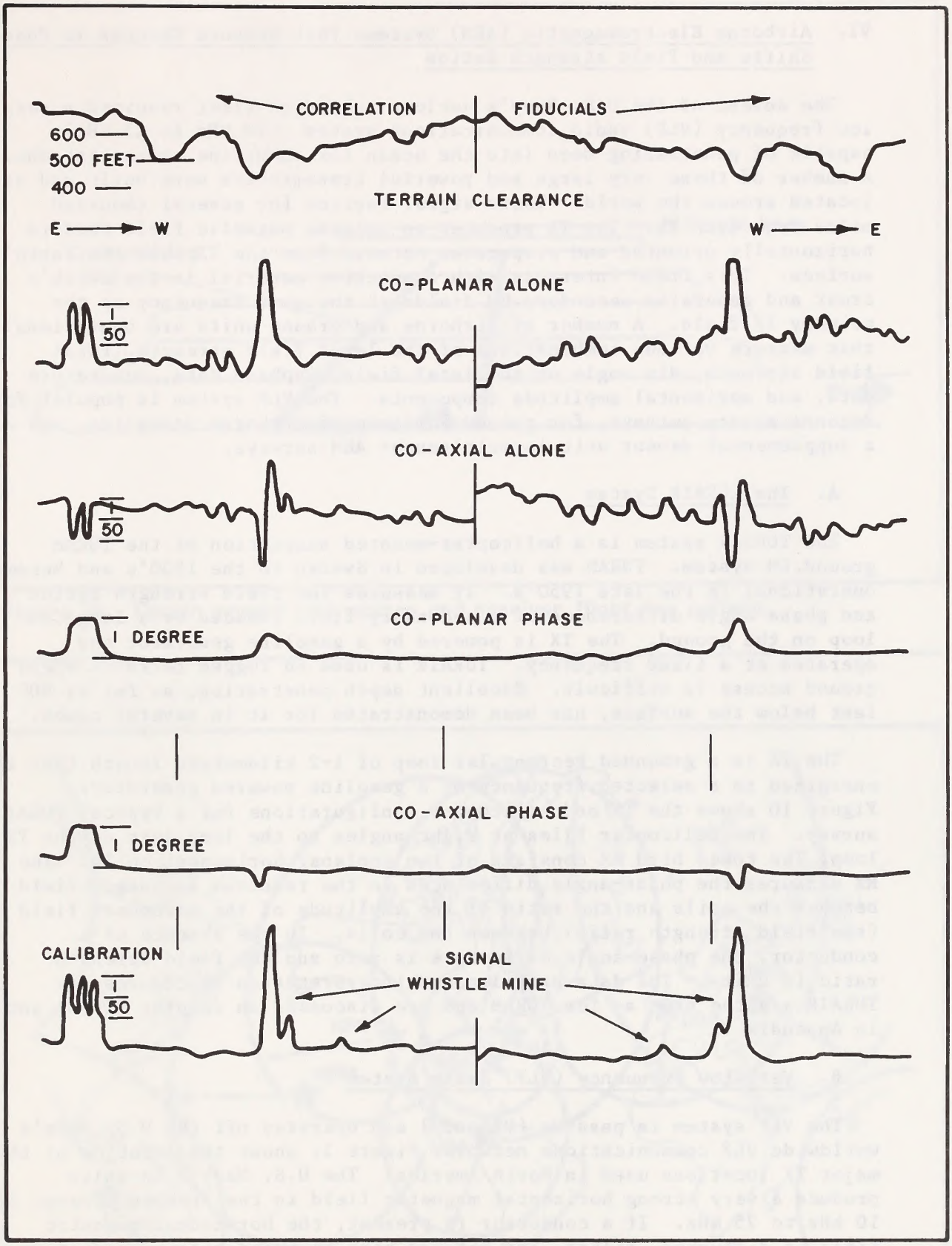

Figure 9. Response of the INCO Ltd System to the Whistle Mine.

VI. Airborne Electromagnetic (AEM) Systems That Measure Changes in Phase Shifts and Field strength Ratios

The advent of the U.S. Navy's nuclear submarine fleet required a very low frequency (VLF) radio communications system (10 kHz to 25 kHz) capable of penetrating deep into the ocean for submarine communications. A number of these very large and powerful transmitters were built and are located around the world. Their signal carries for several thousand miles from each TX. The TX produces an intense magnetic field that is horizontally oriented and propagates outward from the TX over the earth's surface. This field interacts with conductive material in the earth's crust and generates secondary EM fields at the same frequency as the primary TX field. A number of airborne and ground units are operational that measure various combinations of the local field strength, total field strength, dip angle of the local field, inphase data, quadrature data, and horizontal amplitude components. The VLF system is popular for reconnaissance surveys, for ground followup of airborne anomalies, and as a supplemental sensor unit in multisensor AEM surveys.

A. The TURAIR System

The TURAIR system is a helicopter-mounted adaptation of the TURAM ground.EM system. TURAM was developed in Sweden in the 1930's and became operational in the late 1950's. It measures the field strength ratios and phase-angle differences of a secondary field induced by a large TX loop on the ground. The TX is powered by a gasoline generator and operates at a fixed frequency. TURAIR is used in rugged terrains where ground access is difficult. Excellent depth penetration, as far as 900 feet below the surface, has been demonstrated for it in several cases.

The TX is a grounded rectangular loop of 1-2 kilometers length that is energized to a selected frequency by a gasoline powered generator. Figure 10 shows the TX and helicopter configurations for a typical TURAIR survey. The helicopter flies at right angles to the long axis of the TX loop. The towed bird RX consists of two coplanar horizontal coils. The RX measures the phase-angle differences in the received secondary field between the coils and the ratio of the amplitude of the secondary field (the field strength ratio) between the coils. In the absence of a conductor, the phase-angle difference is zero and the field strength ratio is unity. The data profiles and interpretation procedures for TURAIR are the same as for TURAM and are discussed in Chapter XIV(B) and in Appendix V.

B. Very Low Frequency (VLF) Radio System

The VLF system is passive (RX only) and operates off the U.S. Navy's worldwide VLF communications network. Figure 11 shows the location of the major TX locations used in North America. The U.S. Navy's TX units produce a very strong horizontal magnetic field in the frequency range of 10 kHz to 25 kHz. If a conductor is present, the horizontal magnetic field is disturbed, tilted, and rotated both in phase and in quadrature. The disturbance also causes local variations in the amplitude and field strength of the primary signal. The VLF RX measures these various changes of primary and secondary fields in the survey area. The system is mounted in small aircraft and helicopters and is available in hand-held units for ground operations. The use and interpretation of VLF data are described in Chapter XIV(C) and in Appendices VI and X.

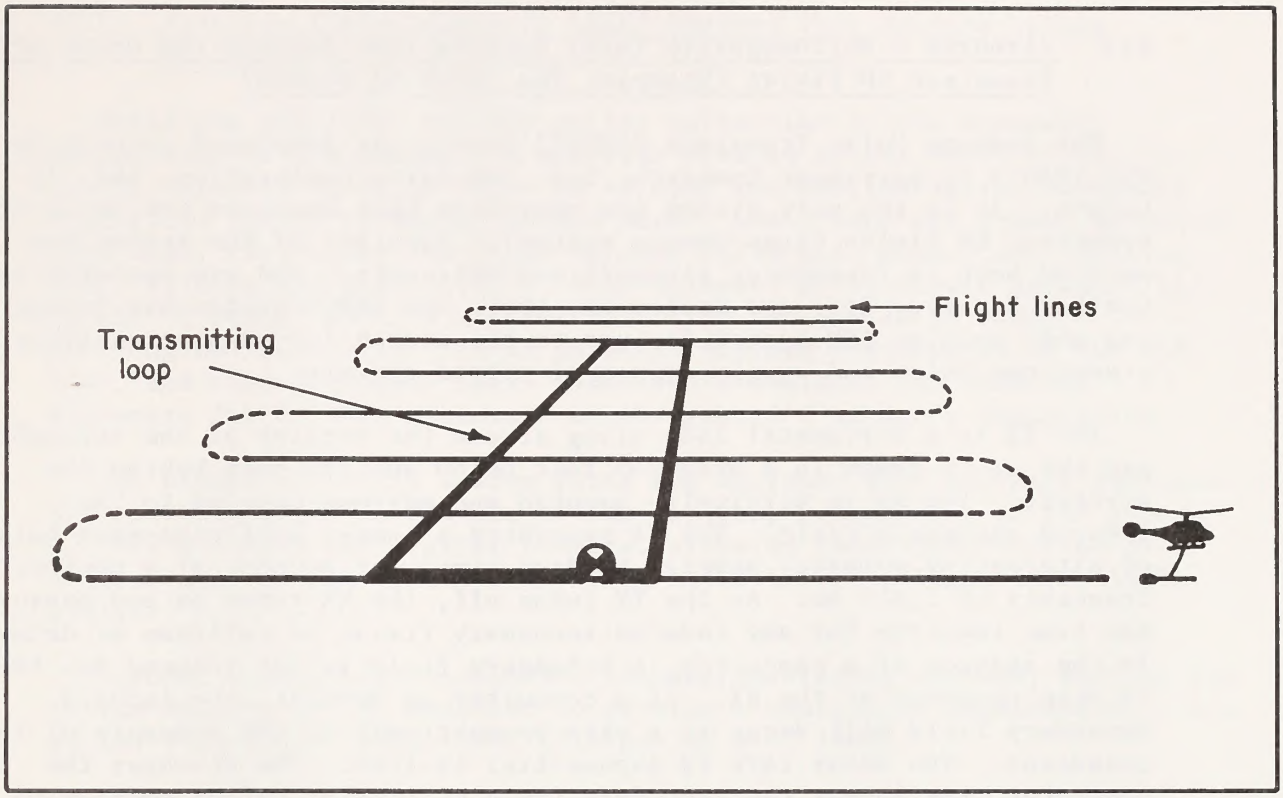

Figure 10. Turair ground loop source and receiver flight line pattern.

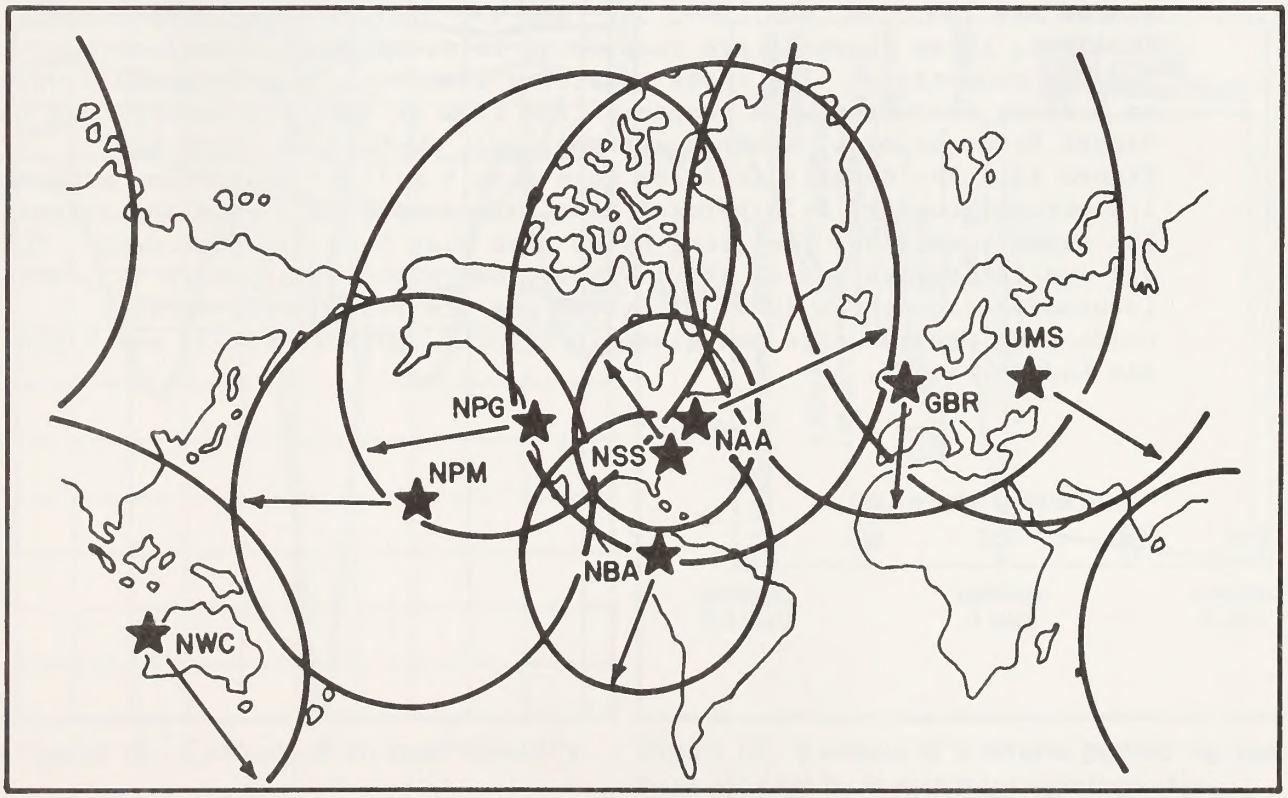

Figure 11. Locations of well-known VLF transmitter stations.
(Station Identification codes and range of signals)

VII. Airborne Electromagnetic (AEM) Systems That Measure the Decay of Transient EM Fields (Example: The INPUT VI System)

The Induced Pulse Transient (INPUT) system was developed jointly in the 1950's by Barringer Research, Ltd. and Selco Exploration, Ltd. in Canada. It is the only system now operating that measures the decay of transient EM fields (time-domain system). Versions of the system are mounted both in fixed-wing aircraft and helicopters and are operated by Questor Surveys, Ltd. and Geoterrex, Ltd. The INPUT system has become the most popular AEM system for use in the search for massive sulfides in greenstone belts and similar types of tilted terrain.

The TX is a horizontal loop slung around the outside of the aircraft and the RX is towed in a bird 200 feet below and 350 feet behind the aircraft. The RX is vertically mounted and maximum coupled to the induced secondary field. The TX generates a square half-sine-wave pulse of alternating polarity several hundred times per second, at a nominal frequency of 1,444 Hz. As the TX turns off, the RX turns on and measures the time required for any induced secondary fields to collapse or decay. In the absence of a conductor, a secondary field is not induced and there is zero response at the RX. If a conductor is present, the induced secondary field will decay at a rate proportional to the strength of the conductor. The decay rate is exponential in form. The stronger the conductor, the longer the secondary field will exist before collapsing totally.

The INPUT VI system measures the decay of the secondary field at six time intervals (channels) which are located at 200, 500, 750, 1,100, 1,500, and 2,100 microseconds after the TX has turned off. The channel widths are 250, 300, 400, 500, 550, and 270 microseconds, respectively. The first three channels are responsive to overburden as well as to bedrock conductors. The three remaining channels normally respond only to bedrock conductors. A response tape from an INPUT VI survey over the Magusi River deposit, located near Noranda, Quebec, is given in Figure 12. The deposit contains more than 4 million short tons grading 1.2 percent copper, 3.55 percent zinc, and recoverable gold and silver. The deposit is 1,500 feet long by 90 feet wide by 1,350 feet deep. The use and interpretation of INPUT VI data are given in Appendix I. Further information about the INPUT VI system and its response to various conducting environments was given in Palacky and West (1973) and Klein and LaJoie (1980).

VIII. Airborne Electromagnetic (AEM) Systems That Measure Ground Resistivity

Units are available for the aerial collection of the apparent resistivity of the ground. A modified version of the INPUT VI has the six RX channels reset to focus on surface and shallow-depth, secondary electrical fields in soils, ground water, coal, sand and gravel deposits, lake beds, clay beds, and other related horizontal conductors (Whiting, 1982; Palacky and West, 1973). Also marketed by Barringer Research Ltd. is the "E Phase" unit, a passive unit that is mounted in small, twin-engined aircraft. Its RX measures various frequencies in the VLF, low-, and high-frequency radio bands and translates the received secondary fields into a measure of the ground's apparent resistivity.

The DIGHEM II/III/IV system units are equipped with software packages that provide a direct readout of the apparent resistivity of the ground in both analogue and digital formats, allowing rapid construction of contour maps of the ground's apparent resistivity (Fraser, 1978, 1979, 1981a).

Several of the multi-frequency inphase/quadrature systems, such as the TRIDEM system, can be modified to provide a continuous measurement of the ground's apparent resistivity (Pitcher et al., 1980).

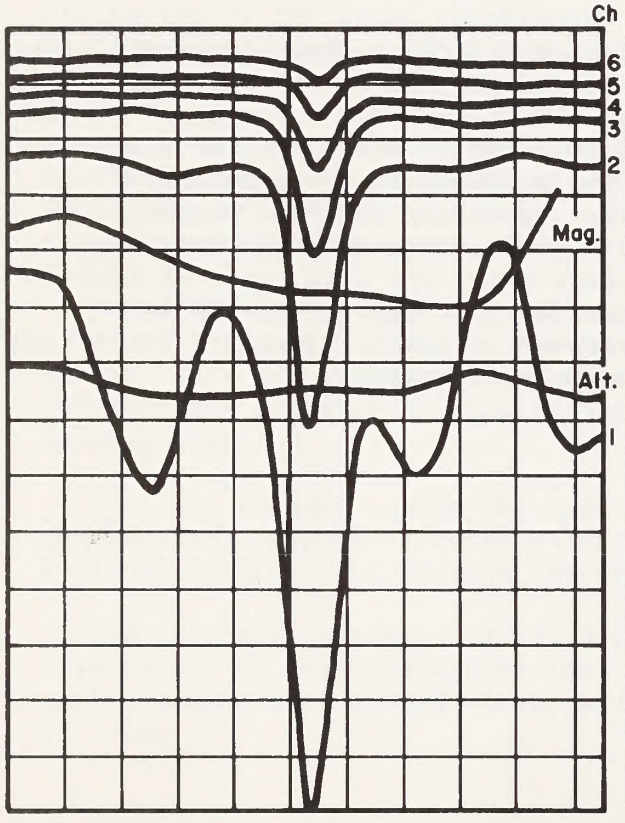

Figure 12. Example of an input discovery.

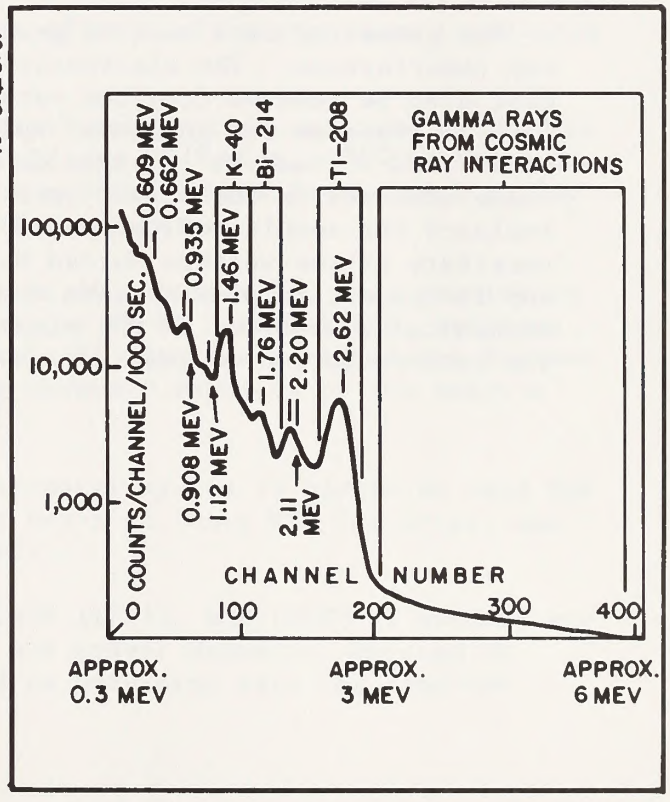

Figure 13. Example of a natural gamma ray spectrum obtained by multichannel spectrometer.

IX. Airborne Gamma-Ray Spectrometry

The emphasis in the early 1970's on uranium exploration led to the development of units capable of simultaneously detecting uranium (U), thorium (Th), and potassium (K), and quantifying the amounts of these elements in parts per million (ppm) in the ground below the RX. The amount of K is measured as K^{40}, the radioactive isotope of K. The amount of U is measured as the amount of Bi^{214}, which is a daughter product of uranium decay. Likewise, the amount of Th is measured as the amount of Tl^{208} present in the survey area. Conversions to ppm U or Th assume that the U and Th are in geochemical equilibrium with the Bi^{214} and Tl^{208} in the survey area. This may not be the case in some locations.

The daughter products of U and Th, and the K^{40} isotope of K, emit gamma-rays at specific energies and frequencies. Figure 13 shows the energy spectrum of natural gamma-rays and those frequencies of interest to us. The selected frequencies are received and recorded by a thallium-activated, sodium chloride photovoltaic cell. The gamma-rays hitting the cell generate a voltage in the cell that is of the same frequency as the gamma-ray. The voltages produced are filtered and the three frequencies of interest are allowed into the recording unit. The units in use can be calibrated to translate the received voltages into ppm U, Th, and K^{40}, assuming isotopic equilibrium between the parent elements and the daughter products. Gamma-ray spectrometer units are portable and can be mounted in aircraft, trucks, or can be hand carried. Units are available for the direct assaying of drill holes.

Raw gamma-ray data must be processed to remove atmospheric and cosmic ray interference. The electronic effects of the instruments themselves must also be removed from the data. These procedures are given in Hansen (1981). Because the gamma-ray spectrometer is measuring the distribution of K^{40}, Tl^{208}, and Bi^{214}, data on the geochemical distribution of these elements in the survey area are necessary in order to properly evaluate the results of the survey. This information is especially necessary in the western United States where the arid cycle of erosion and infrequent rainfall create anomalies that are due mainly to mechanical dispersion of the elements of interest. Appendix 2 contains the interpretation of gamma-ray spectrometer data.

X. Advantages and Disadvantages of the Various AEM Systems

The searches for massive sulfide deposits in North America, Australia, the Baltic region, and southern Africa allow comparisons of the relative effectiveness of these systems to be made. The single-frequency, inphase, quadrature, and the dual-frequency quadrature systems will easily locate large conductive bodies, but they have poor responses to sulphide bodies of small volume or short (less than 800 feet) strike length. The amount of data collected is limited, which hampers the evaluation of the conductor and the proper selection of drill targets. Depth penetration is good to moderate. The DIGHEM II/III system has an advantage with its RX coil configuration, which allows detection of conductors lying parallel to the flight line.

The multi-frequency, inphase/quadrature, and quadrature systems yield more data than the single-frequency, inphase/quadrature systems for the evaluation of a conductor and for the selection of drilling sites. Depth penetration is good and their ability to resolve closely spaced conductors is adequate.

The VLF system has two drawbacks:

1. The system is very sensitive to horizontal conductors (lake bottoms, clays, water saturated soils, etc.), which greatly limits its depth penetration in areas where these features exist.

2. The primary magnetic field produced by the U.S. Navy's TX is channelled by the local topography. In hilly terrains, the VLF data must be filtered to remove the topographic effects. This procedure is covered in Appendices VI and X.

The TURAIR system has excellent depth penetration and does not suffer from electromagnetic coupling of the TX and RX, which is a common problem with inphase/quadrature systems. The major drawback is the need to lay out and retrieve the ground TX loop and generator.

The INPUT VI system has excellent depth penetration, good resolution of closely spaced multiple conductors, no TX-RX interference, and good quality data for conductor evaluation. It also has achieved the highest success rate in terms of discovering economic deposits of the massive sulphide type.

The four-channel, gamma-ray spectrometer system is now being used for the regional mapping of rocks on the basis of their K^{40} (as K-spar and K-mica), uranium, and thorium contents.

The "E Phase" system, TRIDEM, DIGHEM II/III, and INPUT VI systems are also useful in the location of sand and gravel deposits, mapping of soils, location of ground water, and in providing data for land-use planning.

XI. General Ground Electromagnetic (EM) Surveying Techniques

Mineral properties are surveyed by first establishing a survey base line that is parallel to the strike of the conductor, if it is known. If it is not known, then the base line is laid out parallel to the general strike of the rock units in the survey area. The base line is either cut or flagged, depending on the terrain and instrument requirements. It is chained with stations at 100-foot intervals. The survey lines are established at right angles to the base line, usually at 300- or 400-foot intervals along the base line. VLF or high-resolution EM surveys may use 100-foot spacing for the survey lines. The survey lines are cut or flagged and the lines are chained with stations at 100-foot intervals along the line. The base line is the zero reference line for the survey grid.

Normal survey practice is to take instrument readings at each 100-foot station along the base and survey lines. In areas of anomalous EM responses, the station interval is reduced to 50, or even to 25 feet, until the EM anomaly is crossed completely.

XII. The Major Ground EM Systems

The systems used in ground EM surveying are analogues of the AEM systems and can be divided into the same general operating categories. In the 1920's and 1930's, the electrical resistivity and vertical loop EM (VLEM) systems were developed and placed into general use in North America. The horizontal loop EM (HLEM or "Slingram") and TURAM systems were developed in Sweden in the 1930's and were brought to North America shortly after the end of World War II. Induced Polarization (IP) was developed from the electrical resistivity system by Newmont Mining Corporation in the early 1950's to locate deposits of disseminated sulfides in the southwestern United States. In the mid 1970's a ground-based, transient-decay (time-domain) system was developed jointly by the Geological Survey of Canada and Crone Geophysics, Ltd. and is now in widespread use. The advent of microprocessing technology has created and permitted the marketing of a variety of new down-hole geophysical logging and exploration units that operate on the IP, electrical, and transient decay principles.

Table 2 gives a listing of the ground EM and other geophysical systems in use today. The table shows the system, its uses, field costs, and the form of interpretation to be used.

	Method (A) Active (P) Passive	Parameter Measured: Designation	Parameter Measured: Unit	Characteristic Physical Property	Main Causes of Anomalies
ELECTRICAL	RESISTIVITY (A)	Apparent resistivity	Ω-m	Resistivity Conductivity	Conductive veins, sedimentary layers, volcanic intrusions, shear zones, faults, weatherings, hot waters
ELECTRICAL	INDUCED POLARIZATION (A)	Time domain: chargeability polarizability Frequency domain: frequency effect Phase domain: phase shift	ms ple mr	Ionic-electronic Over voltage	Conductive mineralizations: disseminated or massive (graphite, sulfides), clay
ELECTRICAL	SELF POTENTIAL (P)	Natural potential	mV	Conductivity Oxydability	Massive conductive ores Graphite Electro-filtration Faults
ELECTRICAL	MISE-A-LA-MASSE (A)	Applied potential	mV	Conductivity	Extension of previously located conductive orebodies
ELECTRICAL	TELLURIC (P)	Relative ellipse area Ratios—apparent resistivity	Ω-m	Conductance	Basin and Range studies Conductance of sedimentary series Salt domes, geothermal
ELECTRICAL	MAGNETOTELLURIC (P) MT, AMT (A) CS-AMT	Apparent impedance (resistivity and phase)	Ω-m degrees	Resistivity Conductivity	Conductive veins, sedimentary layers, shear zones, faults, weatherings, resistive basements, bedded ores
ELECTRICAL	ELECTROMAGNETIC (A)	Phase difference Tilt angle Amplitude ratio Sampling of decay curve induced in receiving coil by eddy currents In-phase, out-of-phase components	degrees Ω-m σt	Electrical conductivity	Conductive mineralizations Surficial conductors Shear zones
	MAGNETIC (P)	Earth magnetic field Vertical component Z, Total intensity Horizontal gradient Vertical gradient	$1\gamma = 10^{-5}$ gauss	Magnetic susceptibility	Contrasts of magnetization Magnetite content of the materials
	GRAVITY (P)	Gravity field	milligal (1 gal = 1 cm/s^2)	Density	Deposits of heavy ores Salt domes (light) Basement rocks
	RADIOACTIVITY (P)	Intensity and spectral composition of gamma rays	cps	Radioactivity	Radioactive elements Uranium-Thorium-K_{40}
SEISMIC	REFRACTION (A)	Traveling time of seismic waves	milliseconds feet per second	Seismic wave velocity Dynamic modulus	Contrasts of velocity: markers at variable depth Fissured rocks
SEISMIC	REFLECTION (A)				
	THERMOMETRY (P)	Temperature	°C	Geothermal gradient and temperature	Abnormal flux of heat Thermal inertia of rocks

Table 2. Application of geophysical techniques.

Applications		Geophysical Crew		
Direct Detection	Indirect Detection	Production	Survey Cost	Interpretation
Massive sulfides Oil shales Clays Geothermal reservoirs	Bulk material Base metals Coal & natural steam	Depending upon depth of investigation El. soundings: 20 to 250 E.S./month Resistivity profiling: 20 to 100 line km/month Resistivity maps: 5 to 20 sq km/month	750/day	Curve matching Computer modeling
Conductive: sulfides oxides mn oxides	Associated minerals (zinc, gold, silver, tin, uranium, etc.)	800 to 2000 stations/month 20 to 70 line km/month	850/day	Curve matching Computer modeling
Sulfides: pyrite pyrrhotite copper Mn ore	Associated minerals (lead, gold, silver, zinc, nickel)	2500 to 3500 stations/month 60 to 200 line km/month	250/day	Rules of thumb Curve matching Visual interpretation
Conductive ores	Associated minerals (zinc, tin)	5 to 15 sq km/month	400/day	Computer reduced, computer modeling, visual interpretation
Structural studies Steam	Regional exploration	20 to 500 sq km/month	450/day	Computer reduced Curve matching Visual
Massive sulfides Clays Natural steam	Shear zones General tectonics General structure	Up to 3 stations/day Up to 20 stations/day	1200/day to 1000/station	Computer reduced Computer inversion Visual interpretation
Conductive: sulfides oxides Mn oxides	Kimberlites Associated minerals Ground follow up (lead, nickel), shear zones, weathered zones, conductivity maps	50 to 150 line km/month 6000 to 10,000 line km/month	750/day (ground) 70-95 km air	Curve matching Visual interpretation Computer modeling
Magnetite Pyrrhotite Titano-magnetite	Molybdenum Iron ore Chromite Copper ore Kimberlites Asbestos Geological mapping in terms of magnetic changes (basic rocks . . .) and/or discontinuities inventory of mineral resources	4000 to 8000 stations/month 80 to 300 line km/month (on shore) 20 to 80 line km/working day (off shore) 1000 to 15,000 line km/month	300/day (ground) 25-30 km air	Computer reduced Rule of thumb Computer modeling Computer inversion Visual interpretation
Chromite Pyrite Chalcopyrite Lead	Placer configuration Karstic cavities Basement topography Structure	400 to 1500 stations/month 20 to 50 stations/working day Surface meter combined with seismic turnover	450/day	Computer reduced Computer modeling Computer inversion Curve matching
Uranium Thorium Phosphates	Ground follow up Geological structural mapping (differentiation in granites)	80 to 400 line km/month (ground) 1000 to 15,000 line km/month (air)	350/day 25-60 km	Computer reduced Rations of responses Geologic correlation
Buried channels Faults Morphological traps Basement topography	Tin, diamonds Heavy minerals Natural steam Uranium	10 to 50 line km/month (on shore) 10 to 40 line km/working day (off shore)	350/day 1200-5000/day	Computer interpreted Computer inverted
Thermal springs	Natural steam Boron, sulfur, Subterranean volcanism		1000/day	Computer reduced

XIII. Inphase/Quadrature Systems

The Horizontal Loop Electromagnet (HLEM) system is the only ground EM system operating in the horizontal coil inphase/quadrature mode at present. The HLEM is maximum coupled and consists of separate TX and RX coplanar coils that are connected by a shielded coaxial cable of a fixed length. The lengths are standardized in the industry in units of 100, 200, 300, 400, 600, and 800 feet. The system is carried and operated by two persons and normally requires cut lines and chained grids. The coils, TX and RX, are suspended around the waist and are held up by a shoulder harness.

The system measures changes in the inphase and quadrature components of a secondary field produced by the interaction of the primary transmitted field and a conductor. Frequencies used range from 200 Hz to 3,600 Hz, but the most common frequencies are from 800 to 1,600 Hz. The TX sends a reference signal to the RX via the shielded cable. The RX compares the received secondary signal with the reference signal. The differences are displayed on the RX dials as percent change in the secondary field as compared to the primary field for both the inphase and quadrature components. The TX is battery powered and depth penetration is one-half of the cable length in nonconducting ground. Penetration can be less if the ground is conductive.

As a conductor is approached with a HLEM unit, the readings at the RX will increase from background values of near zero to positive values as the edge of the conductor is reached. The readings will decrease to large negative values over the conductor's center and will then increase to positive values as the other edge of the conductor is reached. After this edge is crossed, the readings will return to background values again. A typical HLEM profile over a conductor is shown in Figure 14. If the positive shoulders of the profile are asymmetrical, the conductor dips toward the larger shoulder.

The HLEM system can determine the dip, depth, and conductivity-thickness product of the conductor. Conductor quality is related to the ratio of the maximum negative inphase value to the negative quadrature value, measured at the center of the conductor. The higher the ratio, the stronger the conductor is. The depth and thickness of the conductor are determined from the coil spacing and the plotting of the negative inphase and quadrature values on a phasor diagram. These diagrams are normally supplied by the manufacturer of the unit used for the survey. If they are not availabe, the general phasor diagrams for interpretation of HLEM data given in Appendix III may be used.

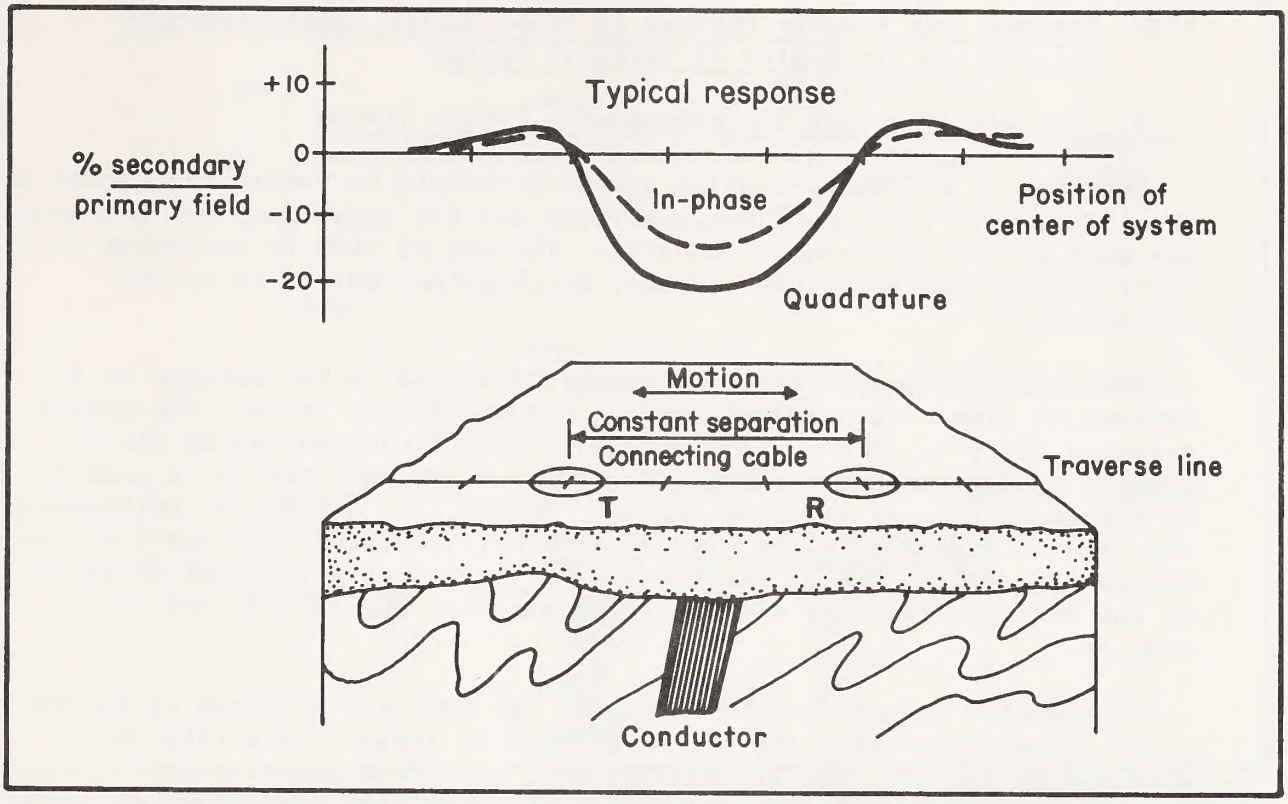

Figure 14. Field setup and results over a steeply dipping bedrock conductor using HLEM.

Normal survey practice is to record readings every 100 feet on the survey line, with readings taken every 50 or 25 feet in anomalous zones. Either the TX or the RX may proceed first down the survey line. The cable must be kept tight and the coils must be kept in the same plane at each reading. Otherwise, serious errors will be introduced into the received data. The readings are plotted midway between the coils. The HLEM system is very sensitive to topographic interference and is not usable in mountainous areas. A subsystem has been developed to operate in mountainous areas and is called the Shootback HLEM system. It was jointly developed by Noranda Mines, Ltd. and Crone Geophysics, Ltd. in the 1960's and is available on the open market as the Crone CEM unit. The HLEM system is widely used in the world in the search for massive sulfides in "greenstone" belt terrains. The basic use and interpretation of HLEM units and data are given in Appendix III and in Klein and LaJoie (1980), Ward (1979), and Nair et al. (1968). The Shootback variant is explained in Klein and LaJoie (1980) and Grant and West (1966).

XIV. Systems That Measure Changes in Phase Shifts, Field Strength Ratios, and Dip Angles of Vertical Fields

A. The Vertical Loop Electromagnetic (VLEM) System

The VLEM is a minimum-coupled system developed in Sweden and Canada in the 1920's. Various units are available and are updated as new advances are made in the electronics industry. The use of VLEM is declining in favor of the HLEM and TURAM systems, which gather more data on the conductor.

The VLEM system consists of separate TX and RX units operated by a two-person crew. It does not require cut or chained lines. The system measures the tilt or dip angle of a secondary field induced by the TX, usually at frequencies ranging from 400 to 5,000 Hz. The TX is powered by either battery or gasoline engine. The RX is a hand-held inclinometer the size of a walkie-talkie with an internal receiving coil tuned to the proper frequency. The TX generates a horizontal or a vertical EM field at the desired frequency and the TX is aimed at the RX for each survey station.

A conductor present at the RX causes the EM field produced by the TX to be tilted from the plane of the primary TX field. This tilt is measured by the RX. The RX readings will move from positive (or negative) on one side of the conductor, to zero over the conductor's center, and then to negative (or positive) over the other side of the conductor. Away from the conductor, the RX readings will be near zero. Depth penetration is usually one-half of the TX-RX separation.

Normal survey practice is for the TX and RX to move parallel to each other along adjacent survey lines and to "face" each other at the corresponding station on each line (that is both the TX and RX will be at station 10N [1000 feet north of base line] on their respective lines). This method is called the broadside or parallel line mode of VLEM surveying. It is used to locate a conductor for further detailed VLEM surveying by the fixed TX mode. Figure 15 shows the field procedure and conductor response to a VLEM broadside survey.

If a conductor is located by the broadside method, the TX is brought over and placed at the conductor center (the zero or cross-over point) identified at the RX. The survey procedure is then shifted to the fixed TX mode. In this mode, the TX remains at the conductor center on this line and the RX is operated on the survey lines adjacent to the TX on both sides. The TX remains stationary and is rotated so that it points directly at the RX for each reading on the adjacent survey line. If the TX is powerful enough, the RX can survey several lines (usually to a maximum of 1,200 feet from the TX) before the TX has to be moved to the conductor's center on another line. This process is repeated until the conductor has been fully traced out along strike. Figure 16 shows a typical fixed TX survey and a conductor response to the survey.

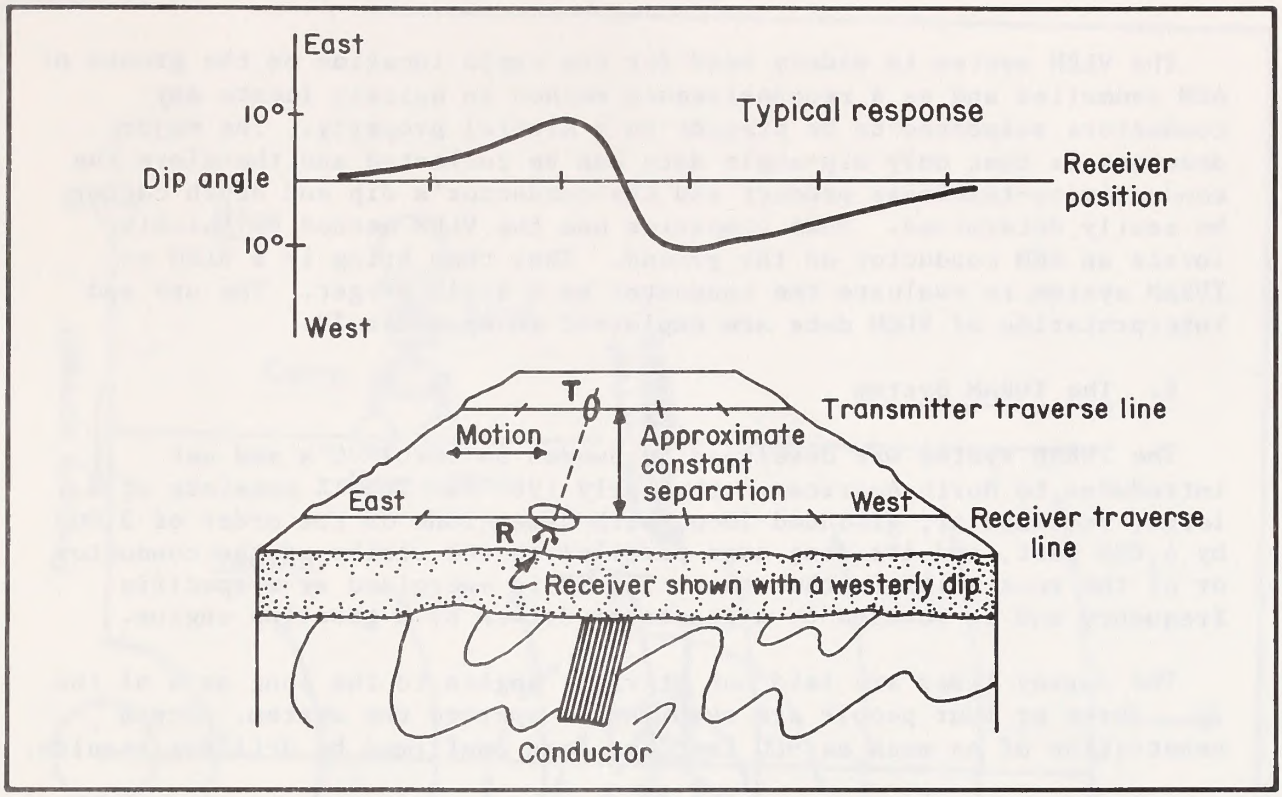

Figure 15. Field setup and results over a steeply dipping bedrock conductor using VLEM. Parallel line technique.

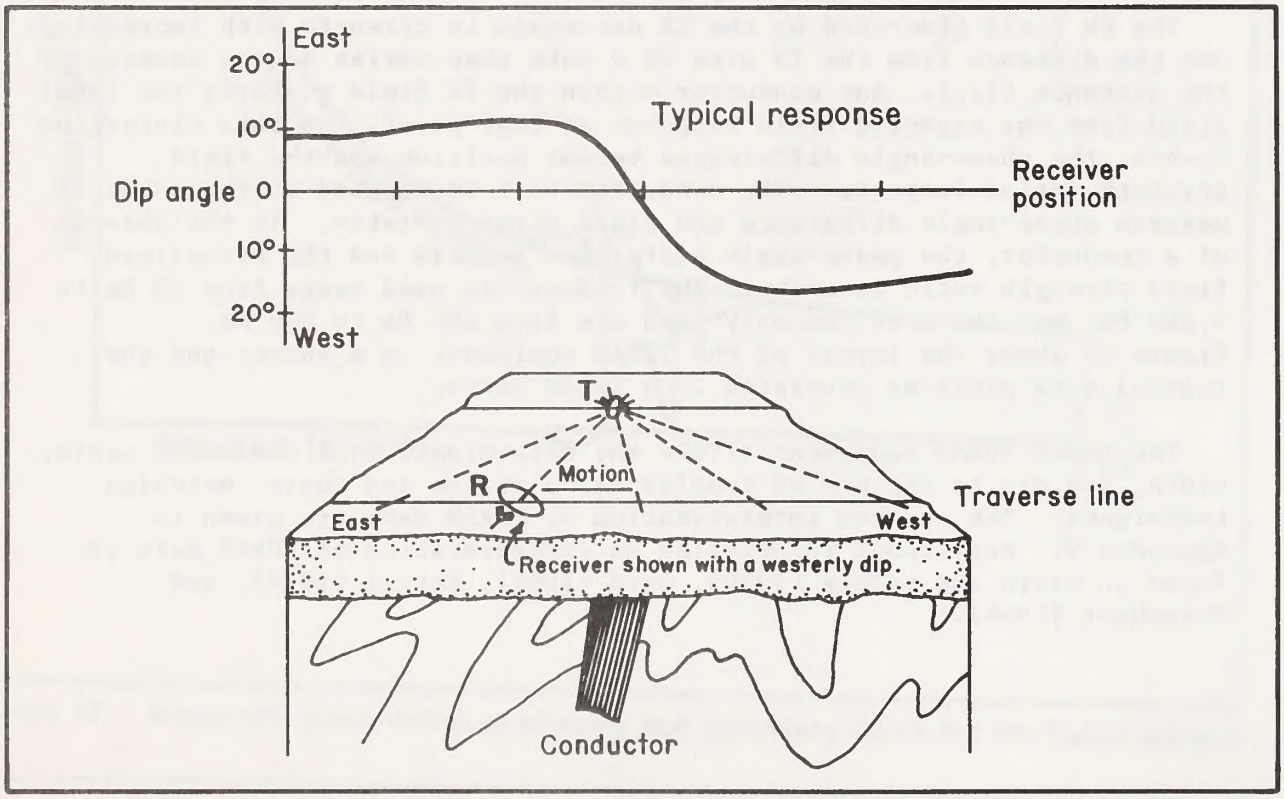

Figure 16. Field setup and results over a steeply dipping bedrock conductor using VLEM. Fixed transmitter setup.

The VLEM system is widely used for the rapid location on the ground of AEM anomalies and as a reconnaissance method to quickly locate any conductors suspected to be present on a mineral property. The major drawback is that only dip-angle data can be collected and therefore the conductivity-thickness product and the conductor's dip and depth cannot be easily determined. Most companies use the VLEM method to quickly locate an AEM conductor on the ground. They then bring in a HLEM or TURAM system to evaluate the conductor as a drill target. The use and interpretation of VLEM data are explained in Appendix IV.

B. The TURAM System

The TURAM system was developed in Sweden in the 1930's and was introduced to North America in the early 1960's. The TX consists of a large, rectangular, grounded loop, with dimensions on the order of 2,000 by 4,000 feet, and its long axis parallel to the strike of the conductor or of the rock units in the area. The TX is energized at a specific frequency and is powered by a generator driven by a gasoline engine.

The survey lines are laid out at right angles to the long axis of the TX. Three or four people are required to operate the system. Depth penetration of as much as 900 feet has been confirmed by drilling results.

The RX consists of two horizontal coplanar coils, maximum coupled, and connected by a shielded reference cable 100 or 200 feet long. The coils measure the difference in the inphase angle of the secondary field and the difference between the signal amplitudes (the field strength ratio) of the secondary field at each survey station.

The EM field generated by the TX decreases in strength with increasing use the distance from the TX wire at a rate that varies as the inverse of the distance (1/r). Any conductor within the TX field distorts the local field from the expected field response at that point. As this distortion occurs, the phase-angle differences become positive and the field strength ratios increase. The conductor will be located at the point of maximum phase-angle difference and field strength ratio. In the absence of a conductor, the phase-angle difference is zero and the normalized field strength ratio is unity. The frequencies used range from 35 Hz to 3,000 Hz, but the most commonly used are from 400 Hz to 800 Hz. Figure 17 shows the layout of the TURAM equipment on a survey and the typical data profiles generated by a TURAM survey.

The newer TURAM equipment allows the determination of conductor depth, width, and dip to the use of complex calculations and curve matching techniques. The use and interpretation of TURAM data are given in Appendix V. Additional information on interpretation of TURAM data is found in Klein and LaJoie (1980), Ward (1966), Seigel (1979), and Bosschart (1964).

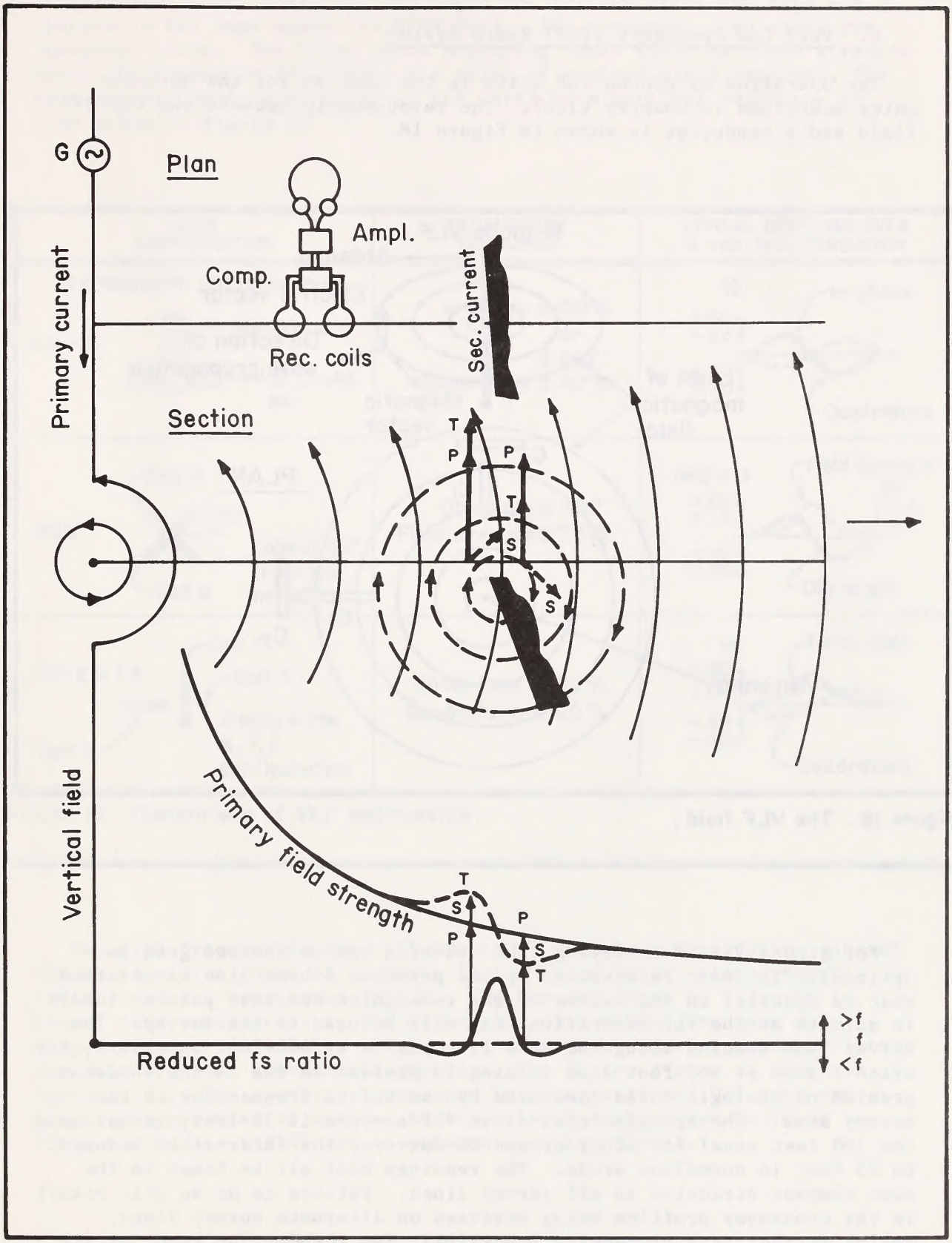

Figure 17. Schematic presentation of primary and secondary fields for the Turam method.

C. Very Low Frequency (VLF) Radio System

The operation of ground VLF units is the same as for the airborne units described in Chapter VI(B). The relationship between the VLF TX field and a conductor is shown in Figure 18.

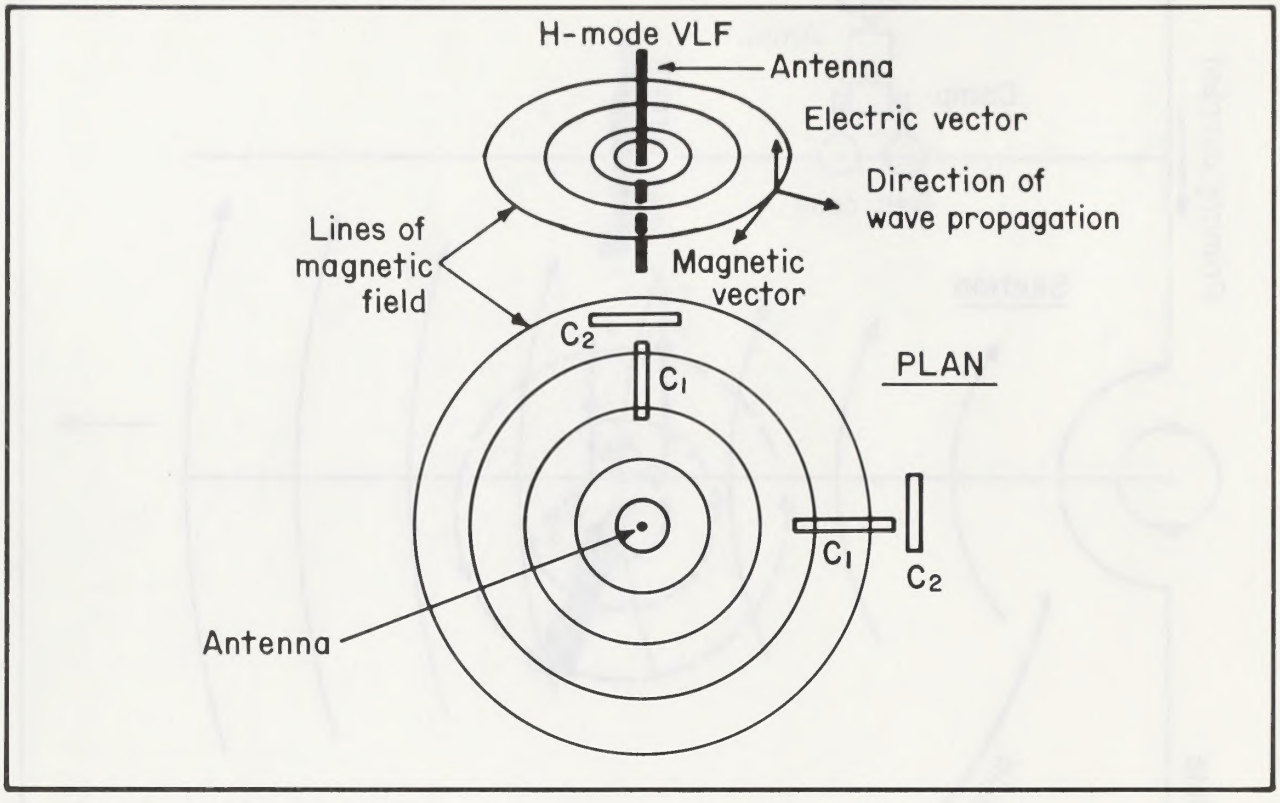

Figure 18. The VLF field.

For ground VLF EM surveying, the use of a cut or chained grid is optional. The unit is operated by one person. A base line is selected that is parallel to the strike of the rock units and that points closely in azimuth at the VLF TX station that will be used in the survey. The survey line spacing along the base line can be at 400-foot intervals, but often a 100- or 200-foot line spacing is preferable due to the inherent problem of geologic noise generated by the VLF TX frequencies in the survey area. The station interval in VLF surveys is 50 feet, rather than the 100 feet usual for other ground EM surveys; the interval is reduced to 25 feet in anomalous areas. The readings must all be taken in the same compass direction on all survey lines. Failure to do so will result in the crossover profiles being reversed on alternate survey lines, making further data processing impossible. The three major types of VLF receivers available are shown in Figure 19.

For those units measuring dip angle and inphase data, the data are plotted in the same manner as VLEM data. The conductor lies under the crossover point. For those units measuring total field or field strength data, the conductor lies under the point of maximum field strength. The response of these three types of VLF units to a vertical conductor is also given in Figure 19.

COILS CONFIGURATION	PARAMETERS MEASURED	TYPICAL RESPONSE OVER A VERTICAL CONDUCTOR
INSTRUMENTS (EM-16 HANDLE) EM-16 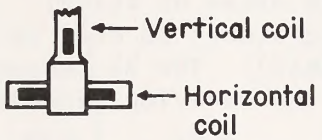	In-phase ±150% or ±56° Quadrature ±40%	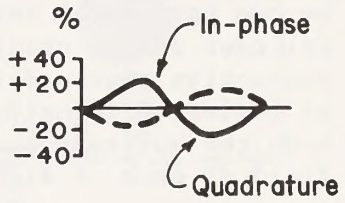
KEM 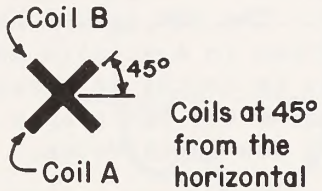	Dip angle ±30° Field strength ±7.5 db	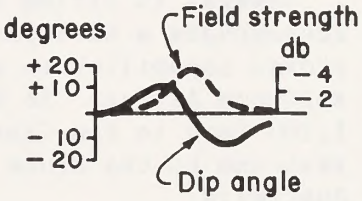
TOTEM I A 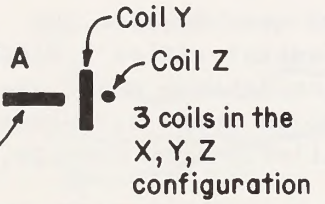	Total field ±100% Quadrature ±100%	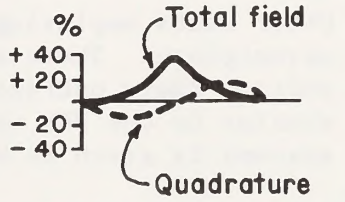

Figure 19. Comparison of VLF instruments.

The high frequencies used (10 kHz to 25 kHz) in VLF surveying subject the RX to a wide range of geologic "noise" from soils, clays, water tables, and the topography itself. The raw data must be filtered to remove this noise prior to the evaluation of a conducting zone or target. Fraser (1969) has developed a four point, moving-average filter for VLF data that solves this problem. The filter system is given in Appendix VI. The operation, use, and interpretation of VLF data are given in Appendices VI and X. Additional information can be found in Klein and LaJoie (1980) and in Hohmann and Ward (1981).

XV. Systems That Measure the Decay of Transient Fields

The Geological Survey of Canada and Crone Geophysics Ltd. have jointly developed the Pulse Electromagnetic (PEM) System. This ground transient-decay system operates in the same manner as the INPUT AEM system described in Chapter VII.

The TX is a large, grounded, rectangular loop. The loop size is commonly 100 to 300 meters on the long edge. The TX is energized either by a battery or by a generator powered by a gasoline engine. The TX can produce in excess of 2,000 watts for deep ground penetration. The RX can be two horizontal coils, rigged as in the TURAM system, or a single RX cylinder can be utilized. The coils are used in areas of thick, conductive overburden (usually laterites); the cylinder is used in areas of resistive formations (as in the Canadian Shield). The RX measures both the horizontal and vertical components of the decaying secondary field at each of eight time channels.

Several TX cycles are available and the RX gates are adjustable to accommodate a wide range of geologic conditions. The PEM system has proven capability to penetrate very thick laterites in Australia and southern Africa. It has successfully penetrated to depths in excess of 1,200 feet in the Canadian Shield. Figure 20 shows the PEM system response to the Elura massive sulfide deposit in New South Wales, Australia.

Other units employing the transient decay method have entered the marketplace. These are the Geonics, UTEM and Geoexploration's SIROTEM units. Their operational procedures and data acquisition modes are similar to the PEM unit. Additional information on these transient decay systems is given in Ward (1979) and is also available from Geonics, Ltd.

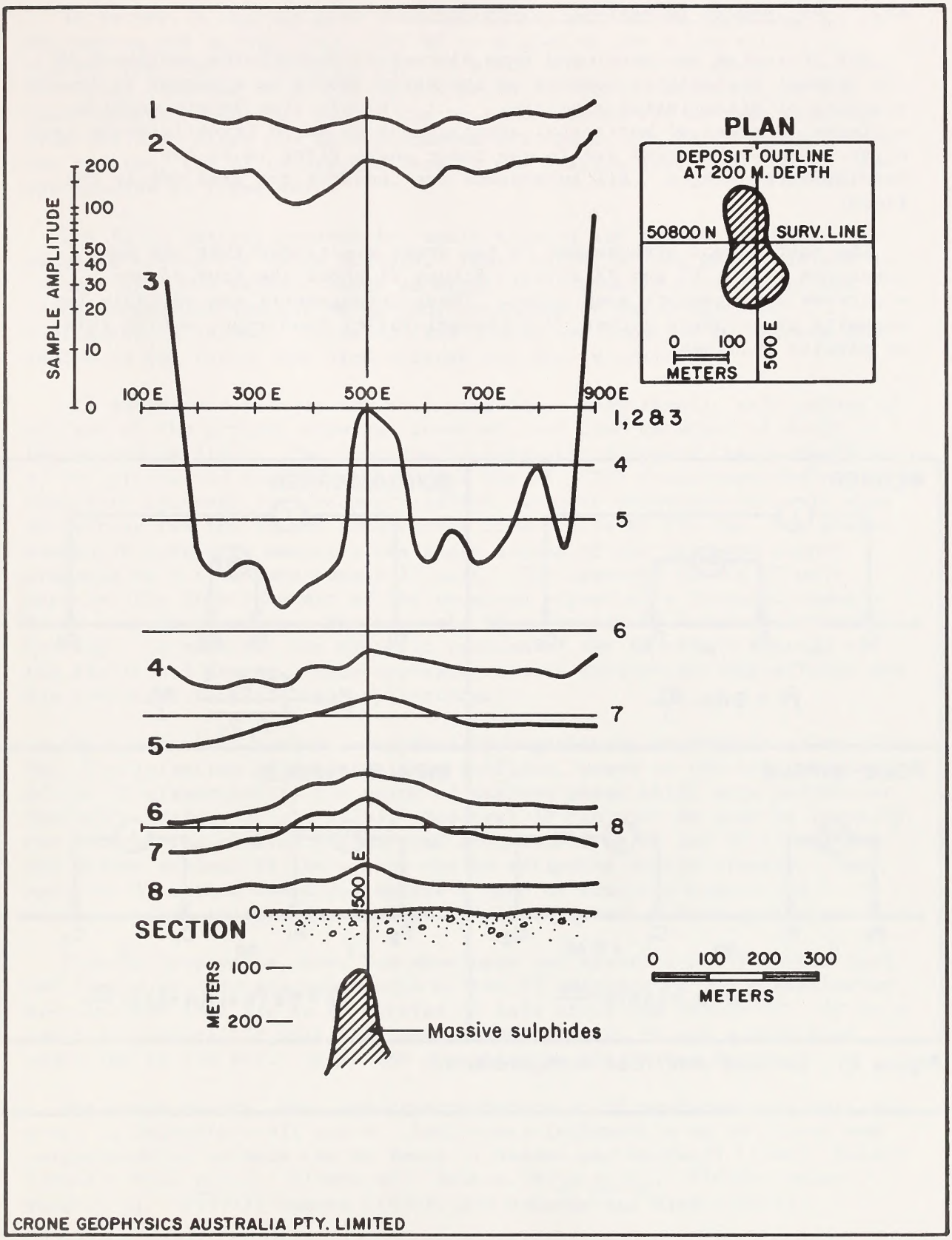

Figure 20. Elura Deposit N.S.W. Australia, Crone Pulse E.M.–P.E.M., Horizontal moving coil method, Coil spacing 200 meters, Tx loop 100m x 100m, Line 50,800.

XVI. The Induced Polarization (IP) System

The IP system was developed from electrical resistivity equipment by the Newmont Exploration Company in the early 1950's as a method to locate deposits of disseminated minerals. It will also locate massive sulfides in areas of horizontal stratigraphy or where thick laterite caps exist. Four subsystems are in use today and a fifth is in the developmental stages. All subsystems are operated the same way in the field.

The most common arrangement is two steel electrodes that are each connected to the TX and RX units. Figure 21 shows the four common electrode arrangements used today. These arrangements are suitable for deposits of porphyry copper, Mississippi Valley lead-zinc, Carlin gold, or massive sulfides.

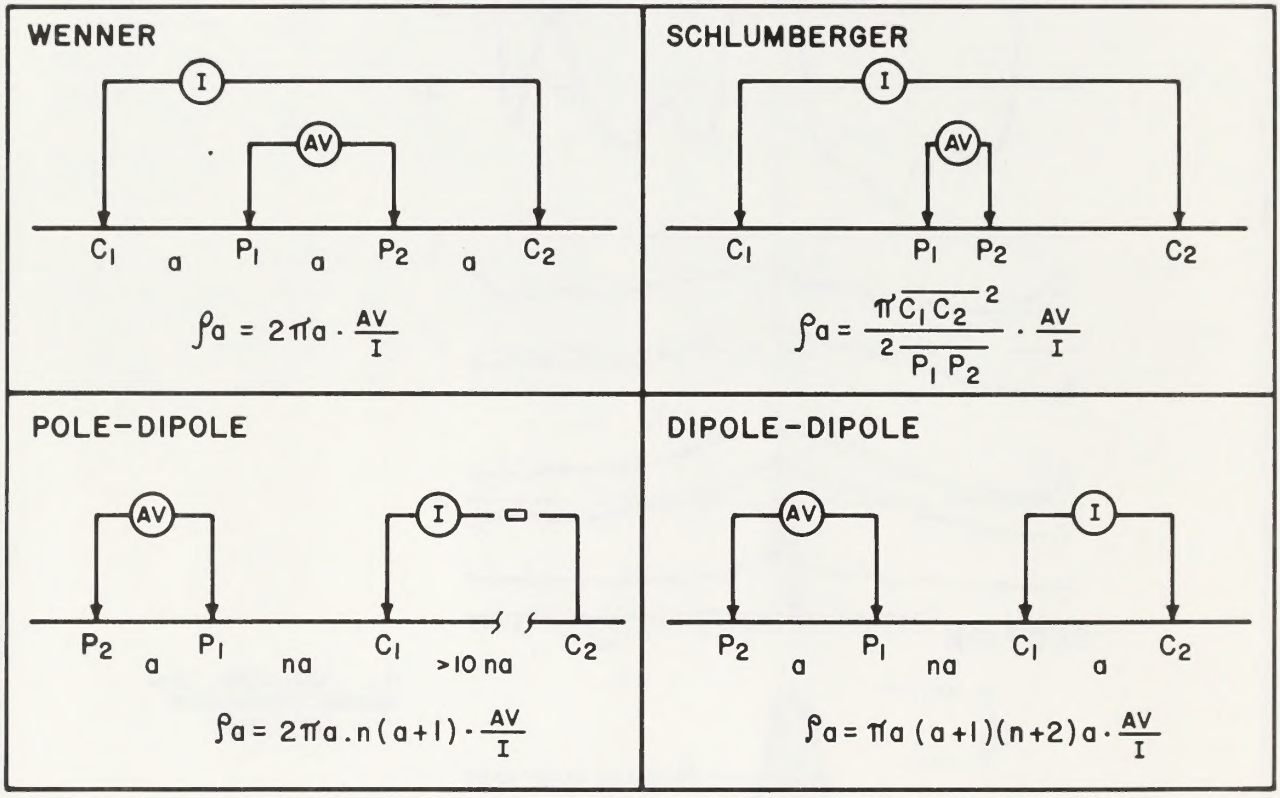

Figure 21. Common electrode configurations.

To survey, a chained grid is established, and the TX is set up at one station on the survey line. The RX is placed at the first recording station and read. The TX is left in place and the RX is moved along the line away from the TX to the next station and read. Depending on the power output of the TX, the RX can be moved out as far as five stations from the TX. After the RX has reached its limit, the TX is moved forward one station, the RX is brought back to one station away from the TX, and the process is repeated.

The TX is battery powered for small surveys and is powered by a gasoline engine for large surveys. Power output of the generator can be as much as 3,000 watts. Depth penetration is usually one-half of the TX-RX separation and can be varied, depending on the electrode configuration chosen. Three to five people are required to operate the system in the field, and line mileage per day is limited.

All subsystems recover the following data: resistivity, self potential voltage of the ground, amperage received, and time constant of decay of the secondary field. The time-domain subsystem recovers the chargeability of the ground and uses DC voltage for the TX. The frequency-domain subsystem recovers the frequency effect (percent polarization). It uses AC voltage for the TX and frequencies from 0.1 Hz to 130 Hz. The phase-domain IP subsystem measures the phase angles of the received signal produced by a frequency-domain TX unit. The spectral domain IP unit measures the time constant of the received signal of a frequency-domain TX at many frequencies. The magnetic IP subsystem is under operational testing. It measures the magnetic portion of the IP effect instead of the electrical fields. This approach reduces ground-coupling effects and has potential for airborne applications.

The spectral IP method is especially significant in that it allows for the discrimination of graphite from sulfides, based on the time constant of the IP dispersion at the point of maximum phase shift at a particular frequency (Pelton et al; 1978). Spectral IP can also be used to identify the size of the mineral grains that are responding to the IP effect and the volume percent of the grains can be estimated fairly closely. The spectral IP method can also isolate a zone of fracture-controlled mineralization lying within a mass of disseminated sulfide minerals.

Phoenix Geophysics, Ltd. has developed and marketed an IP method that can locate oil and gas reservoirs by the IP response of the disseminated hydrocarbons that lie in an alteration halo above the reservoir. It is a modified spectral IP unit that uses a 100-kilowatt TX and a wide band width (DC to 128 Hz). It is now operating in the United States.

The basic theory, use, and interpretation of IP equipment and data are given in Appendices VII and X. Additional information on IP theory and interpretation methods can be found in Madden and Cantwell (1966); Fraser (1981b); Rose et al. (1980a,b); Pelton, Rijo et al. (1978), Pelton, Ward et al. (1978); Sumner (1979); and Hohmann and Ward (1981).

XVII. Magnetometers

Two types of ground magnetometers are in common use today, the fluxgate and the proton precession units. The fluxgate unit has been in use since the 1930's and is being phased out and replaced by the newer (since the 1960's) proton precession equipment.

The fluxgate unit measures the vertical component of the Earth's magnetic field, which limits its effectiveness to the higher magnetic latitudes (more than 30 degrees north or south magnetic declination). A vertical magnetic bar inside the unit, on a triaxial mounting, responds to the pull of the local magnetic field. This pull generates a voltage that is converted to a reading in gammas on the instrument's dial. The unit must be level at each reading and has a bull's-eye level for this purpose. It is operated by one person and cut lines or chained grids are not necessary.

The proton precession unit has separate sensor and electronics packages connected by a cable. The sensor head is filled with kerosene or other organic liquid and is surrounded by an electric coil that produces a magnetic field in the head. This field keeps the protons in the liquid spinning in the sensor's own magnetic field. When a reading is taken, the sensor field is collapsed and the protons spin (precess) in the direction of the Earth's magnetic field. The rate of spin is proportional to the strength of the Earth's magnetic field at that point. The spinning protons create an electric current that is picked up by the sensor head and is transmitted to the electronics unit (the RX). In the RX, the voltage is converted to a direct digital readout, in gammas, of the Earth's total magnetic field. The unit is operated by one person, and cut lines or chained grids are not necessary. The unit may be used at any point on the Earth's surface.

The magnetic gradient (or gradiometer) survey, which uses proton precession equipment, is increasing in use and popularity. Two readings are taken at each station, one above the other, at a constant, fixed separation. The difference, or gradient, between the two readings is plotted. This method offers two distinct advantages over a standard survey. One is that geologic contacts are more sharply defined and more accurately located on the ground. The second is that the data collected need not be corrected for the diurnal magnetic variation or magnetic storm activity. Many ground and airborne surveys now use the gradiometer method as the standard survey .

The one major disadvantage of the proton precession magnetometer is that it cannot operate in zones of steep magnetic gradients (5,000 gammas per meter), which are often found around iron formations and some ultramafic bodies. The fluxgate unit does not suffer from this limitation. The interpretation of magnetic data and survey procedures is given in Appendix VIII. Additional interpretation techniques and field-operation procedures are given in Hood et al. (1979), Breiner (1980), and Wright (1981).

XVIII. Down-hole Electromagnetic (EM) Survey Systems

Three down-hole methods are commonly used in the search for metallic sulfide deposits. One operates as an equipotential electrical method, one uses the IP method, and the third operates as a transient decay-time domain system.

A. The equipotential, or "mise-a-la-masse" method

This system has been in use for several decades. It is used to delineate a massive sulfide deposit or similar type of conductor when a drill hole or adit has penetrated the deposit. The operation is similar to carrying out an IP or resistivity survey. A current electrode is placed into the drill hole or adit so that it is in direct electrical contact with the deposit, the other current electrode is placed outside the deposit at electrical infinity. The deposit is energized by a TX generator with DC voltage, and the electrical potential (voltage) is measured over a grid that covers the search area. The sulfide body will be outlined by the concentric lines of equal voltage. The operation and interpretation of data from this method are given in Hallof (1980). Figure 22 shows a cross section of a deposit energized by the mise-a-la-masse method.

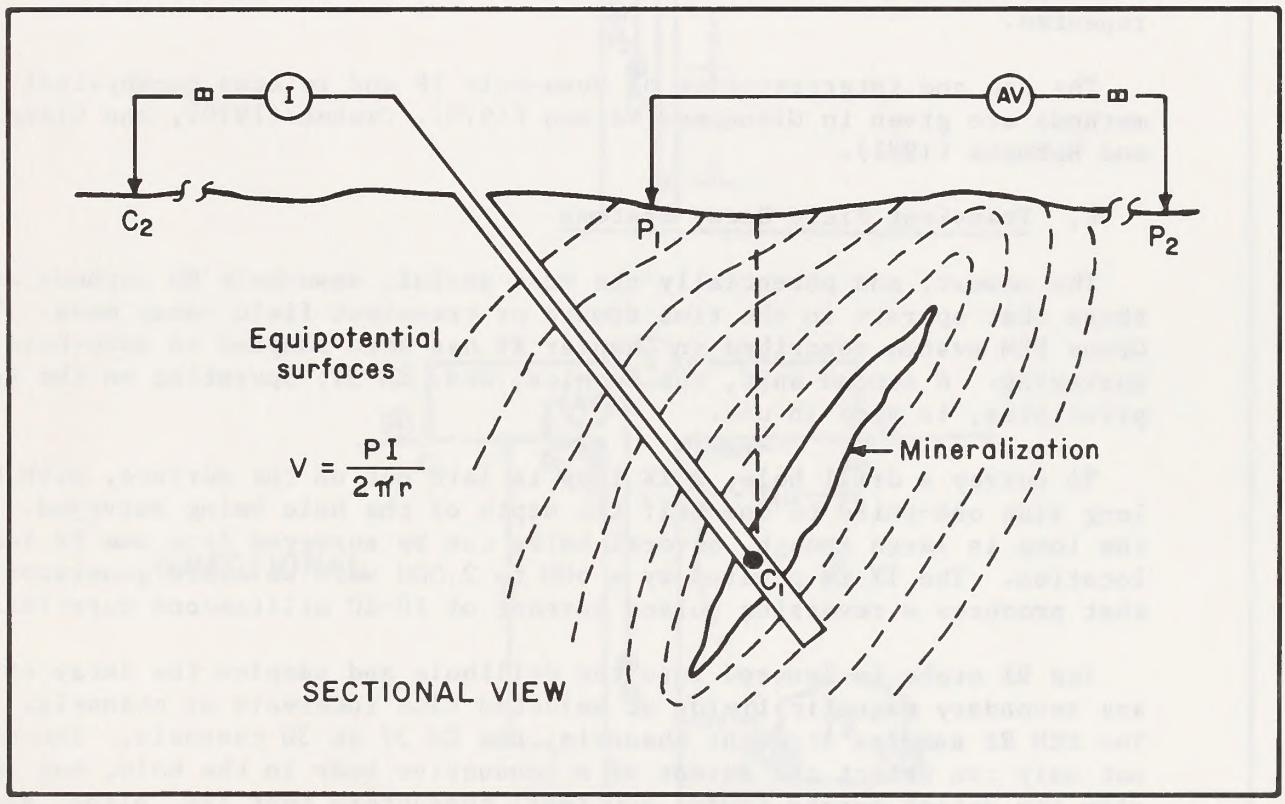

Figure 22. The Mise-à-la-masse method.

B. Induced Polarization

The IP method can be used in down-hole surveying in either the pole-pole or the dipole-dipole configurations. Figure 23 shows the down-hole setups for these two configurations. In the pole-pole configuration, the current electrodes (the TX) are placed with one electrode at electrical infinity from the drill hole, the other current electrode is placed into the hole with the potential electrode (the RX). The potential electrodes (the RX) are placed with one electrode on the surface opposite the current electrode at a distance from the drill hole equal to the TX-RX (current-potential electrode) spacing in the drill hole. The other potential electrode is held at a fixed separation (that depends on the survey requirements) from the current electrode in the hole. These two electrodes are then lowered into the hole, maintaining their fixed separation, and the readings are taken.

In the dipole-dipole configuration, the TX electrodes are set up as for the pole-pole configuration. The RX electrodes are both placed in the drill hole at a fixed separation from each other (see Figure 23). The current electrode is placed in the hole and is stopped at fixed multiple intervals of the RX electrode separation and the readings taken. After the RX has reached its response limit from the TX (usually four to five times the RX separation), the RX is lowered deeper into the hole to a depth equal to the RX electrode separation, the TX is brought back up to one unit of the RX separation from the RX, and the process is repeated.

The use and interpretation of down-hole IP and related geophysical methods are given in Glenn and Nelson (1979), Czubek (1979), and Glenn and Hohmann (1981).

C. Transient Field Decay Systems

The newest, and potentially the most useful, down-hole EM methods are those that operate in the time domain or transient-field decay mode. The Crone PEM system described in Chapter XV has been adapted to down-hole EM surveying. A second unit, the Geonics, Ltd. EM 37, operating on the same principles, is also in use.

To survey a drill hole, a TX loop is laid out on the surface, with the long side one-third to one-half the depth of the hole being surveyed. If the loop is large enough, several holes can be surveyed from one TX loop location. The TX is powered by a 500 to 2,000 watt waveform generator that produces a reversing pulsed current of 10-20 millisecond duration.

The RX probe is lowered into the drillhole and samples the decay of any secondary magnetic fields at selected time intervals or channels. The PEM RX samples at eight channels, the EM 37 at 30 channels. The RX not only can detect the extent of a conductive body in the hole, but it also can detect nearby (500-1,500 feet) conductors that are "blind" and not cut by the drill hole. This detection is accomplished by moving the TX loop around the drill hole and observing the current-flow directions at the RX in the hole.

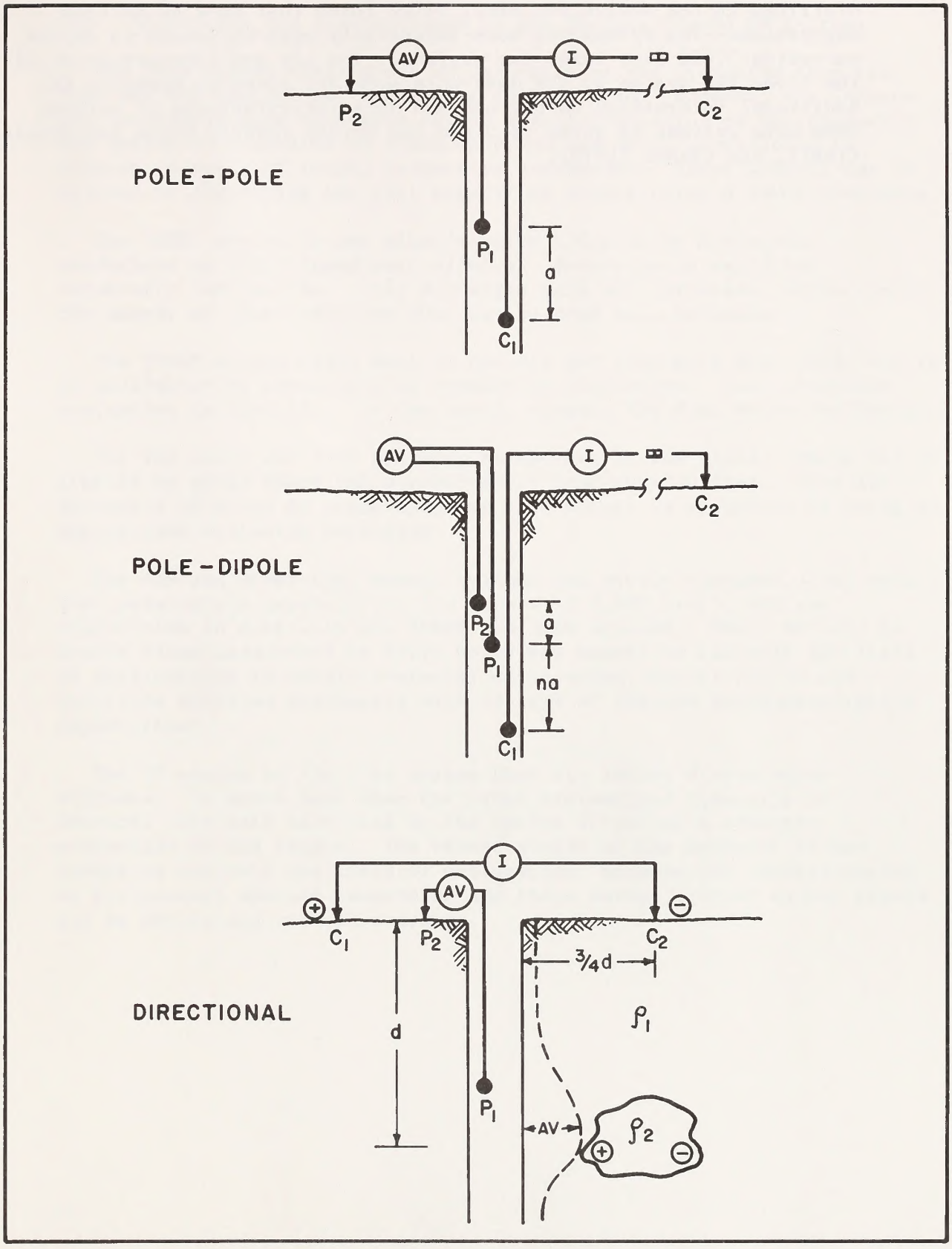

Figure 23. Down-hole logging arrays.

The transient decay system is becoming a popular tool in old mining districts in the search for deep, blind lodes that have no surface expression. The system has been sucessfully used in Canada to depths exceeding 3,000 feet below the surface. The use and interpretation of the Crone PEM system in the down-hole mode are given in Appendix IX. Additional information on the use and data interpretation of various down-hole systems is given in Glenn and Nelson (1979), Glenn and Hohmann (1981), and Czubek (1979).

XIX. Advantages and Disadvantages of the Various Ground EM Systems

The HLEM system costs about 20 percent more per line-mile than the VLEM and VLF systems and requires a chained grid. However, the inphase and quadrature data recovered permit a full evaluation of the conductor. The system is sensitive to topography, and its depth penetration is reduced in areas of thick, conductive overburden. These effects can be reduced by increasing the coil separation and/or using a lower frequency.

The VLEM system is not significantly affected by horizontal conductors or local topograhic effects. Surveying is rapid and relatively inexpensive. Only dip-angle data are collected, which limits the amount of interpretation that can be done on a conductor.

The TURAM system costs more to operate per line-mile than HLEM, but it is unaffected by topography or conductive overburden. Full conductor evaluation is possible. It can locate targets 900 feet below the surface.

The VLF units are fast and easy to operate in the field. Their use is limited to areas where the overburden is less than 50 feet. They are seriously affected by topography but this effect is minimized by using an appropriate filtering technique.

The PEM and other time domain systems are easily operated, they have deep penetration capabilities (in excess of 3,000 feet), and are competitive in cost with the TURAM and HLEM systems. Their ability to locate blind conductors in drill holes has opened an entirely new field of applications in metallic-mineral exploration, especially in old districts explored previously with systems of limited depth-penetration capabilities.

The IP system is the only system that can locate disseminated sulfides. It costs more than the other systems per line-mile to operate. The data collected by the system allow for a complete evaluation of the target. The recent advent of the spectral IP has opened an entirely new field of exploration, because the identification of the mineral species responding and their volume percent in the ground can be determined with this system.

XX. List of Trademarks and Manufacturers Used in this Reference

A. Registered Trade Marks

1. The following are registered trademarks of Barringer Research, Ltd:

   a. E-Phase (operated by Questor Surveys, Ltd.)

   b. INPUT (operated by Questor Surveys, Ltd. and Geoterrex, Ltd.)

2. The following is the registered trademark of DIGHEM, Ltd.:

   a. DIGHEM (operated by DIGHEM, Ltd.)

3. The following are registered trademarks of Scintrex, Ltd.:

   a. TRIDEM (operated by Kenting Earth Sciences, Ltd.)

   b. TURAIR (various contractors)

   c. HEM 701 (various contractors)

4. The following is the registered trademark of Phoenix Geophysics, Ltd.:

   a. QUADREM (operated by Phoenix Geophysics, Ltd.)

B. Addresses of Manufacturers and Contractors Cited in this Reference:

Barringer Research, Ltd.
304 Carlingview Drive
Rexdale, Ontario
Canada

Barringer Research, Ltd.
5161 Ward Road
Wheatridge, Colorado
80033

Crone Geophysics, Ltd.
3607 Wolfedale Road
Mississauga, Ontario
Canada L5C 1V8

DIGHEM, Ltd.
Suite 7010
1 First Canadian Place
Toronto, Ontario
Canada M5X 1C7

Geonics, Ltd.
1745 Meyerside Drive
Unit 8
Mississauga, Ontario
Canada L5T 1C5

Geoterrex, Ltd.
2060 Walkley Road
Ottawa, Ontario
Canada K1G 3P5

Geoterrex, Ltd.
12860 West Cedar Drive
Suite 101
Lakewood, Colorado
80228

INCO Metals, Ltd.
Geophysics Division
Copper Cliff, Ontario
Canada POM 1NO

Kenting Earth Sciences, Ltd.
380 Hunt Club Road
Ottawa, Ontario
Canada

Phoenix Geophysics, Ltd.
200 Yorkland Blvd.
Willowdale, Ontario
Canada M2J 1R5

Phoenix Geophysics, Ltd.
4891 Independence Street
Suite 270
Wheatridge, Colorado
80033

Questor Surveys, Ltd.
6380 Viscount Road
Mississauga, Ontario
Canada L4K 1B5

Scintrex, Ltd.
222 Snidercroft
Concord, Ontario
Canada L4K 1B5

Scintrex, Inc.
1973 West North Templ
Salt Lake City, Utah
84116

XXI. Selected References

Beck, A.E.: (1981): Physical Principles of Exploration Methods; Halsted Press, New York, 234 p.

Becker, A.: (1969): Simulation of Time-Domain Airborne Electromagnetic Systems Responses, Geophysics, Vol. 34, p. 739-752.

Bosschart, R.A.: (1964): Analytical Interpretation of Fixed Source Electromagnetic Prospecting Data; Unpublished Ph.D. Thesis, University of Delft, Holland.

Bosschart, R.A., and Pemberton, R.: (1969): Applications and Limitations of Airborne Electromagnetic Systems in Mineral Exploration; Mining in Canada, May, p. 19-27.

Bosschart, R.A., and Seigel, H.O.: (1974): The TRIDEM Three Frequency Airborne Electromagnetic System; Canadian Mining Journal, April, p. 68-69.

Breiner, S.: (1973): Applications Manual for Portable Magnetometers; Geometrics, Sunnyvale, California, 94086, 58 p.

_____: (1980): Applications for Portable Magnetometers; in Practical Geophysics for the Exploration Geologist, R. Van Blaricom (compiler), Northwest Mining Association, Spokane, Washington, 99201, p. 206-237.

Czubek, J.A.: (1979): Modern Trends in Mining Geophysics and Nuclear Borehole Logging Methods for Mineral Exploration; in Geophysics and Geochemistry in the Search for Metallic Ores, P. J. Hood (editor), Geological Survey of Canada Economic Geology Report 31, Ottawa, Canada, p. 231-272.

Dobrin, M.B.: (1976): Introduction to Geophysical Prospecting; 3rd edition, McGraw-Hill, New York, p. 630.

Duckworth, K.: (1973): An Alternative Approach to TURAM Data Treatment; Canadian Institute of Mining and Metallurgy Bulletin, October, p. 117-124.

Fraser, D.C.: (1969): Contouring of VLF-EM Data; Geophysics, Vol. 34, p. 958-967.

_____: (1972): A New Multicoil Aerial Electromagnetic Prospecting System; Geophysics, Vol. 37, p. 518-537.

_____: (1974): Survey Experience with the DIGHEM AEM System, Canadian Institute of Mining and Metallurgy Bulletin, April, p. 97-103.

_____: (1978): Resistivity Mapping with an Airborne Multicoil-Electromagnetic System; Geophysics, Vol. 43, p. 144-172.

_____: (1979): The Multicoil II Airborne Electromagnetic System; Geophysics, Vol 44, p. 1367-1394.

_____: (1981a): A Review of Some Useful Algorithms in Geophysics; Canadian Mining and Metallurgical Bulletin, April, 1981, p. 76-83.

_____: (1981b): Contour Map Presentation of Dipole-Dipole Induced Polarization Data; Geophysical Prospecting, Vol. 29, p. 639-651.

Glenn, W.E., and Hohmann, G.W.: (1981): Well Logging and Borehole Geophysics in Mineral Exploration; in 75th Anniversary Volume, B. J. Skinner (editor), Economic Geology Publishing Company, New Haven, Connecticut, p. 850-862

Glenn, W.E., and Nelson, P.H.: (1979): Borehole Logging Techniques Applied to Base Metal Ore Deposits; in Geophysics and Geochemistry in the Search for Metallic Ores; P. J. Hood (editor), Geological Survey of Canada Economic Geology Report 31, Ottawa, Canada, p. 273-294.

Grant, F.S., and West, G.F.:(1966): Interpretation Theory in Applied Geophysics; McGraw-Hill, New York, 583 p.

Hallof, P.G.: (1972): The Induced Polarization Method; paper presented at the 24th International Geological Congress, Montreal, Canada, 44 p.

Hallof, P.G.: (1980): IP and Resistivity: Grounded Electrical Methods in Geophysical Exploration, in Practical Geophysics for the Exploration Geologists, R. Van Blaricom (compiler), Northwest Mining Association, Spokane, Washington, 99201, p. 39-151.

Hallof, P.G., Cartwright, P.A., and Pelton, W.H.: (1979): Use of the Phoenix IVP-2 Receiver for Discrimination Between Sulphides and Graphite; paper presented to the Society of Exploration Geophysicists, New Orleans, Louisiana, 20 p.

Hansen, D.A.: (1980): Geological Applications for Portable Gamma-Ray Spectrometers; in Practical Geophysics for the Exploration Geologist, R. Van Blaricom (compiler), Northwest Mining Association, Spokane, Washington, 99201, p. 1-38.

Hohmann, G.W., and Ward, S.H.: (1981): Electrical Methods in Mining Geophysics; in 75th Anniversary Volume, B. J. Skinner (editor), Economic Geology Publishing Company, New Haven, Connecticut, p. 806-828.

Hood, P.J. (editor): (1979): Geophysics and Geochemistry in the Search for Metallic Ores; Geological Survey of Canada Economic Geology Report 31, Ottawa, Canada, 811 p.

Hood, P.J., Holroyd, M.T., and McGrath, P.H.: (1979): Magnetic Methods Applied to Base Metals Exploration; in Geophysics and Geochemistry in the Search for Metallic Ores, Hood, P. J. (editor), Geological Survey of Canada Economic Geology Report 31, Ottawa, Canada, p. 74-104.

Klein, J., and LaJoie, J.J.: (1980): Electromagnetic Prospecting for Minerals; in Practical Geophysics for the Exploration Geologist, R. Van Blaricom (compiler), Northwest Mining Association, Spokane, Washington, 99201, p. 239-299.

Lazenby, P.G.: (1973): New Developments in the INPUT Airborne EM System; Canadian Institute of Mining and Metallurgical Bulletin, April, p. 1-9.

Madden, T.R., and Cantwell, T.: (1966): Induced Polarization, A Review; in Mining Geophysics, Vol. II, Society of Exploration Geophysicists, Tulsa, Oklahoma, p. 373-400.

Nair, M.R., Biswas, S.K., and Mazumdar, K.: (1968): Experimental Studies on the Electromagnetic Response of Tilted Conducting Half-Planes to a Horizontal-Loop Prospecting System; Geoexploration, Vol. 6, p. 207-244.

Van Blaricom, R. (1980). Address of Publication is Northwest Mining Association (NWMA), 633 Peyton Building, Spokane, WA 999201.

Palacky, G.J.: (1975): Interpretation of INPUT AEM Measurements in Areas of Conductive Overburden; Geophysics, Vol. 40, p. 490-502.

Palacky, G.J., and West, G.F.: (1973): Quantitative Interpretation of INPUT AEM measurements, Geophysics, Vol. 38, p. 1145-1158.

Parasnis, D.S.: (1966): Mining Geophysics; Elsevier Publishing Company, New York, 325 p.

_____: (1979): Principles of Applied Geophysics; Chapman and Hall, London 275 p.

Paterson, N.H.: (1961): Experimental and Field Data for the Dual-Frequency Phase-Shift Method of Airborne Electromagnetic Prospecting; Geophysics, Vol. 26, p. 601-617.

Pelton, W.H., Rijo, L., and Swift, C.M. Jr: (1978): Inversion of Two-Dimensional Resistivity and Induced Polarization Data; Geophysics, Vol. 43, p. 788-803.

Pelton, W.H., Ward, S.H., Hallof, P.G., Sill, W.B., and Nelson, P.H.: (1978): Mineral Discrimination and Removal of Inductive Coupling With Multifrequency IP; Geophysics, Vol. 43, p. 588-609.

Pitcher, D.L., Barlow, R.G., and Lewis, N.: (1980): TRIDEM Airborne Conductivity Mapping as a Lignite Exploration Method; Canadian Institute of Mining and Metallurgical Bulletin, May, p. 53-63.

Reedman, J.H.: (1979): Techniques in Mineral Exploration; Applied Science Publications Ltd., London, 533 p.

Howland-Rose, A.W., Linford, G., Pitcher, D.H., and Seigel, H.O.: (1980a): Some Recent Magnetic Induced-Polarization Developments--Part I: Theory; Geophysics, Vol. 45, p. 37-54.

_____: (1980b): Some Recent Magnetic Induced-Polarization Developments-Part II: Survey Results; Geophysics, Vol 45, p. 55-74.

Seiberl, W.A.: (1975): The F-400 Series Quadrature Component Airborne Electromagnetic System; Geoexploration, Vol. 13, p. 99-115.

Seigel, H.O.: (1979): An Overview of Mining Geophysics; in Geophysics and Geochemistry in the Search for Metallic Ores, P. J. Hood (editor), Geological Survey of Canada Economic Geology Report 31, Ottawa, Canada, p. 7-24.

Skinner, B.J. (Editor): (1981): 75th Anniversary Volume; Society of Geologists, New Haven, Connecticut, 06520, 964 p.

Society of Exploration Geophysicists; (1966): Mining Geophysics, 2 Vols., Tulsa, Oklahoma.

Strangway, D.W.: (1966): Electromagnetic Parameters of Some Sulfide Ore Bodies; in Mining Geophysics, Vol. I, Society of Exploration Geophysicists, Tulsa, Oklahoma, p. 227-242.

Sumner, J.S.: (1976): Principles of Induced Polarization for Geophysical Exploration; Cambridge University Press, London, 860 p.

_____: (1979): The Induced Polarization Exploration Method; in Geophysics and Geochemistry in the Search for Metallic Ores, P. J. Hood (editor), Geological Survey of Canada Economic Geology Report 31, Ottawa, Canada, p. 123-134.

Telford, W. M.; Geldart, L. B.; Sheriff, R. E.; and Keys, D. A.: (1976): Applied Geophysics, Cambridge University Press, Cambridge, 860 p.

Van Blaricom, R. (editor): (1980): Practical Geophysics for the Exploration Geologist; Northwest Mining Association, Spokane, Washington, 99201, 303 p.

Ward, S.H.: (1966): The Electromagnetic Method; in Mining Geophysics, Society of Exploration Geophysicists, Vol. II, Tulsa, Oklahoma, p. 224-371.

_____: (1979): Ground Electromagnetic Methods and Base Metals; in Geophysics and Geochemistry in the Search for Metallic Ores, P.J. P.J. Hood (editor), Geological Survey of Canada Economic Geology Report 31, Ottawa, Canada, p. 45-62.

_____: (1981): Gamma-Ray Spectrometry in Geologic Mapping and Uranium Exploration; in 75th Anniversary Volume, Society of Economic Geologists, Economic Geology Publishing Company, New Haven, Connecticut, p. 840-849.

Whiting, T.H.: (1982): Surficial Conductivity Mapping with the INPUT Airborne EM System and its Application to Coal Exploration; unpublished report, Geoterrex PTY, Ltd., 17 p.

Woods, D.V., and Crone, J.D.: (1980): Scale-Model Study of a Borehole Pulse Electromagnetic System; Canadian Institute of Mining and Metallurgy Bulletin, May, p. 96-104.

Wright, P.M.: (1981): Gravity and Magnetic Methods in Mineral Exploration; in 75th Anniversary Volume, B. J. Skinner (editor), Economic Geology Publishing Company, New Haven, Connecticut, p. 829-839.

Glossary

Apparent Resistivity - The ground resistivity calculated from measurements and a geometric factor derived for a homogenous ground condition. Apparent resistivity is an Ohms law ratio of measured voltage V to the applied current I, with a geometric constant K which depends on the electrode array:

$Pa = KV/I$

The units of resistivity are ohm-meters

Coaxial - A TX and RX are said to be coaxial if the axis of the TX and the axis of the RX are fixed on the same line.

Conductivity - The inverse or reciprocal of resistivity, measured in MHOS.

Coplanar - A TX and RX are said to be coplanar if the TX and RX coils or loops lie in the same plane.

Inphase - The real component of a complex number (vector) that describes the real behavior of an electromagnetic wave. The inphase portion propagates in the direction of the wave motion.

MHOS - A MHOS per meter is a unit of conductivity defined as the conductivity of a one meter cube that has a resistance of one ohm between its opposite faces. The reciprocal of ohm-meter.

Quadrature - The imaginary component of a complex number (vector) that completes the description of an electromagnetic wave. The quadrature portion propagates at 90 degree out-of-phase with the transmitted signal and in the same direction as the inphase component.

Resistivity - The ability of a material to resist the flow of electric current. The ratio of electric field intensity to current density.

APPENDIX I

The INPUT System

(Lazenby, P.G.:1973): New Developments in the INPUT Airborne EM System; The Canadian Mining and Metallurgical Bulletin, April, p. 1-9. [Reprinted by permission of The Canadian Institute of Mining and Metallurgy.]

Table of Contents

New Developments in the INPUT Airborne E. M. System

P. G. LAZENBY, Managing Director,
Questor Surveys Limited,
Rexdale, Ontario

ABSTRACT

This paper describes the latest instrumentation improvements in the INPUT Airborne E.M. System, particularly the new electronic signal-processing techniques. Several anomaly examples illustrating these techniques are shown.

INTRODUCTION

THE BARRINGER INPUT® AIRBORNE E.M. SYSTEM became available to the mining exploration industry in 1964. The development of the equipment through to the Mark V stage in 1965 has been described by Bonivell (1967), and since that time anomalies detected by this system have resulted in the discovery of several orebodies in Canada, the U.S.A., South Africa and Australia. From 1965 to 1970 no further instrumentation improvements were made, and during this period four systems were commercially operational, each of which was installed in a PBY Canso aircraft. The choice of the Canso as a suitable platform was governed initially by the size and weight of the original prototype equipment.

In early 1970, Questor Surveys Limited initiated an "in-house" research and development program with two objectives in sight. The first of these was to find a modern aircraft with better performance and less maintenance problems than the ageing Cansos. The second was to improve the equipment by making use of the latest electronic techniques in signal processing.

The replacement aircraft chosen is a turbine-powered Short Skyvan that has STOL (Short Take Off and Landing) characteristics. Long-range fuel tanks are installed and booms are fitted to the nose and tail so that a large transmitting loop can be attached (Fig. 1).

As the Skyvan is considerably smaller than the Canso, the equipment improvements by necessity had to include a reduction in size and weight. However, the main objectives were to increase stability, decrease the noise level and shorten the integration period.

The purpose of this article is to describe some of the changes that have been made in the new installation and to show field examples of the different types of anomaly that can now be recognized in the data obtained from INPUT surveys.

THE SKYVAN INPUT INSTALLATION

The sensitivity of any remote-sensing device is a direct function of the signal-to-noise ratio of the system, so every effort must be made to increase the signal amplitude (the anomaly) and reduce the noise (the background level on the record).

In most towed-receiver airborne E.M. systems, there are two major sources of motion noise:

(1) vibrational noise due to buffeting of the receiving coil at the end of the tow cable;
(2) coupling noise caused by variations in the position of the receiving coil in relation to the transmitting loop.

(In the INPUT system, the second source of noise is not important because the received signal is not detected in the presence of the primary field.)

A simple method of removing vibrational noise is by integration (filtering), and the longer the time constant used the lower the background noise becomes. Unfortunately, long time constants reduce the amplitude of the signal as well as the noise, and the smoothing causes a reduction in resolution and a degradation of the anomaly character.

The Mark V INPUT receiver used an integration time constant of 3-4 seconds. Examination of the results of surveys performed by this system show that, in general, all anomalies tended to look the same. It was for this reason that the new receiver was designed to operate with a time constant of 0.6 seconds.

In order to make use of such a short integration time, vibrational noise had to be reduced. This was accomplished by re-designing the receiver and changing the cable configuration to achieve higher stability. The location of the receiving coil in relation to the transmitting loop and the ground is shown in Figure 2.

®Registered Trade Mark of Barringer Research Ltd.

P. G. LAZENBY graduated from the University of London in 1952 with a B.Sc. in geology. From 1952 to 1957, he was employed by Seismograph Service Corporation of Tulsa, Oklahoma on foreign contract work in seismic exploration for petroleum, and later in the development of acoustical borehole logging equipment. In 1960, Mr. Lazenby came to Canada and joined the Airborne Survey Division of Selco Exploration Co. Ltd. as field manager during the initial development of the prototype INPUT system. In 1967, he became managing director of Questor Surveys Ltd., a company specializing in airborne survey work, and he has lately become involved in research and development work which resulted in the Mark VI INPUT system, a patent for which has been granted. Mr. Lazenby became a member of the Association of Professional Engineers of the Province of Ontario in 1966.

PAPER SUBMITTED: in June of 1972; revised manuscript received on November 8, 1972.

KEYWORDS: Geophysical exploration, INPUT system, Electromagnetic surveys, Channel widths, Decay transients, Conductors.

FIGURE 1 — The turbine-powered Skyvan.

The residual background noise has been measured during calibration flights at high altitude. The results indicate a noise level of 50 ppm (1 mm on the record) of the peak-to-peak amplitude of the primary field at the receiver.

Changes made to the channel gate widths and positions are shown in Figure 3. Note that there is now no overlap of adjacent channels and that channel 1 is 100 microseconds closer to the end of the primary pulse than previously, whereas channel 6 is 100 microseconds farther away.

It would be out of place here to describe the many other design features, both mechanical and electronic, that were incorporated in the new installation. The improvements in both the equipment and aircraft performance have resulted in a system that is practical and effective on a year-'round basis. The following examples illustrate the high sensitivity and resolution that has been achieved.

RESULTS

1. Vertical Dyke

The thin vertical half-plane (semi-infinite thin sheet) is the most common model used in both theoretical and laboratory studies. The response of a towed receiver system over this type of conductor (width ≪ coil separation) has been well documented and is characterized by a small secondary peak which is recorded just before the transmitter passes over the target (Paterson, 1961).

Figure 4 is an excellent field example of the response due to a vertical dyke conductor (pyrrhotite) striking at 90 degrees to the flight direction. This record has also been labelled with the scales and parameters which apply to all of the examples that follow. The direction of flight is from left to right, and the anomaly position corresponds to the location of the receiver coil.

The small secondary peak which is recorded at approximately 500 feet ahead of the main peak is clearly visible. It will always appear ahead of the main peak regardless of the flight direction. The anomaly width (measured at half the maximum amplitude on channel 2) is 300 feet. This is in close agreement with the theoretical and laboratory results.

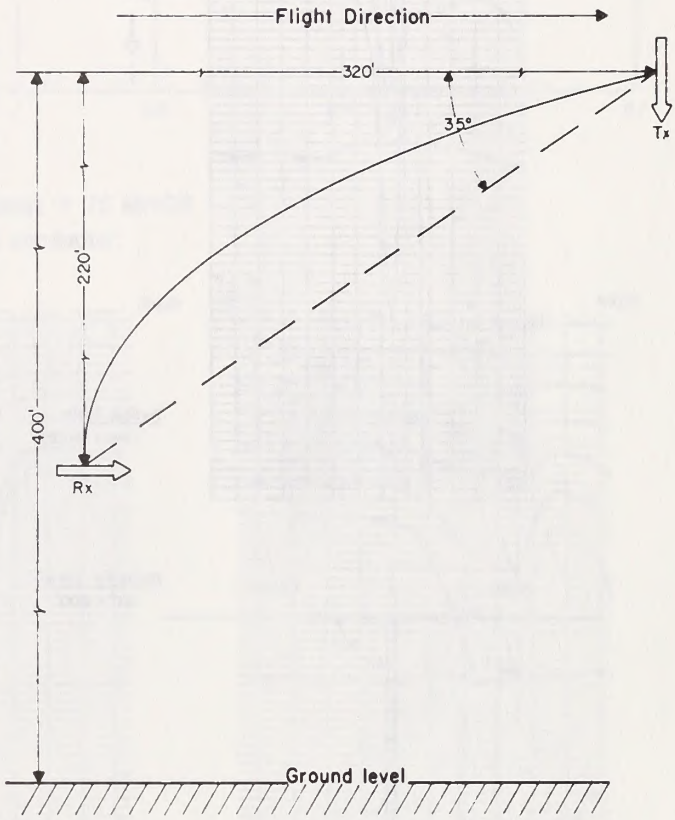

FIGURE 2 — Disposition of transmitting loop and receiving coil.

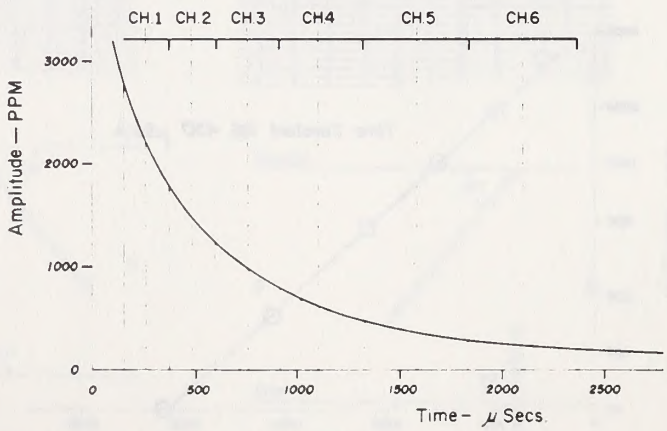

FIGURE 3 — Channel widths and positions.

Figure 5 shows the complete secondary field decay transient of this response at the position of maximum anomaly amplitude. It is plotted on semi-logarithmic paper and indicates that the decay is exponential with a time constant of about 450 microseconds. The amplitude of channel 2 is 1850 ppm. These two values agree closely with those obtained from a vertical dyke model with a thickness-conductivity product of 9.5 mhos. (Channel 2 corresponds in position to channel A of Becker, Gauvreau and Collett, 1972.) Figure 6 shows the relationship between the anomaly amplitude in channel 2 and the time constant of the exponential decay transient as functions of the conductivity-width product. These results have been derived from a combination of actual airborne and ground geophysical measurements over vertical dyke conductors (Palacky, 1972), and the amplitude scale has been adjusted to match the calibration figures of the new system. The time-constant (Tc) is obtained by measuring two amplitudes (A_1 & A_2) at two delay times (t_1 & t_2) on the decay transient and applying the following formula:

$$Tc = \frac{(t_2 - t_1)}{\log_e A_1/A_2} \text{ microseconds}$$

where $t_2 > t_1$ and $A_1 > A_2$.

At this time, no field examples of conductivity-width products in excess of 40 mhos are available, and the curves beyond this figure are theoretical projections indicated by broken lines. The majority of the anomalies used in deriving these results have apparent conductivity-width products of between 5 and 30 mhos, with corresponding time constants of 350-750 microseconds. Figure 7 is a typical example of a curve for the correction of anomaly amplitudes to a flying height of 400 ft. It is based on the fourth power fall-off equation: Ac = Ao $(H/400)^4$, where Ac = corrected amplitude, Ao = observed amplitude and H = flying height. The power value used will vary from approximately 3 to 5 as the thickness-conductivity product changes from 1 to 50 mhos (Palacky, 1972).

2. Variations with Strike

The main variations in the response due to a vertical half-plane conductor which is not at right angles to the flight line are a reduction in the anomaly amplitude and an increase in its width. A secondary variation is an increase in the distance between the secondary peak and the main peak.

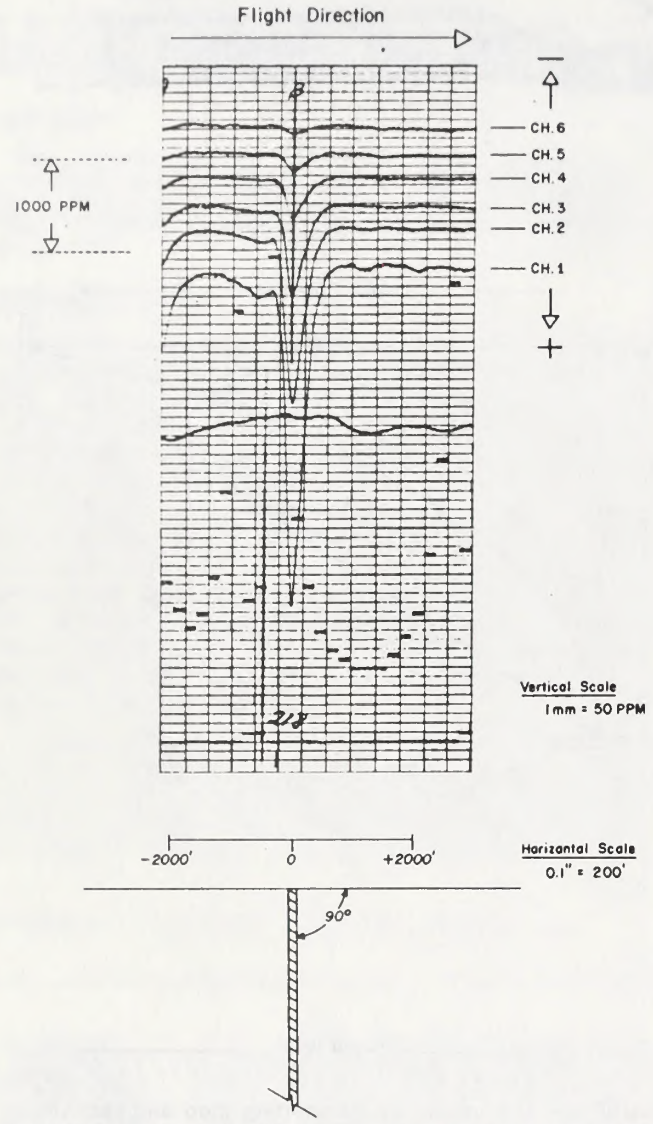

FIGURE 4 — Vertical half-plane conductor, 90-degree strike.

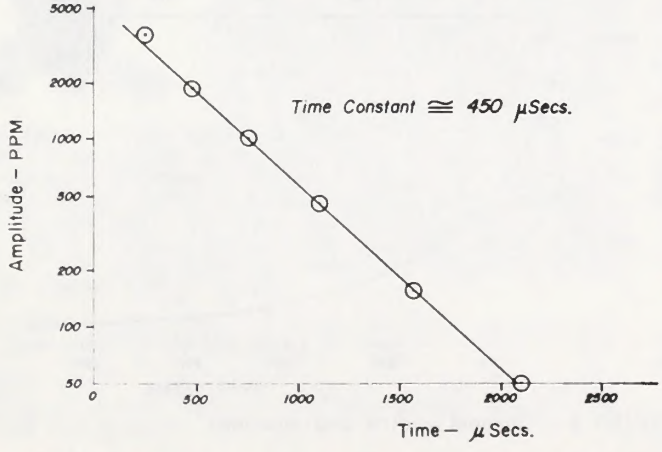

FIGURE 5 — Exponential decay transient for vertical half-plane.

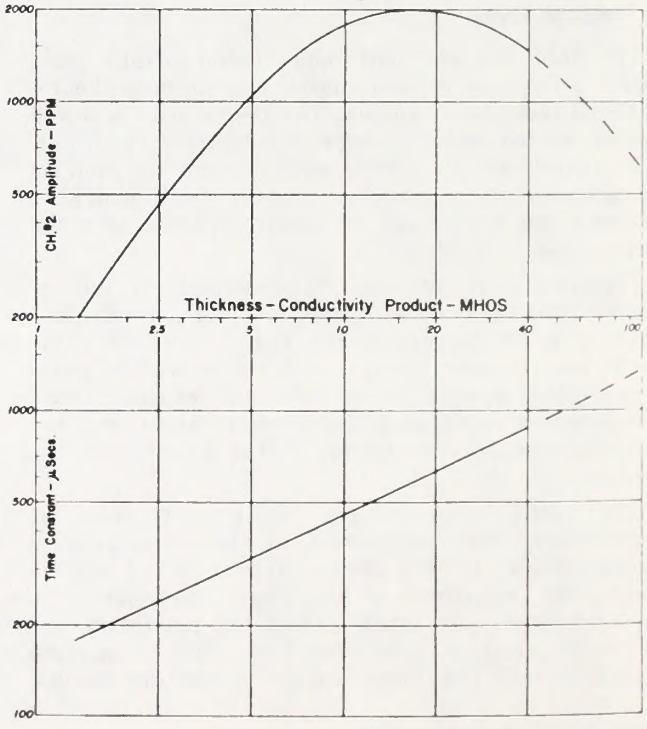

FIGURE 6 — Vertical half-plane conductor.

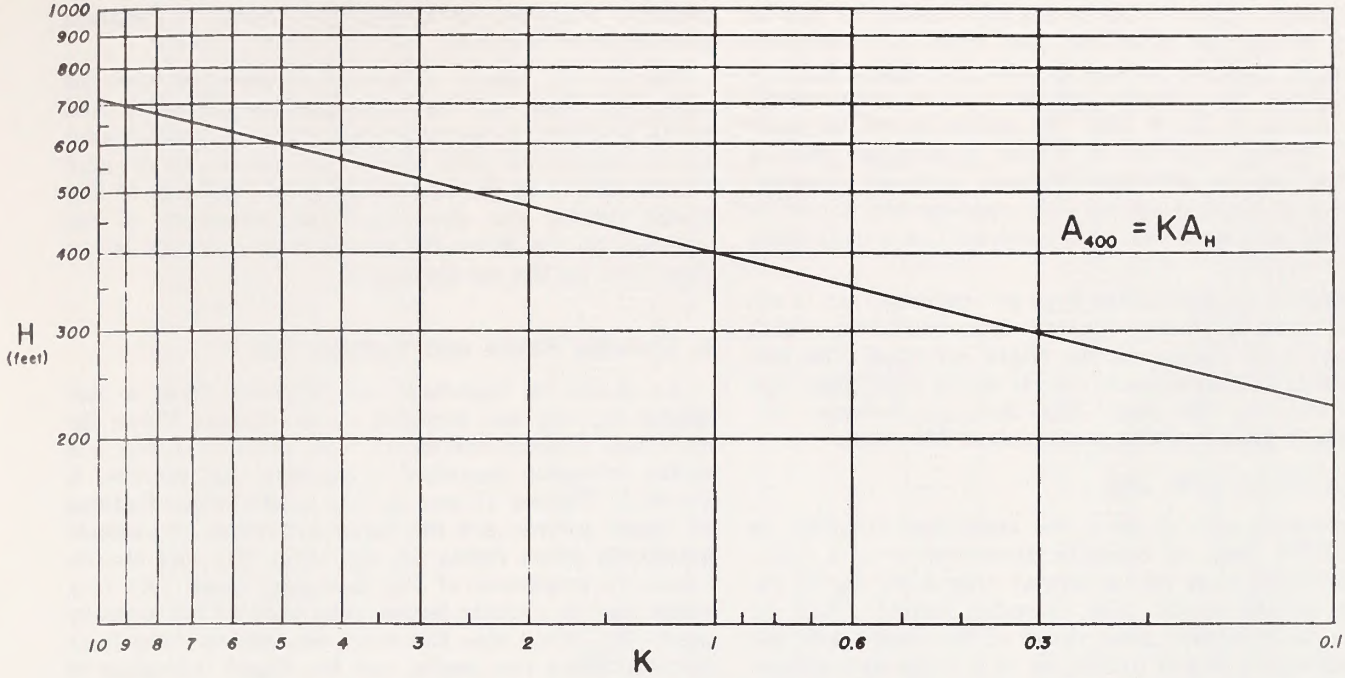

Conductivity–Thickness = 15 MHOS

FIGURE 7 — Amplitude correction curve for vertical half-plane conductor.

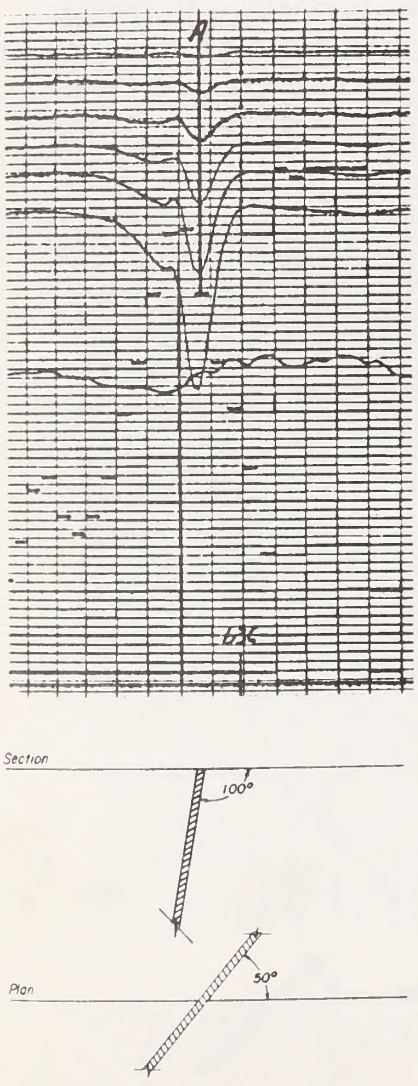

FIGURE 8—Steep dip, 50-degree strike.

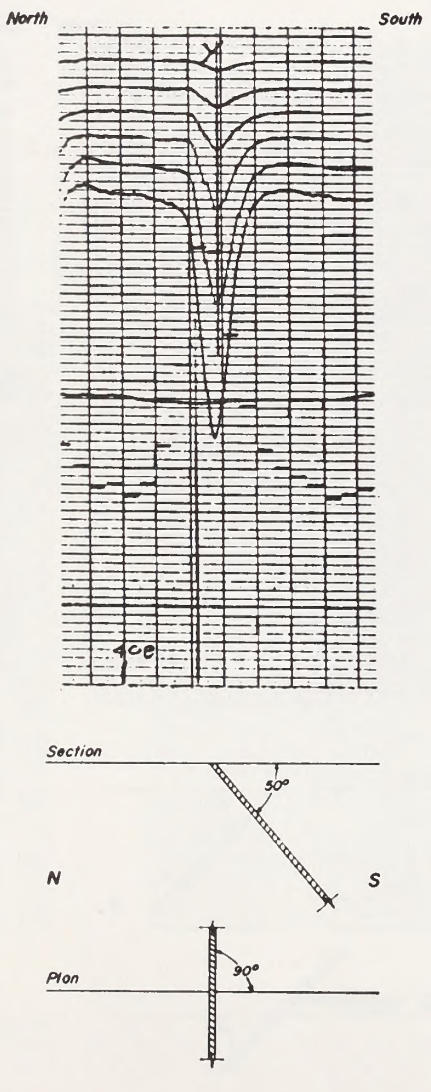

FIGURE 9 — 50-degree dip, 90-degree strike, down-dip record.

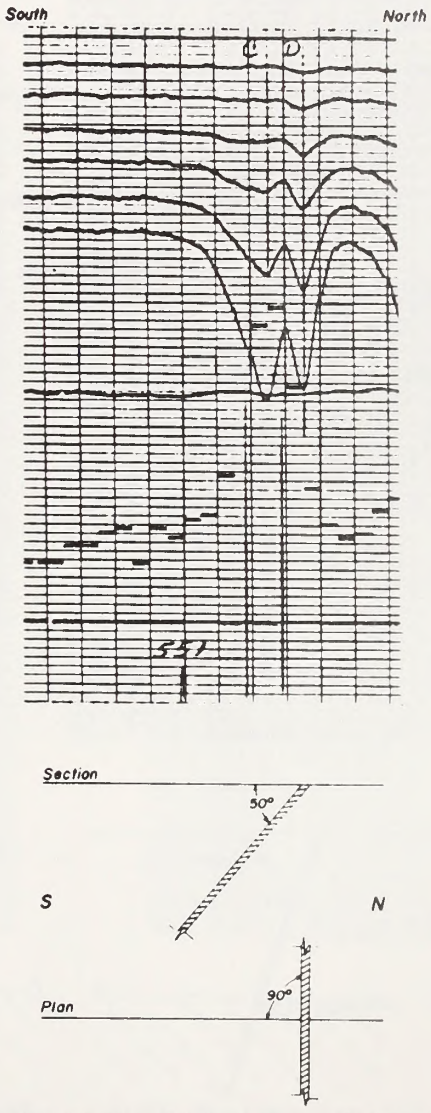

FIGURE 10 — 50-degree dip, 90-degree strike, up-dip record.

Although normally the strike of a conductor can be easily determined from the map, there are instances where an anomaly occurs on only one flight line. In these cases, and before ground work is commenced, it is useful to know that the strike is not at right angles to the direction of flight. Essentially, this is all that can be determined about such an anomaly, because at normal survey line spacing the target is probably too small to be considered as a half-plane conductor.

Figure 8 illustrates the type of response that is obtained from a steeply dipping dyke conductor which strikes at 50 degrees to the flight direction. The amplitude of the main peak (A) is about 1100 ppm, and its width is 600 feet. The distance between the secondary peak and the main peak is 800 feet.

3. Variations with Dip

Figures 9 and 10 show the anomalies obtained on two flight lines in opposite directions over a dyke-like sulphide body which dips at approximately 50 degrees to the south. The downdip record (Fig. 9) shows no secondary peak ahead of the main peak, but it does have a slight indication of a negative response just after the anomaly. A better example of this negative response can be seen in Figure 11, between anomalies FF and GG.

The up-dip record (Fig. 10) illustrates how the secondary peak (C) has increased in amplitude and width relative to the main peak (D). A measurement of the amplitude ratio of the two peaks can be used quantitatively in the estimation of the amount of dip. These results also show that the amplitude of the anomaly on the down-dip record is 60 per cent larger than that on the up-dip record.

4. Variable Strike and Variable Dip

As would be expected, the response from a conductor dipping and striking at 45 degrees shows the combined characteristics of the individual dip and strike examples described previously. An example is shown in Figures 12 and 13. The most obvious features on these records are the large reduction in anomaly amplitude when flying up-dip (Fig. 13) and the increase in amplitude of the secondary peak (A) to a value that is slightly larger than that of the primary peak (B). Note also the large separation (900 feet) between these two peaks, and the slight indication of a negative response after the down-dip anomaly (DD).

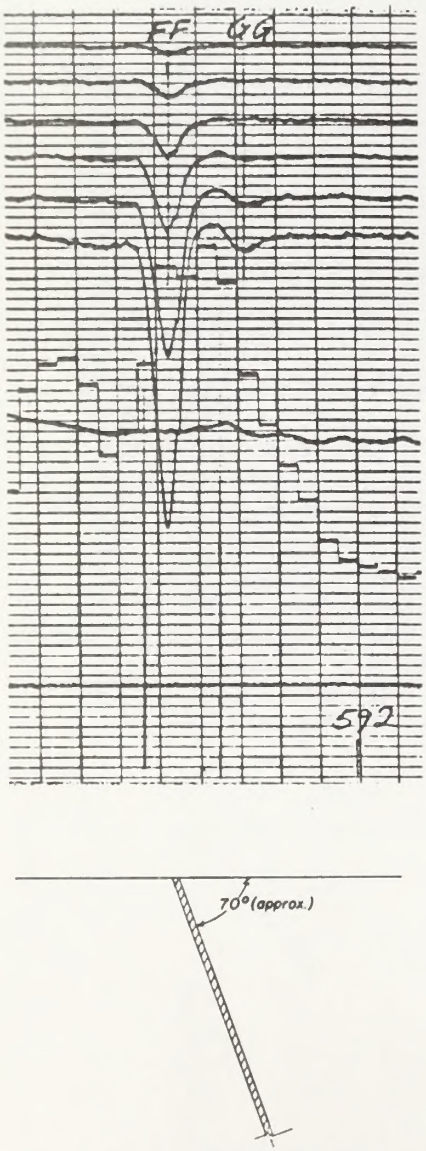

FIGURE 11 — Down-dip record.

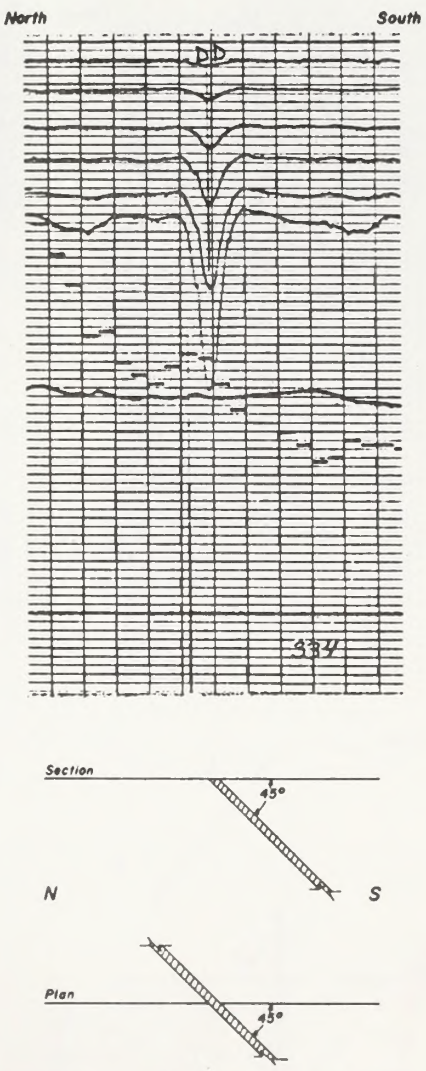

FIGURE 12 — 45-degree dip and strike, down-dip record.

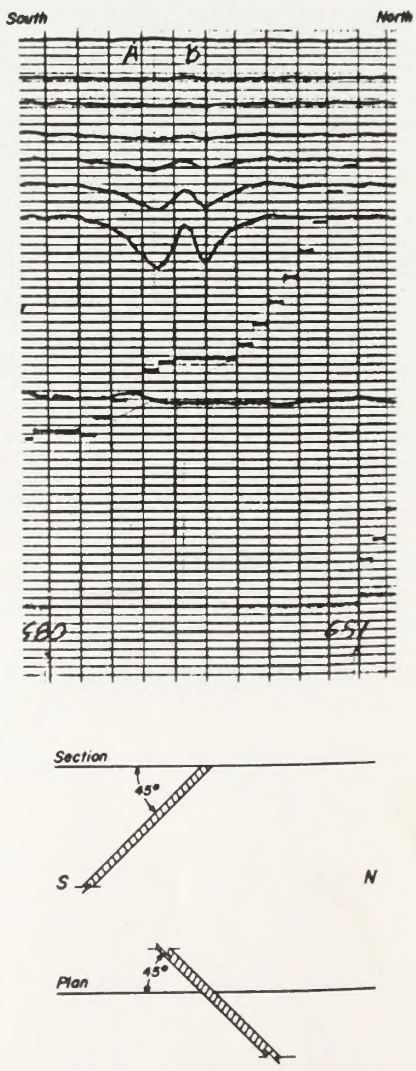

FIGURE 13 — 45-degree dip and strike, up-dip record.

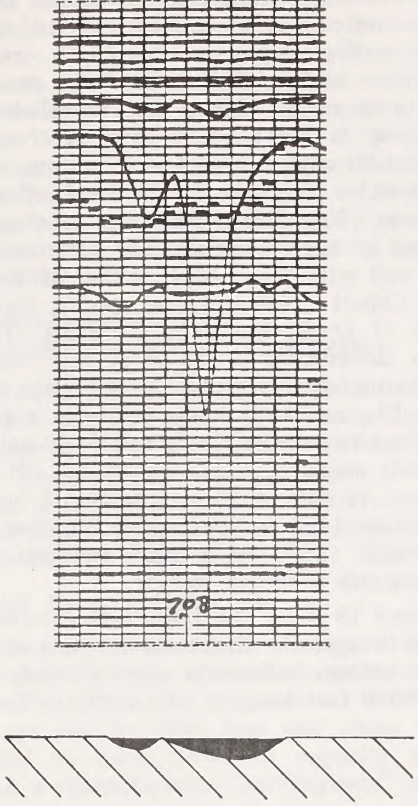

FIGURE 14 — Lake-bottom sediments, low conductivity.

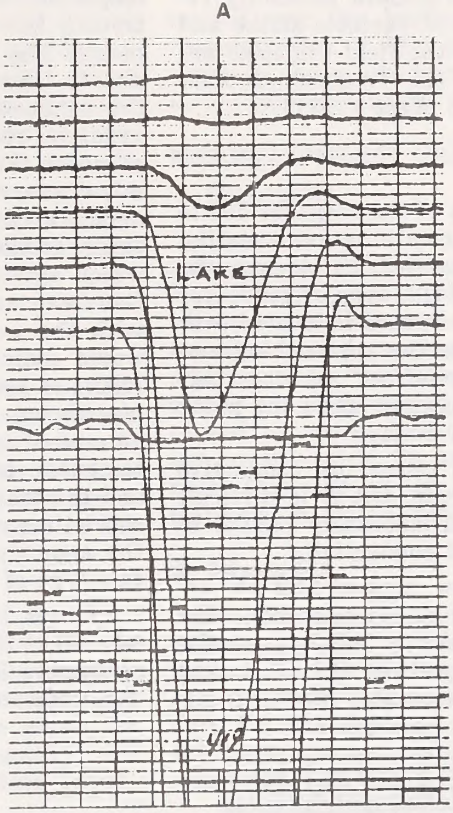

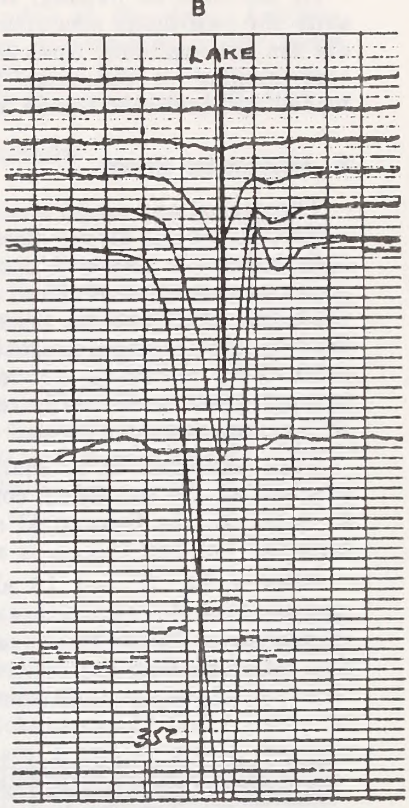

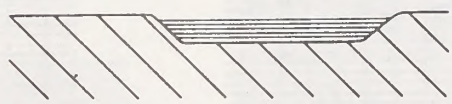

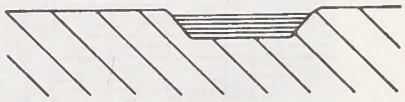

FIGURE 15 — Lake-bottom sediments, high conductivity.

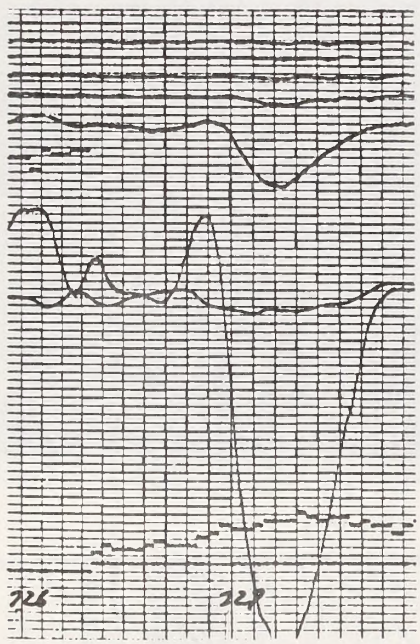

FIGURE 16 — Conductive overburden.

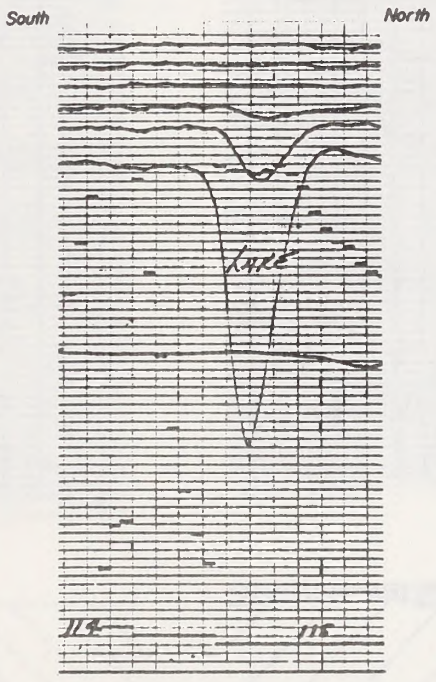

FIGURE 17 — Conductive sediments — variable thickness.

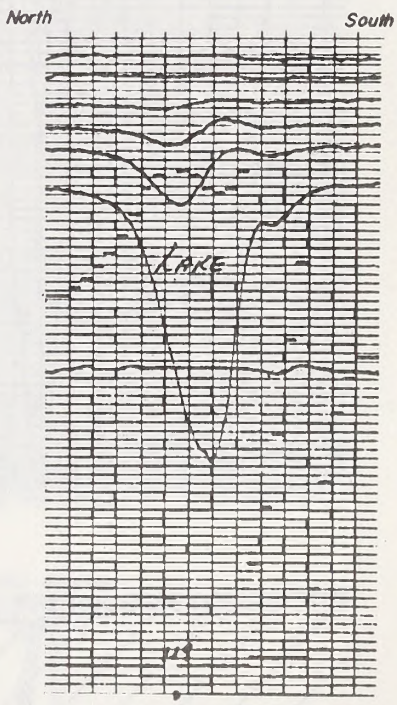

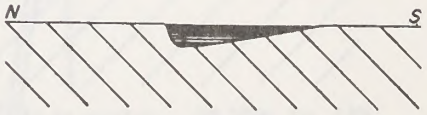

FIGURE 18 — Conductive sediments — variable thickness.

At the time of writing, time-domain modelling results for half-plane conductors of variable strike and dip are not available. However, the field examples are very similar in character to the frequency-domain modelling results of Ghosh and West (1971).

5. Horizontal Sheet

Theoretical and model studies of the response due to a thin, horizontal disc or sheet conductor representing overburden are also well documented. In general, the airborne anomalies produced by this type of conductor are quite broad and the peak response is located over the edge of the sheet nearest to the approaching aircraft. This results in an "edge-effect" or "herringboning" that can be easily recognized when the peaks of the anomalies are plotted on a map.

Field examples of anomalies caused by conductive overburden are extremely common, but it is difficult to duplicate the theoretical and laboratory results in terms of uniform thickness and conductivity.

Figures 14, 15 and 16 show typical INPUT responses due to conductive surface materials. The anomalies in Figure 14 are caused by lake-bottom silts and, although they are relatively sharp, the short time constant of decay (100 microseconds) and the low amplitude of channel 2 (200 ppm) indicate an extremely low conductivity in the order of 10^{-2}-10^{-3} mhos/metre. The anomalies shown in Figure 15 are also due to lake-bottom sediments, but in these examples the conductivity is much higher and a well-defined negative response is recorded as the receiver approaches the distant edge of the sheet. In some cases, a secondary positive anomaly is recorded after the negative response (Fig. 15B). The time constant for these anomalies is approximately 200 microseconds, which agrees well with the model results of Becker, Gauvreau and Collett (1972). These results, together with the work of Dyck, Becker and Collett (1972), would indicate thicknesses of 10-20 ft and conductivities of approximately 1-2 mhos/metre for the examples shown. In Figure 16 the large response is due to an area of conductive overburden of relatively uniform thickness. In this example, channel 1 is just off scale and the transient is still visible on channel 3, but the short time constant (140 microseconds) together with the anomaly width (1600 feet) make recognition of this type of response a simple matter.

Figures 17 and 18 show the responses obtained on two flight lines in opposite directions across a strip of conductive lake-bottom sediments approximately 1000 feet wide and 5000 feet long. A characteristic feature

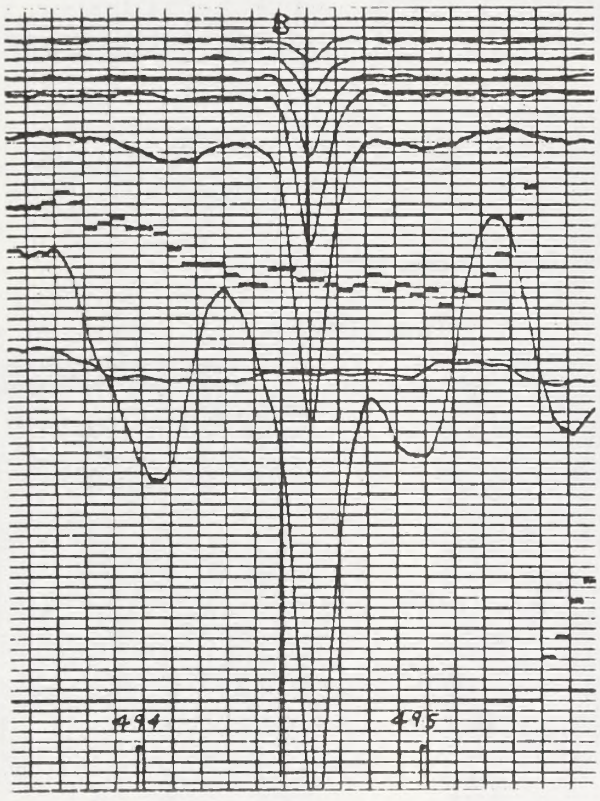

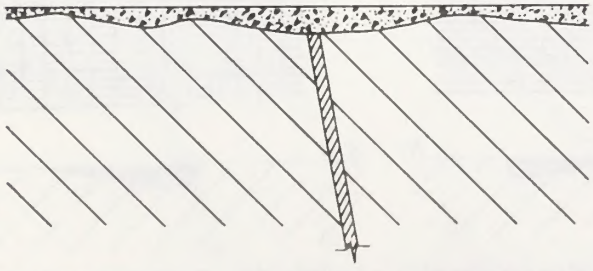

FIGURE 19 — Conductor under conductive overburden.

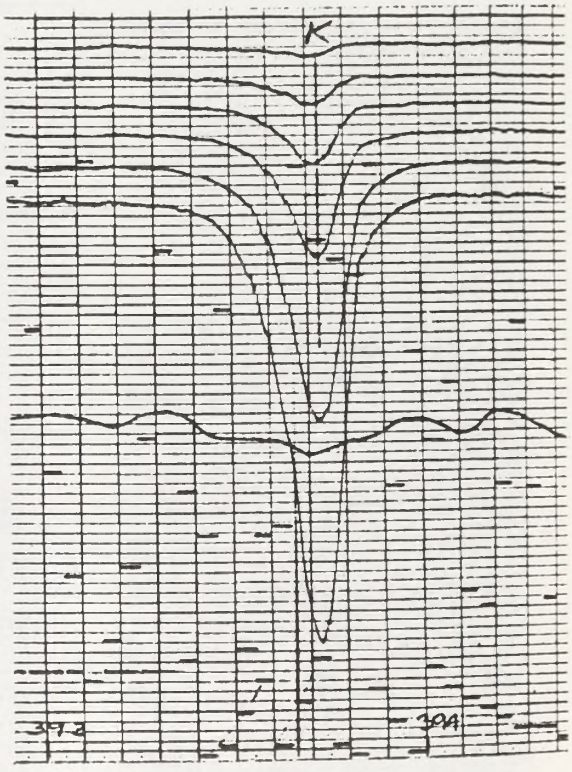

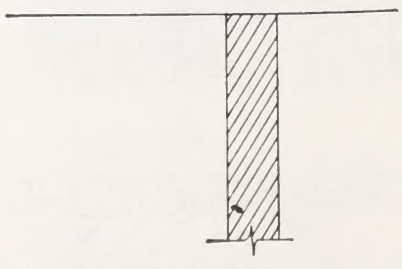

FIGURE 20 — Thick vertical dyke.

of these profiles is the staggering of the anomaly peak from channel to channel. This is indicative of a lateral change in the transient decay rate and therefore a change in the conductivity-thickness product. Time constants measured at intervals across the anomaly increase from approximately 80 microseconds at the south edge to 300 microseconds at the north edge. If we can assume that the conductivity of the sediments is reasonably constant over this distance, the results indicate that in cross section the strip is wedge-shaped and thicker on the north side.

6. Bedrock Conductor Beneath Conductive Overburden

The record shown in Figure 19 is included to illustrate the response obtained from a dipping bedrock conductor beneath a thin layer of conductive clay. It seems likely that in this case there is some enhancement of the anomaly amplitude due to dip in the direction of flight or as a result of eddy currents in the overburden.

7. Thick Vertical Dyke

The response from a body of serpentinized peridotite illustrates the type of anomaly produced by a thick dyke (Fig. 20). The dimensions of this particular body are 800 by 5000 feet and when the anomalies recorded on lines flown in opposite directions are plotted, a characteristic "herringbone" pattern is produced over the leading edge of the dyke. Another characteristic of this type of response is the large width of the anomaly relative to that of a half-plane. In the example shown, it is approximately 1000 feet.

MISCELLANEOUS EXAMPLES

1. Sediments

Figure 21 shows a typical record obtained over a sedimentary formation approximately 1 mile wide. The rock types within this formation are derived from volcanic materials and consist of graphitic siltstones, sandstones and conglomerates. It is virtually impossible to apply any interpretive technique to such a closely spaced group of anomalies. Generally, they are caused by conductors of extensive strike length and are considered to be unattractive economically. However, they can be of considerable value as aids to mapping in drift-covered areas.

2. Magnetite

The conductivity of magnetite iron formations increases as a function of the percentage of iron. Figures 22 and 23 show the anomalies recorded over two different masses of magnetite, each containing about 28-30% Fe. The apparent thickness-conductivity products for these two anomalies are 3 and 12 mhos, respectively, and because the conductivities can be assumed

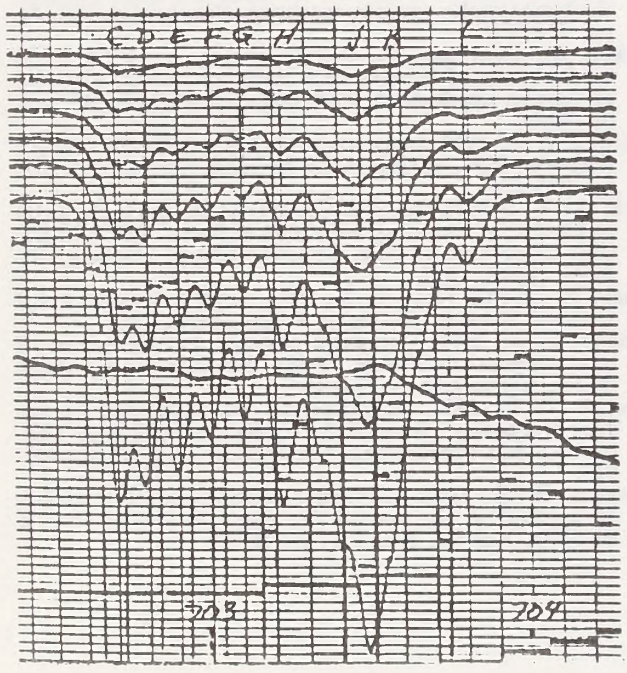

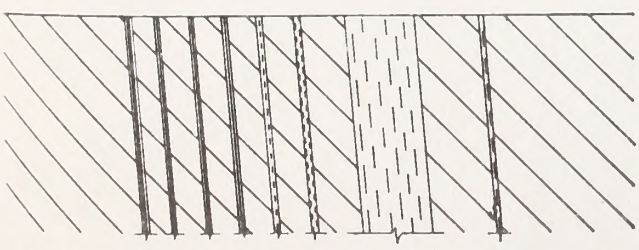

FIGURE 21 — Graphitic sediments.

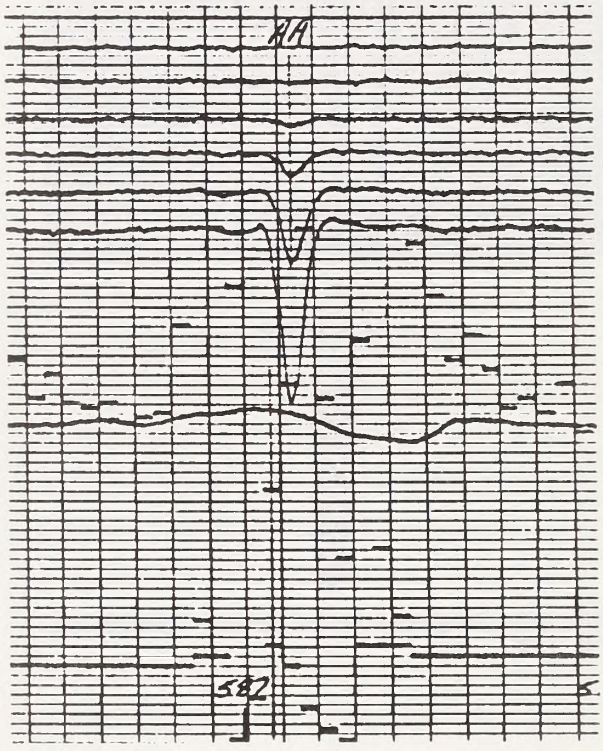

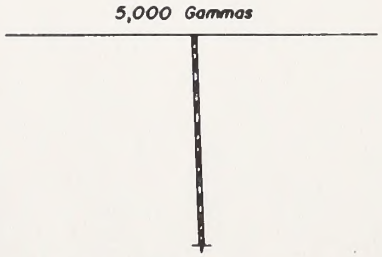

FIGURE 22 — Magnetite in gabbro — 28-30% Fe. 125 ft wide.

to be equal these results indicate that the second conductor is approximately four times as wide as the first. In actual fact, both anomalies are due to disseminated and narrow bands of magnetite in basic rocks and the formation widths are 125 feet for Figure 22 and 510 feet for Figure 23.

CONCLUSIONS

The results presented here illustrate the high resolution capabilities of the new system and demonstrate the increase in definition of anomaly characteristics. The observed amplitude and shape discrepancies between the field data and the laboratory results as noted by Becker, Gauvreau & Collett (1972) have been reduced considerably as a result of the improvements. In many instances it is now possible to match the field data with data obtained by modelling, and also derive a figure for the apparent conductivity-width product together with an indication of the conductor attitude. The examples can be used as aids in interpretation and discrimination, but, as Paterson (1971) has pointed out, conductivity-width measurements must be considered as apparent rather than real, and are more useful in the grading of anomalies on a relative basis than in estimates of "true" conductivity.

The research and development program outlined in the introduction to this article took almost two years to complete. The design work has been made available to Barringer Research Ltd., and equipment designated by the name "Barringer/Questor Mark VI INPUT" will be manufactured by them in order to up-date the current installations.

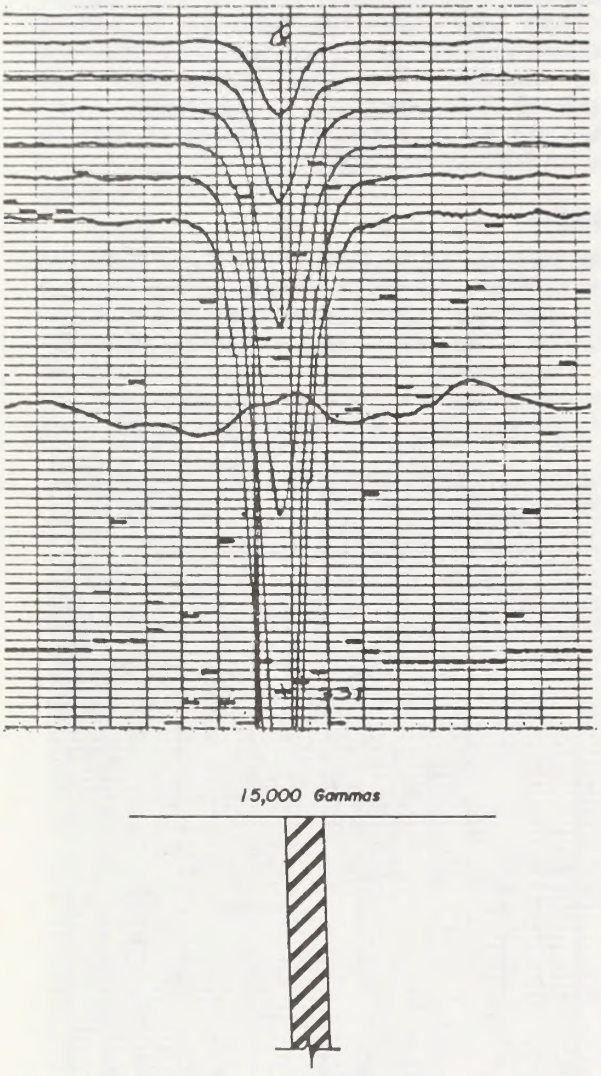

FIGURE 23 — Magnetite in anorthosite — 28-30% Fe, 510 ft wide.

ACKNOWLEDGMENTS

The author would like to thank Dr. A. Laurin for his permission to use the anomaly examples, and Dr. A. Becker for his comments and suggestions for improvements in the presentation of this material.

REFERENCES

Becker, A., 1969, Simulation of time-domain, airborne, electromagnetic system response. Geophysics, Vol. 34, pp. 739-752.

Becker, A., Gauvreau, C., and Collett, L. S., 1972, Scale model study of time-domain electromagnetic response of tabular conductors. CIM Bulletin, Vol. 65, No. 725, pp. 90-96.

Boniwell, J. B., 1967, Some recent results with the INPUT Airborne E.M. System. CIM Bulletin, Vol. 60, No. 659, pp. 325-332.

Dyck, A. V., Becker, A., and Collett, L. S., 1972, Surficial conductivity mapping with the airborne INPUT system. Presented at CIM Annual General Meeting, Ottawa, April, 1972.

Ghosh, M. K., and West, G. F., 1971, AEM analogue model studies; Norman Paterson & Associates Ltd.

Palacky, G. J., 1972, Computer-assisted interpretation of multi-channel airborne E.M. measurements. Ph.D. thesis, University of Toronto.

Paterson, N. R., 1961, Experimental and field data for the dual-frequency phase-shift method of airborne electromagnetic prospecting. Geophysics, Vol. 26, pp. 601-617.

Paterson, N. R., 1971, Airborne electromagnetic methods as applied to the search for sulphide deposits. CIM Bulletin, Vol. 64, No. 705, pp. 29-38.

APPENDIX II

The Interpretation of Gamma-Ray Spectrometry

Roger A. Haskins

INTERPRETATION

Figure 1 is the reduced copy of a flight tape taken from survey line ML3 flown in the California Desert in the late 1970s. The object is to outline areas of anomalous uranium mineralization. The primary parameter here is the uranium to thorium ratio (eU/Th). First a base line is drawn on the profiles which is eyeballed in. It should be placed so as to cut along the average level of response. Using this base line, the anomalous responses are bracketed by vertical lines which extend to cover all of the profile data. This allows easy comparison to be made of the various data elements of the anomaly. By extending the lines to the bottom, the anomaly's position and width on the ground can be recovered from the flight lines. These lines will have been previously plotted on topographic maps or air photos.

The anomalies have been identified by letters (A-G). Anomaly A is over the Avawatz Mountains proper and G is the furthest east. Anomaly A is 6,500 feet wide on the ground and has three sharp spikes of high magnetic responses associated with it. The spikes must probably represent magnetite lodes in the limestones which flank the granitic core of the mountains. The anomaly is related to the eastern edge of the granite. The granite has higher U and Th content than the limestones and related sedimentary rocks to the east of it.

Anomalies B, D, and G probably represent various sedimentary units with enriched uranium contents. If a favorable hydrologic system has been flowing through these units they may contain uranium deposits. The size of the anomalies are B: 7,500 feet; D: 12,500 feet; and G: 2,500 feet.

Anomalies C, E, and F are of particular interest as they are steep, narrow, and considerably higher in amplitude above their adjacent profiles. Anomaly C is 2,500 feet wide and could represent a locally enriched geologic formation or a uranium deposit. Anomaly E is 2,500 feet wide but has additional response that is only 300 feet wide rising from it. This anomaly points out a zone of enrichment of uranium in a unit that is already enriched. This would be a definite follow-up target on the ground. Anomaly F is a single spike that is 150 feet wide and sharply defined. This spike probably represents a zone of uranium mineralization. This anomoly would also be a prime candidate for ground follow-up work.

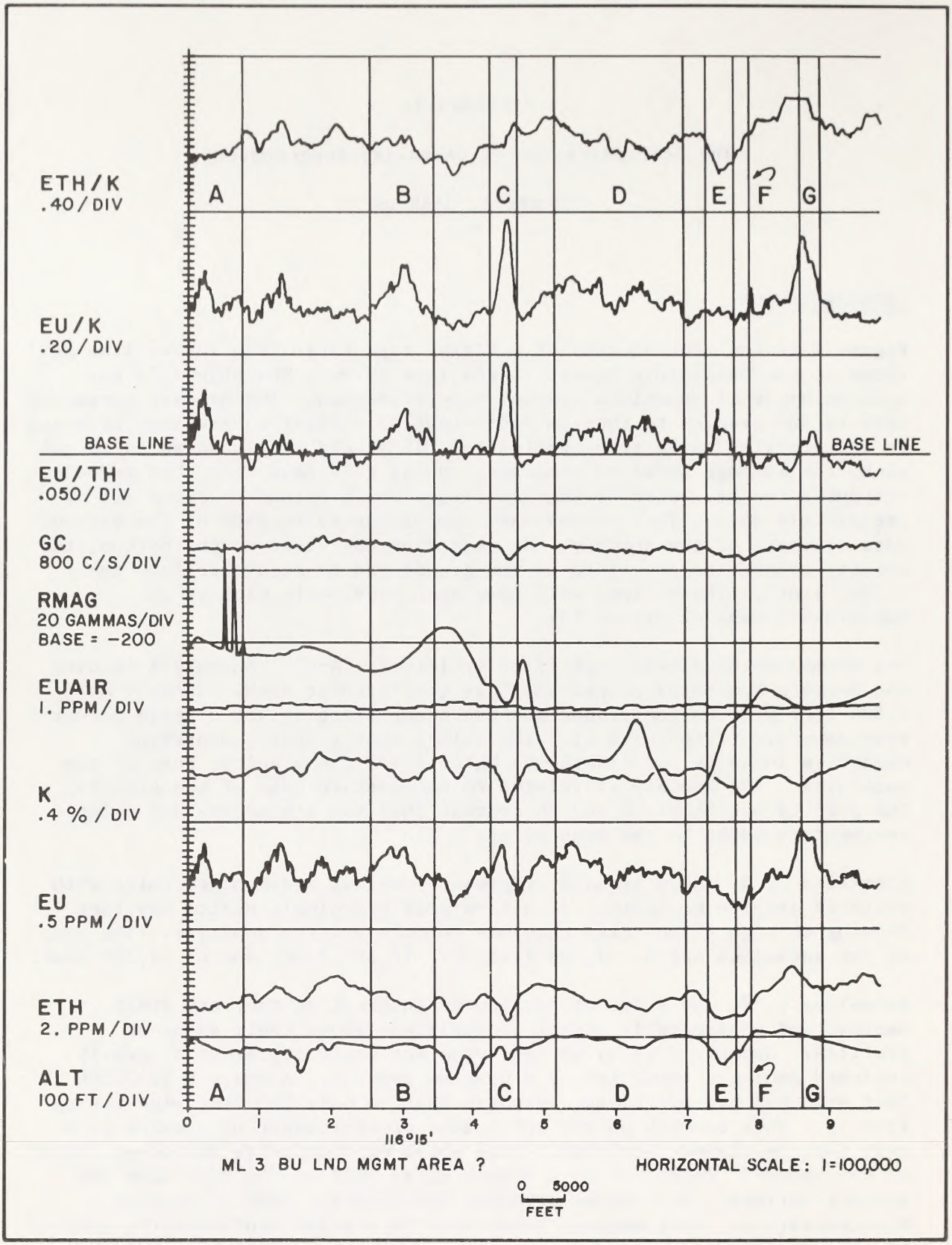

Figure 1. Flight Tape of Four Channel Gamma-ray Spectrometer Profile Flown Over the Avawatz Mountains in the California Desert Conservation Area.

SUMMARY

In conclusion, Figure 1 shows two different, but very useful, types of information with regard to uranium. One is the outlining of geologic formations that have higher than average uranium contents and are therefore potential hosts for uranium deposits. This is shown by anomalies A, B, C, D, and G. The second is the picking up of localized zones of probable uranium mineralization, as characterized by anomalies E and F.

Similar baselines can be constructed for the individual K^{40}, U, and Th profiles and areas of anomalous element concentration can be outlined for various inventory needs. However, if uranium mineralization alone is the target, then the ratio of U/Th is the best parameter to begin with.

APPENDIX III

Horizontal Loop (HLEM) Systems

(Strangway, D.W.:1966): Electromagnetic Parameters of Some Sulfide Ore Bodies; in Mining Geophysics, Vol. I, p. 227-242. [Reprinted by permission of the Society of Exploration Geophysicists, Tulsa, Oklahoma.]

Table of Contents

ELECTROMAGNETIC PARAMETERS OF SOME SULFIDE ORE BODIES

DAVID W. STRANGWAY*

A series of model experiments has been carried out as an aid to the interpretation of horizontal-loop (Slingram) electromagnetic surveys. The model used was a large conducting sheet with various orientations subjected to various frequencies. It is shown how it is possible to derive the dip, depth, and conductivity-thickness product of such bodies. The interpretation procedure has been applied to a set of field data and it is concluded that the conductivity-thickness product is a useful parameter in the study of massive-sulfide deposits. These examples show that many sulfide conductors have conductivity-thickness products between one and 30, a surprisingly small range considering the possible range of values for conductivity and for thickness in natural deposits.

Introduction

The horizontal-loop electromagnetic system is widely used in prospecting for massive-sulfide deposits. The system consists of a transmitting coil and a receiving coil. The transmitter generates a frequency which is usually set between 400 cps and 3,600 cps. This signal is detected by the receiving coil, and a cable connecting transmitter and receiver allows the received signal to be completely cancelled when no geologic conductor is present. If a conducting body is present, the transmitted signal will generate eddy currents in that body. These eddy currents in turn generate a secondary magnetic field which is detected and measured by the receiving coil. It is customary to measure the component in-phase with the primary transmitted signal and that which lags it by 90 degrees (i.e., the quadrature component, sometimes called the out-of-phase component). One of the most serious difficulties in the use of these systems has always been the interpretation of the data. The present paper discusses a procedure of interpretation for tabular conductors and then shows results encountered over some typical sulfide conductors.

Theoretical analysis of the response of a dipping tabular conductor to an alternating vertical magnetic dipole is difficult. For the case of a semi-infinite sheet it has so far only been possible to calculate the high-frequency or infinite conductivity response. Wait (1951, 1954, 1955, 1956) and Slichter and Knopoff (1959) have presented theoretical solutions for the case of a conducting half-space and for the case of a horizontally stratified earth. Wesley (1958) has published an approximate solution for the case of a vertically dipping dike, but West (1960) has shown that in many circumstances this latter solution is inadequate. Because of the complexity involved in deriving theoretical solutions for typical field conditions, several workers have turned to the use of scale models. With these models a variety of conditions can be simply and efficiently studied and the theoretical solutions expanded over a wide range. In fact, the theoretical solutions are often used to ensure that the model apparatus is functioning correctly. To achieve the maximum capability of the model and to study the in-phase-quadrature relationship a multiple-frequency system is desirable. Variable-frequency model studies have been reported by West (1960) and by Dolan (1960). In the case of tabular conductors, West (1960) has shown that the most useful response parameter is the one he calls α which is equal to $\sigma\mu\omega sl$. Where

σ = conductivity—mho/m
μ = permeability—henry/m
ω = frequency—cps
s = conductor thickness—meters
l = coil separation—meters

* Department of Geology and Geophysics, Massachusetts Institute of Technology, Cambridge.

As long as the value of α is unchanged, then the secondary magnetic field generated by the body will be the same. This makes modelling particularly simple for we may change two or more of the quantities in the response parameter and still get the same response curve as long as the numerical value of α is unchanged. In laboratory model experiments, of course, the coil separation and conductor thickness are of necessity much less than the same quantities in a real electromagnetic survey. This means that in order to model field conditions we must increase the conductivity of the model ore body, permitting the use of readily available materials such as copper, aluminum, or nonmagnetic stainless steel. By using one coil configuration and one conducting body we may then vary the quantity α by varying the transmitted frequency, thus reproducing a wide range of conditions. In a simple laboratory model we are limited by not being able to reproduce the inhomogeneities of a naturally occurring sulfide deposit.

In the present study, model frequencies between 200 cps and 20 kc/sec were used. Using a coil separation (l) of one foot and a stainless-sheet as a model, the values of α that could be modeled ranged from one to 105. As will be seen shortly this range of values of α is sufficient to cover the useful prospecting range over most natural sulfide deposits.

Interpretation

A series of model curves using a stainless-steel sheet was run and the results compiled in the manner devised by Hedstrom and Parasnis (1959). In Figure 1 a few typical curves have been shown. This figure shows the effect of varying dip. As has long been known, the shape of the horizontal-loop curve depends strongly on the dip of the conducting sheet. In the vertical case the curve is completely symmetrical while in the case of a horizontal sheet the curve is asymmetrical (except in a few special cases). In Figure 2 this fact is put in graphical form. Based on the ratio of areas under the two shoulders of the curve it is possible to derive a value for dip. This ratio varies from one for a symmetrical, vertical case to zero for a horizontal sheet, enabling one to determine a value of dip from typical field curves. Comparison with various field cases shows that the technique is reasonably accurate (see examples).

Horizontal sheets have wide variations in their response curves (see Figure 1) with only small variations in response parameter α. In some cases a positive response, in some no response, and in some a negative response over the center of a sheet are encountered. This makes recognition and interpretation of anomalies associated with horizontal conductors difficult unless two or more frequencies or coil separations are used in the field. It is, however, important to observe that as the coil system moves over the edge of a horizontal sheet there is always a negative response like that normally encountered directly over dipping tabular conductors. It will be shown that both the center and edge effects can be used for interpretation.

It is interesting to consider the effect of a lateral increase in conductivity in a horizontal sheet. This could represent a conducting orebody surrounded by a poorly-conducting overburden or surface layer. In the case where the response to the horizontal layer is positive, the local field at the high-conductivity portion is enhanced rather than reduced. This means that the response of the more highly conducting portion is generated by a larger field than normal and therefore the amplitude of the expected anomaly will be enhanced.

Using the technique developed by Hedstrom and Parasnis (1958) a series of parametric curves has been drawn. Figures 3 to 7 show some of the familes of curves that can be drawn for various dips. The maximum anomalies in both in-phase and quadrature components are plotted and curves drawn through them joining points of equal depth to the surface of the body in units of coil separation and of equal response parameter. In carrying out an interpretation one should first estimate the dip and then refer to the most appropriate curve 90, 60, 30, or 0 degrees dip. In the case of the horizontal sheet, two separate sets of curves can be used to

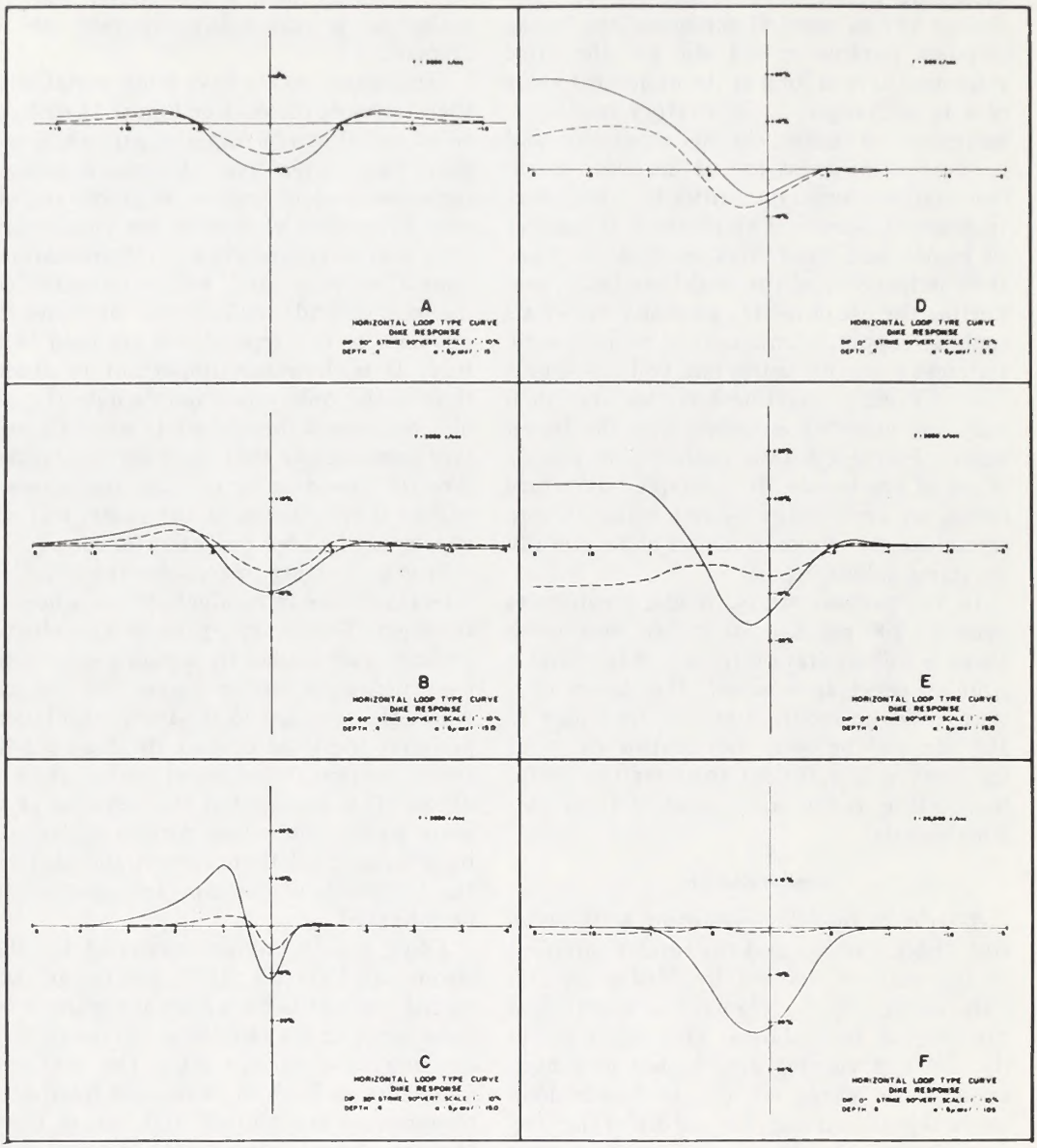

FIG. 1. Typical horizontal loop profiles over semi-infinite sheets.

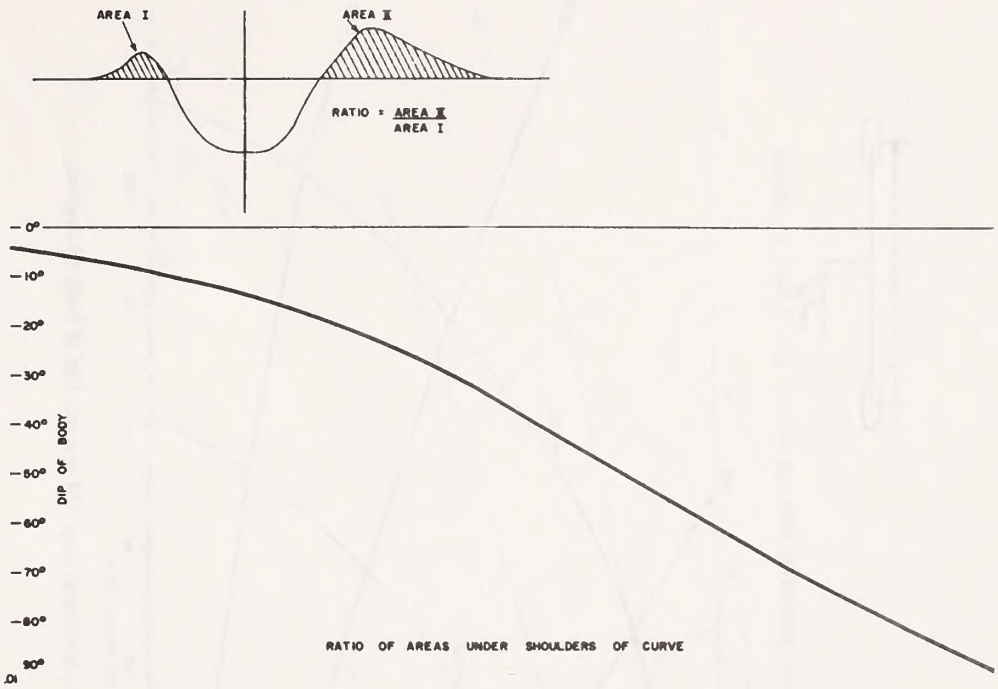

FIG. 2. Determination of dip of tabular conductor.

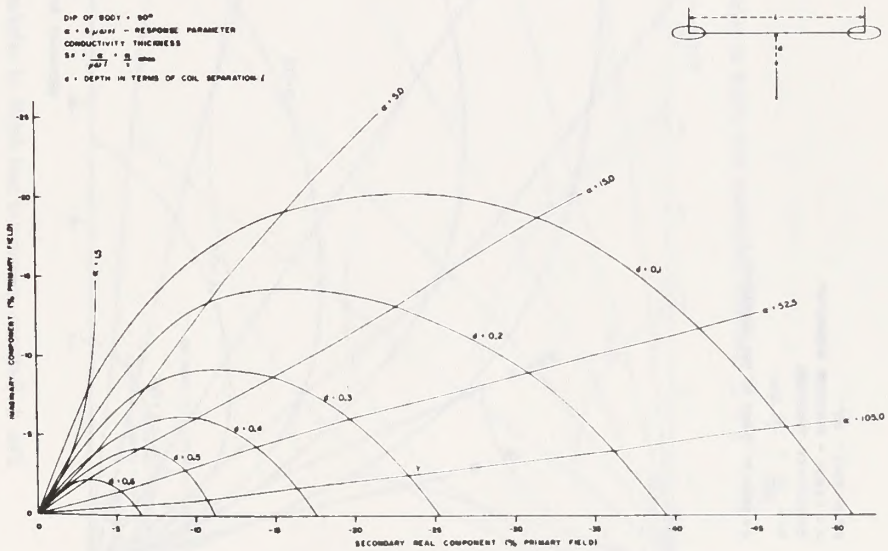

FIG. 3. Response parameter and depth of tabular conductors, horizontal loop EM system. Dip of body 90 degrees.

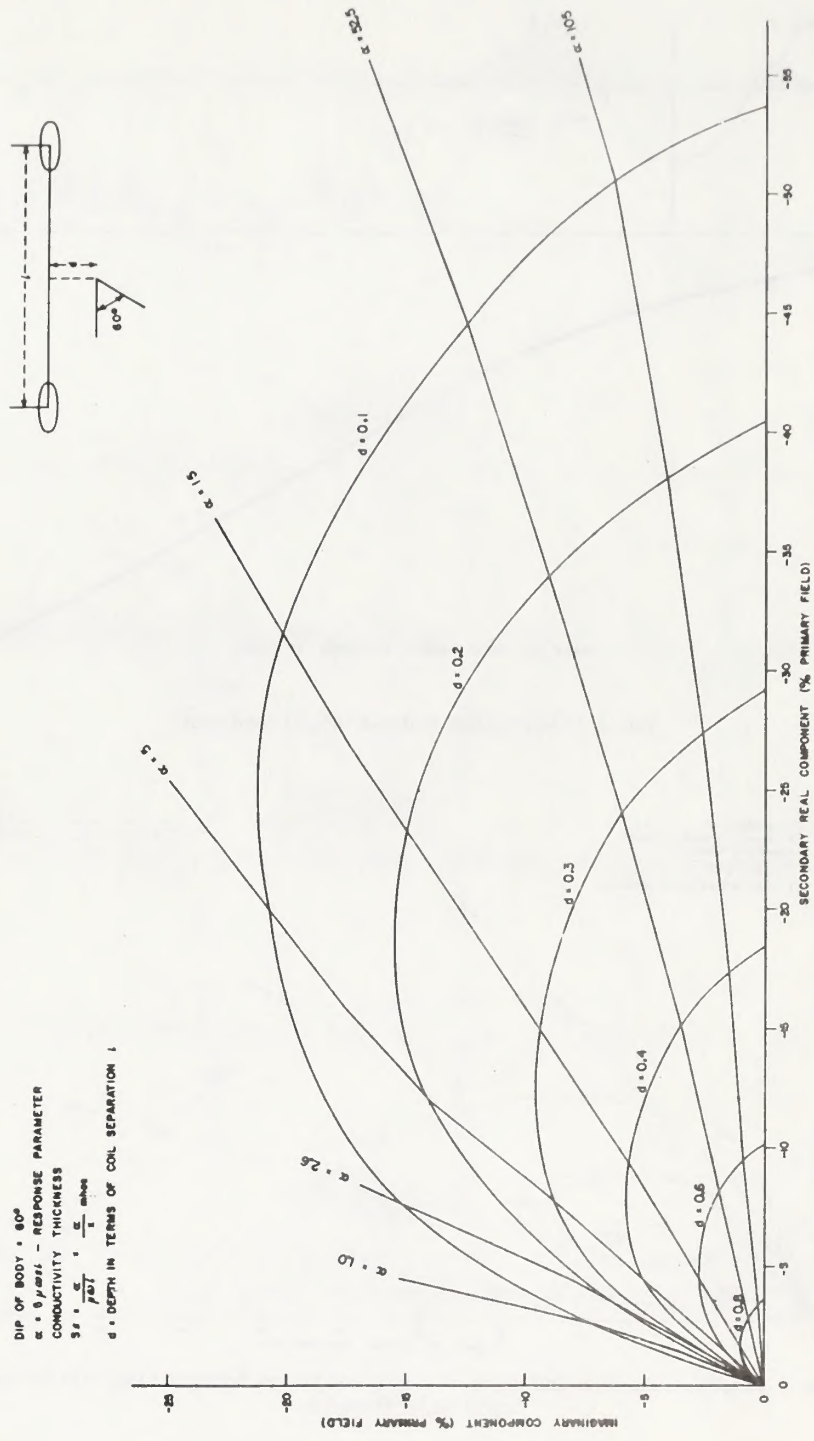

FIG. 4. Response parameter and depth of tabular conductors, horizontal loop EM system. Dip of body 60 degrees.

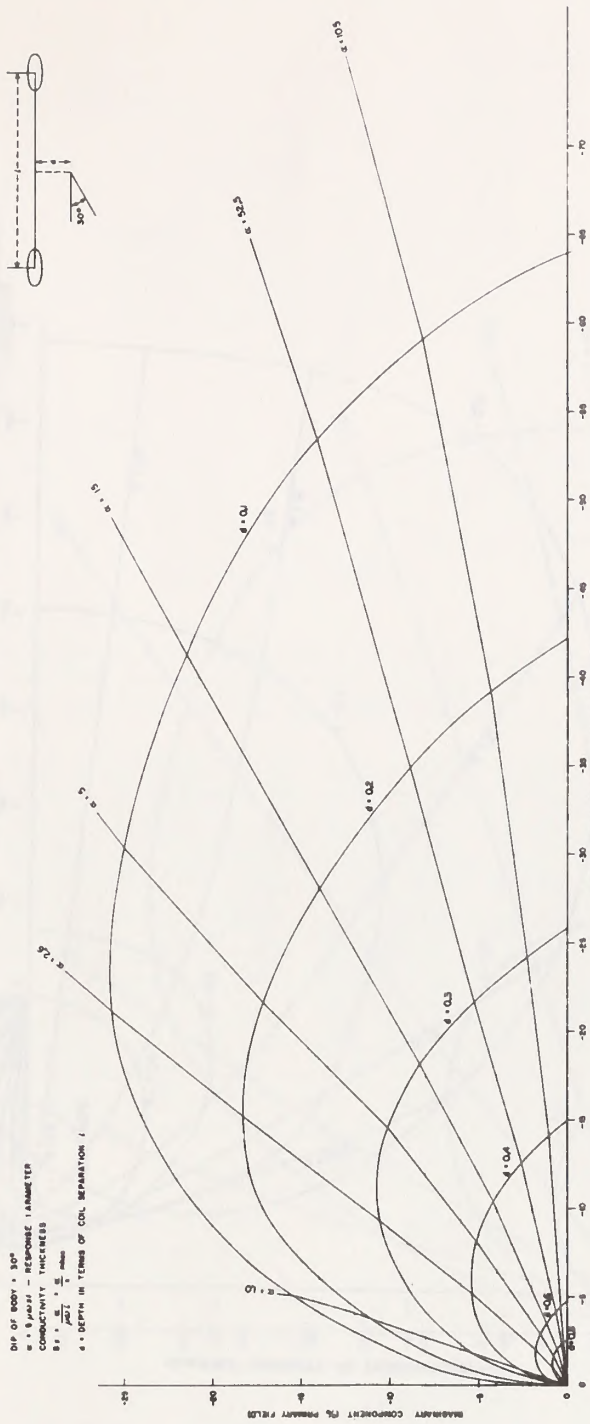

FIG. 5. Response parameter and depth of tabular conductors, horizontal loop EM system. Dip of body 30 degrees.

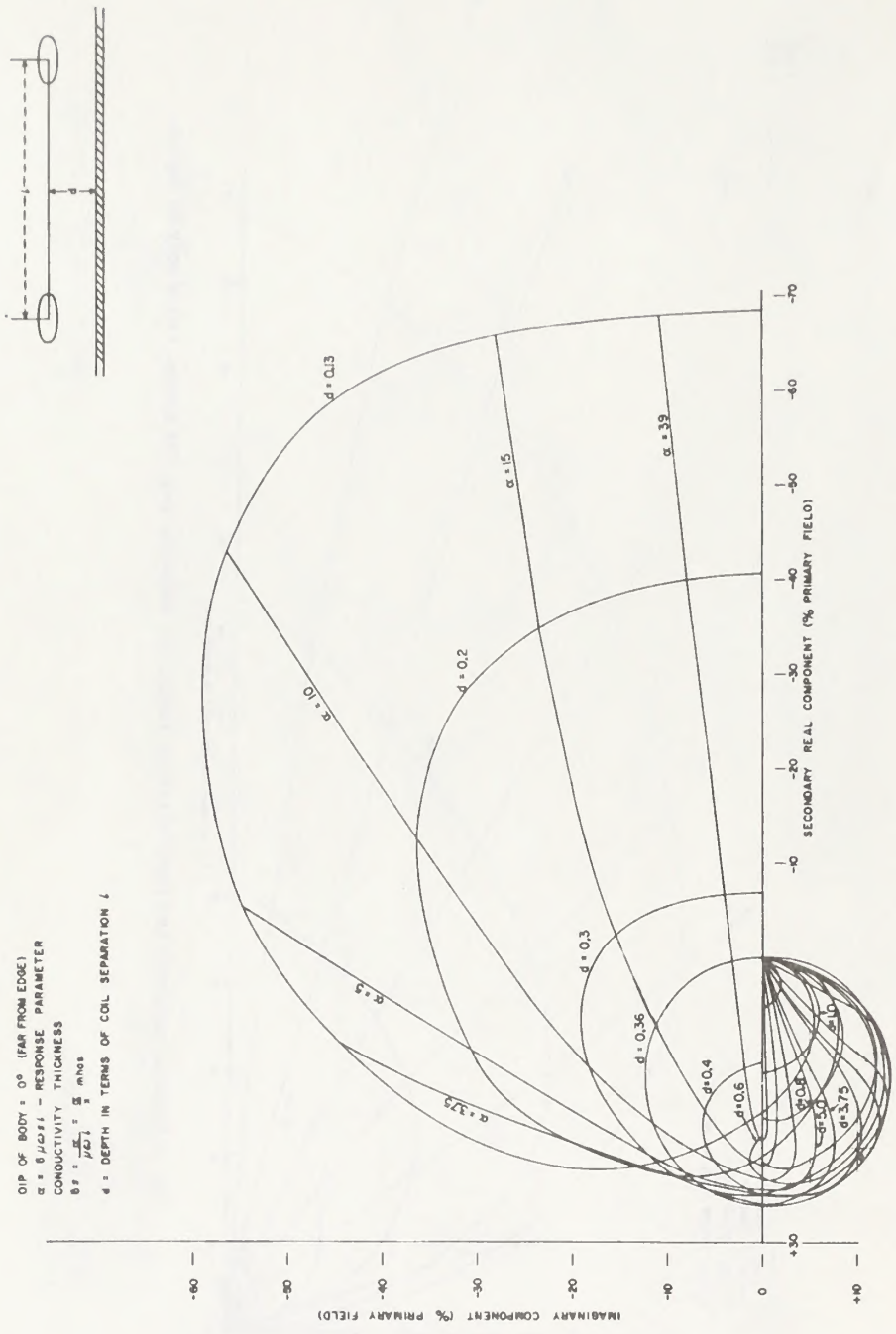

FIG. 6. Response parameter and depth of tabular conductors, horizontal loop EM system (modified from Hedstrom and Parasnis, 1958). Dip of body zero degrees. Reprinted by permission of *Geophysical Prospecting*.

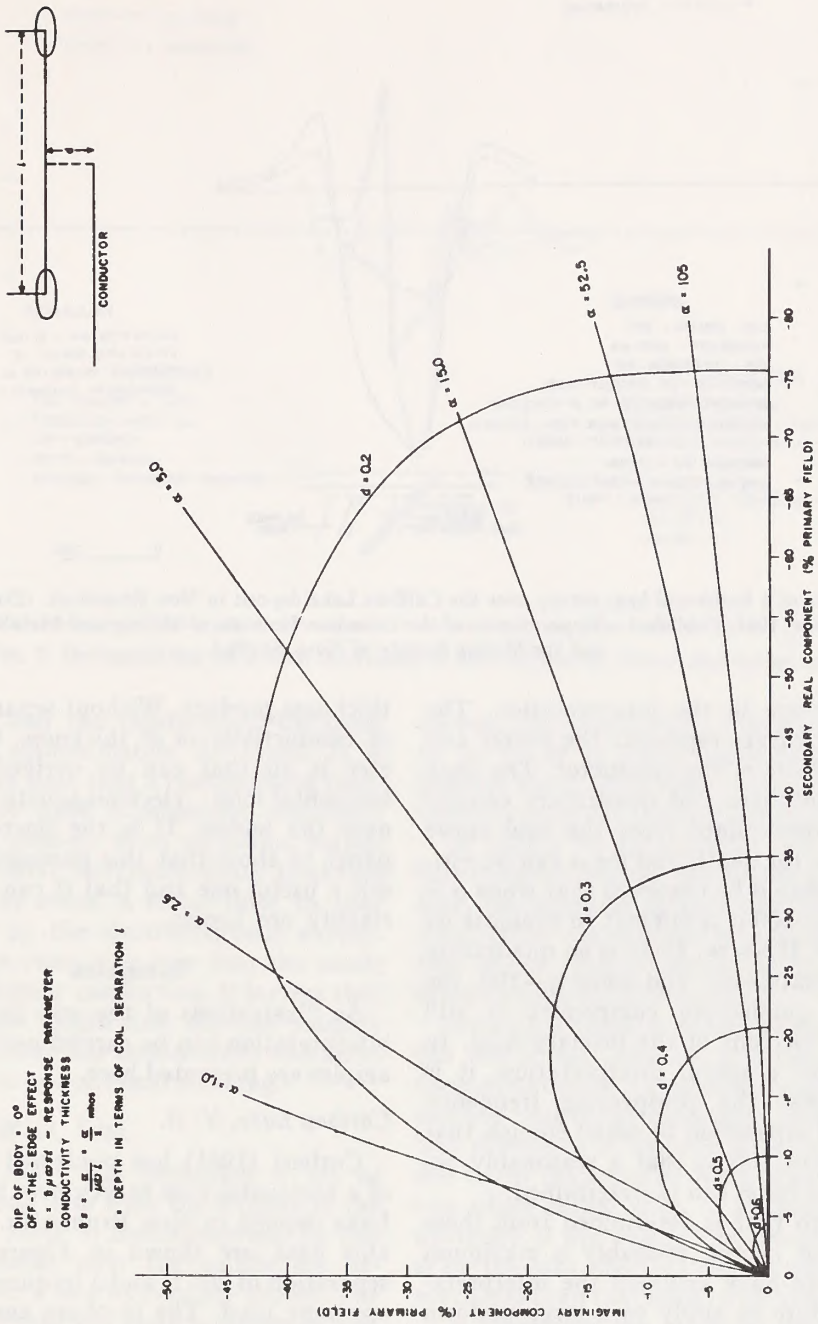

FIG. 7. Response parameter and depth of tabular conductors, horizontal loop EM system. Dip of body zero degrees; off-the-edge-effect.

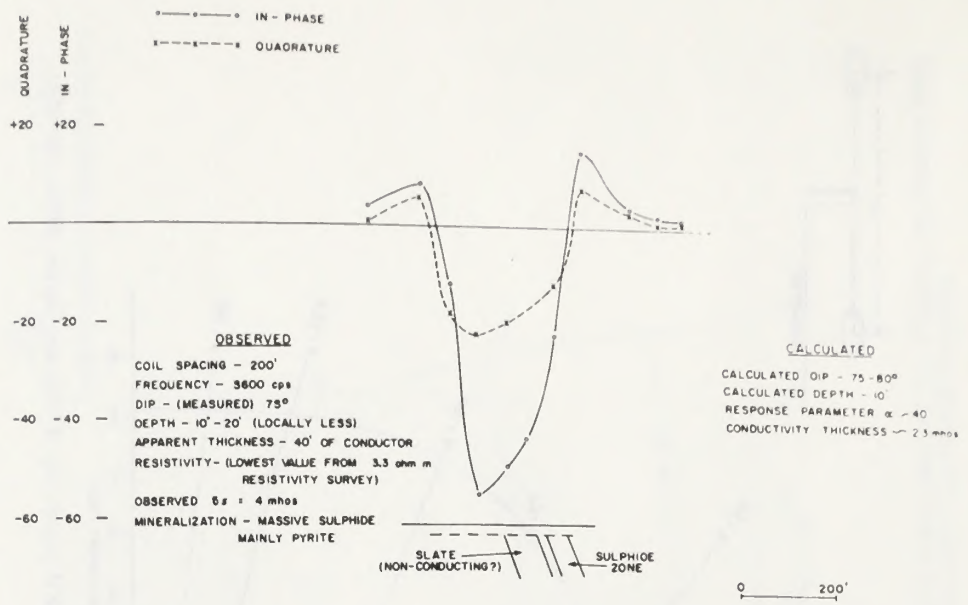

FIG. 8. Results of a horizontal loop survey over the Caribou Lake deposit in New Brunswick. (Data from J. D. Corbett, 1961, Published with permission of the Canadian Institute of Mining and Metallurgy and the Mining Society of Nova Scotia.)

give confidence in the interpretation. The two sets of curves represent the center and the edge effects of the conductor. The peak values of in-phase and quadrature components are determined from the field curve and a value for depth and for α can be estimated. It should be observed that when α is greater than 100 it is difficult to evaluate its exact value. If $\alpha = \infty$, there is no quadrature response whatsoever, and when $\alpha = 100$, the secondary quadrature component is still only a few percent of the primary field. In order to get a useful interpretation, it is essential that the prospecting frequency and/or coil separation be small enough that α is less than 100 so that a reasonably accurate value for σs can be determined.

The depth that is determined from these curves is, of course, probably a maximum depth, as we have assumed the interpretation procedure to apply to a large uniform sheet. If coil separation, l, and frequency, ω, are known and magnetic permeability μ is assumed to be one, it is then possible to evaluate the quantity σs or the conductivity-thickness product. Without separate studies of conductivity or of thickness, this parameter is all that can be derived from the horizontal-loop electromagnetic response over the bodies. It is the purpose of this paper to show that this parameter is of itself a useful one and that it can be used to classify ore bodies.

Examples

As illustrations of the way in which the interpretation can be carried out several examples are presented here.

Caribou Lake, N. B.

Corbett (1961) has published the results of a horizontal-loop survey over the Caribou Lake deposit in New Brunswick. The available data are shown in Figure 8. A coil separation of 200 ft and a frequency of 3,600 cps were used. The in-phase anomaly indicates a steep dip of about 75 to 80 degrees which is close to the reported value of 75 degrees. Using the peak in-phase and quadrature response the depth is found to be less

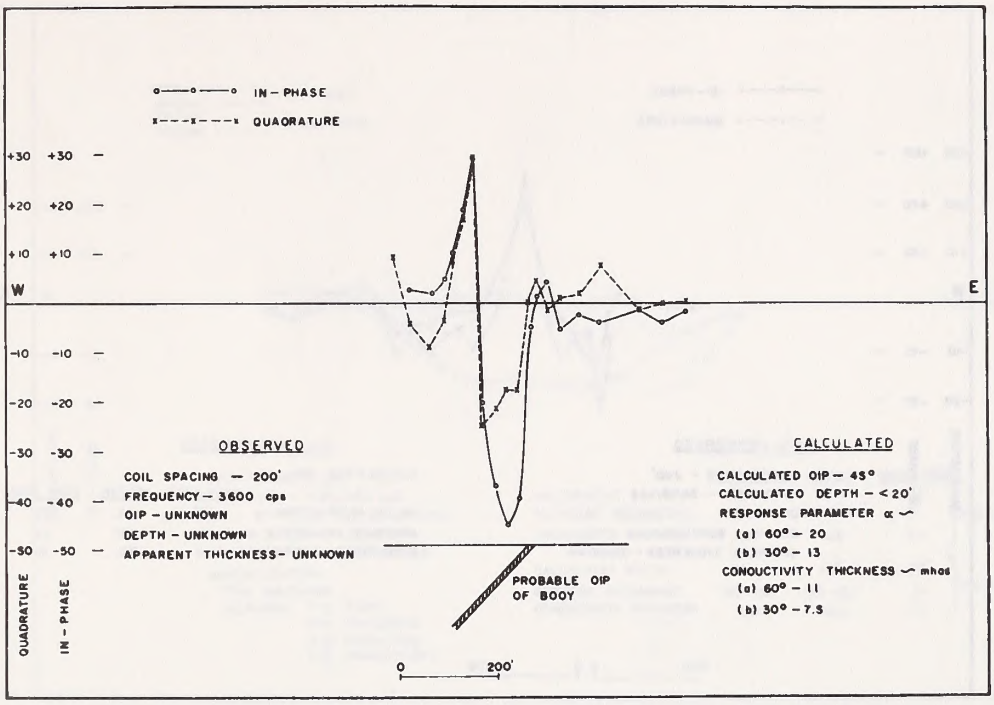

FIG. 9. Horizontal-loop data from the vicinity of the Coronation Mine in Saskatchewan.

than 20 ft and the conductivity-thickness product is approximately 23 mhos. It is interesting to note that a conventional resistivity survey gave a minimum resistivity value of 33 ohm-m. With an actual sulfide thickness of 40 ft, the conductivity-thickness product is 44 mhos, a value close to that determined by the electromagnetic survey. Although we cannot be sure that the whole sheet is uniformly conducting, it is clear that the estimated depth and dip are roughly correct and that the conductivity-thickness product has a real physical meaning.

Coronation Mine, Sask.

Rattew (1961) has presented a set of horizontal loop data from the vicinity of the Coronation Mine in Saskatchewan. In this paper anomalies over the sulfide ore deposit and over a nearby lake are shown. The anomaly over the ore body is shown in Figure 9. This interpretation gives an estimated dip of 45 degress. The depth is estimated as less than 20 ft. Depending on whether one uses the 30- or the 60-degree parametric curves, the conductivity-thickness is found to be 7.5 or 11 mhos respectively. The σs product has a value close to one, not greatly different from the Caribou Lake value.

In Figure 10 an anomaly over a nearby lake is shown. We see that at the edges of the lake, the anomaly in both the in-phase and quadrature components is negative. These two edges give σs values of 1.1 and 0.4 mhos and depths of about 50 ft.

Since this depth is considerably less than the 200-ft coil spacing, it seems that the approximation of a thin sheet is an adequate one and that the σs value has a real meaning. The difference at the two edges is probably due to the thickness or depth of water on the two edges rather than to a change in conductivity of the water. The average value of σs for the lake edges is then 0.8 mho, a value much less than that found over the ore body.

In examining the center of the lake it is seen that both in-phase and quadrature components show a strong positive anomaly as expected over a horizontal layer in some cases. The two values are +20 percent and

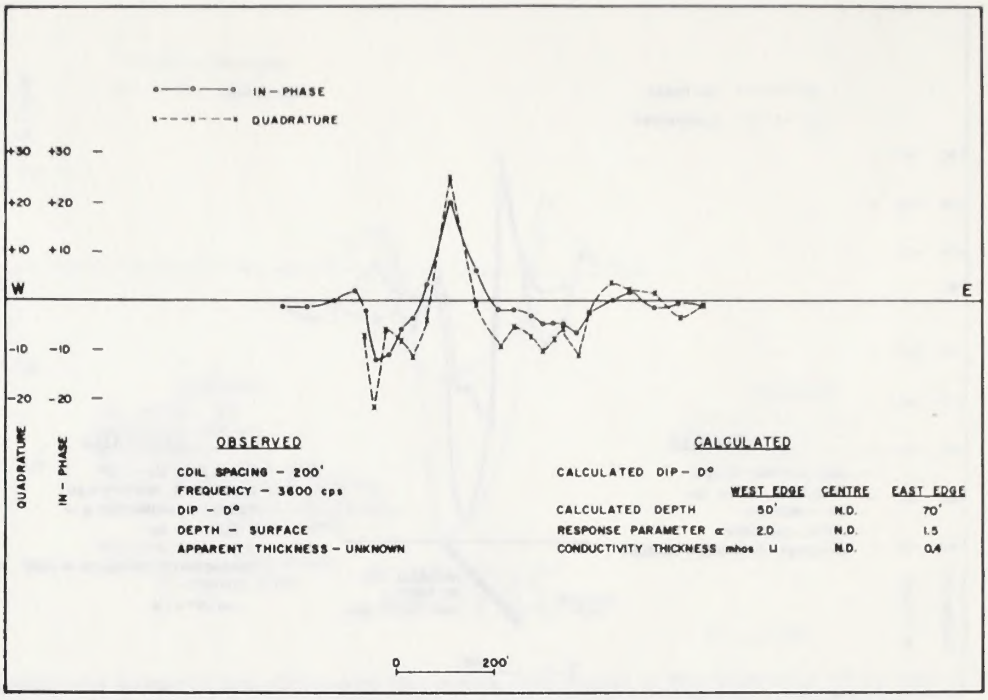

FIG. 10. Lake Anomaly from Coronation Mine area, Saskatchewan.

+25 percent respectively, a combination of values not found in Figure 7. We are forced to conclude that the thin-sheet approximation does not hold over the center of the lake where the water depth is probably considerable. If a sufficiently high conductivity is involved, the current flow will be concentrated near-surface. In other words, if the skin depth for the lake is considerably less than the coil separation, one would still expect the thin sheet approximation to hold since the material at depth is not sampled. It is useful to estimate the skin depth δ in this case. Typical swamp and lake waters have a conductivity of about 10^{-2} mho/m. The skin depth is given by $\delta = \sqrt{2/\sigma\mu\omega}$ where σ, μ, ω are as previously defined. This yields a value of 83 m or about 250 ft, a value greater than the coil separation of 200 ft. Therefore the thin sheet assumption is inadequate. Slichter and Knopoff (1959) show that large positive anomalies such as these can be expected over half-spaces or thick layers.

Clearwater, N. B.

Fleming and Brooks (1960) have reported on a survey over a flat-lying sulfide deposit in the Clearwater, New Brunswick, area. This deposit was surveyed using five separate coil configurations and frequencies. The interesting features of these surveys are shown in Figures 11, 12, and 13, where the approximate ore body configuration is shown together with the electromagnetic curves. In Figures 11 and 12, the results of 200-ft and 100-ft coil separation surveys are shown. It is interesting to note that the anomalies over the center of the deposit have opposite signs as expected under certain conditions over horizontal conductors when α is changed. In Figure 13 the high frequency 3,600 cps survey shows that the in-phase anomaly over the center of the deposit is negative, while the quadrature component is close to zero.

A study of the profiles reveals that the anomaly on the edge of the conductors is negative in all cases except for the north end

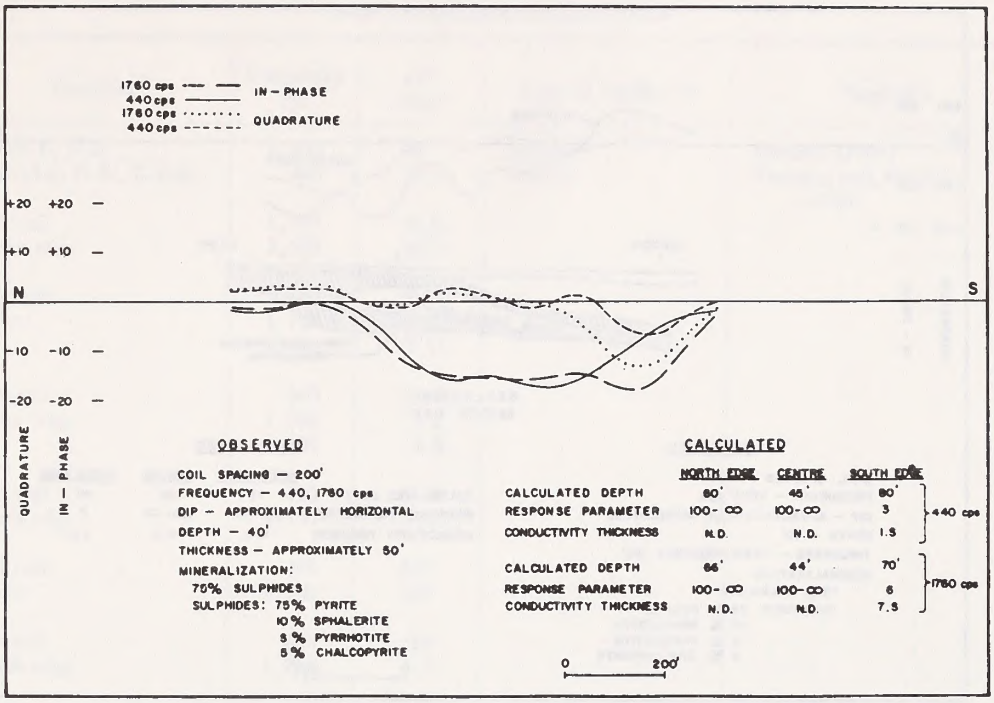

FIG. 11. Results from a 200-ft coil separation survey at Clearwater, New Brunswick. L.16 E.

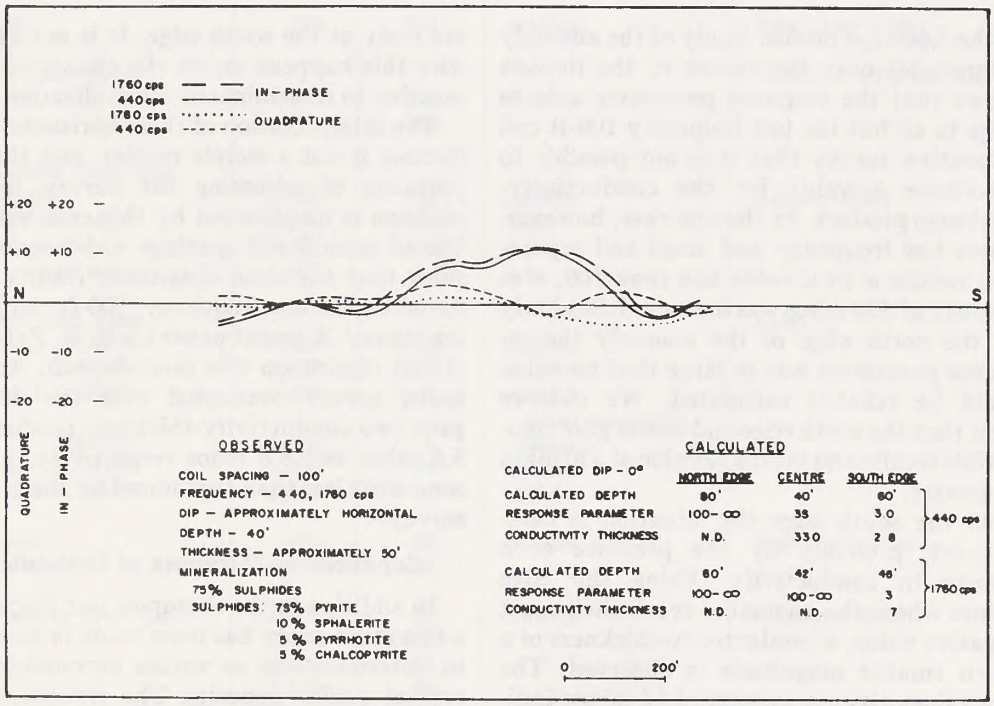

FIG. 12. Results of a 100-ft coil separation survey at Clearwater, New Brunswick. L.16 E.

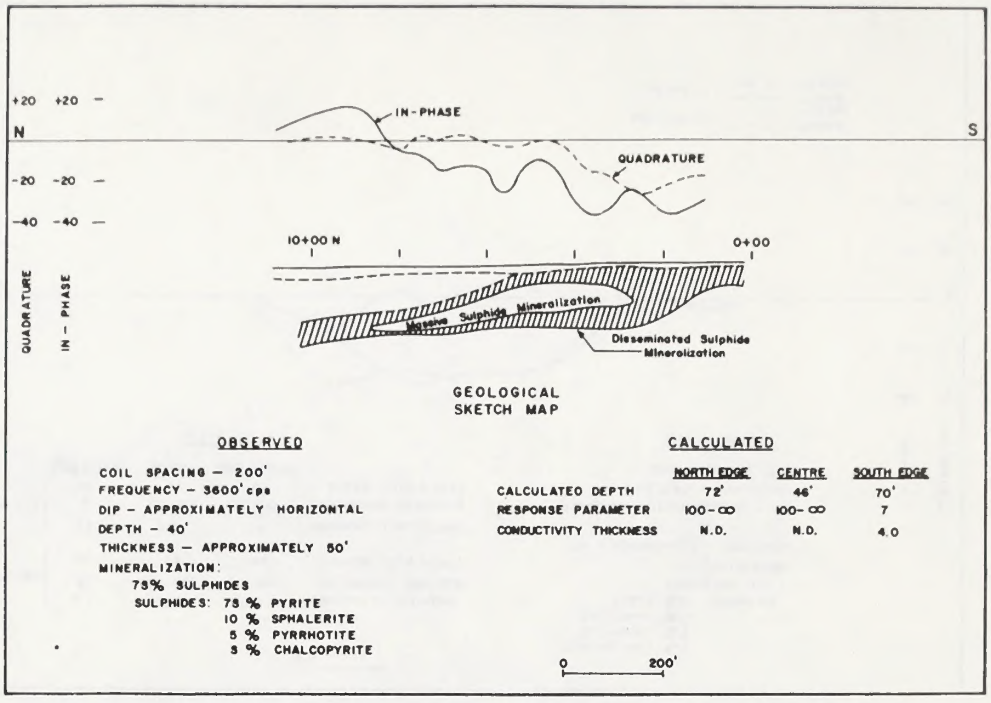

FIG. 13. High frequency survey from Clearwater, New Brunswick. L.16 E.

of the 3,600 cps profile. Study of the anomaly magnitudes over the center of the deposit shows that the response parameter α is so large in all but the low-frequency 100-ft coil separation survey that it is not possible to determine a value for the conductivity-thickness product. In the one case, however, where low frequency and small coil separation reduce α to a value less than 100, a σs product of 330 mhos was measured. Similarly on the north edge of the anomaly the response parameter was so large that no value could be reliably calculated. We observe then that the north edge and center give compatible results and yield a σs value of 330 mhos or greater.

At the south edge the situation is complicated, probably by the presence of a change in conductivity. Using the edge values where the anomalies reach their most negative value, a conductivity-thickness of a much smaller magnitude is observed. The five values give an average of 12 mhos, indicating a distinct change in character of the ore body at the south edge. It is not known why this happens unless the change is from massive to disseminated mineralization.

The interpretation of these horizontal conductors is not a simple matter, and the importance of adjusting the survey to the problem is emphasized by this case history. Use of several coil spacings and frequencies show that the most diagnostic results were found on the low frequency, 100-ft coil spacing survey. A recent paper by N. R. Paterson (1961) reports on this same deposit. An airborne survey conducted over the deposit gave two conductivity-thickness products of 5.6 mhos and 8.8 mhos respectively, values somewhat less than that found by the ground survey.

Conductivity-Thickness of Orebodies

In addition to the examples just discussed, a literature study has been made in an effort to determine the σs values encountered in typical sulfide deposits. The interpretation procedure used was that just discussed. In

Table 1. Conductivity-thickness values

Location	Frequency cps	σs* mhos	Type of conductor	Reference
Caribou L, N.B.	3,600	23	sulfides	Corbett (1961)
Clearwater, N.B., L.16E.	440	N.D.	sulfides	Fleming and Brooks (1960)
200-ft coil	1,760	N.D.		
north edge	3,600	N.D.		
200-ft coil	440	N.D.		
center	1,760	N.D.		
	3,600	N.D.		
200-ft coil	440	15.0		
south edge	1,760	5.7		
	3,600	4.0		
100-ft coil	440	N.D.		
north edge	1,760	N.D.		
100-ft coil	440	330		
center	1,760	230		
100-ft coil	440	14		
south edge	1,760	7		
New Hosco, Que.	876	94	sulfides	McKay & Paterson (1960)
Quebec	2,400	60	sulfides	Bear Creek Files
Quebec	876	140	sulfides	Bear Creek Files
Garon Lake, Que.				McKay & Paterson (1960)
L.4	876	33	sulfides	
L.8	876	140		
Coronation Mine, Sask.				
orebody	3,600	10	sulfides	Rattew (1962)
lake—east edge	3,600	0.4	lake	
—center	3,600	N.D.	lake	
—west edge	3,600	1.1	lake	
Mosher Lake, Sask.				Byers
Zone A L.3200N	3,600	17	sulfides	
L.3800N	3,600	9	sulfides	
Zone B L.3800N	3,600	1	sulfides (dual conductor)	
L.4200N	3,600	5	sulfides	
Zone C L.6600N	3,600	34	sulfides	
Zone D L.7600N	3,600	10	sulfides	
Minnesota	440	23	massive sulfides	Bear Creek Files
	1,760	53		
Desmazures Twp., Que.	3,600	57	sulfides	Bosschart (1961)
	3,600	N.D.		
	3,600	63		
	3,600	60		

* N.D.—not determinable.

Table 1 (Continued)

Location	Frequency cps	σs* mhos	Type of conductor	Reference
Central Sweden	520	31		Tornquist & Bosschart (1958) (Coil separation assumed to be 60m.)
Kankberg, Sweden			sulfides	Malmquist (1958)
L.5440W	3,600	45		
L.5400W	3,600	57		
L.5360W	3,600	25		
L.5300W	3,600	9		
West				
Example 1	876	20	Magnetite & pyrrhotite	West (1960)
Example 3	1,000	10	sulfides	
Example 4	1,000	31	sulfides	

Table 1 the results of this study are compiled. Results from New Brunswick, Quebec, Ontario, Minnesota, and Sweden are shown.

In studying these data it is quite clear that the range of values of σs is strikingly small. Where small values of α were used and a value of σs could be determined, it is readily seen that the values range from one to about 300 mhos. When we consider the fact that in nature σ may vary over a very wide range as may s, this small range is quite striking. Even a set of data collected by Bosschart (1961) from Quebec and Ontario intended to show very high conductivity showed values of σs of the same order of magnitude as the other sulfide deposits studied. All the data from Bosschart's paper are not presented, as several cases were clearly due to multiple conductors. Of the single-conductor cases, only one had an α value so large that it was not possible to evaluate the σs product. A lower-frequency or shorter-coil spacing would have made the value of α less than 100, so that a σs value could have been determined.

In the previously mentioned paper by Paterson (1961) a study of conductivity thickness using an airborne electromagnetic system has been reported. It is interesting to study his data taken from several sulfide deposits in Canada. The conductivity-thickness values given in his paper show a range of 2.2 to 12.8 mhos for 17 separate determinations. This range is somewhat less than that reported in this paper, and it seems that a value between one and 300 mhos is typical for massive-sulfide deposits.

Conclusions

It is concluded that dip, depth, and conductivity-thickness product of tabular conductors can be estimated from horizontal-loop surveys and that it is a useful parameter with sufficient variation to allow distinction between various types of conducting bodies. Typical values for sulfide deposits range between about one and 300 mhos. In planning surveys or designing equipment these typical values need to be considered.

Acknowledgments

The work reported in this paper was conducted in the laboratories of the Geophysics Division of Bear Creek Mining Company. Ralph C. Holmer and G. R. Rogers of that organization instigated this study and encouraged it at all stages. A great deal of the work carried out followed the example of G. F. West of the University of Toronto.

References

Bosschart, R. A., 1961, On the occurrence of low resistivity geological conductors: Geophys. Prosp., v. 9, no. 2.

Byers, A. R., Comparison of electromagnetic geophysical prospecting methods over known sulphide zones in the Flin Flon area, Sask.: Report No. 28, Department of Mineral Resources, Saskatchewan Government.

Corbett, J. D., 1961, An empirical demonstration of geophysical methods across the Caribou deposit, Bathurst, N.B.: Transactions C.I.M.M., v. 64.

Dolan, W. M., 1960, A versatile approach to electromagnetic scale modelling: Paper presented at SEG meeting, Galveston, Texas, no. 10.

Fleming, H. W., and Brooks, R. B., 1960, Geophysical case history of the Clearwater deposit, Northumberland Co., New Brunswick, Canada: Transactions A.I.M.E., v. 217.

Hedstrom, H., and Parasnis, D. S., 1958, Some model experiments relating to electromagnetic prospecting with special reference to airborne work: Geophysical Prospecting, v. 6, no. 4.

——— 1959, Reply to comments by N. R. Paterson: Geophys. Prosp. v. 7, no. 4.

McKay, D. G., and Paterson, N. R., 1960, Geophysical discoveries in the Mattagami district, Que.: C.I.M.M. Trans., v. 53.

Malmquist, D., 1958, The geophysical case history of the Kankberg deposit in the Skellefte district, North Sweden, *in* Geophysical surveys in mining hydrological and engineering surveys: Leiden, E.A.E.G.

Paterson, N. R., 1961, Experimental and field data for the dual-frequency phase-shift method of airborne electromagnetic prospecting: Geophysics, v. 26, no. 5, p. 601–617.

——— 1959, Comments on paper "Some model experiments. . . . " by Hedstrom and Parasnis: Geophys. Prosp., v. 7, no. 4.

Rattew, A. R., 1962, Helicopter-borne electromagnetic, magnetic and radiometric survey, Coronation Mine, Sask.: C.I.M.M. Trans., v. 55.

Slichter, L. B., and Knopoff, L., 1959, Field of an alternating magnetic dipole on the surface of a layered earth: Geophysics, v. 24.

Tornquist, G., and Bosschart, R. A., 1958, Some recent results of geoelectrical prospecting in Sweden, *in* Geophysical surveys in mining, hydrological and engineering surveys: Leiden E.A.E.G.

Wait, J., 1951, Oscillating magnetic dipole over a horizontally stratified earth: Can. Jour. Phys., v. 29.

——— 1954, 1955, 1956, Mutual coupling of loops over a homogeneous ground: Geophysics, v. 19, 290–296, v. 20, p. 630–637, v. 21, p. 479–484.

Wesley, J. P., 1958a, Response of a dike to an oscillating dipole: Geophysics, v. 23, no. 1. p. 128–133.

——— 1958b, Response of a thin dike to an oscillating dipole: Geophysics, v. 23, no. 1, p. 134–143.

West, G. F., 1960, Quantitative interpretation of electromagnetic prospecting measurements: Unpublished Ph.D. thesis, University of Toronto.

APPENDIX IV

Vertical Loop (VLEM) Systems

(Ward, S.H.:1966): The Electromagnetic Method; in Mining Geophysics, Vol. II, p. 356-362. [Reprinted by permission of the author and the Society of Exploration Geophysicists, Tulsa, Oklahoma.]

Table of Contents

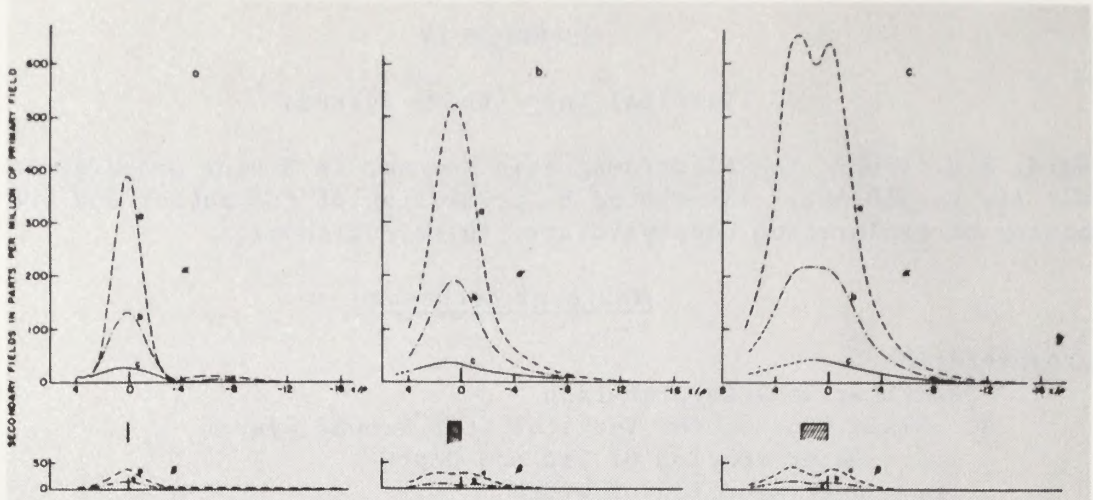

FIG. 152. Effect of conductor width on profiles obtained with Varian-T.G.S. helicopter system. Conductor length 9 ρ; depth extent 8 ρ; dip 90°; height variable: $a=3\ \rho$, $b=4\ \rho$, $c=6\ \rho$; width variable 0.125 ρ, ρ, 2 ρ. Conductivity 565 mho-m. α is the in-phase response and β is the quadrature response. Courtesy Texas Gulf Sulphur Co.

that the curves presented might also be applicable to the Aero Canso system and to the Newmont-Aero helicopter system.

Note that the half-plane is detected at about four times the coil separation on either side of the sheet.

(ii) *Effect of strike.*—The system is relatively insensitive to the direction of flight within plus or minus 30 degrees of normal to the strike of a conductor. Since this is a reasonable tolerance to place on the selected flight direction, the effect of larger deviations from normal to strike would not appear pertinent.

(iii) *Effect of dip.*—As the dip of a large sheet conductor flattens from 90 degrees, the amplitude of the peak response increases substantially, the curve becomes asymmetrical, and three peaks gradually replace the single one.

The hangingwall of the sheet lies under the long flank of the profile and the upper edge of the conductor always lies vertically below the largest peak in the profile.

All of the above features are evident in Figure 150.

(iv) *Effect of multiple conductors.*—Resolution of adjacent sheet conductors by the Varian-T.G.S. helicopter system is indicated in Figure 151. For a system height above conductor of 3ρ, the two sheets are not resolved until they are 2 ρ apart, while for a system height of 5 ρ the two sheets are not resolved until they are 4 ρ apart. Assuming a normal flying altitude of 150 ft and an overburden 50 ft thick, conductors 150 ft apart and greater may be resolved.

(v) *Effect of width.*—Figure 152 reveals that as width increases the peaks broaden until eventually the peak splits. Thus a wide conductor may not be differentiable from two parallel sheet conductors.

VII. Interpretation

A. *Quantitative interpretation*

The first step in electromagnetic interpretation is that of estimating quantitatively the characteristic parameters of the source such as dip, depth, depth extent, width, and conductivity. The next step usually involves correlation of the deduced parameters with independent estimates based on complementary geophysical data such as gravity and magnetics. The third step is the most difficult since it is the establishment of geologic credibility for the quantitative interpretations. With good geologic control the problem is not so severe, but usually we lack such control and must rely upon inference and experience gained from previous case histories.

Most quantitative interpretation—step I—is based on scale model observations over a half-plane or the thicker semi-infinite dike. Provided we analyze a profile over the center of a body of limited strike length, this procedure may be extended to most practical situations we meet. When the depth extent becomes very shallow or the dip very flat, then other models must be introduced. We may match a field curve with one or more members of a catalogue of field curves, or we may analyze certain characteristics of the field curves in terms of the variability of these characteristics and their relationship to source parameters as determined in scale model experiments. Usually we choose the latter procedure.

To see the manner in which quantitative interpretation is normally carried out, let us discuss each method in turn.

(a) *Fixed transmitter vertical loop ground system*

(i) *Determination of dip and depth.*—Several empirical formulas have arisen which enable us to predict the dip and the depth of a sheet conductor from the asymmetry of the dip angle profile and from the maximum dip angle observed. All of them assume that the transmitting coil is vertically above the top edge of the conductor. The most useful method for determining dip and depth is that due to Grant and West (1965). Figure 153 is a reproduction of a figure from their text. A measure of the ratio of maximum dip angle on the footwall to maximum dip angle on the hangingwall plus a measure of the peak-to-peak amplitude permits entry to the diagram. First the dip is obtained directly or by interpolation, then the depth may be

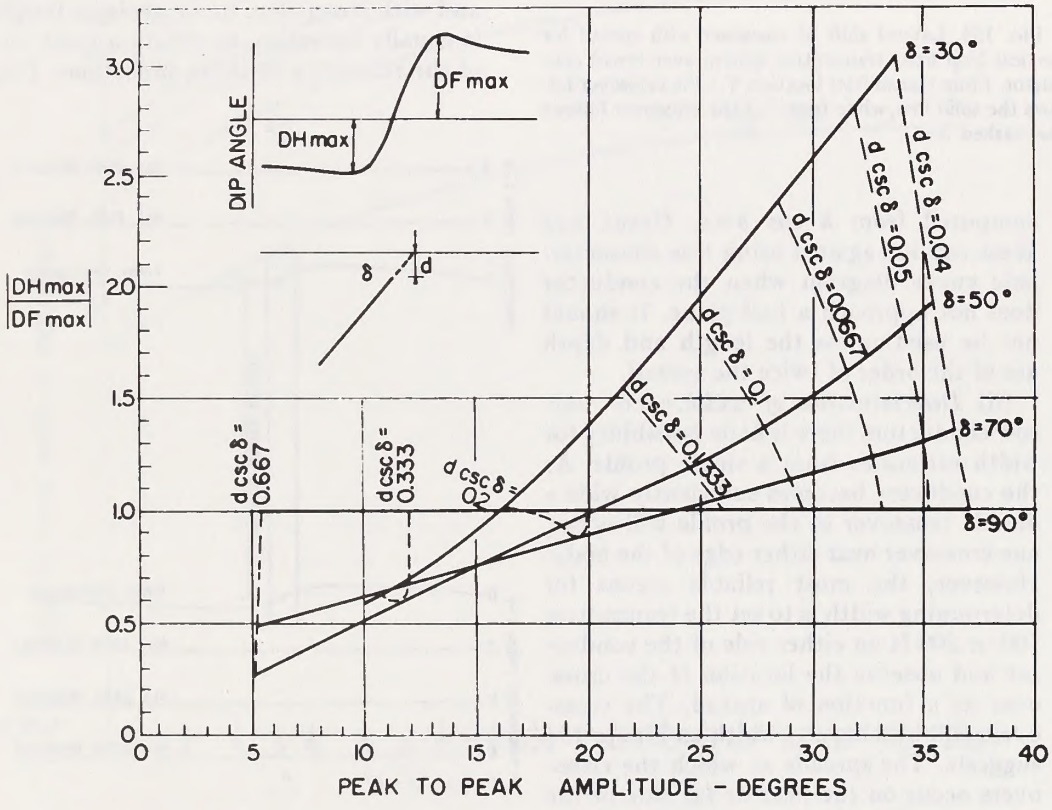

FIG. 153. Characteristic curve diagram yielding depth and dip of conductive half-plane for the vertical loop, fixed-transmitter method. The depth d is given in units of the spread ρ (after Grant and West, 1965).

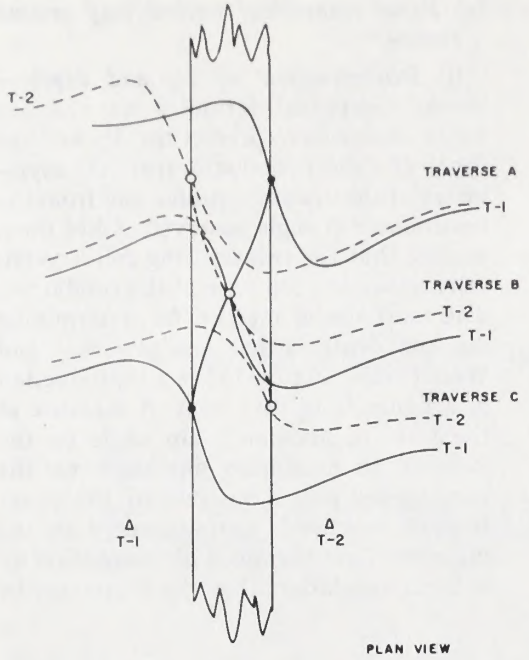

FIG. 154. Lateral shift of crossover with spread for vertical loop fixed transmitter system over broad conductor. From transmitter location T-1 the crossover follows the solid line, while from T-2 the crossover follows the dashed line.

computed from $h \cos \delta = c$. Grant and West caution against using this characteristic curve diagram when the conductor does not approach a half-plane. It should not be used unless the length and depth are of the order of twice the spread.

(ii) *Determination of width.*—For narrow conductors there is little possibility for width estimates from a single profile. As the conductor becomes sufficiently wide a double crossover in the profile will occur, one crossover near either edge of the body. However, the most reliable means for determining width is to set the transmitter 100 or 200 ft on either side of the conductor and observe the location of the crossover as a function of spread. The crossovers will bracket the width as Figure 154 suggests. The spreads at which the crossovers occur on the near or far side of the conductors are functions of conductor width, length, and depth extent.

(iii) *Determination of strike length.*—A profile containing a crossover will occur, when the transmitter is vertically above the conductor, even when the receiving coil is several hundred feet off the end of the conductor. Thus, strike length determination is usually made by setting the transmitter 400 to 800 ft off the end of the conductor, along strike, and traversing every 100 or 200 ft until a crossover is obtained. If this procedure is carried out off both ends, a minimum strike length is that between the first crossovers obtained with the strike offset transmitters. The procedure is illustrated in Figure 155.

(iv) *Determination of strike.*—Where only a single narrow conductor exists, a line joining the crossovers will trace the strike of the conductor. For broad conductors or multiple conductors, allowance must be made for the shift of the crossover with spread, with transmitter location, and with frequency. Some geologic insight is usually necessary to obtain a good idea of the reliability of strike inflections. Usu-

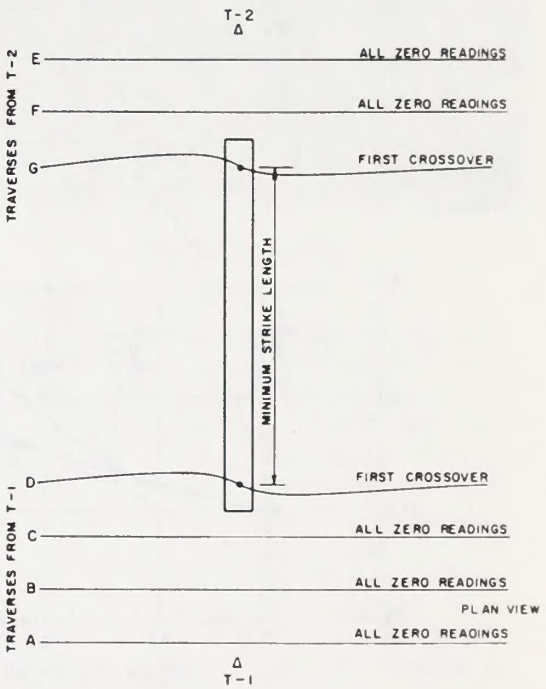

FIG. 155. Transmitter offset off ends of conductor for determination of minimum strike length.

ally it suffices to cross hatch a zone in which conductors are known to occur and thus obtain a mean strike for complex situations.

(v) *Determination of depth extent.*—Criteria for determination of depth extent are not very sensitive unless the ratio of depth extent to depth becomes very small. We have seen from the model curves that shallow depth extent manifests itself in a drop in the flanks of the dip angle profile. Usually one merely notes qualitatively that the depth extent is apt to be limited and employs gravity or magnetics to make a quantitative estimate of the depth extent.

(vi) *Determination of conductivity-thickness product.*—If we plot the ratio of peak high frequency response versus peak low frequency response for various depths and dips of a half-plane, a set of characteristic curves will result, one set for each dip. Such curve families may be obtained by means of scale model experiments and the curves for any given set are drawn for constant depth and for constant induction number $\theta = \sigma\mu\omega t\rho$. Alternatively, we may plot the peak-to-peak response versus known induction number, from model experiments, for each depth. Figure 156 is such a set of curves pertaining to a vertical sheet conductor. This set demands an

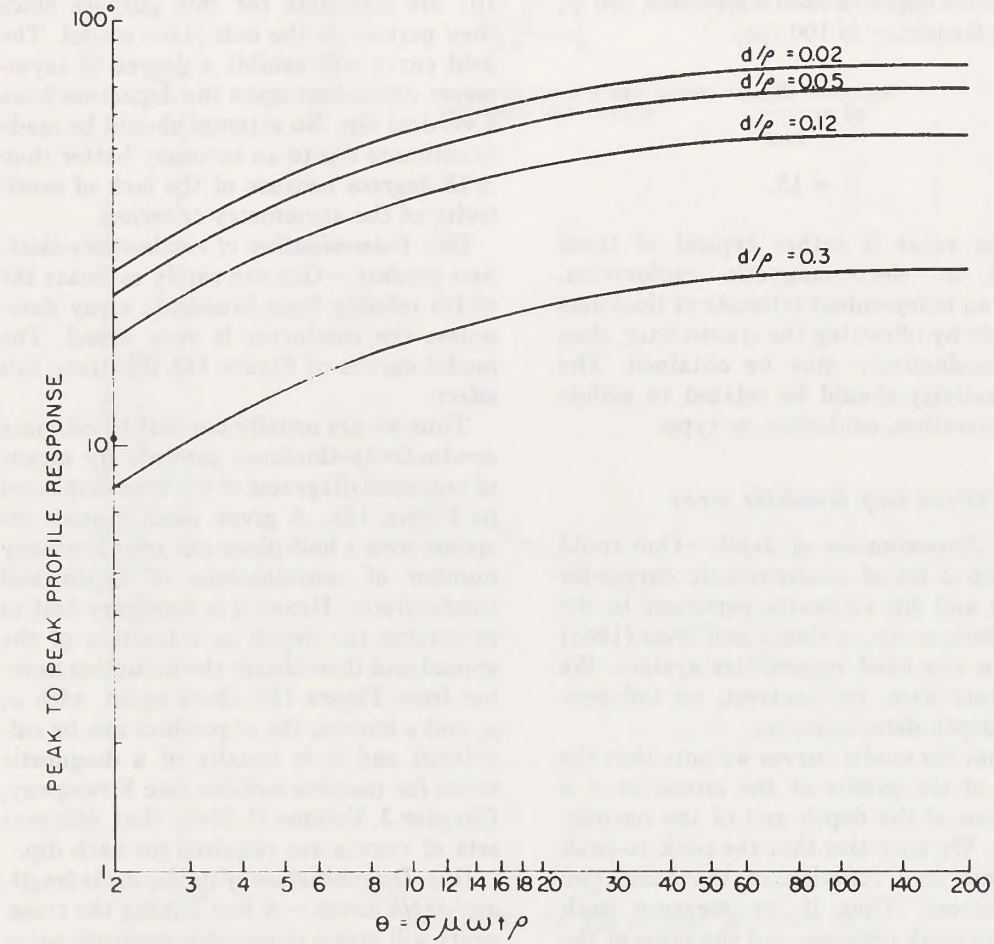

Fig. 156. Universal curves for estimating conductivity-thickness product with vertical loop, fixed transmitter electromagnetic system. Vertical half-plane model. Courtesy Newmont Exploration Ltd.

independent estimate of depth whereas the dual frequency set does not.

To use Figure 156 we note the peak-to-peak response as, say, 40 degrees. This response can arise from a thin sheet of induction number 4.4 and depth 0.02 ρ, or from an induction number of 12 and a depth of 0.12 ρ, or from any similar combination. The independent estimate of depth from Figure 153 permits us to obtain the induction number uniquely.

Since we know the frequency and spread and are prepared to assume the permeability as that of free space in most instances, then we can obtain the conductivity-thickness product. That is, for a peak-to-peak response of 40 degrees and estimated depth of 12 m a spread of 100 m, and a frequency of 100 cps,

$$\sigma t = \frac{\theta}{\mu\omega\rho}$$

$$= 15.$$

This value is rather typical of those found in electromagnetic exploration. Once an independent estimate of thickness is made by offsetting the transmitter, then the conductivity may be obtained. The conductivity should be related to sulfide concentration, oxidation, or type.

(b) *Vertical loop broadside array*

(i) *Determination of depth.*—One could develop a set of characteristic curves for depth and dip estimates pertinent to the broadside array, as Grant and West (1965) did for the fixed transmitter system. We illustrate here, for contrast, an independent depth determination.

From the model curves we note that the slope of the profile at the crossover is a function of the depth and of the conductivity. We note also that the peak-to-peak response is a function of the same two parameters. Thus if we measure both peak-to-peak response and the slope at the crossover as functions of depth and conductivity, we should be able to estimate both parameters. However, we may note that a decrease in conductivity will lower all points by the same fraction so that the ratio of slope to peak-to-peak response should be independent of conductivity. On the other hand, increasing the depth decreases the dip angle an amount dependent upon how far the measuring station is from the conductor axis. Thus a plot of slope to peak-to-peak amplitude versus depth may be obtained from model data and used to interpret field data. Figure 157 is such a plot, the depth and the slope are normalized by the spread ρ.

(ii) *Determination of dip.*—The dip of the conductor is often crudely estimated by curve matching. The curves of Figure 107 are adequate for this purpose since they pertain to the half-plane model. The field curve will exhibit a degree of asymmetry dependent upon the departure from a vertical dip. No attempt should be made to estimate dip to an accuracy better than ± 15 degrees because of the lack of sensitivity of the asymmetry criterion.

(iii) *Determination of conductivity-thickness product.*—One can rarely estimate the width reliably from broadside array data, unless the conductor is very broad. The model curves of Figure 114 illustrate this effect.

Thus we are usually content to estimate conductivity-thickness product by means of universal diagrams of the type displayed in Figure 158. A given peak-to-peak response over a half-plane can arise from any number of combinations of depth and conductivity. Hence it is necessary first to determine the depth as a fraction of the spread and then obtain the induction number from Figure 158. Once again, with ω, μ, and ρ known, the σt product can be calculated and it is usually of a diagnostic value for massive sulfides (see Strangway, Chapter 3, Volume I). Note that different sets of curves are required for each dip.

(iv) *Determination of strike, strike length, and depth extent.*—A line joining the crossovers will give a reasonable approximation to the strike throughout the length of the conductor. Strike length may be deter-

mined approximately from the termination of the line of crossovers.

Depth extent is not generally a parameter which can be obtained with the broadside array unless the depth extent is less than the spread, as Figure 109 indicates.

(c) *Horizontal loop electromagnetic system.*—A sound basis for interpretation of horizontal loop data is contained in Strangway's article in Chapter 3 of Volume I. No additional comments are necessary.

(d) *Hunting Canso Airborne System*

(i) *Determination of conductivity-thickness product.*—An interpretation scheme for this method is contained in an article by Paterson (1961a). Some elements of that scheme follow.

First, Paterson assumed a half-plane as the basic model. Then he determined the fall-off law for the half-plane, as depicted in Figure 140. From this he constructed a correction graph by which he could convert the response at any aircraft height to

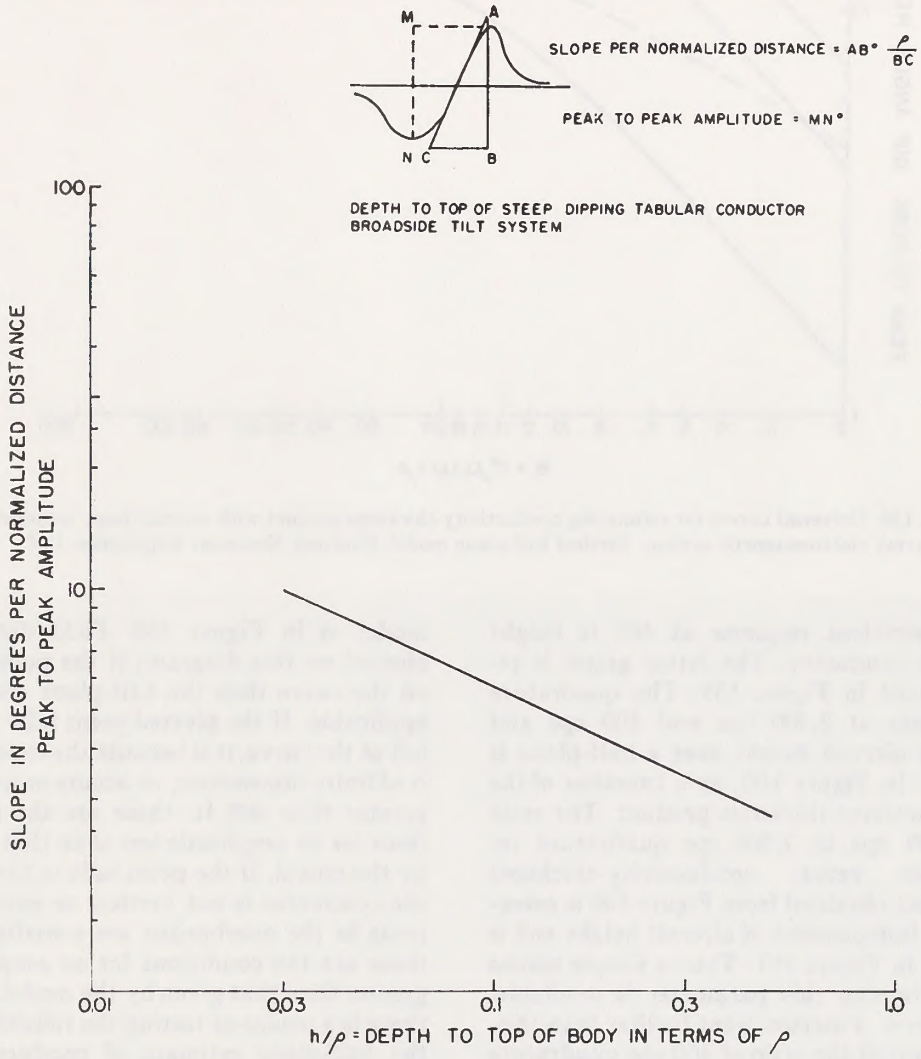

FIG. 157. Diagram for estimating depth from profiles obtained with broadside array vertical loop electromagnetic system. Vertical half-plane model. Courtesy Newmont Exploration Ltd.

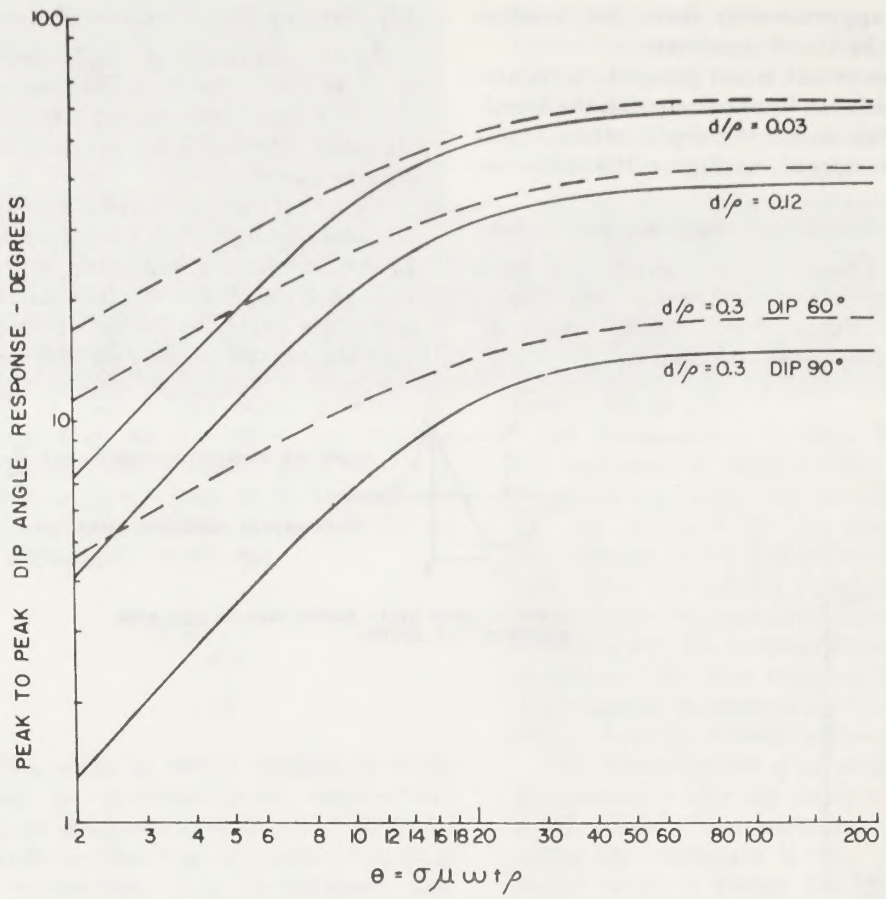

FIG. 158. Universal curves for estimating conductivity-thickness product with vertical loop, broadside array electromagnetic system. Vertical half-plane model. Courtesy Newmont Exploration Ltd.

an equivalent response at 400 ft height above conductor. The latter graph is reproduced in Figure 159. The quadrature response at 2,300 cps and 400 cps and 400-ft aircraft height over a half-plane is given, in Figure 160, as a function of the conductivity-thickness product. The ratio of 400 cps to 2,300 cps quadrature responses versus conductivity-thickness product obtained from Figure 160 is essentially independent of aircraft height and is given in Figure 161. Thus a simple means of obtaining this parameter is available. However, Paterson went further than this. He plotted the ratio of 400 cps quadrature to 2,300 cps quadrature versus 400 cps quadrature response for the half-plane model as in Figure 162. Field data are plotted on this diagram; if the points fall on the curve then the half-plane model is applicable. If the plotted point falls to the left of the curve, it is because the conductor is of finite dimensions, or occurs at a depth greater than 400 ft; these are the conditions for an amplitude less than that given by the model. If the point falls to the right the conductor is not vertical or eddy currents in the overburden are contributing; these are the conditions for an amplitude greater than that given by the model. Thus there is a means of testing the reliability of the half-plane estimate of conductivity-thickness product. A more conventional phasor diagram for estimating the conduc-

Appendix V

APPENDIX V

The TURAM System

(Duckworth, K.:1973): An Alternative Approach to TURAM Data Treatment; The Canadian Mining and Metallurgical Bulletin, October, 1973. [Reprinted by permission of The Canadian Institute of Mining and Metallurgy.]

Table of Contents

An Alternative Approach to Turam Data Treatment

K. DUCKWORTH, Assistant Professor,
Department of Geology,
University of Calgary,
Calgary, Alberta

ABSTRACT

The treatment of Turam data by conventional procedures does not permit the interpreter to make any estimate of induced current magnitudes. This problem may be overcome by using an alternative data treatment procedure. It is shown that the conventional and alternative procedures are equally satisfactory in terms of their ability to provide the location of line currents and estimates of conductor quality. A full description and evaluation of both procedures is presented in conjunction with field examples to show how the alternative procedure may assist interpretation when used to complement the conventional approach.

INTRODUCTION

IN THE SEARCH for ore structures which are buried at depths greater than 200 feet, the Turam electromagnetic prospecting system is known to have a marked advantage over most of the other electromagnetic systems. This advantage is due to the type of primary field source used by this system, which is able to transmit a field which loses power with distance much less rapidly than do most source fields. With the inevitable increase in our need to search at greater depth, it is probable that the Turam system will see increasing use.

In anticipation of an increase in interest in this prospecting system, the present discussion is concerned with providing the potential user with a knowledge of some features of the system which have not received much attention in other publications. The particular aim of the discussion is to illustrate features of the conventional data treatment procedures which can mislead the interpreter and to present an alternative procedure which in some respects the user may find more helpful. In suggesting that the new data treatment procedure be followed, it is recommended that it only be used as an additional aid to complement the conventional approach.

Recent discussions of the Turam system have been presented by Grant and West (1965), Keller and Frischknecht (1966), and Parasnis (1966), but the most comprehensive study available is that by Bosschart (1964). However, in order to facilitate the understanding of the present discussion for the reader who is not familiar with the system, a brief review of the working principles and the conventional data reduction procedures is presented here. In addition, field examples of some of the features discussed are given.

K. DUCKWORTH obtained a B.Sc. in physics from the University of Leeds, England, in 1960 and a Ph.D. in applied geophysics from the same institution in 1964. His thesis involved the investigation of Upper Coal Measure structures in the north of England by means of gravity surveys.

He joined the Australian Bureau of Mineral Resources in 1964, and was posted to the Uranium Group based in Darwin. His duties involved organizing and conducting geophysical surveys in the area around the Rum Jungle mine. As a result of this work, he developed an interest in the application of electromagnetic depth sounding to mining problems.

Dr. Duckworth joined the University of Calgary in 1968 as Assistant Professor in the Geology Department. His research interests currently center around the development of electromagnetic prospecting techniques.

PAPER SUBMITTED: in June of 1972; revised manuscript received in April of 1973.

KEYWORDS: Geophysical exploration, Turam data, Data treatment, Electromagnetic surveys, Induced currents, Conductors, Magnetic fields, Argand diagrams, Field strength, Reduction procedures.

OPERATING PRINCIPLES

The Turam system is characterized by its use of a fixed source of primary electromagnetic field. The normal form of this source is a large rectangular loop of wire lying on the ground surface. The dimensions of this rectangle are usually so large that, if work is conducted near one of the long sides of the loop and remote from the ends, the source may be effectively approximated as a single, infinitely long, horizontal, straight wire. The passing of an alternating current through this wire generates an alternating magnetic field around the wire which obeys an inverse first-power law of attenuation as distance from the wire increases. The geometry of this primary field is such that any current which it induces to flow in a subsurface conductor will tend to flow parallel to the source line. This can be appreciated by considering that the efficiency of the induction process is maximum for structures parallel to the source line and zero for structures perpendicular to the source line. Experience and theory show that such currents behave as concentrated line currents which are confined to the edges of conductive structures. For example, the currents induced into a thin tabular conductive ore structure with large dip would behave as a single line current flowing along the top edge, as shown in Figure 1. (This model assumes infinite depth and strike extent to avoid consideration of return current paths.) If the strike direction of a structure is known the source line is normally laid parallel to it, in order to maximize the induction process. In addition, if the dip of a structure is known, the induction process can be further improved by placing the source on the up-dip side of the structure, as shown by Bosschart (1964).

The induced secondary currents also generate magnetic fields so that, in the environment of the source wire, the observed magnetic field is the vector resultant of the primary and secondary fields. It is the

spatial behaviour of this resultant field which is of interest and the Turam system normally only investigates the behaviour of the vertical component of the resultant field. This is achieved in practice by sampling the horizontal gradient of the vertical component.

To appreciate the behaviour of the resultant vertical component, consider points A and B situated on a traverse line perpendicular to the source line in Figure 1. The induction process causes the induced current to have a phase lag of 90° + δ with respect to the primary current. Thus the secondary field will also lag behind the primary field by this same amount at all points in space. This is shown in the two Argand (vector-phase) diagrams in Figure 1, which represent the field relationships at A and B respectively. We can see that in moving from A to B there is a marked change in the magnitudes of the primary field, P, and the secondary field, S, but their phase relationship is constant. The vector combination of P and S gives a resultant vertical component, R, with a phase angle, θ, with respect to P. The magnitudes of R and θ are evidently dependent upon the magnitudes of P and S, which in turn are functions of spatial position. The parameters which are in fact observed with the Turam system are the field strength ratio (FSR), i.e. R_A/R_B, and the phase angle difference ($\triangle\theta$), i.e. $\theta_B - R_A$. This is achieved by operating two receiving coils simultaneously at points A and B and comparing the received signals by means of a polar AC potentiometer. Surveying procedure consists of traversing these two coils at fixed spacing along the same line over the conductive structure and observing the variation of the FSR and $\triangle\theta$ parameters along that line.

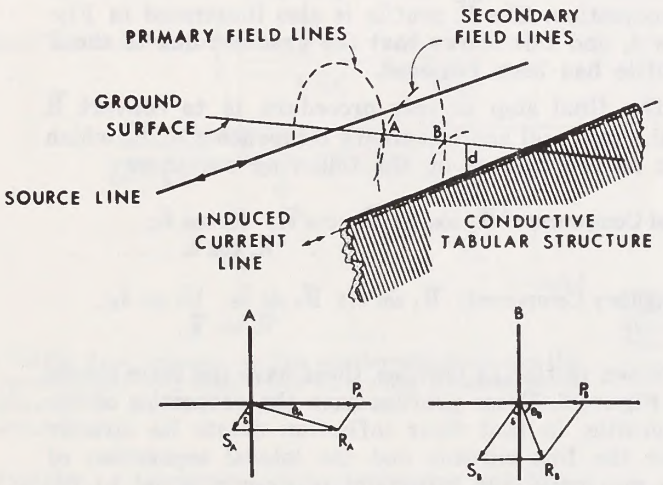

FIGURE 1 — Magnetic field relationships at two points on a Turam traverse over a thin steeply dipping tabular conductor.

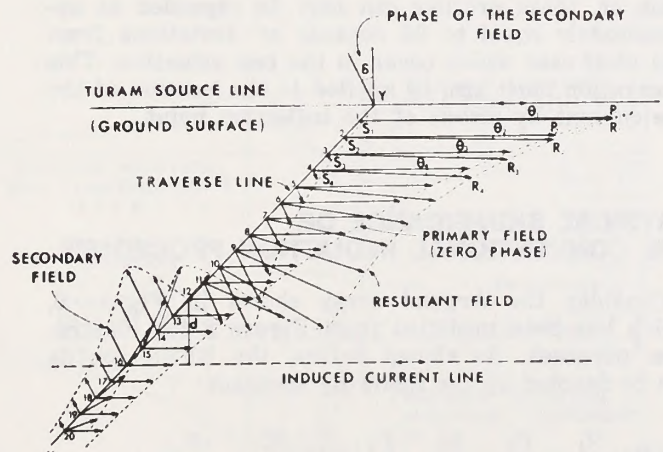

FIGURE 2 — The behaviour of primary, secondary and resultant magnetic fields represented by an array of Argand diagrams (phase plotted opposite to normal convention and scale modified to facilitate illustration).

The behaviour of the P, S, R and θ parameters along a traverse line which crosses a single induced line current is shown in Figure 2, which consists of an array of Argand diagrams. (The depth of the line current is equal to twice the station spacing.) Notable features are the attenuation of the P vectors as distance from the source increases and the reversal of phase of the S vectors as the point of observation crosses the induced current line. A clearer view of the R and θ behaviour is shown in Figure 3, which is a view along the XY axis of Figure 2. It should be noted that phase lag has been plotted in an anticlockwise sense to facilitate these illustrations, but that this does not affect the behaviour of R and θ. In addition, the scale of the vector amplitudes was increased in Figure 3 for the sake of clarity.

An alternative presentation of the variation of these parameters is shown in Figure 4, where each parameter is represented by a magnitude profile. The FSR and $\triangle\theta$ profiles of Figure 5 were derived direct from the R and θ profiles of Figure 4 by a digital procedure which simulated the mode of action of the Turam system. This shows that we can expect a peak in the FSR profile almost directly over the line current and a corresponding negative trough in the $\triangle\theta$ profile.

It is evident from this illustration that the FSR and $\triangle\theta$ anomalies do not provide the exact location of the line current. However, if we are able to transform the data so that it gives us the S profile, or a

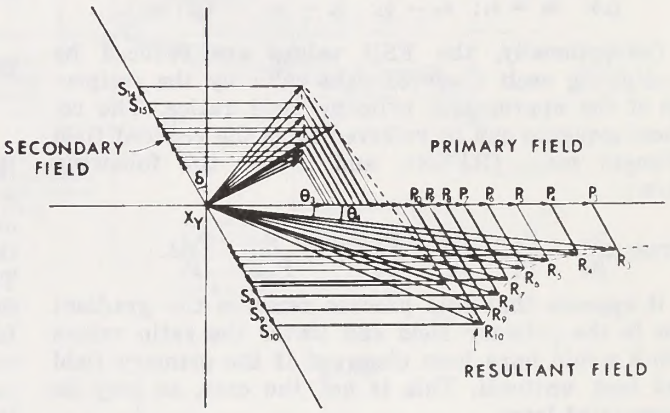

FIGURE 3 — The superimposed Argand array derived from Figure 2 to facilitate illustration of the behaviour of R and θ.

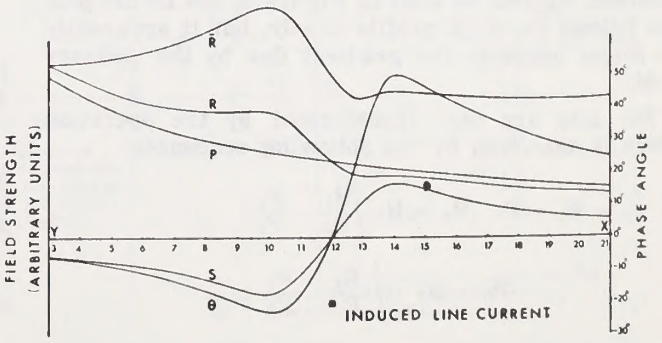

FIGURE 4 — Magnitude profiles of the magnetic fields ($\overline{R}$ being the reduced magnetic field).

profile which has the same properties as the S profile, we can not only locate the line current but measure its depth. This is based on the following considerations.

The secondary field vertical component function has the form

$$S = K \frac{i\,x}{x^2 + d^2} \qquad (1)$$

where K is a constant (magnitude dependent on system of units)

i = the induced current
x = horizontal displacement from the line current
d = the depth of the line current

This function is zero for $x = 0$ and symmetrical, so that the inflection point on the S profile of Figure 4 must lie over the line current. Taking the first horizontal derivation we get

$$\frac{dS}{dx} = Ki \frac{d^2 - x^2}{(d^2 + x^2)^2} \qquad (2)$$

This function is zero when $d = \pm x$, so the displacement of the maximum and minimum from the inflection point on the S profile is exactly equal to the depth to the line current.

CONVENTIONAL REDUCTION AND INTERPRETATION PROCEDURE

Turam survey data can be described by the following sequences, which use the notation of Figure 2.

$$\text{FSR: } \frac{R_1}{R_2}, \frac{R_2}{R_3}, \frac{R_3}{R_4}, \ldots \frac{R_n}{R_{n+1}}; \ldots$$

$$\Delta\theta: \ \theta_2 - \theta_1; \ \theta_3 - \theta_2; \ \theta_4 - \theta_3; \ldots \theta_{n+1} - \theta_n; \ldots$$

Conventionally, the FSR values are reduced by multiplying each observed data value by the reciprocal of the appropriate primary field ratios. The reduced sequence can be referred to as the reduced field strength ratio (RFSR), and it has the following form:

$$\text{RFSR: } \frac{R_1}{R_2} \cdot \frac{P_2}{P_1}; \frac{R_2}{R_3} \cdot \frac{P_3}{P_2}; \ldots \frac{R_n}{R_{n+1}} \cdot \frac{P_{n+1}}{P_n}; \ldots$$

It appears that this process removes the gradient due to the primary field and leaves the ratio values which would have been observed if the primary field had been uniform. This is not the case, as may be appreciated later.

The initial presentation of data is in the form of RFSR and $\Delta\theta$ profiles, the latter being plotted as observed. As can be seen in Figure 5, the RFSR profile follows the FSR profile closely, but it apparently no longer contains the gradient due to the primary field.

The data are next transformed by the operation which is described by the following sequences:

$$\bar{R}: \ \bar{R}_1 = R_1 = P_1; \ \bar{R}_2 = R_1 \Big/ \frac{R_1}{R_2} \cdot \frac{P_2}{P_1}; \ldots$$

$$\ldots \ \bar{R}_3 = \bar{R}_2 \Big/ \frac{R_2}{R_3} \cdot \frac{P_3}{P_2}; \ldots$$

[i.e., $\bar{R}_1 = P_1$; $\bar{R}_2 = \bar{R}_1/(\text{RFSR})_1$; $\bar{R}_3 = \bar{R}_2/(\text{RFSR})_2$; ...]

$$\bar{\theta}: \ \bar{\theta}_1 = \theta_1 = 0; \ \bar{\theta}_2 = \bar{\theta}_1 + \Delta\theta_{21}; \ \bar{\theta}_3 = \bar{\theta}_2 + \Delta\theta_{32}. \ldots$$

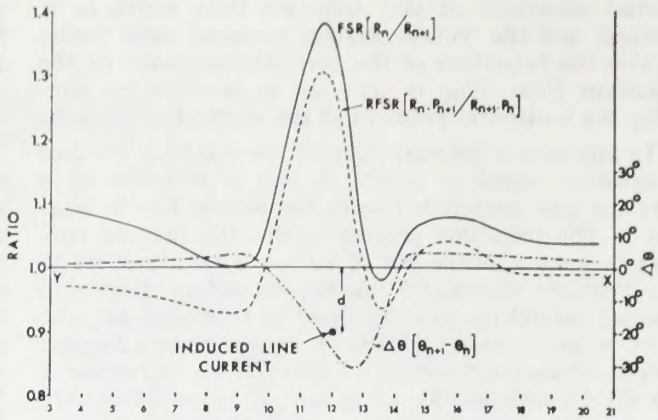

FIGURE 5 — Profiles of field strength ratio (FSR), reduced field strength ratio (RFSR) and phase difference ($\Delta\theta$) over a single induced line current.

This involves the assumption that at some point, such as 1 in Figure 2, the primary and resultant fields are almost identical and, in the case shown, this can be seen to be a good approximation. The $\bar{\theta}$ values are denoted here in this way to correspond to the use of the $\bar{R}$ notation, but they could be denoted by θ as this is the sequence which would provide the θ profile of Figure 4 — subject to the quality of the initial approximation. The $\bar{R}$ profile is also illustrated in Figure 4, and this shows that the gradient due to the P profile has been removed.

The final step in this procedure is to convert $\bar{R}$ and $\bar{\theta}$ into real and imaginary components of $\bar{R}$, which can be represented by the following sequences:

$$\text{Real Component: } \bar{R}_1 \cos\bar{\theta}_1; \ \bar{R}_2 \cos\bar{\theta}_2; \ \bar{R}_3 \cos\bar{\theta}_3; \ldots \ldots \bar{R}_n \cos\bar{\theta}_n; \ldots$$

$$\text{Imaginary Component: } \bar{R}_1 \sin\bar{\theta}_1; \ \bar{R}_2 \sin\bar{\theta}_2; \ \bar{R}_3 \sin\bar{\theta}_3; \ldots \ldots \bar{R}_n \sin\bar{\theta}_n; \ldots$$

When plotted as profiles, these have the form shown in Figure 8. These profiles have the properties of the S profile, in that their inflection points lie directly over the line current and the lateral separation of the maximum and minimum is exactly equal to 2d. They do, however, differ from the S profile in that they are not symmetrical about the inflection point. In practice, the separation of the maximum and minimum on these profiles can only be regarded as approximately equal to 2d because of deviations from this ideal case which occur in the real situation. This reservation must also be applied to the location of the line current by means of the inflection point.

PHYSICAL SIGNIFICANCE OF THE CONVENTIONAL REDUCTION PROCEDURE

Consider the Argand array shown in Figure 6, which has been modified from Figure 2 for illustration purposes. As shown before, the RFSR profile can be denoted by the following sequence:

$$\text{RFSR: } \frac{R_1}{R_2} \cdot \frac{P_2}{P_1}; \frac{R_2}{R_3} \cdot \frac{P_3}{P_2}; \ldots \frac{R_n}{R_{n+1}} \cdot \frac{P_{n+1}}{P_n}; \ldots$$

Now consider the projection of the vectors R_1, R_2, R_3 . . . to form the vectors X_1, X_2, X_3 . . . as shown in

Figure 6. By the geometry of the diagram we can say that

$$\frac{R_2}{X_2} = \frac{P_2}{P_1} ; \frac{R_3}{X_3} = \frac{P_3}{P_1} ; \ldots\ldots \frac{R_n}{X_n} = \frac{P_n}{P_1} ; \ldots\ldots$$

$$\text{i.e. } X_2 = \frac{R_2 P_1}{P_2} ; X_3 = \frac{R_3 P_1}{P_3} ; \ldots\ldots X_n = \frac{R_n P_1}{P_n} ; \ldots\ldots\ldots$$

and $X_1 = R_1$, as can be seen.

Thus

$$\frac{X_1}{X_2} = \frac{R_1}{R_2} \cdot \frac{P_2}{P_1} ; \frac{X_2}{X_3} = \frac{R_2}{R_3} \cdot \frac{P_3}{P_2} ; \ldots\ldots\ldots$$

$$\ldots\ldots\ldots\ldots \frac{X_n}{X_{n+1}} = \frac{R_n}{R_{n+1}} \cdot \frac{P_{n+1}}{P_n} \ldots\ldots\ldots\ldots$$

However, this is the RFSR sequence, so that $X_n = \overline{R}_n$, and we see that the conventional reduction procedure is equivalent to this proportionate amplification of each R vector.

The effect of applying this construction to the whole of Figure 2 is shown in Figure 7. This permits us to see that the real and imaginary components of $\overline{R}$ must reach their maximum and minimum at the same point, as does the S profile. This diagram omits P_1 and P_2 for convenience in illustration, but this does not affect the principles described here.

By plotting the real and imaginary values of X from Figure 7 we get the real and imaginary component profiles of $\overline{R}$ referred to earlier, as shown in Figure 8.

A consideration which has received little attention in the literature is the possibility that the magnitudes of the RFSR and $\triangle\theta$ anomalies are dependent on the distance between the source and target. It is evidently desirable that a conductor should not generate different Turam anomalies when the source distance is changed.

However, it is inevitable that an increase in the distance of the source from the target will cause an attenuation of the magnitude of the induced current. We must ask whether it is possible for the RFSR and $\triangle\theta$ anomalies to retain the same magnitudes when the source-to-target distance is increased. In one idealized case this is possible, as shown in the vector diagram of Figure 9. This shows the effect of moving the source away from the target in steps. With the target situated only eight stations away from the source, the induced current and its magnetic field are quite

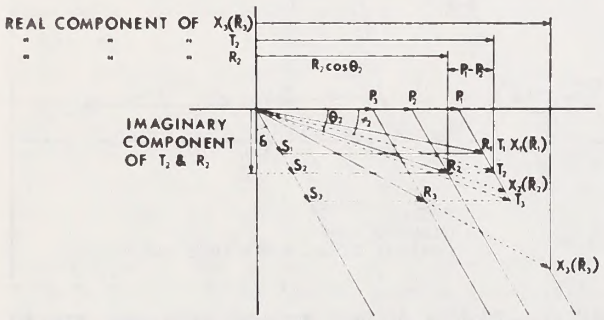

FIGURE 6 — (above) — The relationship between the conventional and alternative reduction procedures is shown by the relationship between the X and T vectors.

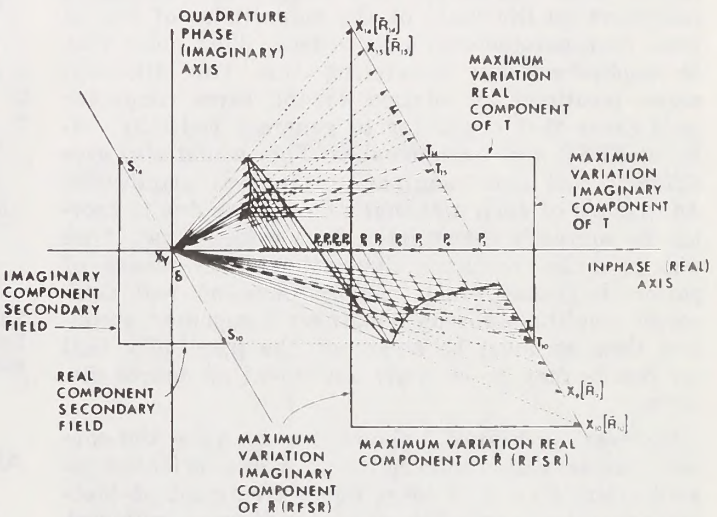

FIGURE 7 — (right) — The conventional and alternative reduction procedures applied to the Argand array shown in Figure 3.

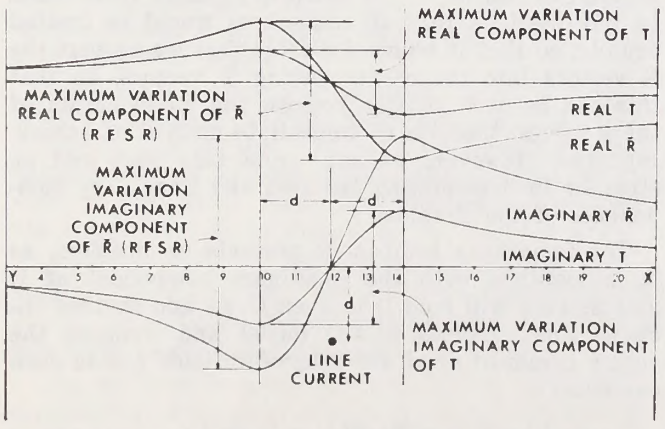

FIGURE 8 — Real and imaginary field component magnitude profiles derived by the conventional ($\overline{R}$) and alternative (T) reduction procedures.

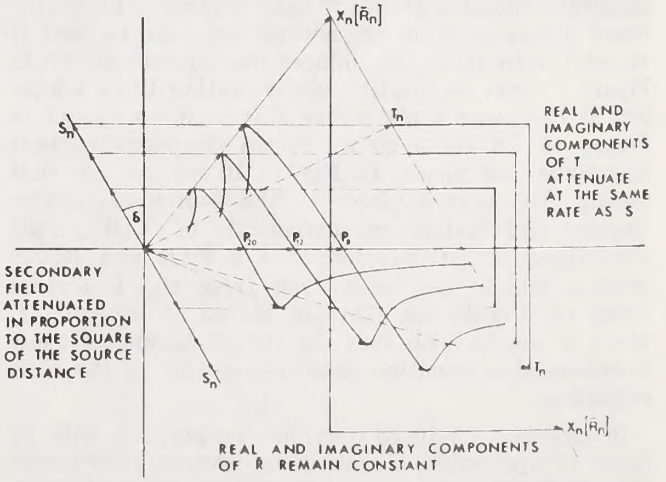

FIGURE 9 — The real and imaginary components of R will remain constant with increasing source distance if the magnitude of S experiences an inverse first-power attenuation. The components of T exactly reflect the behaviour of S

strong. Moving the source to a position twenty stations from the target causes marked attenuation of the secondary field due to the attenuation of the primary field at the target. If, as shown here, the rate of attenuation of the P and S fields is the same, then the magnitudes of the projected $X(\overline{R})$ vectors are independent of the change in source distance. Therefore, in this special case, the RFSR and $\triangle\theta$ profiles which may be derived from the $X(\overline{R})$ and θ profiles will also be independent of source distance.

In this special case, the S field must be experiencing an inverse first-power law of attenuation of its peak magnitude as source distances increase in order to correspond to the same law which controls attenuation of the P field.

In practice, we may expect that an inverse first-power law of attenuation of the induced current and S field will quite often fail to operate. This may be appreciated when we consider that the influence of conductor geometry (such as dip) on the inductive linkage will also vary with change of source distance. This geometric contribution will not follow any uniform law, so that only in the absence of its influence will the conditions described above be achieved.

Therefore, we may expect that the RFSR and $\triangle\theta$ anomalies, along with the real and imaginary components of $\overline{R}$, may often display an irregular dependence on source distance. This means that comparing conductors on the basis of the magnitudes of any of these four parameters is hazardous. This point may be emphasized by considering that two different source positions in relation to the same conductor could cause that conductor to generate radically different RFSR and $\triangle\theta$ anomalies. This would also give different real and imaginary component amplitudes. An example of such a change of response due to moving the source is shown later. It is evident that if we wish to make conductor size estimates by means of phasor diagrams which employ plots of real component amplitude versus imaginary component amplitude then we must be aware of the possibility that our results may be strongly dependent on source distance.

However, as Figure 9 shows, we can view the conventional reduction procedure as being oriented toward attempting to achieve equal treatment of identical conductors regardless of source distance, although this also means that it gives very unequal treatment to identical induced currents if they happen to lie at different distances from the source. This can be seen if we arbitrarily move the induced line current shown in Figure 7 from its location under station 12 to a location at the same depth under station 8, as shown in Figure 10. In doing so we retain the same current magnitude and phase. In Figure 10 we can see that moving the current closer to the source attenuates the real and imaginary components of $X(\overline{R})$. This also causes an attenuation of the FSR and RFSR profiles, which can be derived from the R and $\overline{R}$ values of Figure 10. This is shown in Figure 11, where it can be seen that the RFSR anomalies show an enhanced attenuation compared to that of the FSR anomalies.

In practice, induced current magnitude will be found to approximately obey an inverse first-power law of attenuation in a considerable number of cases. The main concern of the present discussion is to emphasize that exceptions are quite common, as shown by the practical examples given later.

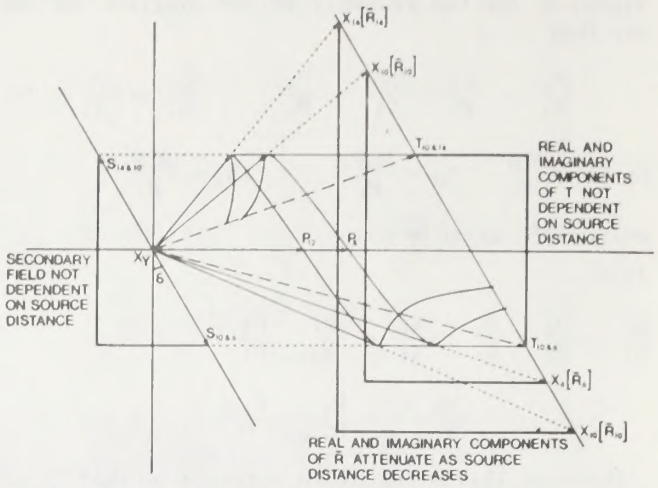

FIGURE 10 — Line currents of magnitude and phase equal to those of the line current in Figure 7 are here situated under Stations 8 and 12. The components of T may be seen to be invariant with change of source distance, whereas the components of $\overline{R}$ are attenuated.

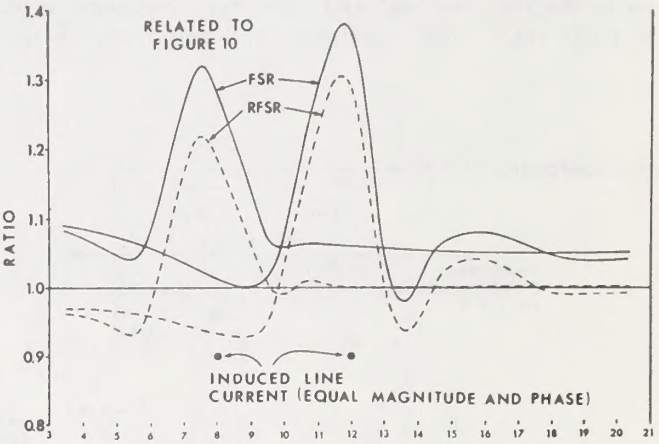

FIGURE 11 — Profiles of field strength ratio and reduced field strength ratio over equal line currents, showing the attenuation of both profiles as source distance is reduced.

AN ALTERNATIVE REDUCTION PROCEDURE

If we return to Figure 6, we can see that if the primary field had been uniform and of magnitude equal to P_1 the resultant field would have been described by the vectors T_1, T_2, T_3 — and not by the vectors, $\overline{R}_1$, $\overline{R}_2$, $\overline{R}_3$, . . . A uniform primary field would be our ideal, in that all conductors would be treated equally, so that it seems desirable that we convert the R vectors into the corresponding T vectors. In that this can be seen to also require the modification of the θ values, there is no immediate method of achieving this. However, we can avoid this step and go straight to determining the real and imaginary components of the T values.

The imaginary component presents no problem, as it is identical with the imaginary component of R and S. This will hold true even if we add further induced line currents to the model and compute the vector resultant of all the magnetic fields due to such currents:

$$\text{e.g.: } T_2 \sin \phi_2 = R_2 \sin \theta_2 = S_2 \sin \delta$$

where ϕ_n is the phase angle of T_n

i.e. Imaginary Component of $T_n = R_n \sin \theta_n$

The real component may be derived by considering the geometry of Figure 6. The vector difference of T_2 and R_2 is equal to the vector difference of P_1 and P_2 and also equal to the vector difference of the real components of R_2 and T_2:

i.e. Real Component of $T_n = R_n \cos \theta_n + (P_1 - P_n)$

If we apply this construction, as shown in Figure 7, we can see that the real component variation of the T vectors has the same amplitude as the real component variation of the S vectors. A plot of magnitudes of the real and imaginary components of T which were derived from Figure 7 is shown in Figure 8. It is readily appreciated that these profiles have all the properties of the S profile, including the symmetry. This latter point may be valuable in that recognition of the inflection point may be easier with these symmetrical profiles than with the unsymmetrical profiles derived from $\overline{R}$.

We could, of course, convert the real and imaginary components of T_n into values of S_n by using the following expression:

$S_n = [(\text{Real Variation } T_n)^2 + (\text{Imag. Variation } T_n)^2]^{1/2}$

However, this will not be valid if we have more than one induced line current operating. It is also possible to derive values of T_n and θ_n, but these would not serve any additional purpose in the interpretation.

We can see in Figure 10 that identical currents must generate identical real and imaginary components of T, regardless of source distance. Thus we now have a data treatment procedure which automatically treats induced currents in proportion to their magnitude. The magnitude of the induced current is easily derived from S by use of equation (1). In practice this can be useful in that lacking any knowledge of the geometry of a conductor, we may gain some information about geometry if we find that on increasing the source distance the induced current magnitude does not show an inverse first-power attenuation. The conventional procedure tends to discard this information.

We may also compute the phase of the induced current from either the $\overline{R}$ or T components:

$$\text{i.e. } \delta = \tan^{-1}\left[\frac{\text{Real Component Variation } (\overline{R} \text{ or T})}{\text{Imaginary Component Variation } (\overline{R} \text{ or T})}\right]$$

This is a measure of the quality of the conductor in that δ tends to 90 degrees for very good conductors and 0 degrees for poor ones.

Thus, this alternative procedure can provide us with the location, depth, magnitude and phase of a single isolated induced current. The conventional procedure does not attempt to provide a current magnitude; in fact, as we have seen, it tends to standardize the response of all line currents.

It can be seen that the two procedures are complementary and that the alternative procedure can be viewed as current-oriented whereas the conventional procedure is conductor-oriented.

The alternative procedure does not in fact achieve a synthesis of the data which a truly uniform primary field would provide, because it does not compensate for the decrease in induced current magnitude with increasing source distance.

The location of the line current can be determined by the use of either the real or imaginary components of T, and it is inevitable that if a Turam anomaly is generated by a single isolated line current both real and imaginary components will give exactly the same location. However, in practice the main induced current may often be accompanied by a number of other weaker satellite currents of different phase, flowing in paths close to that of the main current. If these currents go unrecognized and the interpreter assumes that only a single line current exists, then the interference of these unrecognized currents can cause the real and imaginary profiles to provide separate locations for the line current both laterally and in depth. This is to be expected regardless of which reduction procedure is used.

We can summarize the alternative data treatment procedures by means of the following sequences.

As before, the observed data consist of

$$\text{FSR: } \frac{R_1}{R_2}\ ;\ \frac{R_2}{R_3}\ ;\ \frac{R_3}{R_4}\ ;\ \ldots\ldots\ \frac{R_n}{R_{n+1}}\ ;\ \ldots\ldots$$

$$\Delta\theta = \theta_2 - \theta_1;\ \theta_3 - \theta_2;\ \theta_4 - \theta_3;\ \ldots\ldots\ \theta_{n+1} - \theta_{nj}\ \ldots\ldots$$

Now we can convert directly to R and θ (instead of to RFSR and then $\overline{R}$ and θ).

$$\text{R:]}\ R_1 = P_1;\ R_2 = R_1 \cdot \frac{R_2}{R_1};\ R_3 = R_2 \cdot \frac{R_3}{R_2};\ \ldots\ldots\ldots$$

$$[\text{i.e. } R_1 = P_1;\ R_2 = R_1/(FSR)_1;\ R_3 = R_2/(FRS)_2;\ \ldots\ldots]$$

$$\theta;\ \theta_1 = 0;\ \theta_2 = \theta_1 + \Delta\theta_{21};\ \theta_3 = \theta_2 + \Delta\theta_{32};\ \ldots\ldots\ldots$$

The real and imaginary components of T are then given by:

Real Component T:

$$R_1 \cos\theta_1 + (P_1 - P_1);\ R_2 \cos\theta_2 + (P_2 - P_1);$$
$$\ldots\ldots\ldots\ldots R_3 \cos\theta_3 + (P_3 - P_1)\ldots\ldots$$

Imaginary Component T:

$$R_1 \sin\theta_1;\ R_2 \sin\theta_2;\ R_3 \sin\theta_3\ ;\ \ldots\ldots\ldots\ldots\ldots$$

This process is slightly less lengthy than the conventional one, which requires an extra step in the construction of the RFSR sequence. As in the conventional procedure an approximation is made in stipulating $R_1 = P_1$. This approximation will be unsatisfactory if the target lies near the source and its use will cause asymmetric profiles of real and imaginary components of T to be derived.

FIELD EXAMPLES

The field examples shown in Figures 12 and 13 are taken from work performed in the Northern Territory of Australia. The conductors involved proved to be uneconomic graphitic shale beds, but they provide good examples of the type of Turam anomaly which can be misleading.

In Figure 12, the traverse line is shown crossing two conductors which were on the limb of a small chevron anticline. This RFSR profile is a good example of Turam response which shows the influence of the dip of the conducting structures. The model experiments performed by Bosschart (1964) showed that structures which dip away from the source may be expected to be more effectively linked with the

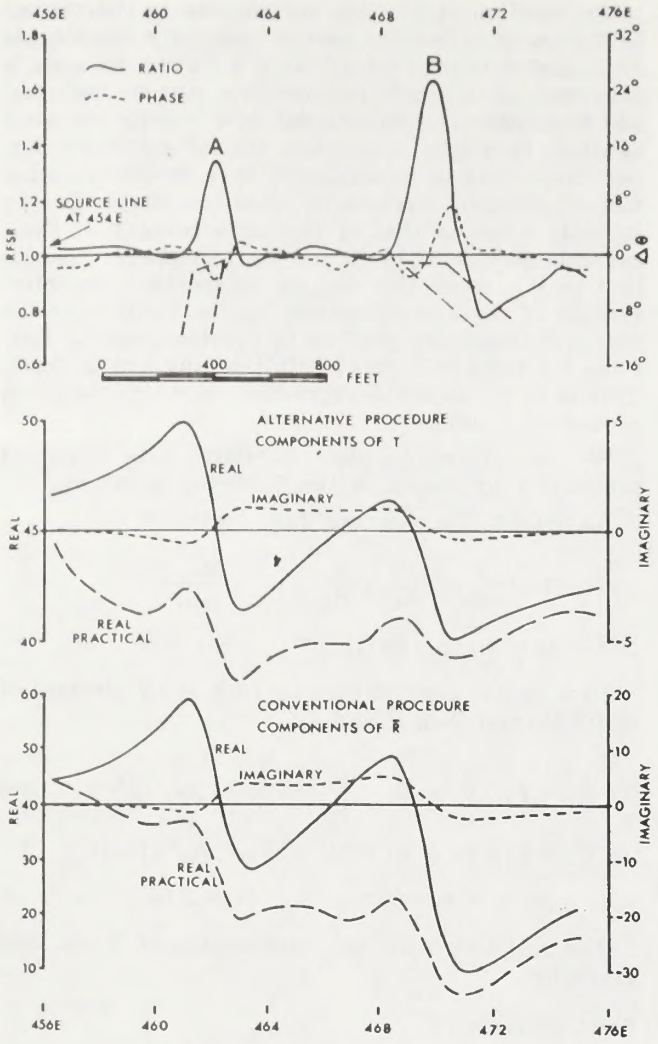

FIGURE 12 — Field example.

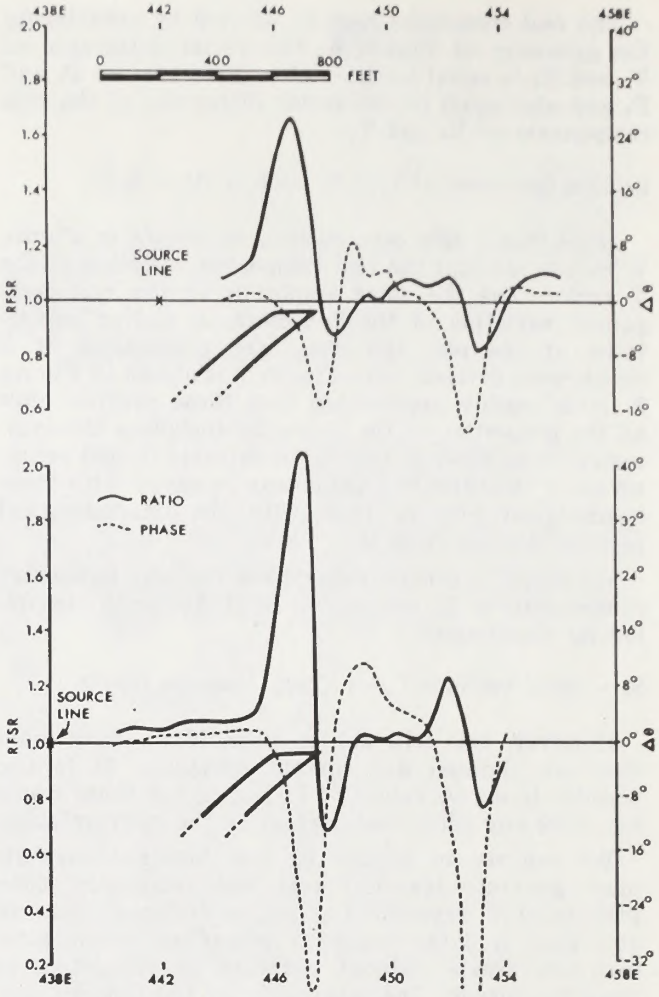

FIGURE 13 — Field example.

source field than those which dip toward it. This permits us to predict that conductor B should give a relatively better response than conductor A, although it is surprising that its response is twice that of A considering that it is twice as far from the source as A.

A study of the induced currents in these two conductors, using a curve matching technique (Duckworth, 1972), revealed that anomaly A was caused by a single isolated current whereas anomaly B was caused by a close grouping of currents. This grouping consisted of a dominant current with a number of much weaker parallel satellites. It was found that the magnitude and phase of this dominant current were almost equal to those of the current which generated anomaly A. However, the dominant current at B was slightly weaker than that at A and located at greater depth.

The conventional and alternative data treatment methods were applied to this profile, resulting in the profiles shown in Figure 12. It is evident that both methods were being influenced by some unrecognized features near the source and that anomaly B is probably not a good representation of an anomaly due to an isolated line current. In order to provide some clarification of the situation, synthetic data were generated using single line currents at A and B and employing the magnitude and phase relationships discussed above. The profiles derived in this way are therefore free of the noise associated with the practical profiles.

If anomalies A and B are compared in the synthetic profile of the real component of T we can see that the amplitude of B is smaller than A, as we would expect due to the smaller magnitude of the current at B and its greater depth although almost equal phase. This effect appears to be reflected in the practical profile of the real component of T.

If we consider the synthetic profile of the real component of $\overline{R}$ we see a much stronger anomaly at B than at A. This is an example of enhancement of the anomaly due to the greater distance between the source and B. In fact, this enhancement is not as great as it would have been if A had not been present, because the presence of A severely attenuated the primary field acting at B. These effects appear to be again reflected in the practical profile. Here we can see that magnitudes of the real components of $\overline{R}$ are unrelated to current magnitude.

Concerning depth, we can see that all four real component profiles agree; detailed examination shows that they all place the current at B at a greater depth than that at A.

Conductor quality is shown by the real/imaginary ratio to be very high, using either data treatment method, and detailed study shows that both methods give the same results in this context.

This example appears to confirm that the two data treatment methods are equally good at locating the induced line current and at evaluating conductor quality. However, if an estimate of the magnitudes of the induced currents is required only the alternative procedure can supply it.

The case shown in Figure 13 illustrates the effect which was observed when the source line was moved away from a shale conductor which dipped toward the source. The evident enhancement of the RFSR anomaly was probably caused by a combination of two processes. The first of these was enhancement of the $\overline{R}$ and RFSR response by the process illustrated in Figure 10. The second was a possible enhancement of the inductive linkage as the source distance increased. This could happen with a conductor which dips toward the source, as this shale did. This inductive enhancement would have maintained the magnitude of the induced current at a higher value than an inverse first-power law of attenuation would have allowed.

It can be seen, therefore, that we might select those parts of this conductor which were most remote from the source as being the best drilling targets on the basis of the stronger RFSR response over such areas. The conversion to real and imaginary components of $\overline{R}$ would not clarify this situation, but an appreciation of the induced current magnitudes might do so. Here then is another case in which the alternative data treatment procedure could be useful.

CONCLUSIONS

In cases where a Turam anomaly can be recognized as being generated by a single isolated line current, the alternative procedure permits the magnitude of that current to be computed. This cannot be achieved by means of the conventional procedure. In addition, the location of the current line laterally and in depth can be determined with an accuracy at least equal to that of the conventional approach. In terms of the amount of data manipulation required, the alternative procedure is slightly less lengthy than the conventional one.

Both procedures provide equally good estimates of conductor quality, on the basis of the real to imaginary component ratio.

The conventional procedure has an advantage in that it tends to treat conductors equally, regardless of source distance, provided that their geometry does not influence the induction process. In practice, conductor geometry in conjunction with source distance may often influence the response, and in this case a knowledge of induced current magnitude is valuable. The alternative procedure may be characterized by the fact that it tends to give equal treatment to the induced line currents regardless of source distance.

It is believed that the Turam user may find that the concurrent use of the alternative and conventional procedures may help resolve some of the ambiguities found in Turam data.

ACKNOWLEDGMENTS

This paper arose from work which was supported by a grant from the National Research Council of Canada. The author is indebted to the director of the Australian Bureau of Mineral Resources for permission to use field data gathered when employed as an officer of that organization.

REFERENCES

Bosschart, R. A., 1964, Analytical interpretation of fixed source electromagnetic prospecting data, Waltman-Delft.

Duckworth, K., 1972, Turam interpretation by curve matching using a line current approximation, Geophysical Prospecting, Vol. 20, No. 3, pp. 514-528.

Grant, F. S., and West, G. F., 1965, Interpretation theory in applied geophysics, McGraw-Hill.

Keller, G. V., and Frischknecht, F. C., 1966, Electrical methods in geophysical prospecting, Pergamon.

Parasnis, D. S., 1966, Mining Geophysics, Elsevier.

Appendix VI

GEOPHYSICS, VOL. 34, NO. 6 (DECEMBER 1969), P. 958–967, 6 FIGS., 1 TABLE

CONTOURING OF VLF-EM DATA†

D. C. FRASER*

Prospecting for conductive deposits with ground VLF-EM instruments has received considerable impetus with the recent development of lightweight receivers. The large geologic noise component, which results from the relatively high-transmitted frequency, has caused some critics to avoid use of the technique. Those who routinely perform surveys with a VLF-EM unit find that, in some areas, a 5-degree peak-to-peak anomaly can be significant, whereas anomalies having amplitudes in excess of 100 degrees may occur as well. Consequently, there is a dynamic range problem when presenting the results as profiles plotted on a field map.

A data manipulation procedure is described which transforms noisy noncontourable data into less noisy contourable data, thereby eliminating the dynamic range problem and reducing the noise problem. The manipulation is the result of the application of a difference operator to transform zero-crossings into peaks, and a low-pass smoothing operator to reduce noise. Experience has shown that field personnel can routinely perform the calculations which simply involve additions and subtractions.

INTRODUCTION

VLF-EM data can be exceedingly difficult to interpret because a large geologic noise component can result from the relatively high-transmitted frequency of about 20,000 Hz. Routine surveys can yield useless data unless special care is taken both in survey procedure and in data presentation.

The purpose of this paper is to describe the survey procedure and the method of data presentation in use by the Keevil Mining Group and to illustrate the advantages of this approach.

VLF-EM GROUND SURVEY PROCEDURE AND DATA TREATMENT

The primary field

VLF-EM transmitter stations are located at several points around the globe. They broadcast at frequencies close to 20,000 Hz, which is low compared to the normal broadcast band. The purpose of these stations is to allow governmental communication with submarines, and the low frequency allows some penetration of the conductive ocean water. Skin depth is approximately $3.6\sqrt{P}$ meters, where P is the resistivity of a homogeneous halfspace in ohm-m, on the assumption that the frequency is 20,000 Hz and that the halfspace is magnetically nonpolarizable. Consequently, depth of exploration is severely restricted for overburden resistivities less than 200 ohm-m.

Since the area to be prospected normally is of considerable distance from the transmitter stations, the primary field is uniform in the area, allowing rather simple mathematics to be used in anomaly prediction and analysis.

Survey procedure and data treatment

The survey procedure first consists of selecting a transmitter station which provides a field approximately parallel to the traverse direction, i.e., approximately perpendicular to the expected strike of a conductor. The following points relate to the method of data treatment.

1. Readings should be taken every 50 ft, as will be shown below.
2. Transmitter stations should not be changed

† Manuscript received by the Editor April 24, 1969; revised manuscript received August 18, 1969.

* Keevil Mining Group Limited, Geophysical Engineering & Surveys Limited, Teck Corporation Limited, Toronto, Ontario, Canada.

for a given block of ground, to avoid distortion in the contour presentation. Hence, fill-in lines should be run with the same transmitter station as other lines in the block. The field direction of this station should be shown on the data map.

3. List the dip angle[1] data in tabular form, as follows:
   a) list in the direction of north (top of paper) to south, or from west to east;
   b) designate south or east dips as negative; and
   c) perform calculations as shown in Table 1.

   Thus, the filtered output or contourable quantity simply consists of the sum of the observations at two consecutive data stations subtracted from the sum at the next two consecutive data stations. The theoretical basis for this procedure will be described below.
4. The right-hand column (filtered data) is suitable for contouring. Normally, negative values are not contoured since, being caused by dip angle flanks, they do not aid interpretation but only confuse the picture. The positive values generally are contoured at 10-unit intervals, and the zero contour is shown only when it brackets an anomaly. In quiet areas, 5-unit contours may be meaningful.

[1] This paper assumes that data is recorded as for the Crone Radem which defines a north-dipping field as a south "dip" on the instrument. This convention was chosen because a south reading is interpreted as arising from a conductor to the south.

Example

Figure 1 presents dip-angle data, according to the Crone convention, in the vicinity of the Temagami mine of Copperfields Mining Corporation Limited in Ontario. This figure illustrates that several conductors are present yielding large dip angles. A complex pattern has resulted which requires some thought to interpret properly.

Figure 2 presents the filtered data in contoured form where only the 0, 20, and 40 contours are shown for simplicity. The conductor pattern is immediately apparent, even to exploration personnel untrained in VLF-EM interpretation. The three anomalies correlate with a zone of nearly massive pyrite and two brecciated fault zones. Depth to bedrock is 15 ft.

In practice, all the data of Figures 1 and 2 are

Table 1. Example of calculations

Location	Measured dips	Apply sign and form the moving sum of pairs of entries	Take first differences of alternate entries
3+00S	6S	−6	
		(−6)+(−7)=	−13
3+50S	7S	−7	
		(−7)+(−8)=	−15 (−23)−(−13)= −10
4+00S	8S	−8	
			−23 (−39)−(−15)= −24
4+50S	15S	−15	
			−39 + 7
5+00S	24S	−24	
			−16 +57
5+50S	8N	+ 8	
			+18 +38
6+00S	10N	+10	
			+22 + 8
6+50S	12N	+12	
			+26 + 6
7+00S	14N	+14	
			+28 (+34)−(+26)= + 8
7+50S	14N	+14	
		(14)+(20)=	+34
8+00S	20N	+20	

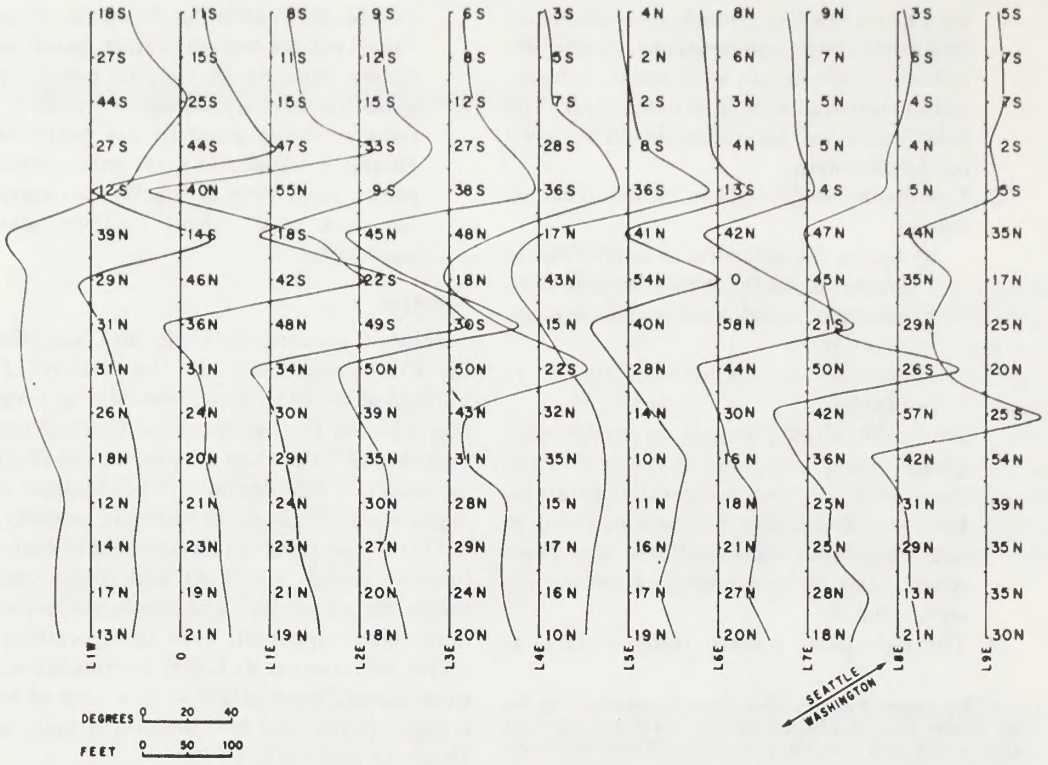

FIG. 1. Dip-angle data in the vicinity of the Temagami mine. The arrow defines the VLF-EM primary field direction from the transmitter at Seattle, Washington.

placed on a single map. The above example illustrates that this very simple one-dimensional filtering scheme yields a practical and effective approach to VLF-EM data handling.

The filter improves the resolution of anomalies, thereby making them easier to recognize. An inflection on the dip profile from a conductor subordinate to a larger one yields a positive peak, thereby emphasizing the presence of such a conductor. Figure 3 illustrates this effect where nine lines were run over an SP (self-potential) anomaly in the Temagami area. The dip-angle anomaly is very poorly resolved due to the regional south dips produced by an areally large conductor to the south of the map area. The contoured VLF-EM data yields a clearly defined anomaly which was located over the negative center of the SP.

THE FILTER AND ITS EFFECT ON ANOMALIES

The filter operator

The filter operator was designed to meet the following criteria:

1. It must phase shift the dip-angle data by 90 degrees so that crossovers and inflections will be transformed into peaks to yield contourable quantities.
2. It must completely remove dc and attenuate long spatial wavelengths to increase resolution of local anomalies.
3. It must not exaggerate the station-to-station random noise.
4. It must be simple to apply so that field personnel can make the calculations without difficulty.

The first two criteria are met by using a simple difference operator, i.e.

$$M_2 - M_1,$$

where M_1 and M_2 are any two consecutive data points.

The third criterion is met by applying a smoothing or low-pass operator to the differences, i.e.

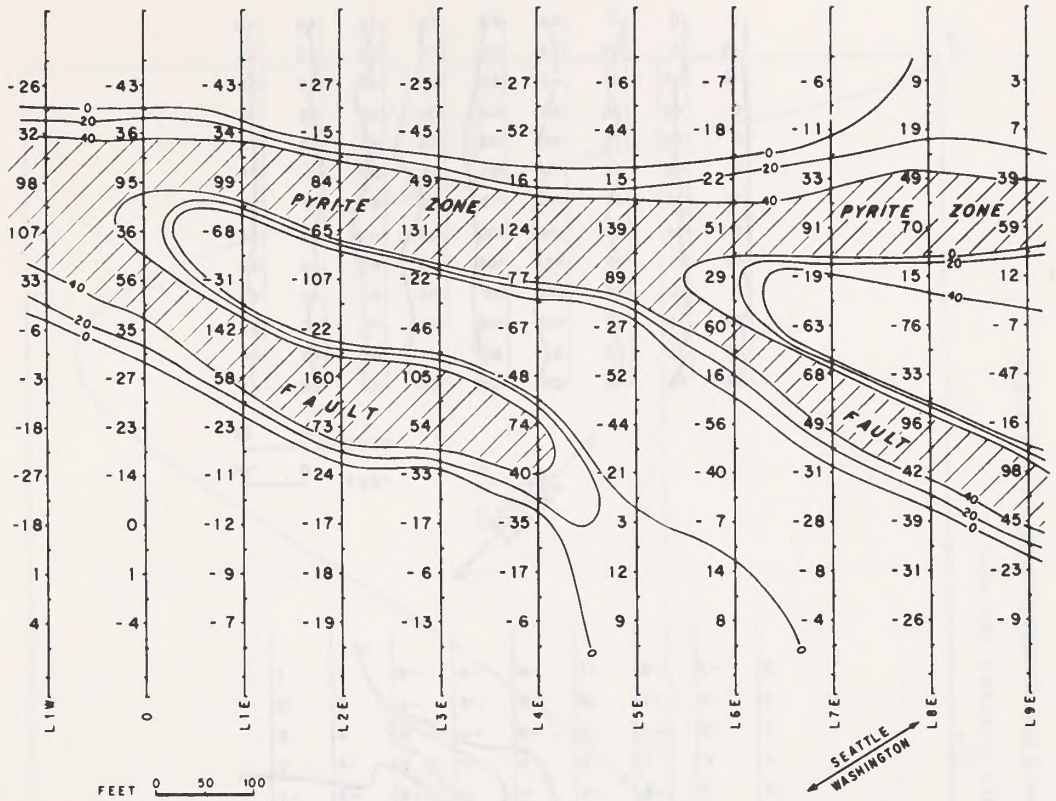

FIG. 2. Filtered data computed from the map of Figure 1.

$$\tfrac{1}{4}(M_2 - M_1) + \tfrac{1}{2}(M_3 - M_2) + \tfrac{1}{4}(M_4 - M_3),$$

where M_1, M_2, M_3, and M_4 are any four consecutive data points. The filtered output then is

$$\tfrac{1}{4}(M_2 - M_1) + \tfrac{1}{2}(M_3 - M_2) + \tfrac{1}{4}(M_4 - M_3) = \tfrac{1}{4}[M_3 + M_4 - M_1 - M_2].$$

The final criterion is enhanced by eliminating the constant, so that the plotted function becomes

$$f_{2,3} = (M_3 + M_4) - (M_1 + M_2),$$

which is plotted midway between the M_2 and M_3 dip-angle stations.

This filter has its frequency (wavenumber) response displayed in Figure 4, for a station spacing of 50 ft. Its characteristics are as follows:

1. All frequencies are shifted by 90 degrees.
2. Noise having a wavelength equal to the station spacing and dc bias are completely removed.
3. Maximum amplitude occurs for wavelengths of 250 ft, or five times the station spacing.

The frequency (wavenumber) response of the filter is shown for a station spacing of 50 ft, because this is the most suitable spacing for defining sulfide bodies within a few hundred feet of surface. This will be demonstrated below.

The dike model

A conducting dike in a VLF-EM field will produce a secondary induction field from eddy currents maintained in it by the primary field. These eddy currents will tend to flow in such a manner as to form line sources concentrated near the outer edges of the dike since the field is uniform (Figure 5a). This dike may be replaced by a loop of wire of dimensions traced out by the main current concentration in the dike. The secondary field geometry of the loop and dike then will be practically identical, as has been shown by Fraser (1966), Parry (1966), and Parry et al (1965). This

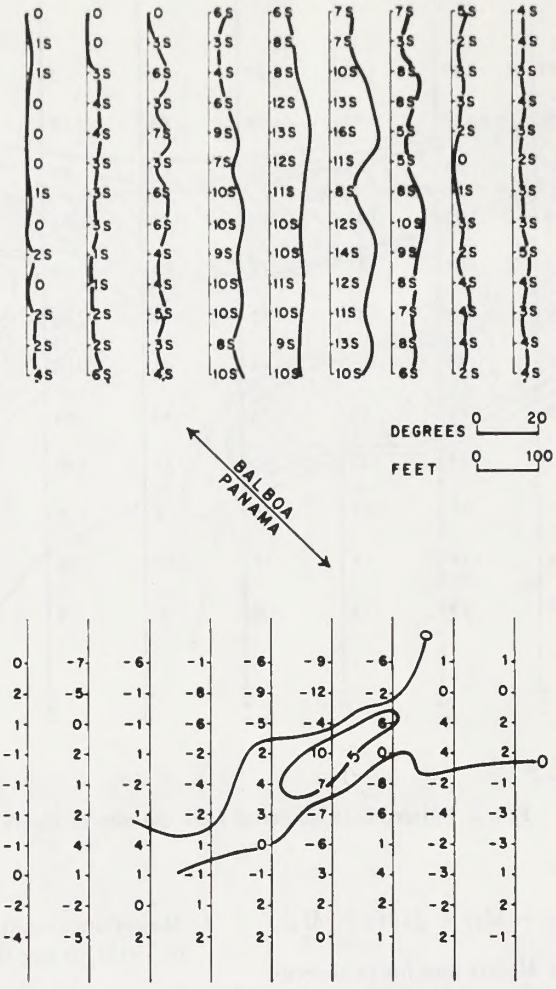

FIG. 3. Dip-angle (upper map) and filtered data (lower map) over a small grid in the Temagami area. The arrow defines the VLF-EM primary field direction from the transmitter at Balboa, Panama.

allows a mathematical model of a dike to be constructed because the field from a line source is known.

For brevity, only a dike which is large in depth extent and in length will be considered herein. Only the top line source of Figure 5a will contribute to the measured dip angles because the other current line sources are very far away.

The horizontal Hs_x and vertical Hs_z secondary fields are (Figure 5b)

$$Hs_x = kH_0 \frac{z}{x^2 + z^2}$$

$$Hs_z = kH_0 \frac{x}{x^2 + z^2},$$

where k is a positive constant having the dimension of length and is related to the conductivity and dimensions of the dike, and where H_0 is the primary VLF-EM strength at the dike. The measured dip angle is

$$\alpha = \tan^{-1}\left[\frac{H_{0_z}}{Hs_x + H_0}\right]$$

$$= \tan^{-1}\left[\frac{kx}{kz + x^2 + z^2}\right].$$

Model dip profiles can be computed for various depths z only by assuming a value for k.

As a means of testing the effect of the filter operator, a single k value was chosen to yield a

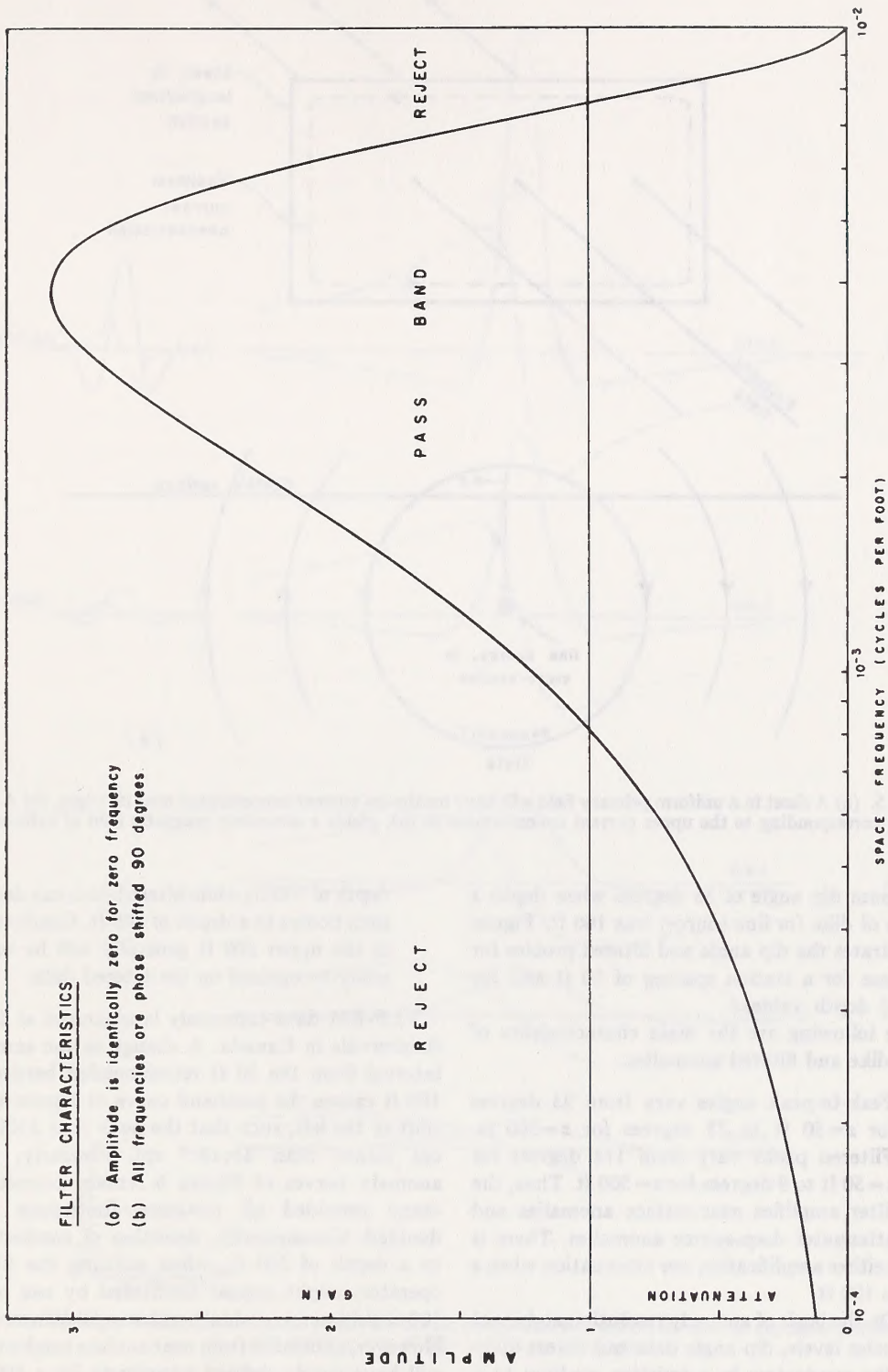

FIG. 4. Frequency response of filter operator for station spacing of 50 ft.

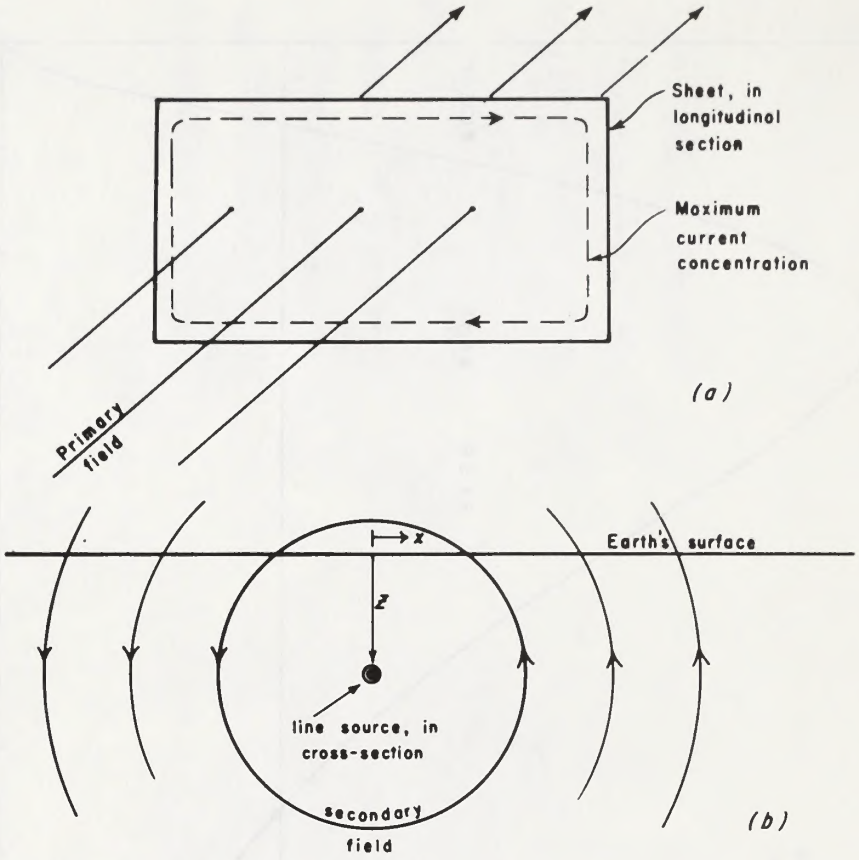

FIG. 5. (a) A sheet in a uniform primary field will have maximum current concentrated near its edges. (b) A line source, corresponding to the upper current concentration in (a), yields a secondary magnetic field of cylindrical shape.

maximum dip angle of 35 degrees when depth z to top of dike (or line source) was 100 ft. Figure 6 illustrates the dip angle and filtered profiles for this case for a station spacing of 50 ft and for several depth values.

The following are the main characteristics of these dike and filtered anomalies:

1. Peak-to-peak angles vary from 93 degrees for $z=50$ ft to 25 degrees for $z=500$ ft. Filtered peaks vary from 118 degrees for $z=50$ ft to 8 degrees for $z=500$ ft. Thus, the filter amplifies near-surface anomalies and attenuates deep-source anomalies. There is neither amplification nor attenuation when z is 100 ft.
2. On the basis of anomaly resolution and usual noise levels, dip angle data can detect dike-like conductors in a resistive medium to a depth of 500 ft, while filtered data can detect such bodies to a depth of 300 ft. Conductors in the upper 200 ft generally will be more easily recognized on the filtered data.

VLF-EM data commonly is measured at 100-ft intervals in Canada. A change in the sample interval from the 50 ft recommended herein to 100 ft causes the passband curve of Figure 4 to shift to the left, such that the peak is at 2×10^{-3} cpf rather than 4×10^{-3} cpf. Similarly, the anomaly curves of Figure 6 remain correct in shape provided all distance dimensions are doubled. Consequently, detection of conductors to a depth of 500 ft, when utilizing the filter operator, might appear facilitated by use of a 100-ft station interval rather than a 50-ft interval. However, anomalies from near-surface conductors will have poorly defined waveforms for a 100-ft

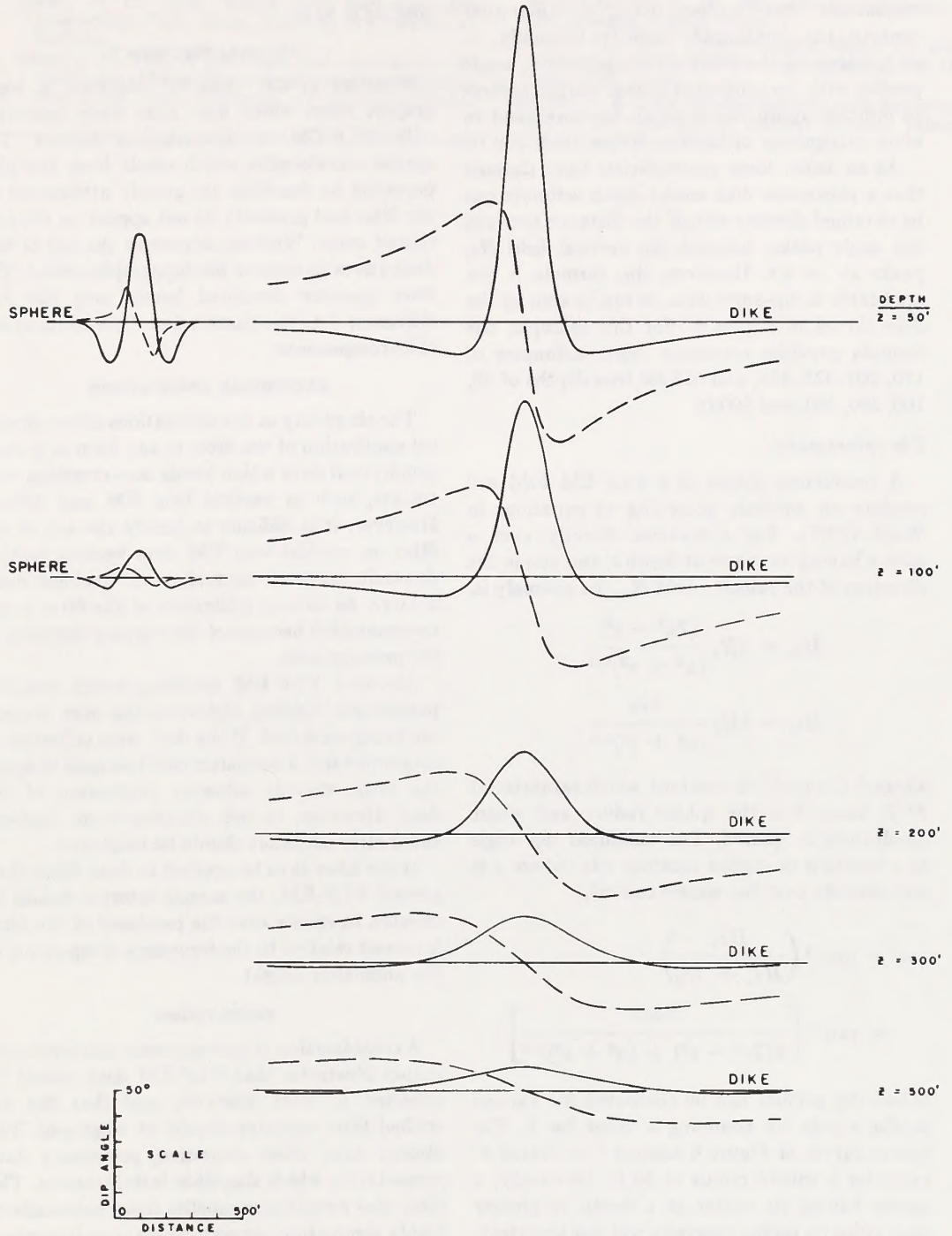

FIG. 6. Dip-angle (dashed) and filtered (solid) curves for model dike and sphere for several depths of burial, where z is depth to top of dike and to center of sphere.

data station interval, and will alias as deeper conductors. This "geologic noise" will somewhat confuse the contoured output. Generally, a comparison of the 50-ft data station dip angle profiles with the contoured filtered output suffices to indicate approximate depth to source and to allow recognition of sources deeper than 300 ft.

As an aside, some geophysicists have claimed that a reasonable dike model depth estimate can be obtained directly as half the distance between dip angle peaks, because the vertical field Hs_z peaks at $x = \pm z$. However, this formula is not applicable to dip-angle data, as can be seen by the dike curves of Figure 6. For this example, the formula provides erroneous depth estimates of 150, 200, 325, 425, and 625 for true depths of 50, 100, 200, 300, and 500 ft.

The sphere model

A conducting sphere in a VLF-EM field will produce an anomaly according to equations in Ward (1967). For a traverse directly over a sphere having its center at depth z, and run in the direction of the primary field H_0, the anomaly is,

$$Hs_x = kH_0 \frac{(2x^2 - z^2)}{(x^2 + z^2)^{5/2}}$$

$$Hs_z = kH_0 \frac{3xz}{(x^2 + z^2)^{5/2}},$$

where k is a positive constant which saturates at $R^3/2$, where R is the sphere radius, and where quadrature is ignored. The measured dip angle as a function of station location x is (where x is zero directly over the sphere center),

$$\alpha = \tan^{-1}\left(\frac{Hs_z}{Hs_x + H_0}\right)$$

$$= \tan^{-1}\left[\frac{3kxz}{k(2x^2 - z^2) + (x^2 + z^2)^{5/2}}\right].$$

Model dip profiles can be computed for various depths z only by assuming a value for k. The sphere curves of Figure 6 assume a saturated k-value for a sphere radius of 50 ft. Obviously, a sphere having its center at a depth of greater than twice its radius generally will not be detectable. However, the filter operator aids in the recognition of a spherical conductor because it amplifies the anomaly, for the small sphere sizes usually encountered in nature, assuming data spacing is 50 ft.

TOPOGRAPHIC EFFECT

Whittles (1969) recently described a topographic effect which may arise when surveying with VLF-EM in mountainous regions. The spatial wavelengths which result from the phenomenon he describes are greatly attenuated by the filter and generally do not appear on the contoured maps. Whittles advocates the use of first derivatives to remove the topographic effect. The filter operator described herein uses the first difference (i.e., the discrete first derivative) as one of its components.

ADDITIONAL APPLICATIONS

The simplicity of the calculations allows practical application of the filter to any form of ground geophysical data which yields zero-crossings over tragets, such as vertical loop EM and Afmag. However, it is difficult to justify the use of the filter on vertical loop EM data because neither dynamic range of anomalies nor geologic noise is large. In Afmag, utilization of the filter is not recommended because of the varying direction of the primary field.

Airborne VLF-EM systems, which measure parameters yielding zero-crossings over targets, are being marketed. If the data were collected on magnetic tape, a computer could be used to apply the filter, thereby allowing contouring of the data. However, in this situation more sophisticated filter operators should be employed.

If the filter is to be applied to data other than ground VLF-EM, the sample interval should be selected to ensure that the passband of the filter is correct relative to the frequency components of the anomalies sought.

CONCLUSIONS

A consideration of geologic noise and conductor shapes illustrates that VLF-EM data should be collected at 50-ft intervals, and that the described filter operator should be employed. The filtered data, when contoured, provides a data presentation which simplifies interpretation. The filter also amplifies anomalies from near-surface, highly conducting ore pods which is an important feature in several mining districts such as at Tribag and Temagami, both in Ontario, and in Louvicourt Township of Quebec.

REFERENCES

Fraser, D. C., 1966, Rotary field electromagnetic prospecting: Ph.D. thesis, Univesity of California at Berkeley.

Parry, J. R., 1966, A theoretical and experimental investigation of finite dikes in a uniform electromagnetic field: M.Sc. thesis, University of California at Berkeley.

——— Fraser, D. C., and Ward, S. H., 1965. Investigation of finite dikes in a uniform electromagnetic field: Presented at the 35th Annual International SEG Meeting, Dallas, Texas.

Ward, S. H., 1967, Electromagnetic theory for geophysical applications, *in* Mining Geophysics, Vol. II: Tulsa, SEG, p. 80.

Whittles, A. B., 1969, Prospecting with radio frequency EM-16 in mountainous regions: Western Miner, February 1969, p. 51–56.

APPENDIX VII

The Induced Polarization (IP) Method

Hallof, P. G.:(1972): The Induced Polarization Method; Phoenix Geophysics Ltd. [paper presented to the 24th International Geological Congress, Montreal, Canada, August; reprinted by permission of the author] 44 p.

Table of Contents

Hallof, P. G., Cartwright, P. A., and Pelton, W. H.;(1979): The Use of the Phoenix IPV-2 Phaw IP Receiver for Discrimination Between Sulphides and Graphite; [paper presented to the Society of Exploration Geophysicists Annual Meeting, New Orleans, Louisiana, November, reprinted by permission of the authors] 21p.

Table of Contents

The Induced Polarization Method

by

P.G.Hallof

*Presented at the 24th. International Geological Congress, Montreal, Canada, August 1972.

PHOENIX Geophysics Limited

200 YORKLAND BLVD., WILLOWDALE, ONTARIO, CANADA M2J 1R5

TITLE: The Induced Polarization Method

AUTHOR: Philip G. Hallof

ABSTRACT:

In recent years, the use of the induced polarization method (IP) in base metal exploration has increased dramatically. More consistent and widespread use of IP has resulted in the discovery of many ore bodies and demonstrated the numerous exploration situations in which the method can be of use. For this reason, there is currently a great interest in induced polarization among exploration geologists.

Induced polarization effects can be expected in any rocks that contain metallic minerals. When the method is used in mineral exploration, electrical current is applied to the ground and the resulting voltages are measured and analyzed to detect the possible presence of metallic minerals. There are several measurement techniques in common use; however, measurements made in the time domain and in the frequency domain are mathematically equivalent.

There are differences in the sensitivity, stability, power, etc. of the current source and in the voltmeter employed in the two types of measurement. These requirements result in some differences in the size and weight of the equipment necessary to complete any given survey, with the chosen electrode configuration, in a particular geological setting. The type of measurement dictates, to some extent, the type of electrode configuration that can be employed. The electrode configuration used does influence the magnitude, width, etc. of the anomaly detected for any geological situation; the effectiveness of the IP method is dependent upon the electrode configuration used.

The induced polarization method found its original application in the search for disseminated mineralization that could not be detected using other geophysical techniques. The method is very useful in this type of exploration and large zones of disseminated mineralization can be detected at depths of 1,000 feet, or more. The method has also been successfully used in the search for zones of concentrated (but less than massive) sulphide mineralization of the stratabound type. Examples from lead-zinc deposits in limestones in the U.S. and Canada demonstrate this success.

Even in the search for massive sulphide zones that might normally be detectable by electromagnetic methods, there are situations in which the IP method must be used. These include areas of thick overburden and regions in which deep weathering have created a highly conductive surface layer.

THE INDUCED POLARIZATION METHOD

Introduction

This review of the induced polarization method has been prepared primarily for geologists and exploration people rather than for geophysicists. I have therefore concentrated on field data demonstrating the usefulness of the induced polarization method and the applicability of the various electrode configurations that are in common use.

Only a small amount of theoretical work and mathematical development will be included. For a more complete discussion of the induced polarization phenomena and mathematical techniques for interpretation, etc., the reader is referred to one of several review papers that have appeared in print.

Madden and Cantwell (1967)
Seigel (1967)
Hallof (1967)

The first two references have particularly good bibliographies on the induced polarization method.

The IP Phenomenon

When used in mineral exploration, the term "induced polarization" refers to the measurement of the frequency dependence or the time dependence of electrical potentials and current flow in the earth. In unmineralized rocks, current flow is carried by ionic solutions in the pore spaces of the rocks. The resistivity is largely dependent upon the porosity of the rocks and the salinity of solutions in the pore spaces. The resistivity (impedance) of the rocks is independent of the frequency of the applied current.

However, if metallic mineral particles are present within the rock,

complex electro-chemical reactions at the surface of the metallic minerals will enter into the current flow (Madden and Cantwell, 1967). Metallic minerals conduct electricity by electrons and the overall effect is that the resistivity of the mineralized rock will decrease as the frequency of the applied current is increased.

A simple representation of the inverse resistivity (conductivity) of the physical situation shown in Figure 1 is the curve in Figure 2. In the range of frequencies used for mineral exploration, the electro-chemical reactions at the surface of metallic minerals are controlled by the WARBURG CONDUCTION. A study of these reactions has suggested the equivalent circuit shown in Figure 3.

For simple, one-dimensional current flow through a mineral electrode, the impedances measured will be similar to those shown in Figure 4. Other examples of the frequency dependence of resistivity for mineralized rocks are available (Wait, 1959; Hallof, 1967). A linear system which

GENERALIZED GEOMETRY FOR METALLIC MINERAL IN ROCK PORE SPACE

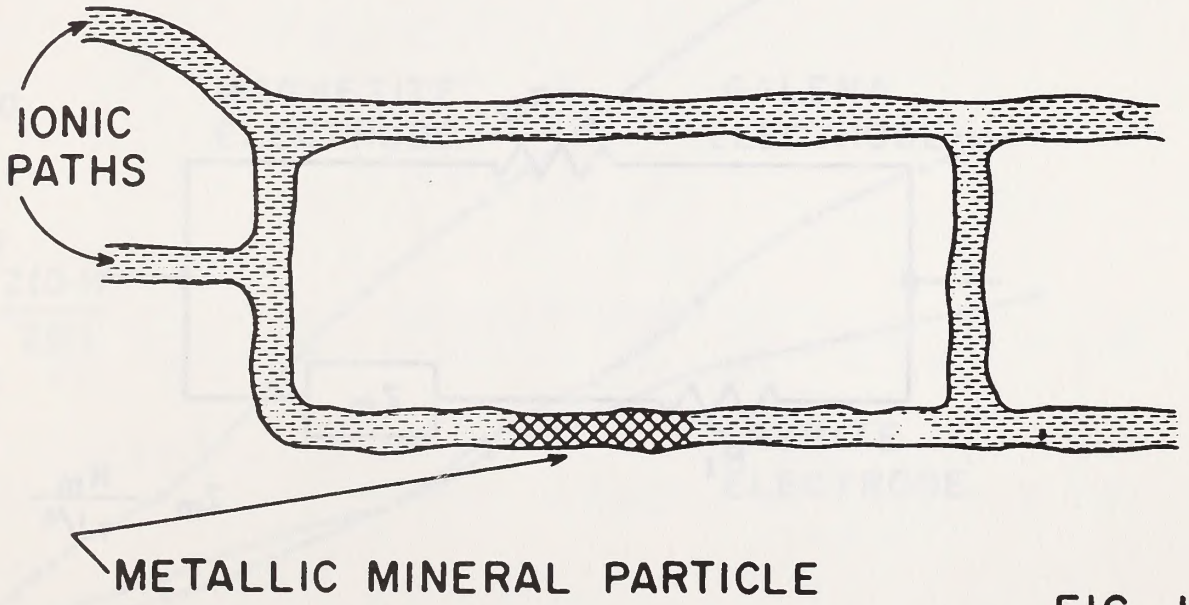

FIG. 1

LOG-LOG PLOT FOR CONDUCTIVITY VS FREQUENCY

MINERALIZED ROCK

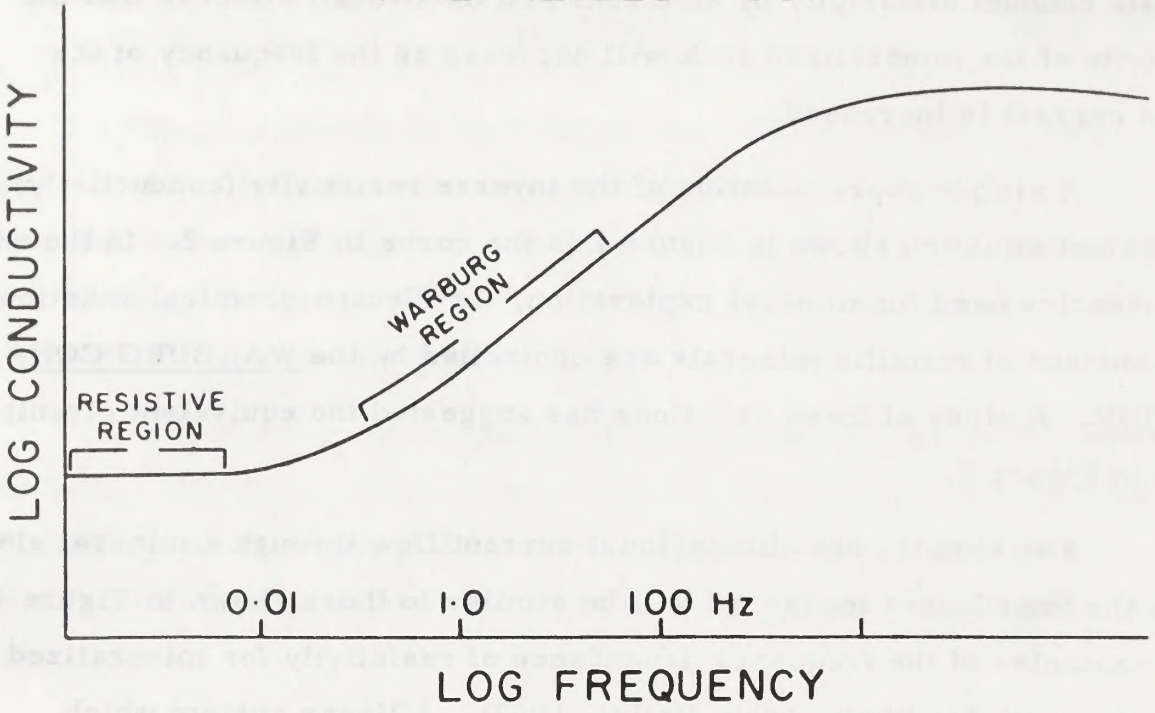

FIG. 2

EQUIVALENT CIRCUIT FOR ELECTRICAL CONDUCTION

IN MINERALIZED ROCKS

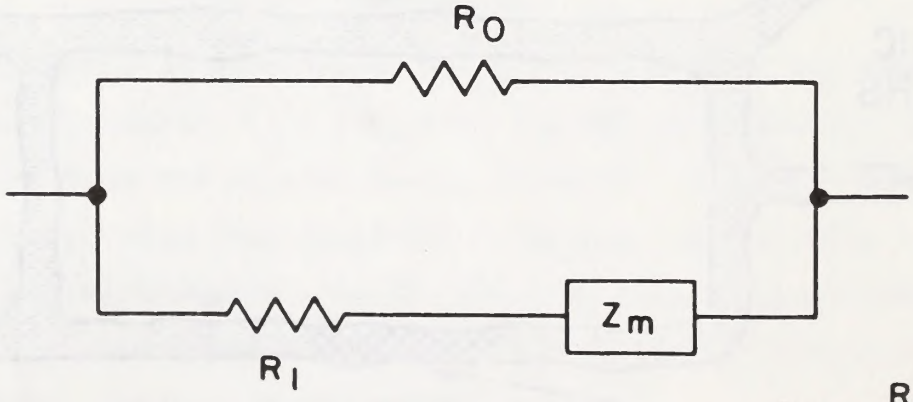

FIG. 3

exhibits this type of behaviour is capable of storing energy; i.e., a polarization can be induced by current flow.

There are two entirely equivalent ways to measure this induced polarization (Hallof, 1967):

Figure 5 - Measurement in Time Domain (left side)

Figure 5 - Measurement in Frequency Domain (right side)

For the simple equivalent circuit shown in Figure 3, Madden and Cantwell (1967) have shown that the following approximate functions are valid for low frequencies and relatively long times.

a) Transfer Impedance $$Z(f) \simeq Z_R(dc)\left[1 - \frac{R_o}{Z_m(1.0\,Hz)} f^{\frac{1}{4}}\right]$$

b) Step-function Current Response $$V(t) = Z_R(dc)\left[1 - \frac{1}{1.78} \times \frac{R_o}{Z_m(1.0\,Hz)} t^{-\frac{1}{4}}\right]$$

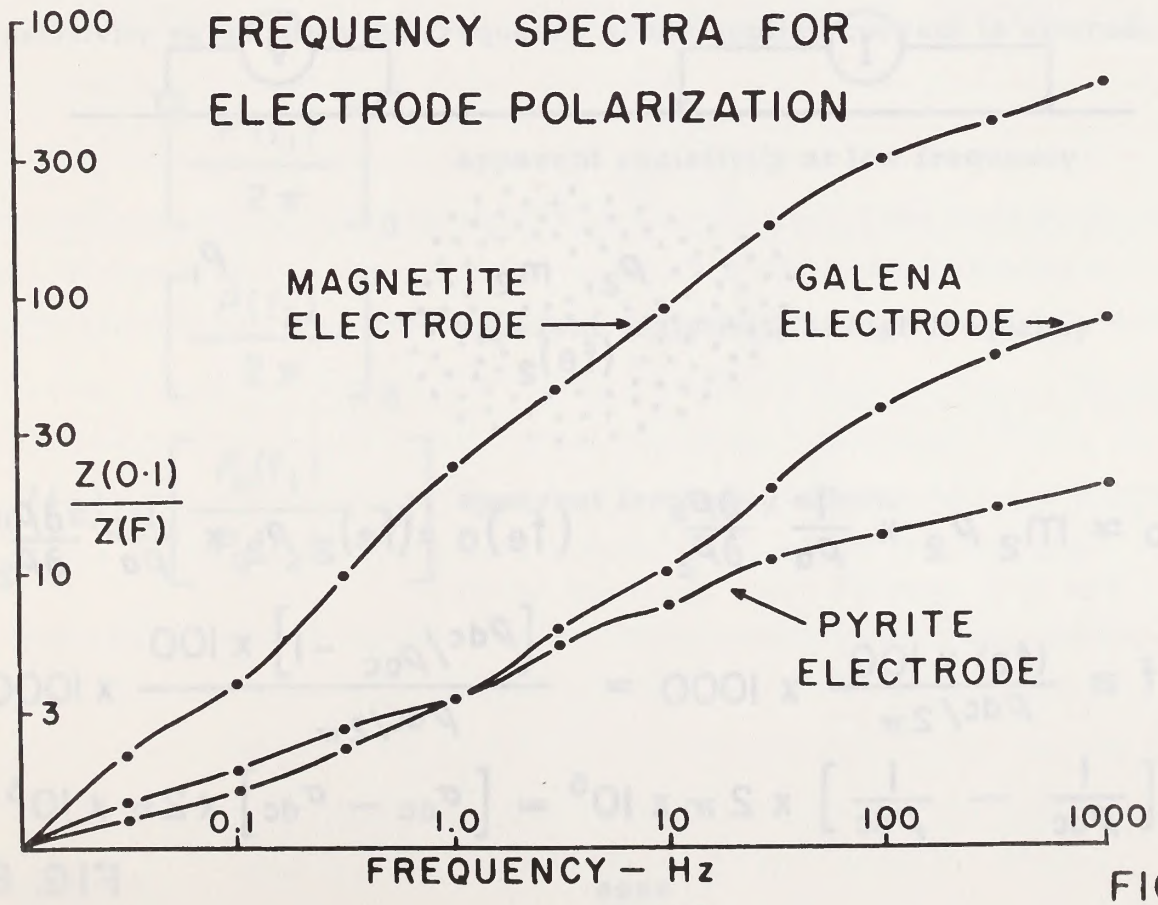

FIG. 4

TIME DOMAIN | **FREQUENCY DOMAIN**

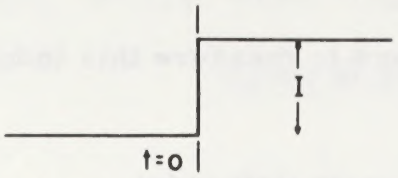

STEP-FUNCTION CURRENT $i(t) = I u(t)$

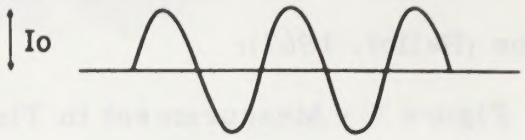

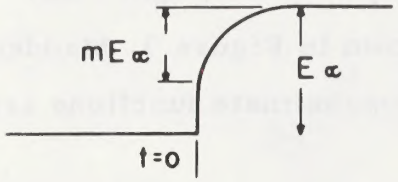

VOLTAGE RESPONSE $E(t)$

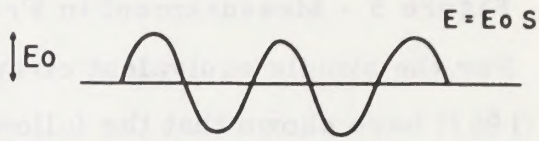

if $\rho_o(w) = \frac{E_o(w)}{I_o(w)}$

$$m \equiv \frac{E(t)_{t\to\infty} - E(t)_{t\to 0}}{E(t)_{t\to\infty}}$$

$$fe \equiv \frac{\rho_{o\,f\to 0} - \rho_{o\,f\to\infty}}{\rho_{o\,f\to\infty}}$$

BY LA PLACE TRANSFORM THEORY

$$m = \frac{fe}{1+fe} \cong fe$$

FIG. 5

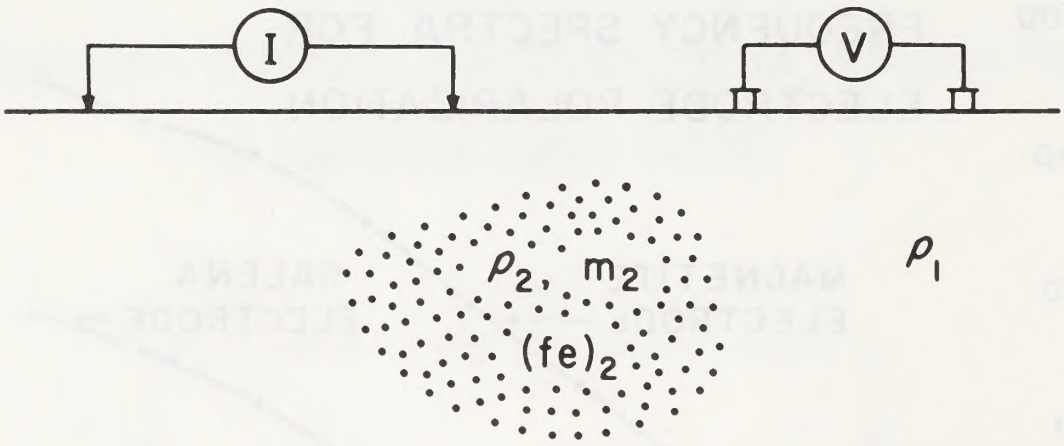

$$ma \simeq m_2 \rho_2 \times \frac{1}{\rho_a} \frac{\partial \rho_a}{\partial \rho_2} \qquad (fe)a = (fe)_2 \rho_2 \times \frac{1}{\rho a} \frac{\partial \rho_a}{\partial \rho_2}$$

$$mf \equiv \frac{(fe) \times 100}{\rho_{dc}/2\pi} \times 1000 = \frac{\left[\rho_{dc}/\rho_{ac} - 1\right] \times 100}{\rho_{dc}/2\pi} \times 1000$$

$$= \left[\frac{1}{\rho_{ac}} - \frac{1}{\rho_{dc}}\right] \times 2\pi \times 10^5 = \left[\sigma_{ac} - \sigma_{dc}\right] \times 2\pi \times 10^5$$

FIG. 6

In carrying out IP field surveys, any four-electrode configuration may be used. Seigel (1967) has shown that for pulse-transient (time domain) IP measurements, the theoretical IP problem can be solved for any geometry for which the apparent resistivity solution is available. The apparent resistivity solutions may arise from theoretical developments or scale modelling. The same development can be used for the variable frequency (frequency domain) IP method (Hallof, 1967) (see Figure 6).

Parameters Measured in Field Surveys

As the use of the IP method in mineral exploration has developed through the years, many different parameters have been used by investigators. However, only a few are in common use. Two of these are:

a) Variable Frequency Method

When applying the variable frequency technique, the apparent resistivity of the earth at any particular place is measured with any electrode configuration. The presence of metallic mineralization is detected as a change in the apparent resistivity value when the frequency of the applied current is altered.

$\left[\frac{\rho(f_1)}{2\pi}\right]_a$ apparent resistivity at low frequency

$\left[\frac{\rho(f_2)}{2\pi}\right]_a$ apparent resistivity at high frequency

$(fe)_a = \left[\frac{\rho_a(f_1)}{\rho_a(f_2)} - 1\right]$ apparent frequency effect.

PARAMETERS MEASURED IN TIME-DOMAIN I.P.

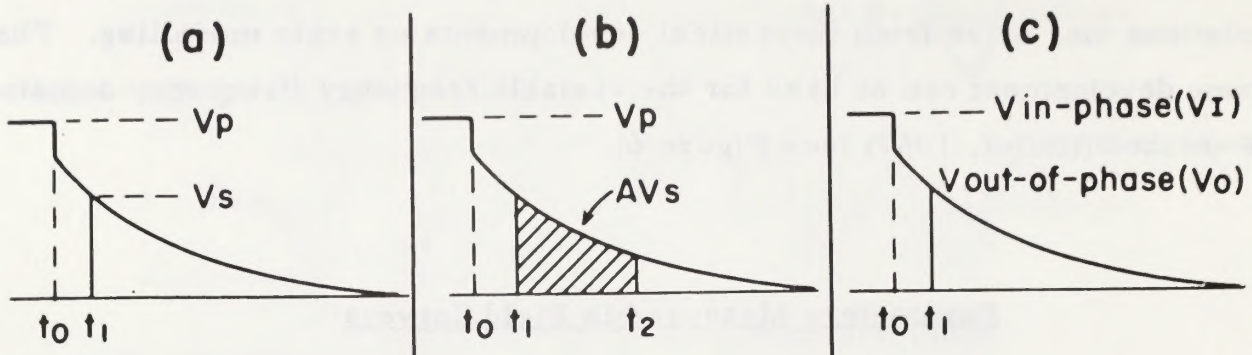

m = chargeability

$$m = \frac{Vs}{Vp}$$

m = chargeability

$$m = \frac{AVs}{Vp}$$

Phase shift (θ) is function of VI and Vo

FIG. 7

ELECTRODE CONFIGURATIONS FOR I P SURVEYS

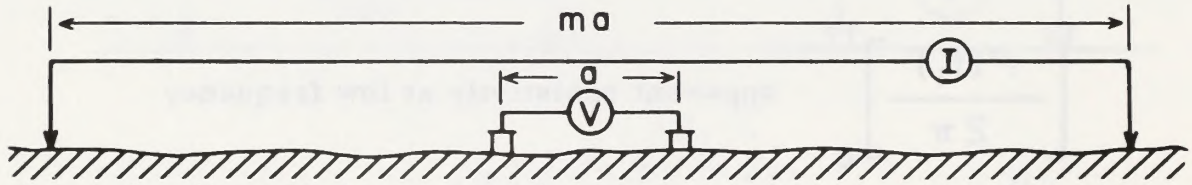

(a) Gradient (Schlumberger) array — where m greater than 15

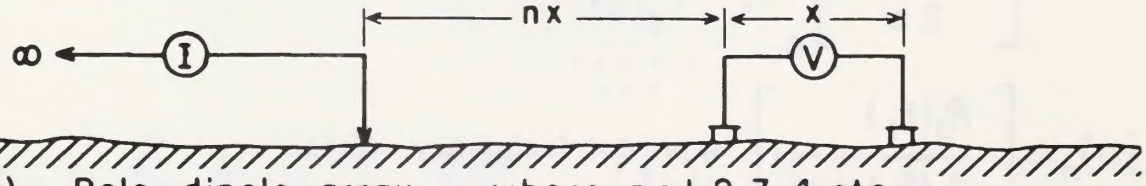

(b) Pole-dipole array — where n = 1,2,3,4 etc.
For n=1 special case is "three array"

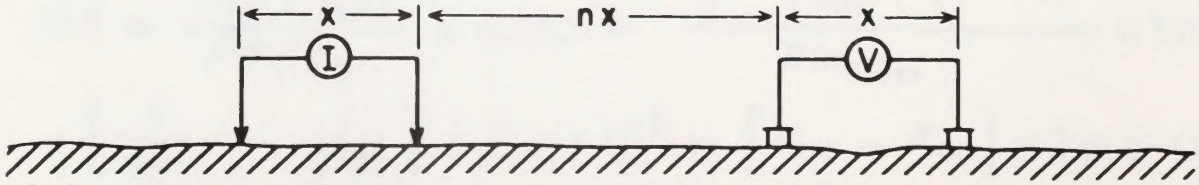

(c) Dipole-dipole array — where n = 1,2,3,4 etc.

FIG. 8

Another parameter that is often useful is the "metal factor", or "metallic conduction factor" (Madden and Cantwell, 1967; Hallof, 1967).

$$Mf = \frac{(fe) \times 100}{\frac{\rho(f_1)}{2\pi}} \times 1000 = \frac{\left[\frac{\rho(f_1)}{\rho(f_2)} - 1\right] \times 100}{\frac{\rho(f_1)}{2\pi}} \times 1000$$

$$= \left[\frac{1}{\rho(f_2)} - \frac{1}{\rho(f_1)}\right] \times 2\pi \times 10^5 = \left[\sigma(f_2) - \sigma(f_1)\right] \times 2\pi \times 10^5$$

b) Pulse-Transient Method

All geophysicists now applying the pulse-transient IP method detect the polarization as a decay in the measured voltage after the applied dc current is terminated. In some cases, the current is applied for a relatively long period of time and the measurement is made once. More often, the measurement is made by averaging several decays, when applying the current in alternate directions in a series of pulses.

The three parameters most commonly measured in the pulse-transient technique are shown in Figure 7. The chargeability shown in Figure 7a is the parameter we have described previously. It is dimensionless and entirely equivalent to the frequency effect. According to Seigel (Seigel, 1967), and others, the decay curve has a constant shape so that the time-averaged chargeability shown in Figure 7b has the same significance. The measurement of the area under the decay curve is somewhat easier and the parameter has the dimensions of millivolt-seconds per volt, or milliseconds.

The parameter shown in Figure 7c measures the slope of the decay curve at some point in time after the applied current is terminated. This is equivalent to the phase-shift for a linear system and it also has the dimensions of milliseconds.

Electrode Configurations Used in Field Surveys

There are numerous electrode configurations that can be used in making IP measurements. However, most of the surveys now done use one of the three electrode configurations shown in Figure 8.

Techniques for Plotting Field Data

For the gradient-array or three-array data, IP results are usually shown as profiles, or occasionally as contoured plan maps when data are available from several lines. If pole-dipole or dipole-dipole data are measured for only a single value of n, the results can also be shown as profiles.

Dipole-dipole data are usually plotted as a "pseudo-section" for several values of n; the separation between the current electrodes and potential electrodes, as well as the location of the electrodes along the survey line, determine the position of the plotting point. The two-dimensional array of data is then contoured (see Figure 9). The contour plots are <u>not</u> sections of the

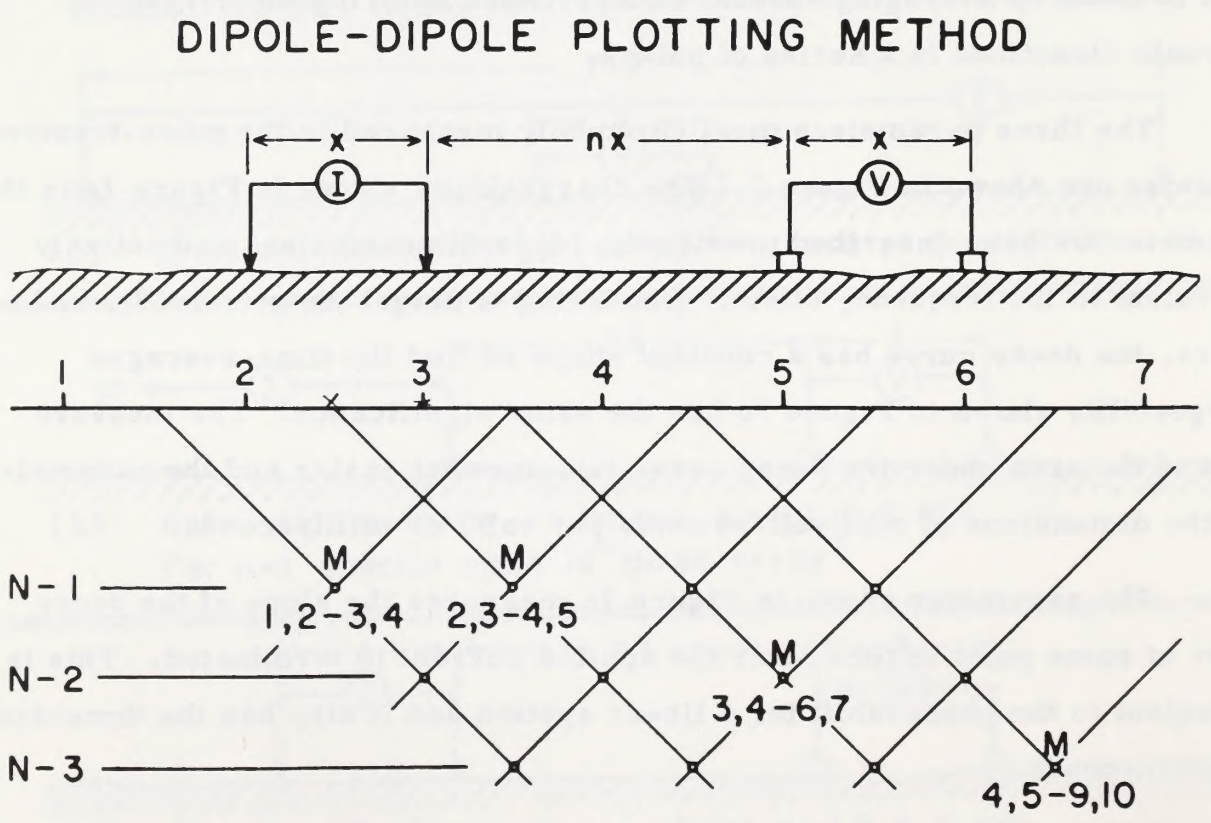

FIG. 9

electrical properties of the earth; they are convenient graphical representations of the measurements made. However, with experience the contour patterns can be interpreted to give some information about the source of the anomaly.

The Use of Scale Modelling Data in Interpretation

One method of gaining experience in the interpretation of IP results is the study of scale modelling data. The advantages of studying modelling data are that the parameters and position of the source are accurately known (this is not always true for field data) and the parameters and position of the source can be varied by the observer, which is obviously not possible in field situations.

Before entering into a discussion of the field applications for the induced polarization method, we will discuss briefly four typical geological situations from model data. The IP scale model data are calculated from the resistivity scale modelling data, using the mathematical expressions derived in Figure 6.

The anomalous sources and the conductive overburden used in the modelling are large in size and it was not possible to make them entirely uniform. There is some variation in parameters. However, all of the examples, with all of the electrode configurations shown in Figure 8, with and without the overburden, were made at the same time, so that comparisons between the various sets of data are reliable.

a) Vertical Source without overburden

The source used in this scale modelling series is relatively large in size compared to the electrode interval (0.5 units x 4.0 units x 8.0 units). The size scale in the model is not determined, so that the electrode interval could be 100' or 1,000'.

For the first series, the source is vertical in attitude, with a depth to the top of 1.0 units (Figure 10 and Figure 11). The resistivity contrast with the background is 20 to 1 and the IP effect of the source is moderate in magnitude.

THEORETICAL INDUCED POLARIZATION AND RESISTIVITY STUDIES SCALE MODEL CASES

VERTICAL SOURCE WITHOUT OVERBURDEN

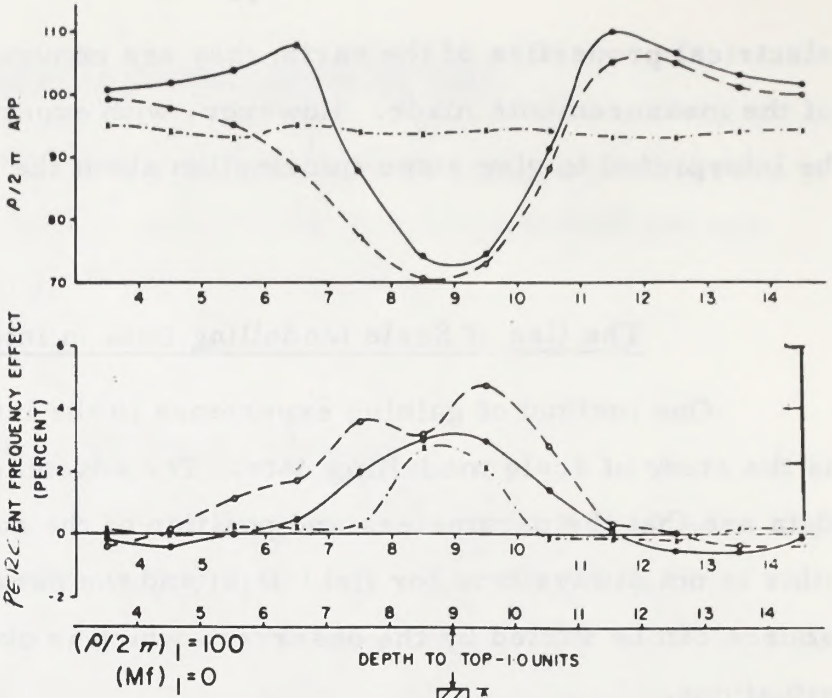

DIPOLE-DIPOLE ARRAY, X=1 UNIT, N=3

POLE-DIPOLE ARRAY, X=1 UNIT, N=3 (REMOTE ELECTRODE - RIGHT)

GRADIENT ARRAY, a=1 UNIT.

$(\rho/2\pi)_1 = 100$

$(Mf)_1 = 0$

PLAN VIEW OF ANOMALOUS ZONE AND SURVEY LINE

LENGTH - 4 UNITS
WIDTH - 0·5 UNITS
DEPTH - 8 UNITS

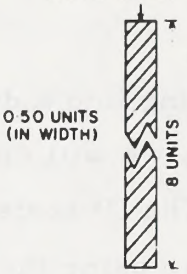

$(\rho/2\pi)_2 = 4.9 \pm 1.5$ (non-uniform)

$(Mf)_2 = 4700 \pm 1000$

$(fe)_2 = 23\% \pm 1.5\%$ (non-uniform)

FIG 1C

THEORETICAL INDUCED POLARIZATION AND RESISTIVITY STUDIES SCALE MODEL CASES

VERTICAL SOURCE WITHOUT OVERBURDEN

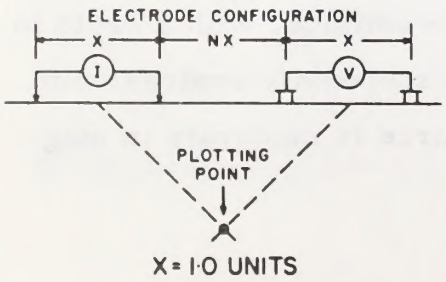

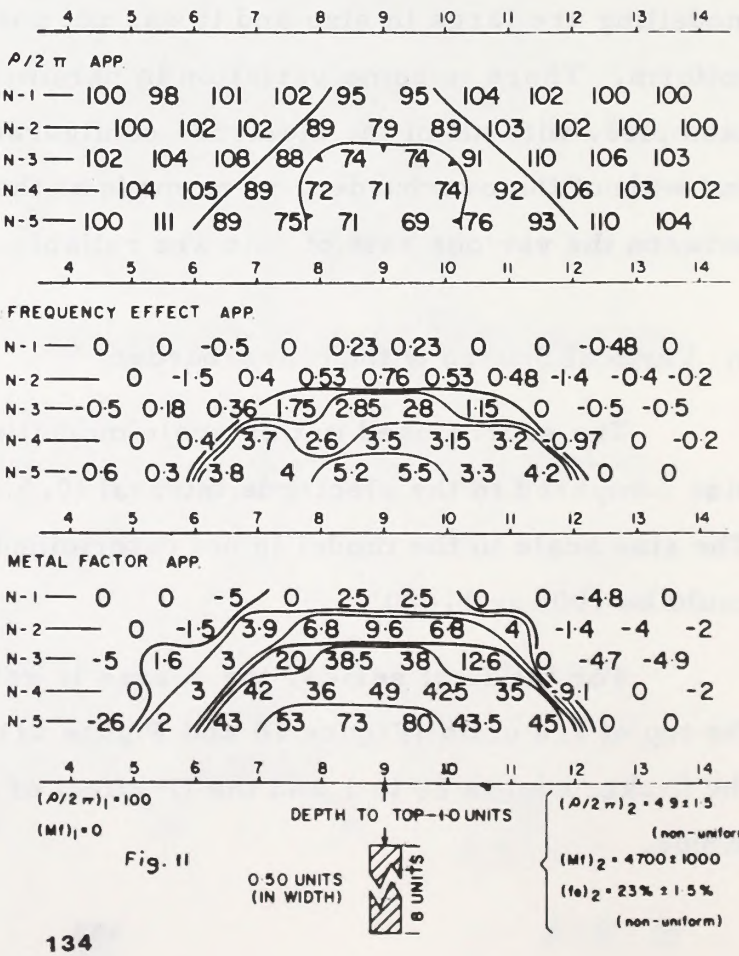

Fig. 11

The profile results shown in Figure 10 show that the gradient array gives no resistivity anomaly and about a 2.0% apparent frequency effect anomaly. The n = 3 measurement for both the pole-dipole and the dipole-dipole electrode configuration gives definite resistivity lows and larger magnitude frequency effects. This insensitivity of the gradient array measurement to a vertical source is to be expected; the vertical source is parallel to the equi-potential lines from the remote current electrodes. There will therefore be little or no distortion of the equi-potential lines and no anomaly is measured on the surface.

In Figure 11 are shown the dipole-dipole data for n = 1,2,3,4,5, plotted in pseudo-section form. The anomalous patterns are typical of those for a relatively narrow, vertical source. The frequency effect anomaly for n = 1 is less than 0.25%. The maximum value of greater than 5.0% is measured for n = 5. Because of the depth of the source and its depth extent, the maximum IP effects are measured for the largest electrode separations. It is, therefore, not possible to determine the width of the source from the anomalous pattern.

b) Vertical Source with overburden

The data in Figure 12 and Figure 13 show the same geometry with a conductive layer that has a thickness of 0.5 units.

Figure 12 shows that the apparent resistivity level measured for the gradient array is 50% higher than that for the other two arrays. However, a small local anomaly from the source at depth is measured for the pole-dipole and the dipole-dipole array.

As would be expected, the presence of the conductive layer has reduced the magnitude of the apparent frequency effect anomalies. The gradient array IP anomaly has almost disappeared. The n = 3 anomaly for the dipole-dipole measurement has been affected the least; it has a magnitude of 3.0%.

THEORETICAL INDUCED POLARIZATION AND RESISTIVITY STUDIES SCALE MODEL CASES

VERTICAL SOURCE WITH OVERBURDEN

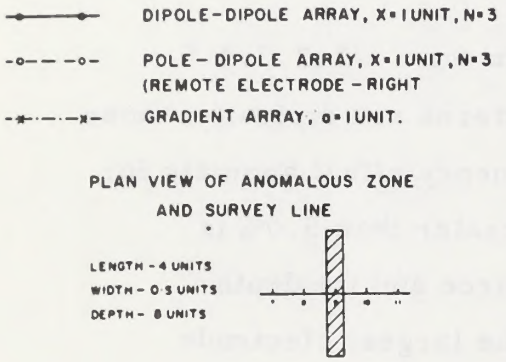

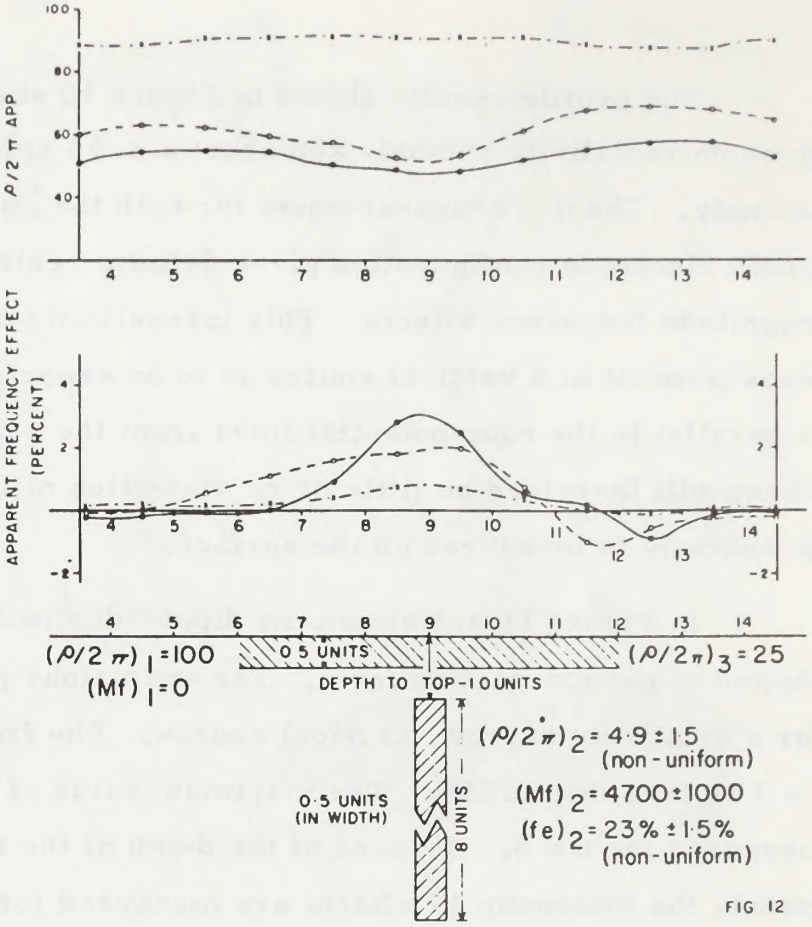

FIG 12

THEORETICAL INDUCED POLARIZATION AND RESISTIVITY STUDIES SCALE MODEL CASES

VERTICAL SOURCE WITH OVERBURDEN

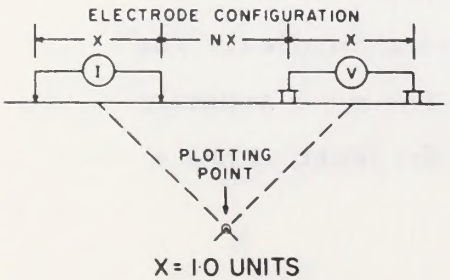

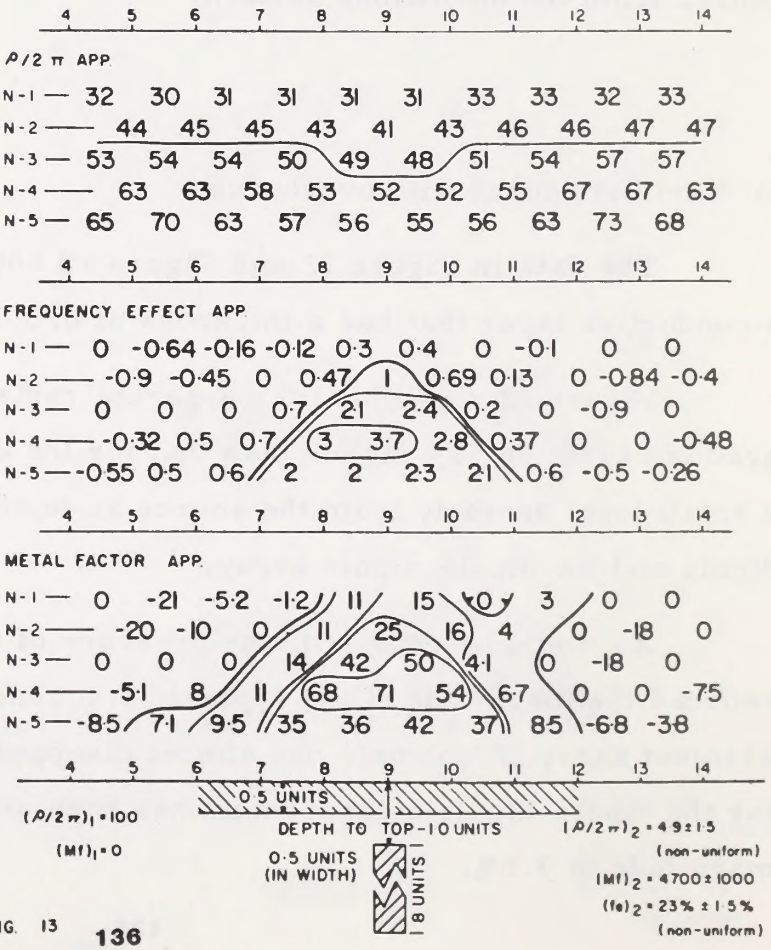

FIG. 13

The dipole-dipole data plotted in Figure 13 can be compared with that in Figure 11 to determine the effect of the conductive surface layer. The apparent resistivity values show the nearly horizontal contours expected for a horizontal surface layer. There is a slight resistivity low over the source. The apparent metal factor anomaly has fewer anomalous values than the pattern in Figure 11 and it appears to be of less width; however, the maximum value of the apparent metal factor is the same in both cases. This is the advantage of the metal factor parameter. It is approximately independent of non-polarizable, conductive zones such as conductive overburden.

c) Horizontal Source without overburden

In Figure 14 and Figure 15, the data are shown for the source in a horizontal position. Since a larger volume of the source is close to the surface (1.0 units to top), the anomalous values measured for all electrode configurations are greater in magnitude. A definite resistivity low is measured for all three configurations. The dipole-dipole data show a maximum apparent frequency effect of about 13.7%, measured for n = 4.

d) Horizontal Source with overburden

As for the vertical source, the presence of the conductive overburden reduced the magnitude of the apparent frequency effects measured (Figure 16 and Figure 17). In this geometry, an anomaly of 5.0% is detected for the gradient array. The anomalous effects are about the same magnitude for all electrode configurations.

The dipole-dipole data in Figure 17 show that the apparent frequency effects are about one-third to one-fourth of the magnitude without overburden. The apparent metal factor values are also lower, but their magnitude is more nearly equal to those in Figure 15.

THEORETICAL INDUCED POLARIZATION AND RESISTIVITY STUDIES SCALE MODEL CASES

HORIZONTAL SOURCE WITHOUT OVERBURDEN

DIPOLE-DIPOLE ARRAY, X = 1 UNIT, N = 3

POLE-DIPOLE ARRAY, X = 1 UNIT, N = 3 (REMOTE ELECTRODE - RIGHT

GRADIENT ARRAY, o = 1 UNIT.

PLAN VIEW OF ANOMALOUS ZONE AND SURVEY LINE

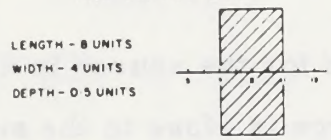

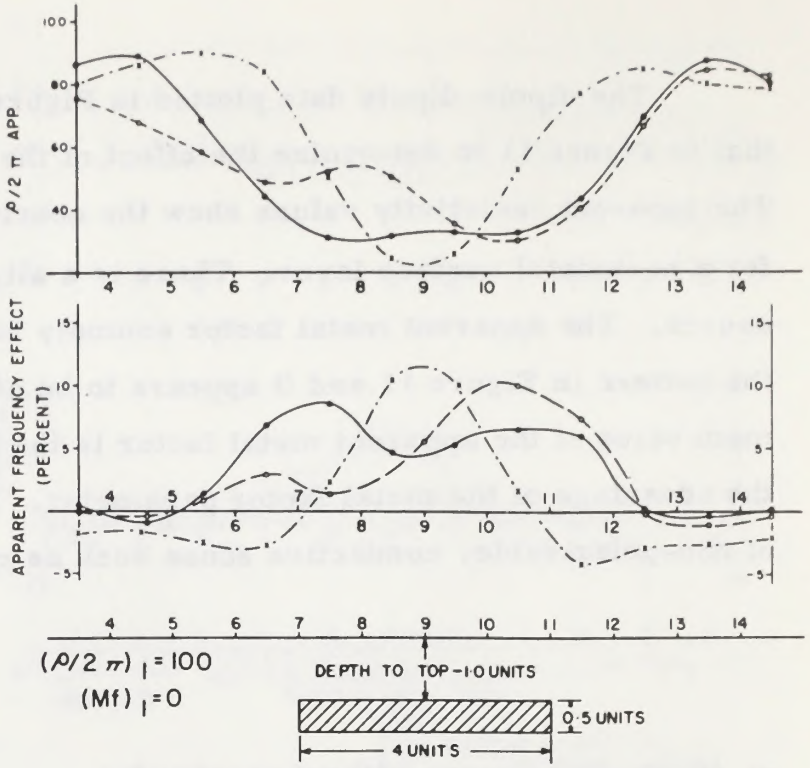

$(\rho/2\pi)_2 = 4.9 \pm 1.5$ (non-uniform)

$(Mf)_2 = 4700 \pm 1000$

$(fe)_2 = 23\% \pm 1.5\%$ (non-uniform)

FIG. 14

THEORETICAL INDUCED POLARIZATION AND RESISTIVITY STUDIES SCALE MODEL CASES

HORIZONTAL SOURCE WITHOUT OVERBURDEN

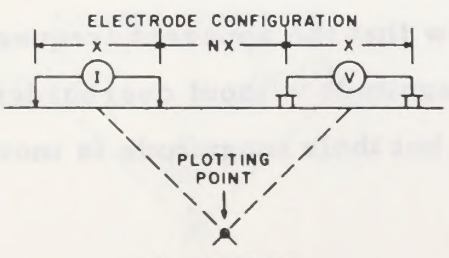

X = 1·0 UNITS

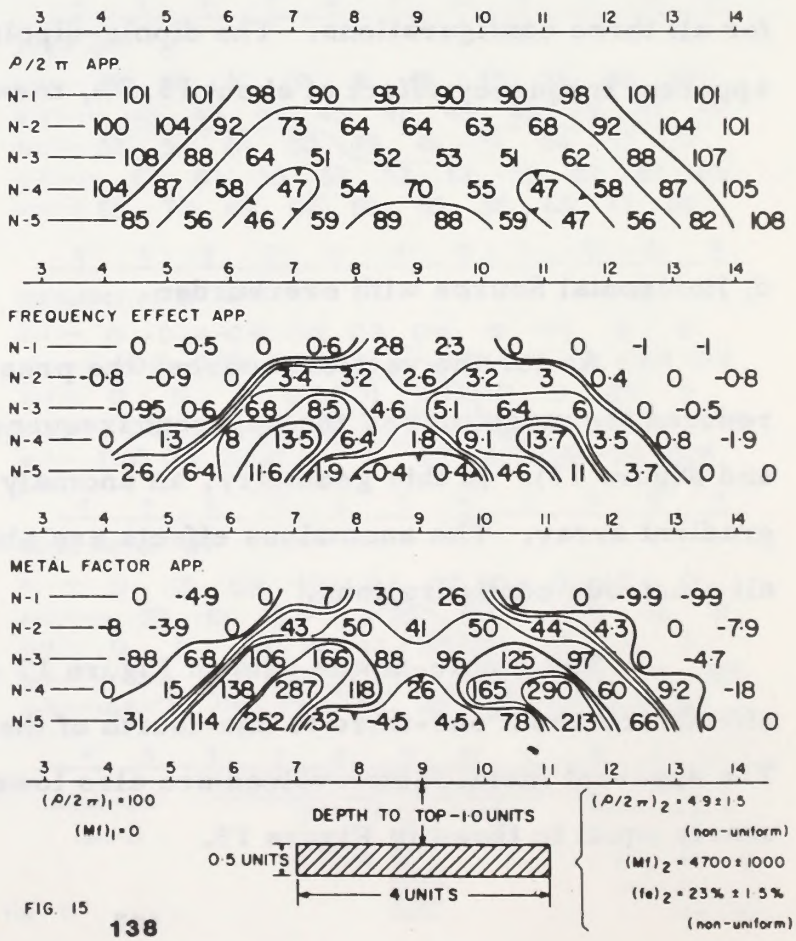

FIG. 15

THEORETICAL INDUCED POLARIZATION AND RESISTIVITY STUDIES SCALE MODEL CASES

HORIZONTAL SOURCE WITH OVERBURDEN

DIPOLE-DIPOLE ARRAY, X = 1 UNIT, N = 3

POLE-DIPOLE ARRAY, X = 1 UNIT, N = 3 (REMOTE ELECTRODE - RIGHT

GRADIENT ARRAY, a = 1 UNIT

PLAN VIEW OF ANOMALOUS ZONE AND SURVEY LINE

LENGTH - 8 UNITS
WIDTH - 4 UNITS
DEPTH - 0.5 UNITS

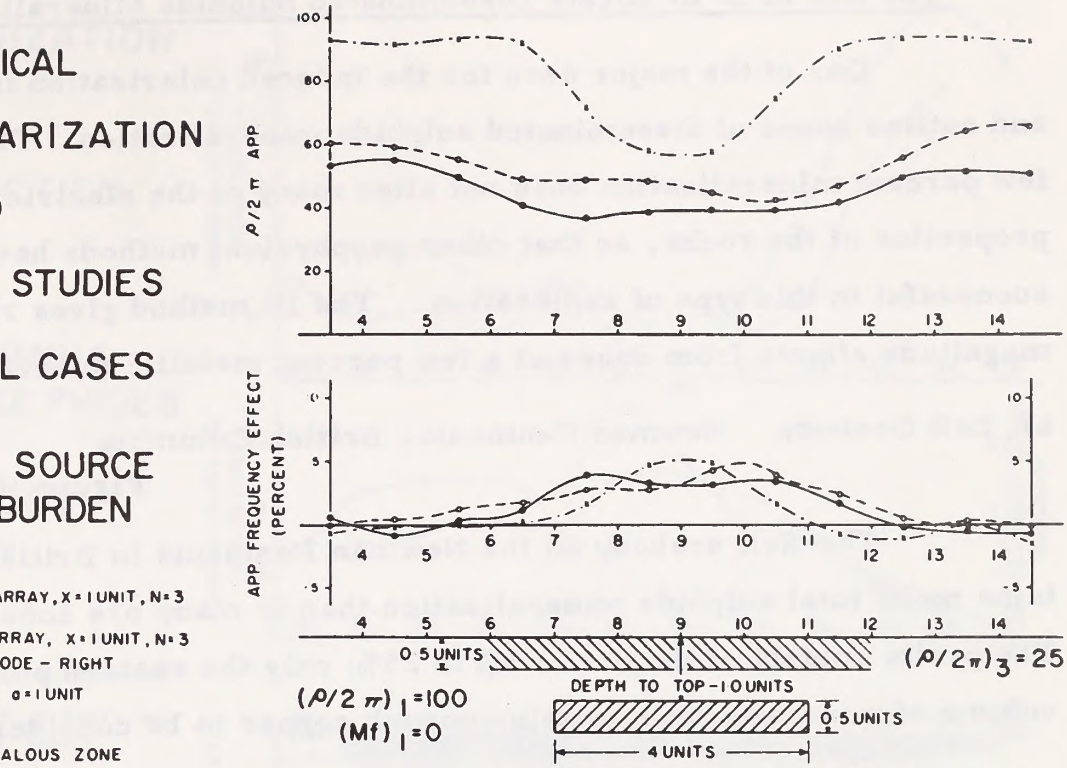

$(\rho/2\pi)_2 = 4.9 \pm 1.5$ (non-uniform)

$(Mf)_2 = 4700 \pm 1000$

$(fe)_2 = 23\% \pm 1.5\%$ (non-uniform)

FIG 16

THEORETICAL INDUCED POLARIZATION AND RESISTIVITY STUDIES SCALE MODEL CASES

HORIZONTAL SOURCE WITH OVERBURDEN

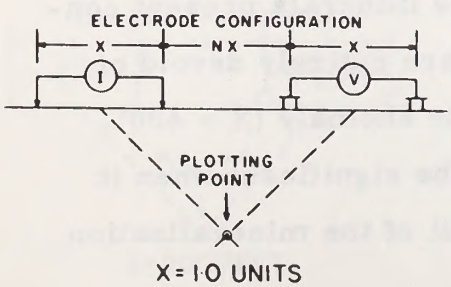

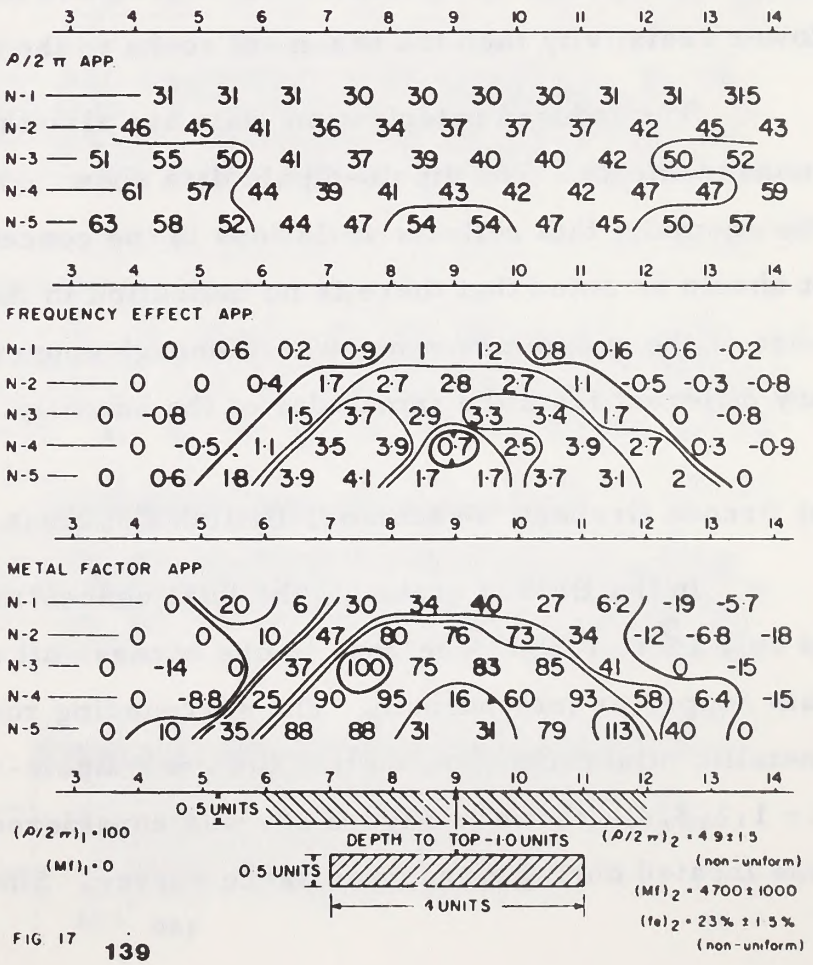

FIG 17

The Use of IP to Locate Disseminated Sulphide Mineralization

One of the major uses for the induced polarization method is to locate and outline zones of disseminated sulphide mineralization. The presence of a few percent mineralization does not alter many of the electrical or physical properties of the rocks, so that other geophysical methods have not been successful in this type of exploration. The IP method gives rise to large magnitude effects from zones of a few percent metallic mineralization.

a) Bell Orebody Newman Peninsula, British Columbia
Figure 18 and Figure 19

The Bell orebody on the Newman Peninsula in British Columbia contains more total sulphide mineralization than in many ore zones of this type. The pyrite content of the ore is 5% to 25%; only the eastern portion of the large volume of mineralization contains enough copper to be considered ore.

Time domain IP data are available for pole-dipole data (three-array), using X = 200', n = 1 and frequency domain data using the dipole-dipole array for X = 200', n = 1,2,3,4. The broad, relatively shallow zone of strongly disseminated sulphide mineralization gives the same results for both types of measurements. The fractured, altered and mineralized rock has a much lower resistivity than the basement rocks to the east.

The induced polarization data are also the same for both types of measurements. The dipole-dipole data show considerable variability within the anomaly; this reflects variations in the concentration of metallic minerals. It should be noted that there is no indication in the IP data that the eastern edge of the anomalous zone, where enough copper is present to make ore, is any different from the remainder of the anomaly.

b) Brenda Orebody Peachland, British Columbia Figure 20

In the Brenda orebody, the total concentration of metallic mineralization is only 1% to 1.5%. The zone is ore because all of the minerals present contain copper or molybdenum. The surrounding rocks are entirely devoid of metallic mineralization, so that the weak dipole-dipole anomaly (X = 400', n = 1,2,3,4), shown in Figure 20, was considered to be significant when it was located during a reconnaissance survey. Since all of the mineralization

INDUCED POLARIZATION AND GEOLOGIC SECTION FROM BRITISH COLUMBIA DISSEMINATED SULPHIDES

BELL OREBODY LINE-22N

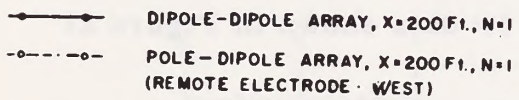

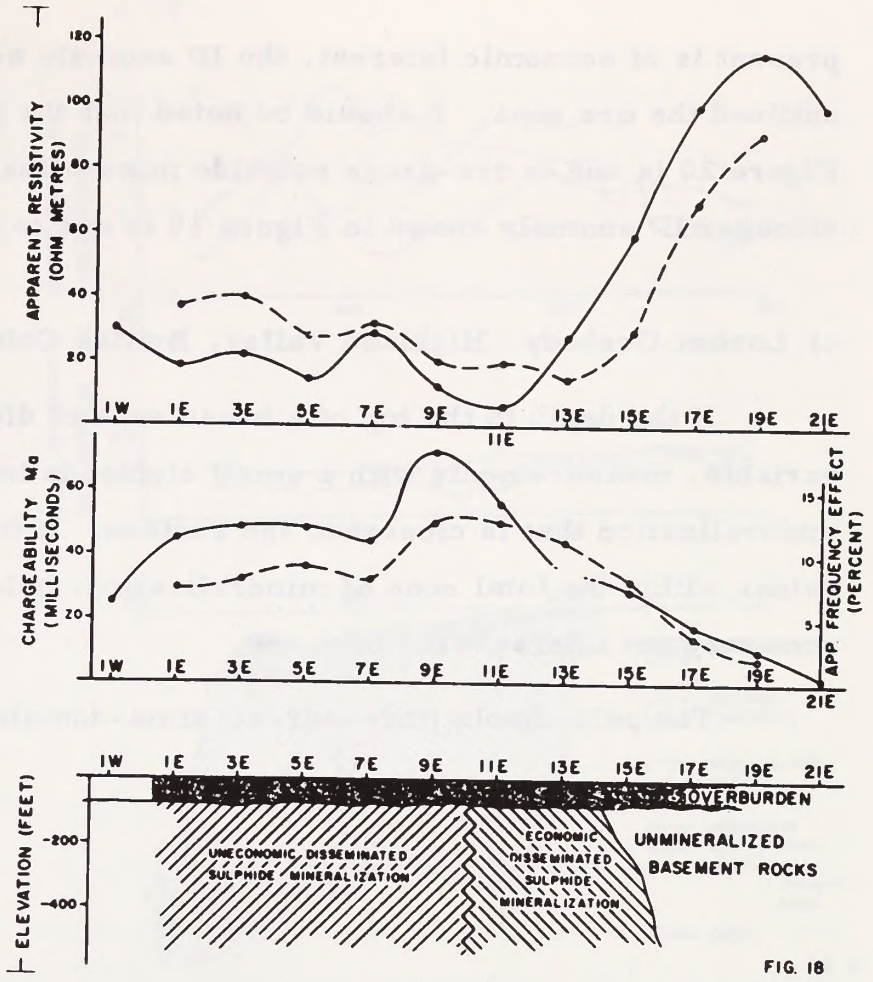

FIG. 18

INDUCED POLARIZATION AND GEOLOGIC SECTION FROM BRITISH COLUMBIA DISSEMINATED SULPHIDES

BELL OREBODY LINE-22N

FREQUENCIES- 0·31/5HZ

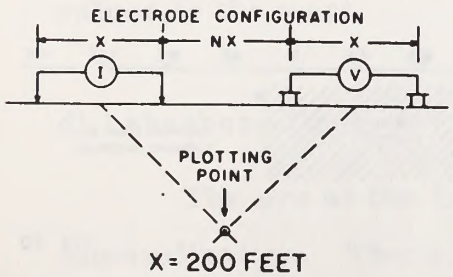

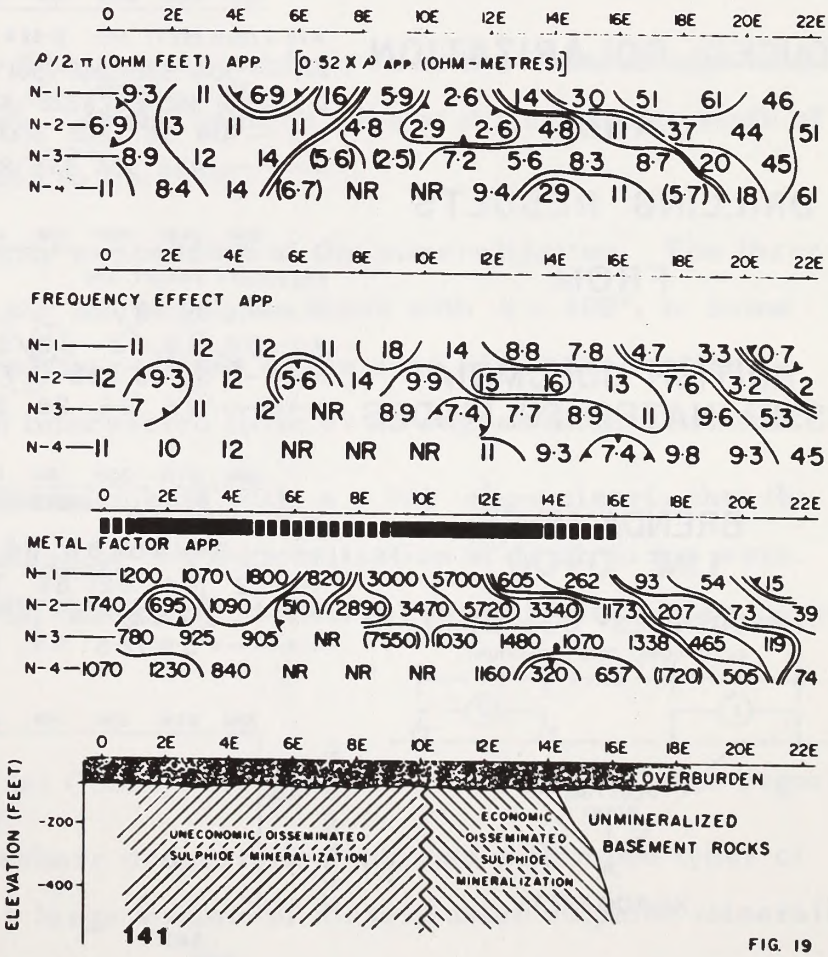

FIG. 19

present is of economic interest, the IP anomaly accurately and completely outlined the ore zone. It should be noted that the weak IP anomaly shown in Figure 20 is due to ore-grade sulphide mineralization, while most of the much stronger IP anomaly shown in Figure 19 is due to pyrite alone.

c) Lornex Orebody Highland Valley, British Columbia Figure 21

If the depth to the top of a broad zone of disseminated mineralization is variable, measurements with a small electrode interval may detect only the mineralization that is closest to the surface. If there is zoning of the copper values within the total zone of mineralization, holes drilled to test the shallow zone may not intersect the best ore.

The pole-dipole (three-array) time-domain IP data shown in Figure 21

INDUCED POLARIZATION
AND
DRILLING RESULTS
FROM
BRITISH COLUMBIA
DISSEMINATED SULPHIDES

BRENDA MINES
LINE 0+00

FREQUENCIES- 0·31/ 2·5 HZ.

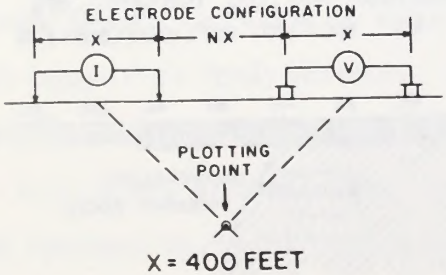

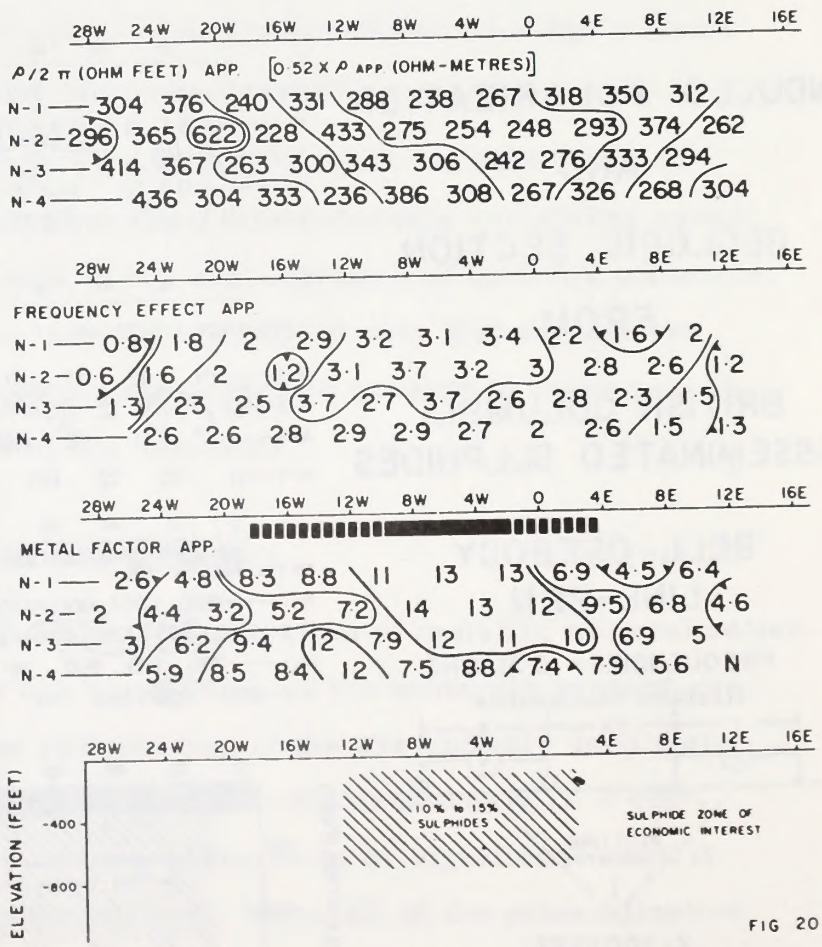

FIG 20

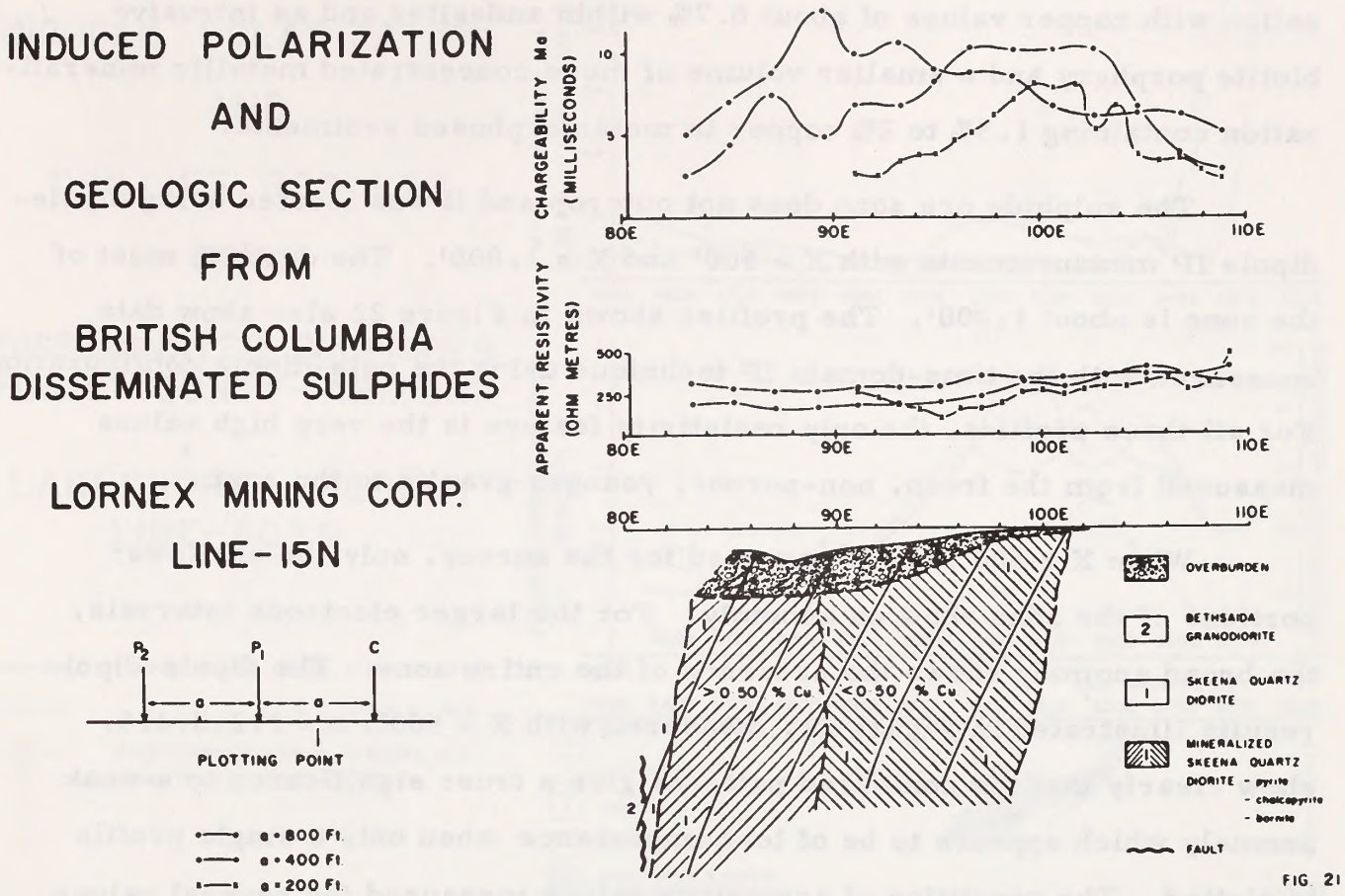

FIG. 21

are from such a situation. The Lornex orebody is at the western edge of a broad zone of mineralization. At the eastern edge of the zone, the depth of overburden is much less than to the west.

There is no resistivity expression of the mineralization. The three-array measurements with a = 200' and also those with a = 400', to some extent, indicate only the shallow portions of the zone of mineralization. Holes drilled in this region intersected little or no copper mineralization.

The three-array measurements with a = 800' show clearly that the strongest IP effects are caused by the mineralization at depth to the west. Drilling has confirmed more concentrated mineralization, with higher copper values, to the west.

d) Lakeshore Orebody Pinal County, Arizona Figure 22 and Figure 23

The ore at the Lakeshore property is contained within two types of mineralization. There is a large volume of disseminated sulphide minerali-

zation with copper values of about 0.7% within andesites and an intrusive biotite porphyry and a smaller volume of more concentrated metallic mineralization containing 1.5% to 2% copper in metamorphosed sediments.

The sulphide ore zone does not outcrop and it was located using dipole-dipole IP measurements with X = 500' and X = 1,000'. The depth to most of the zone is about 1,000'. The profiles shown in Figure 22 also show data measured with the time-domain IP technique using the pole-dipole configuration. For all three profiles, the only resistivity feature is the very high values measured from the fresh, non-porous, younger granite to the east.

When X = 500', n = 3 was used for the survey, only the shallower portions of the zone show an anomaly. For the larger electrode intervals, the broad anomaly shows the presence of the entire zone. The dipole-dipole results illustrated in Figure 22, measured with X = 500', n = 1,2,3,4,5, show clearly that the contoured patterns give a truer significance to a weak anomaly which appears to be of less importance when only a single profile is plotted. The repetition of anomalous values measured for several values of n confirms the presence of an anomalous source.

e) Yalguaraz Zone Mendoza, Argentina Figure 24

If a zone of disseminated sulphide mineralization is large enough, even for concentrations as low as 1.5% to 3.0% total sulphides, it can be detected at considerable depths using IP.

The dipole-dipole (X = 200 meters; n = 1,2,3,4) measurements shown in Figure 24 located a zone of disseminated mineralization under almost 200 meters of valley alluvium. The measurements for n = 1 are not anomalous, but the measurements for n = 4 are definitely anomalous. At Yalguaraz, the altered intrusive at depth has a lower resistivity than the porous alluvium.

The Use of the IP Method to Locate Lead-Zinc Mineralization in Limestones

The induced polarization method has also been found to be very successful in the search for ore zones which are not truely disseminated, but which do

INDUCED POLARIZATION AND DRILLING RESULTS FROM DISSEMINATED SULPHIDES PINAL COUNTY-ARIZONA

LAKESHORE OREBODY LINE-507N

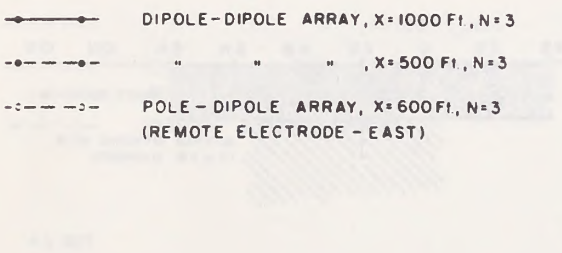

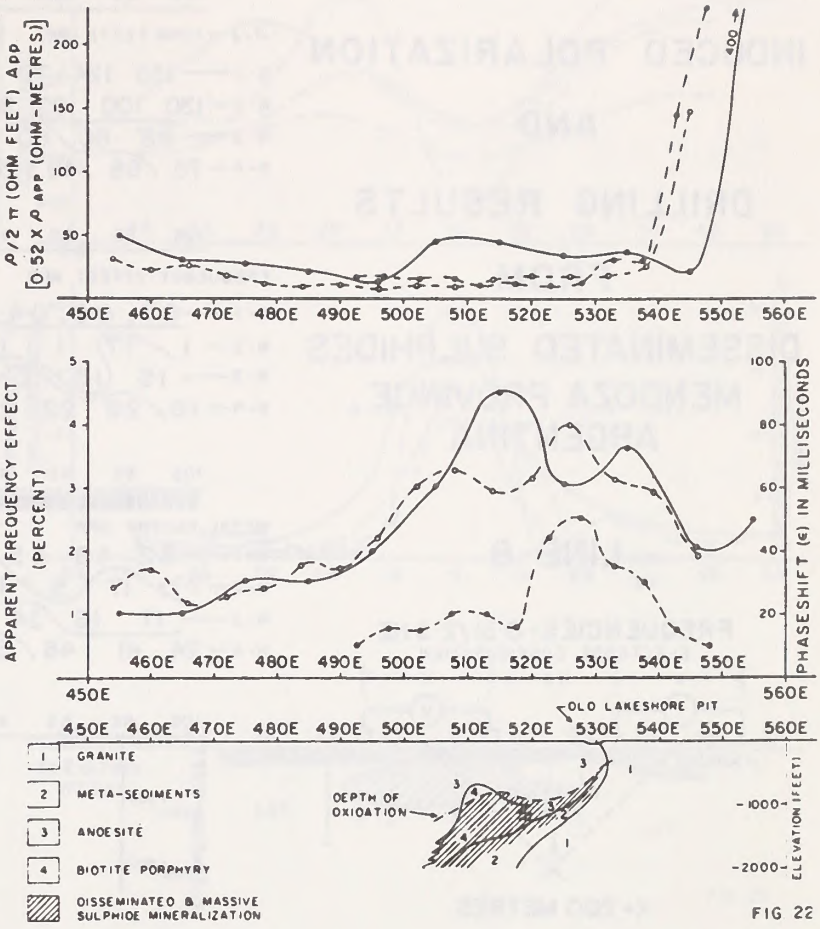

FIG 22

INDUCED POLARIZATION AND DRILLING RESULTS FROM DISSEMINATED SULPHIDES LAKESHORE OREBODY PINAL COUNTY-ARIZONA

LINE-498N

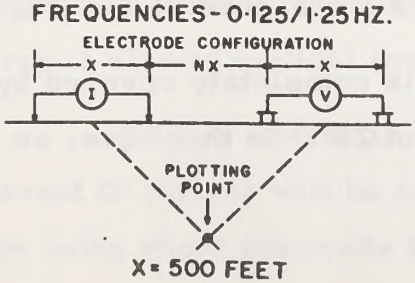

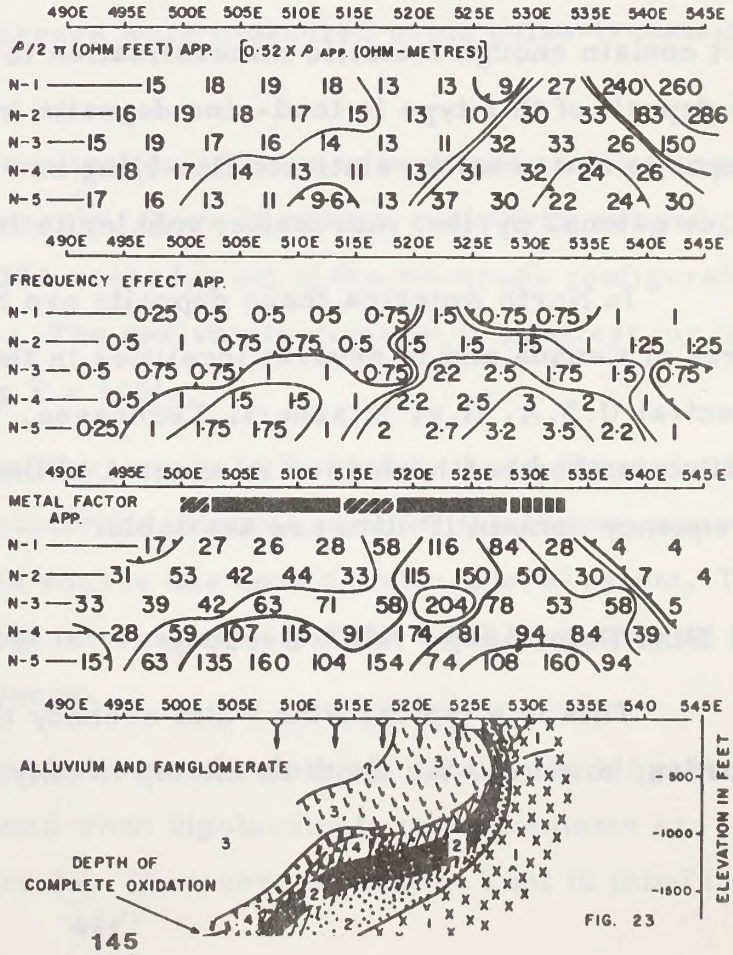

FIG. 23

INDUCED POLARIZATION AND DRILLING RESULTS FROM DISSEMINATED SULPHIDES MENDOZA PROVINCE, ARGENTINA

LINE-8

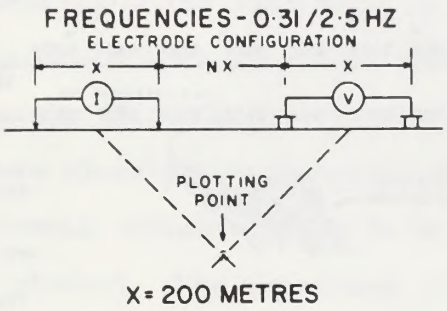

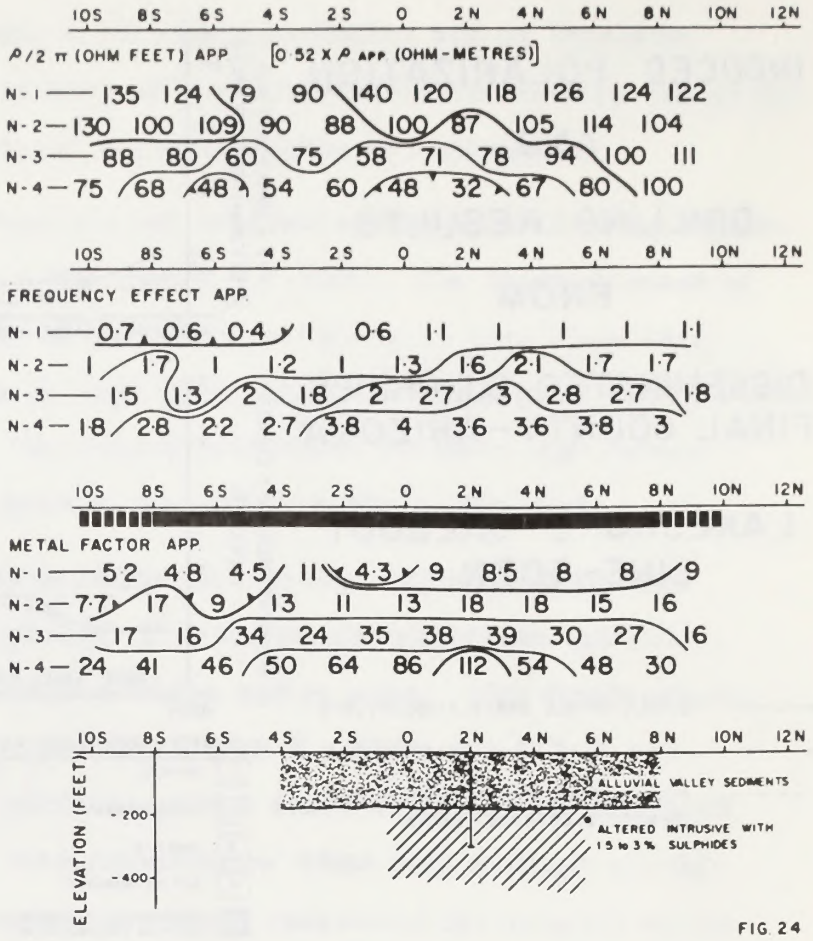

FIG. 24

not contain enough metallic mineralization to be considered massive. One type of deposit of this type is lead-zinc deposits in limestones. These stratabound deposits are usually relatively flat-lying and contain 3% to 30% metallic minerals (i.e. galena, pyrite, marcasite; sphalerite is non-metallic).

In North America, these deposits are being exploited in the Pine Point area of Canada and in several localities in the sedimentary basins of the Central U.S.A. (i.e. Missouri, Tennessee, Wisconsin). The induced polarization method has been used in several of these areas. Both time-domain and frequency domain IP data are available.

a) Pine Point Area N38A Orebody Figure 25, Figure 26 and Figure 27

This is a typical Pine Point orebody that is completely covered by overburden; however, the depth to the top is only about 25'. In this case, as in all

INDUCED POLARIZATION AND DRILLING RESULTS FROM PINE POINT TYPE MINERALIZATION

N-38A OREBODY LINE-P3·0E

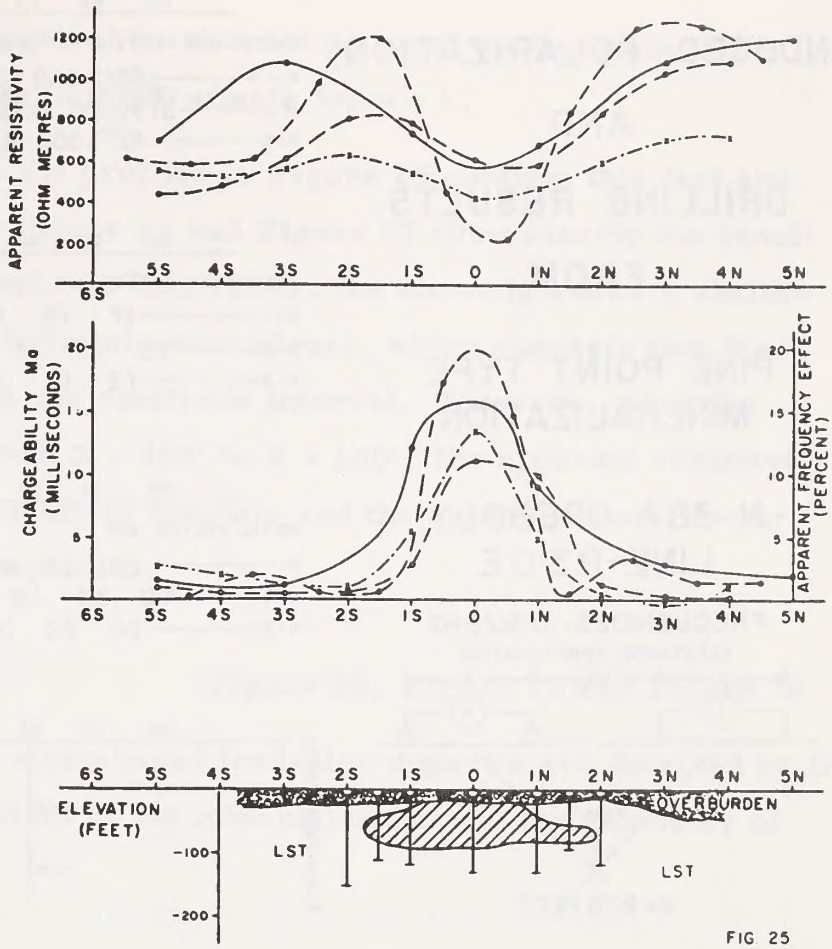

DIPOLE-DIPOLE ARRAY, X=200 Ft., N=1

" " " ,X=100 Ft., N=1

POLE-DIPOLE ARRAY, X=200 Ft., N=1 (REMOTE ELECTRODE - SOUTH)

GRADIENT ARRAY, a=200 Ft.

FIG. 25

of the following cases, the dipole-dipole data is variable frequency IP data, while all of the other electrode arrays were measured using pulse-transient IP equipment.

When this type of mineralization is large enough and shallow enough and contains enough metallic minerals, there is often a resistivity anomaly measured. In the case of the N38A orebody, all of the electrode configurations gave an apparent resistivity low. The resistivity contrast is greatest for the dipole-dipole configuration using X = 100'.

When the source of the IP anomaly is limited in three dimensions, the electrode configuration and electrode interval used for the survey are of greater importance than when the source has considerable lateral extent. The relationship between the electrode interval used and the depth to the top of the source is also of critical importance.

When a source is very shallow and relatively small, the largest apparent IP effects will be obtained when dipole-dipole measurements are made using short electrode intervals. However, it must be kept in mind that

INDUCED POLARIZATION AND DRILLING RESULTS FROM PINE POINT TYPE MINERALIZATION

N-38A OREBODY LINE-P3·0E

FREQUENCIES- 0·31/5HZ

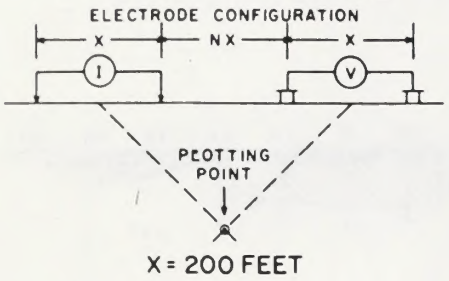

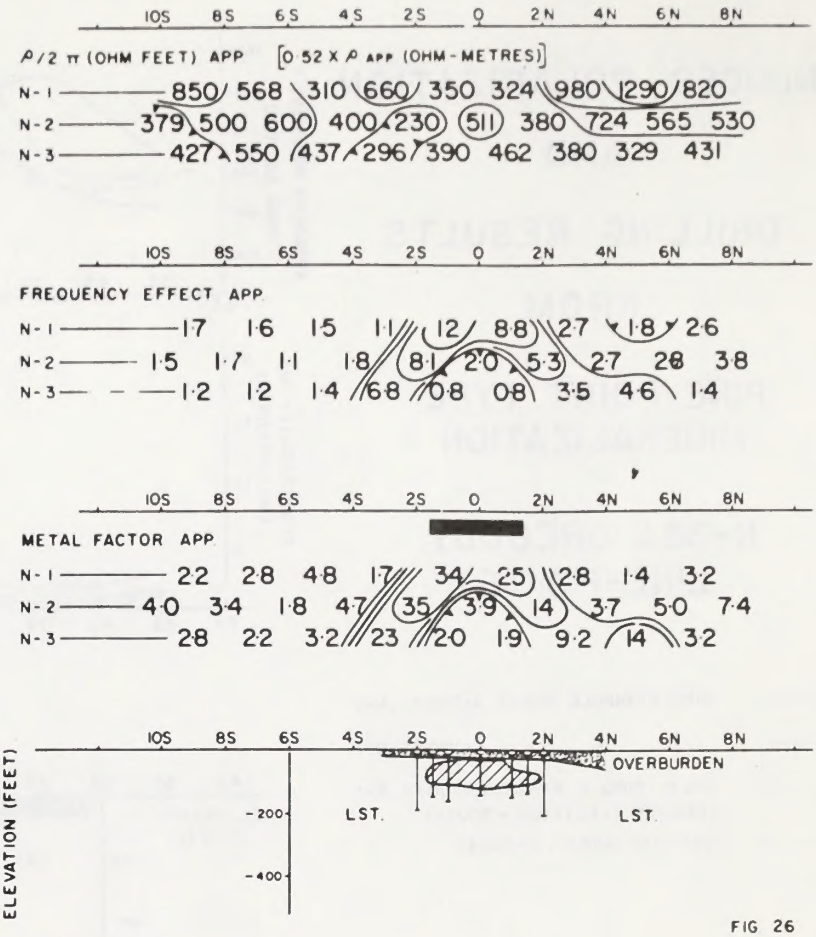

FIG. 26

INDUCED POLARIZATION AND DRILLING RESULTS FROM PINE POINT TYPE MINERALIZATION

N-38A OREBODY LINE-P3·0E

FREQUENCIES- 0·31/5HZ

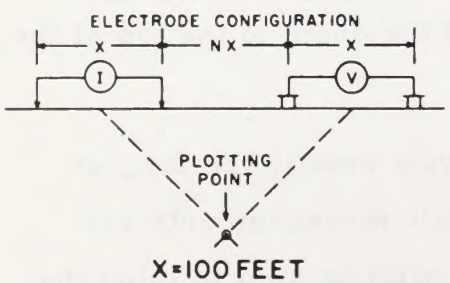

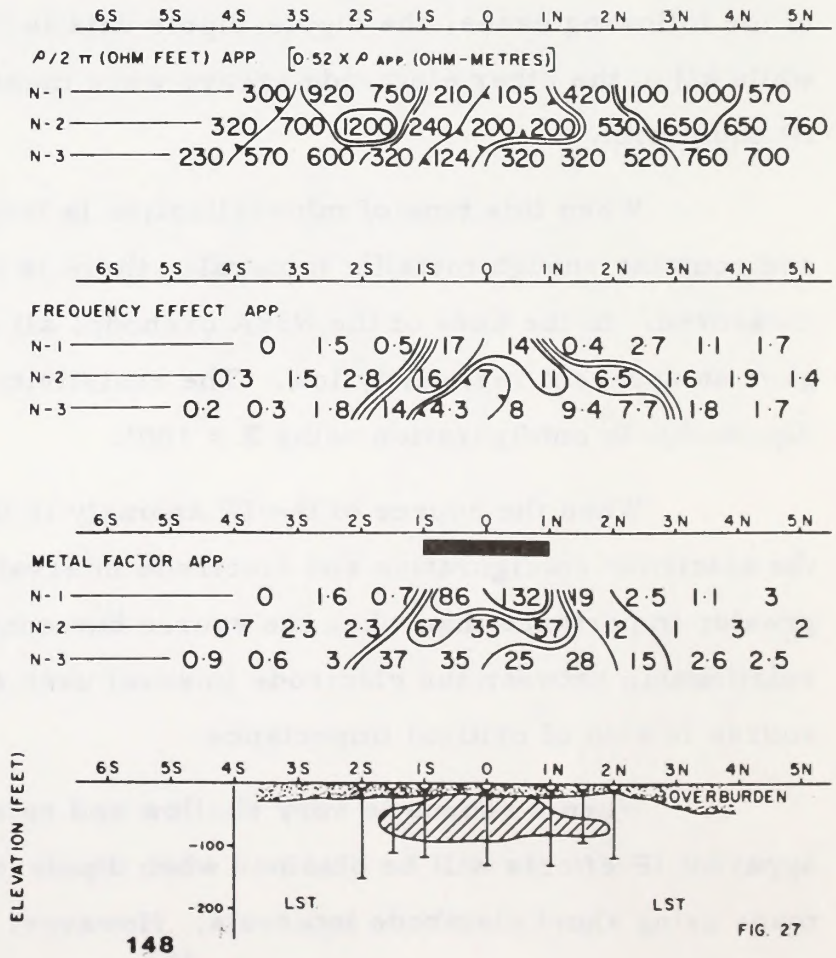

FIG. 27

the electrode interval used must be at least twice as great as the depth to the top of the source to give the maximum IP effects for n = 1.

The results shown in the profiles in Figure 25 confirm this fact and the dipole-dipole data shown in Figure 26 and Figure 27 show clearly the result of changing the electrode interval. In both cases, the anomaly shows a shallow source (i.e. the n = 1 value is definitely anomalous), which suggests that the source is at a depth of less than one electrode interval. However, when the electrode interval is changed from X = 200' to X = 100', the apparent resistivity anomaly, the apparent frequency effect anomaly and the apparent metal factor anomaly are much greater in magnitude.

b) Pine Point K62 Orebody Figure 28, Figure 29 and Figure 30

In many cases where stratabound lead-zinc deposits are detected by IP measurements, the mineral content of the mineralization and the geometry of

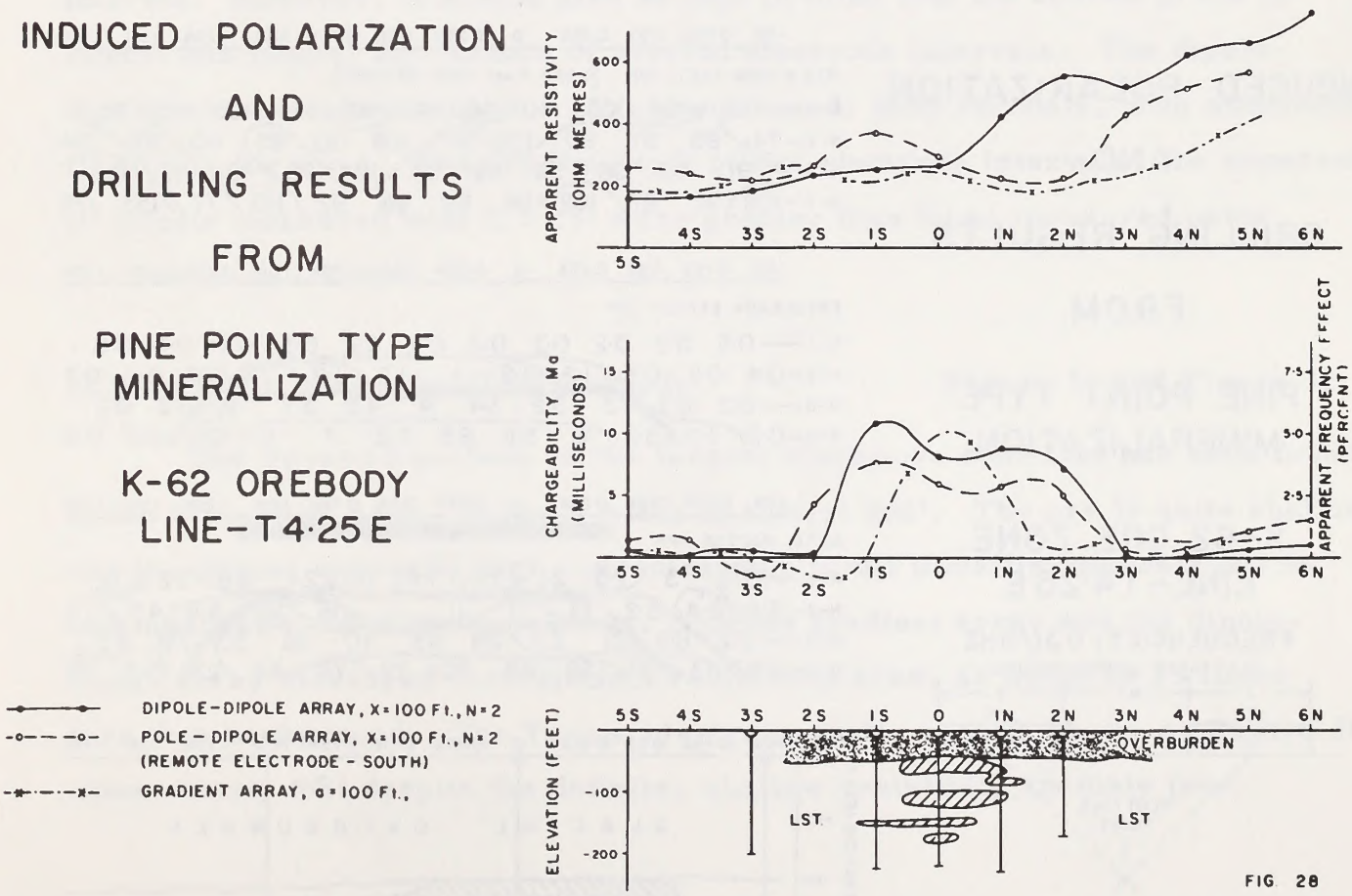

FIG 28

INDUCED POLARIZATION AND DRILLING RESULTS FROM PINE POINT TYPE MINERALIZATION

K-62 ORE ZONE LINE-T4·25E

FREQUENCIES - 0·31/5HZ

ELECTRODE CONFIGURATION

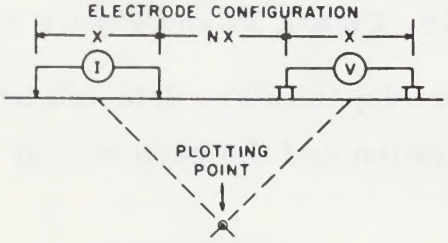

X=200 FEET

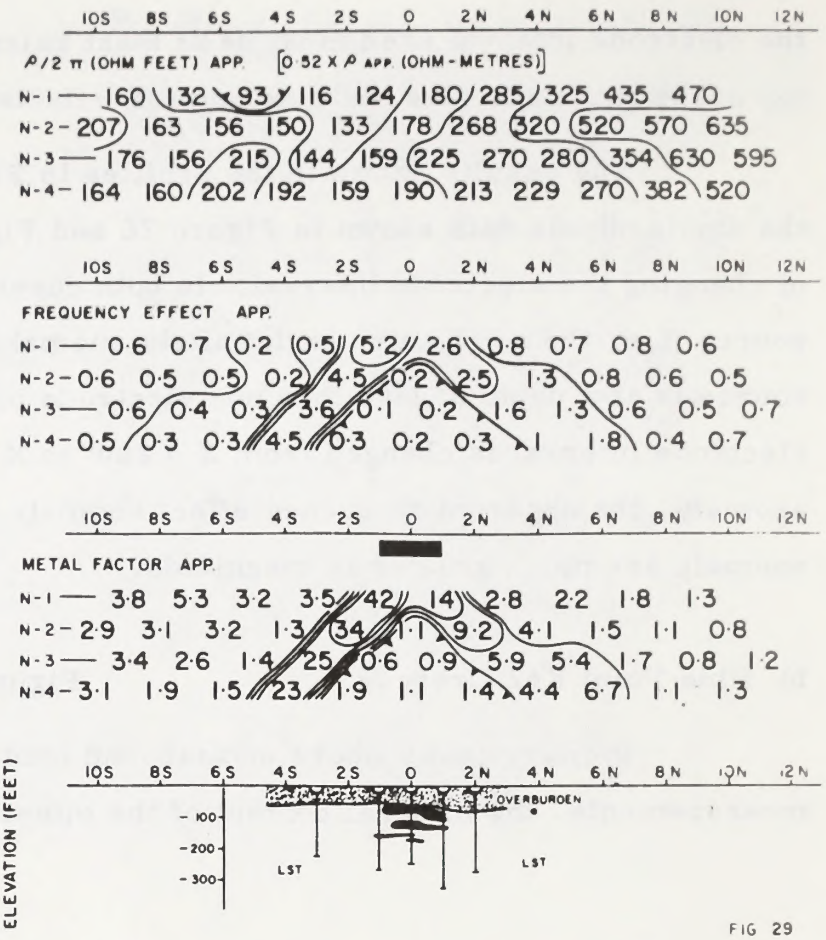

FIG 29

INDUCED POLARIZATION AND DRILLING RESULTS FROM PINE POINT TYPE MINERALIZATION

K-62 ORE ZONE LINE-T4·25E

FREQUENCIES - 0·31/5HZ

ELECTRODE CONFIGURATION

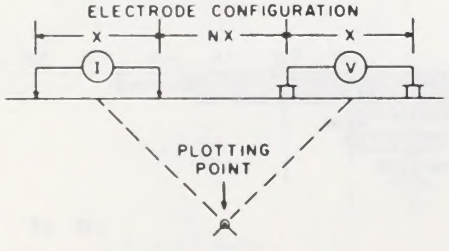

X= 25 FEET

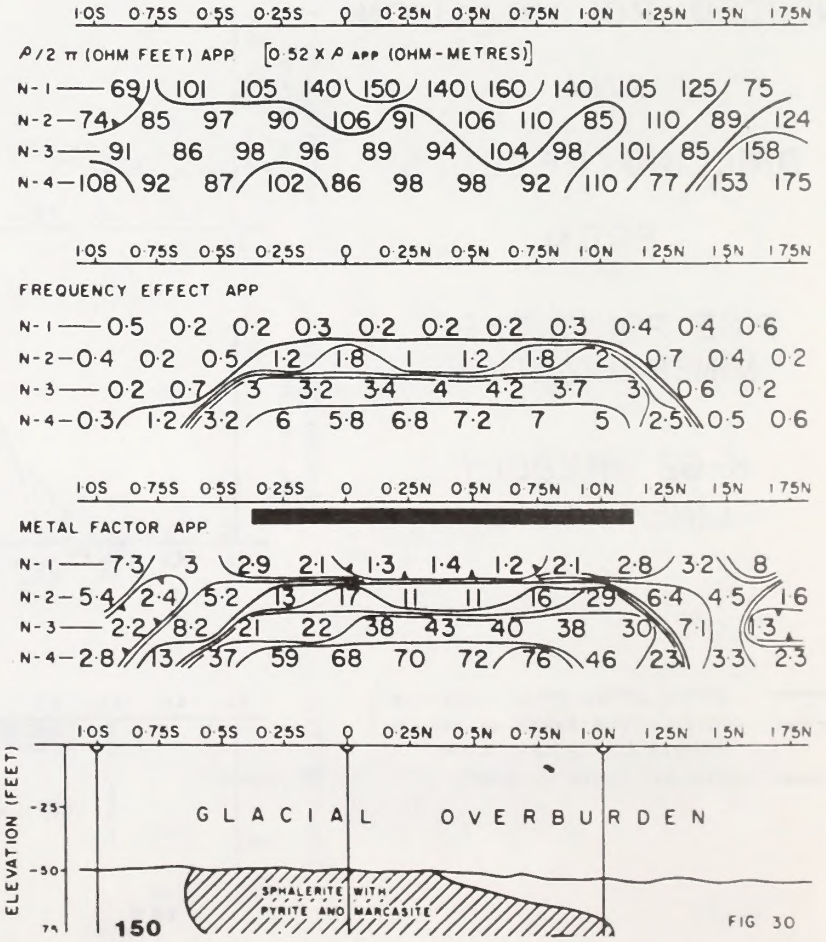

FIG 30

the situation are such that there is no apparent resistivity anomaly measured. This is the case with the K62 orebody at Pine Point.

The resistivity profiles illustrated in Figure 28 show only that the resistiv level in the limestones increases to the north. There is no anomaly from the mineralization. As in the case of the N38A orebody, all of the electrode configurations give rise to a distinct IP anomaly, with the dipole-dipole array giving the largest magnitude anomaly. It should also be noted that none of the profiles suggest the presence of the multiple sources.

The dipole-dipole results shown in Figure 29 and Figure 30 are a dramatic example of the different anomalous magnitudes and anomalous patterns that are measured using widely different electrode intervals over the same zone of mineralization. The measurements with X = 200' show a shallow, narrow anomaly that correlates with the mineralization. As mentioned previously, there is no correlating resistivity low.

The data shown in Figure 30 are from a detailed survey using X = 25'. In this case, the depth to the top of the source is equal to twice the electrode interval. However, it should also be kept in mind that the source of the IP effects has lateral dimensions of several electrode intervals. The dipole-dipole measurements with X = 25' show a broad, deep anomaly, with maximum IP effects for n = 4. Despite the depth of two electrode intervals, the apparent IP effects measured with X = 25' were greater than those measured using X = 100' or X = 200'.

c) Pine Point Area Pyramid Orebody Figure 31 and Figure 32

The Pyramid orebody is the largest single ore zone that has been found in the Pine Point area. It has a width of almost 800'. The ore is quite shallow and it contains unusually high concentrations of the metallic minerals pyrite and marcasite. For these reasons, both the gradient array and the dipole-dipole array measured very distinct resistivity lows, as much as 25 times less than background. The Turam electromagnetic results shown on Figure 31 show clearly that despite the definite, shallow resistivity anomaly (see

GEOPHYSICAL DATA AND DRILLING RESULTS FROM PINE POINT TYPE MINERALIZATION

PYRAMID OREBODY LINE-375W

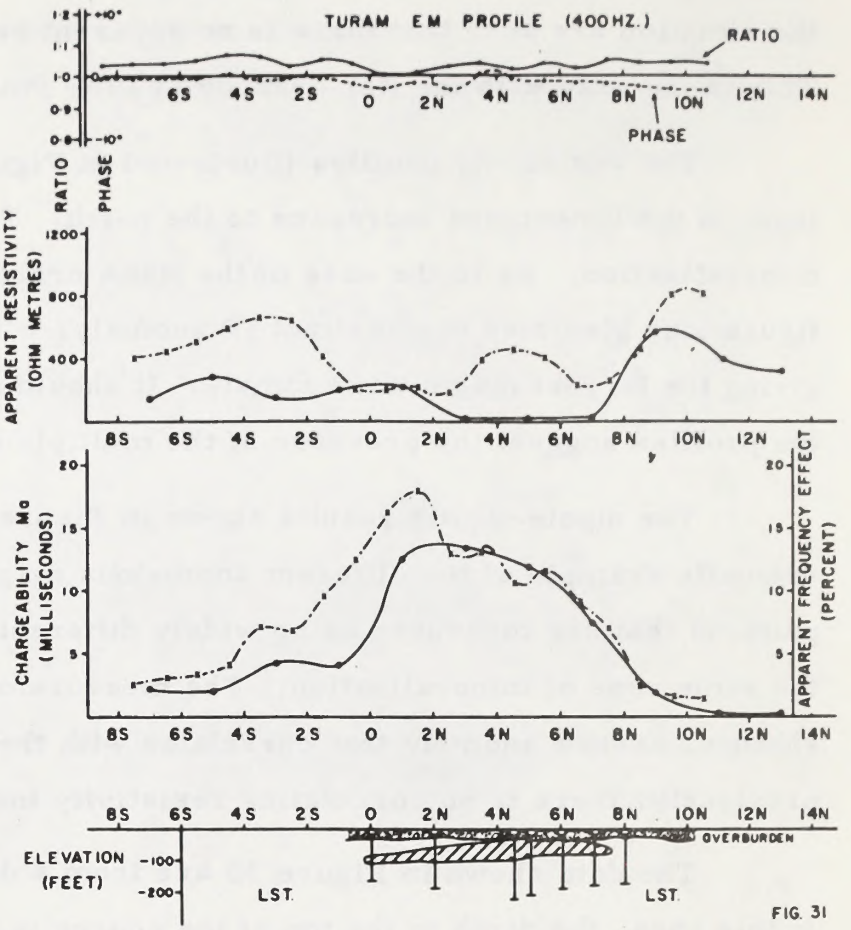

FIG. 31

INDUCED POLARIZATION AND DRILLING RESULTS FROM PINE POINT TYPE MINERALIZATION

PYRAMID OREBODY LINE-375W

FREQUENCIES- 0.31/5HZ

ELECTRODE CONFIGURATION

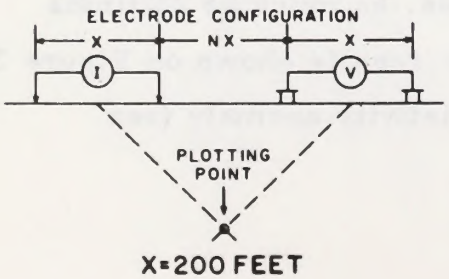

X=200 FEET

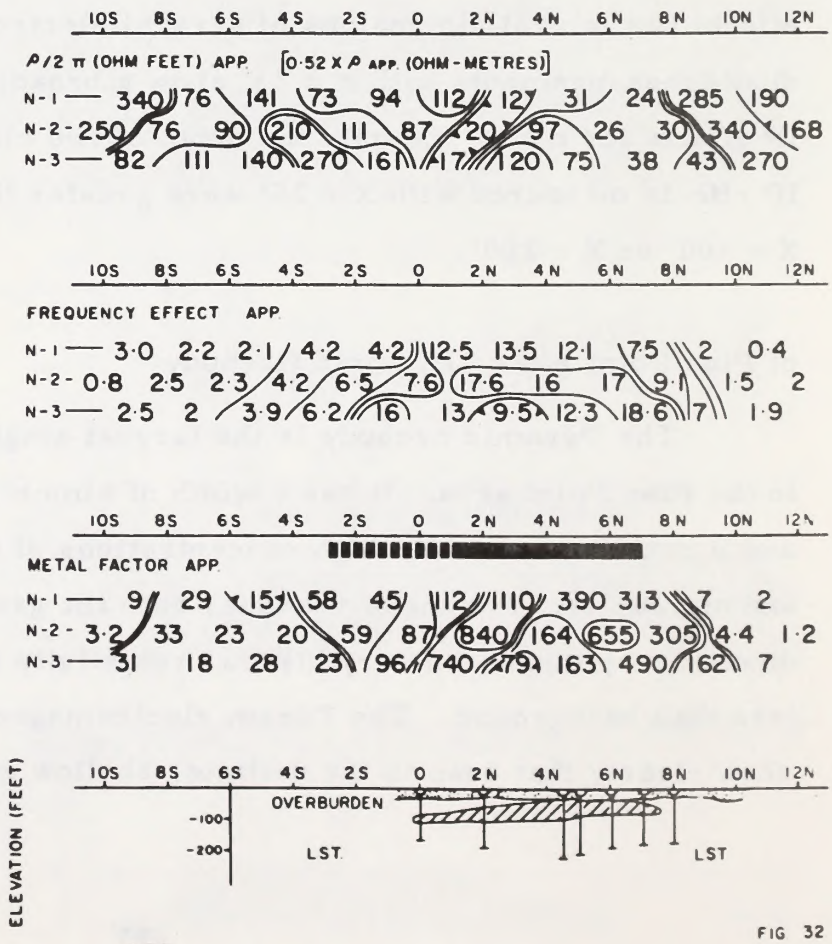

FIG 32

particularly Figure 32), no electromagnetic response can be measured at 400 Hz from this type of mineralization.

The IP profiles in Figure 31 show almost exactly the same anomaly from the gradient array (a = 100') and the dipole-dipole configuration using X = 200', n = 1. This result confirms the scale modelling data; for broad, flat-lying, shallow sources, all of the electrode configurations are equally effective.

d) Pine Point Area Line R0.7W Orebody Figure 33

The results shown in Figure 33 confirm that for relatively small sources, at some depth, all electrode configurations are not equally effective. Here, none of the electrode configurations used give rise to an interpretable resistivity low. The IP profiles show no anomaly for the gradient array (a = 200') measurement. The pole-dipole profiles (X = 200') show low magnitude, but definite, anomalies for both n = 1 and n = 2.

e) Wisconsin Lead-Zinc Field Line 2E Figure 34

The stratabound lead-zinc deposits in limestones are much the same in all parts of the world in which they occur. The data shown in Figure 34 are from a small ore zone located in Wisconsin. The source is at a depth of almost 400'; this is about twice the 200' electrode interval used for the dipole-dipole IP measurements.

The source contains appreciable pyrite and marcasite. There is a low magnitude, but distinct, resistivity low associated with the IP anomaly. The metal factor anomaly pattern suggests a relatively narrow source at some depth. The vertical loop (dip angle) electromagnetic measurements, using 1000 Hz and 5000 Hz, show no anomaly associated with the ore zone.

The Use of the IP Method to Locate Massive Mineralization

In most mineral exploration problems in which the target is massive sulphide mineralization, geophysicists usually choose an electromagnetic

INDUCED POLARIZATION AND DRILLING RESULTS FROM PINE POINT TYPE MINERALIZATION

COMINCO-PINE POINT LINE-R 0·7W

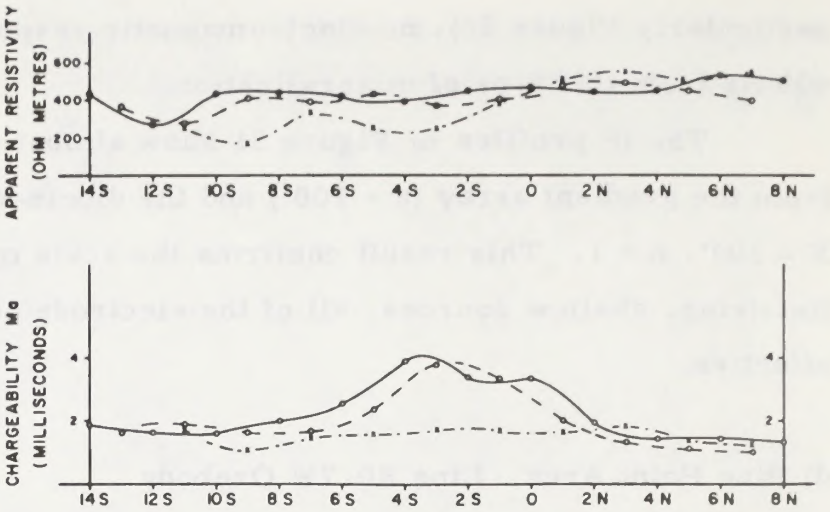

-o- - -o- POLE - DIPOLE ARRAY, X = 200 Ft., N = 1 (REMOTE ELECTRODE - SOUTH)

POLE - DIPOLE ARRAY, X = 200 Ft., N = 2 (REMOTE ELECTRODE - SOUTH)

-x- - -x- GRADIENT ARRAY, a = 200 Ft.

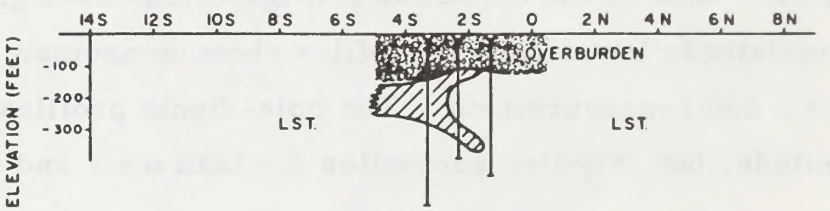

FIG. 33

GEOPHYSICAL DATA AND DRILLING RESULTS FROM PINE POINT TYPE MINERALIZATION

WISCONSIN LEAD-ZINC FIELD LINE-2 E

FREQUENCIES - 0·31/5HZ

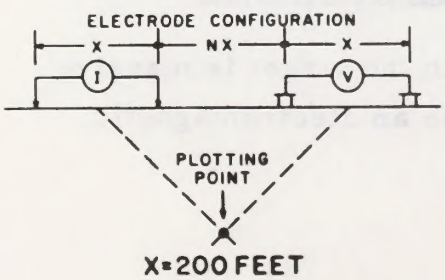

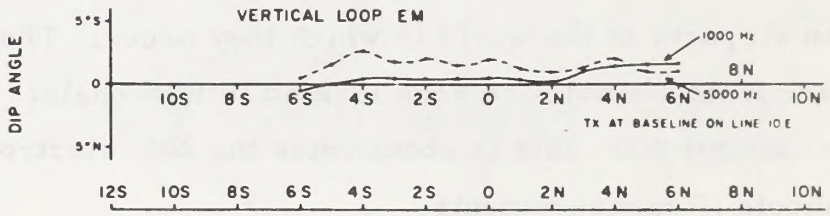

ρ/2π (OHM FEET) APP. [0·52 X ρ APP. (OHM-METRES)]

N-1	480	450	360	540	300	300	230	170	120	160
N-2	700	920	500	200	200	280	240	170	180	
N-3	780	750	600	210	125	170	330	190	190	190

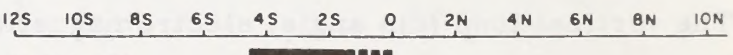

METAL FACTOR APP.

N-1	1·8	2·2	6	2·7	8	3	2·6	0	5	3
N-2	3·1	4·2	6·2	19	14	7·8	6·7	3·4	3	
N-3	3·5	6·6	7·3	17	31	26	9	5·3	2·2	4

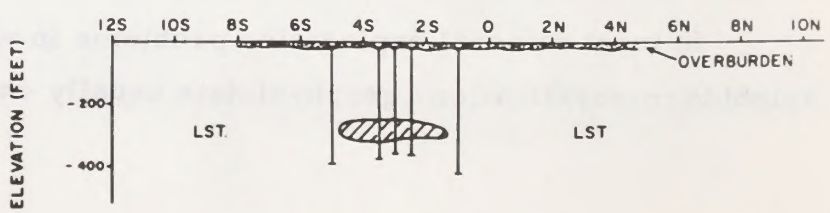

FIG. 34

technique as the primary exploration tool. Many massive sulphide zones are good electrical conductors and in Canada, as in many other parts of the world, the EM methods have been extremely successful in the last twenty years.

In the last few years, the induced polarization method has been applied more often in the search for massive sulphide mineralization. In many of these applications, the IP method has located massive sulphide mineralization that had not been previously detected using EM techniques. A study of several cases where this has occurred is of great importance to the exploration geophysicist and the exploration geologist. Several examples are described below.

a) Shield-type Mineralization Noranda Area, Quebec Figure 35

Copper-zinc ore has been extracted from massive sulphide mineralization in the Noranda area since the last century. In latter years, additional ore has been found by electromagnetic techniques applied on the surface and in drill holes. Recently, some ore has also been found that could not be detected by EM methods.

The IP results shown in Figure 35 located a small ore lens on a mining property near Noranda. The mineralization is not at great depth and the induced polarization and resistivity anomalies are both quite definite. To the east, the horizontal contours exhibited by the resistivity data reflect the presence of the conductive overburden layer.

The electromagnetic profile shown at the top of Figure 35 demonstrates that the zone of mineralization is not an electromagnetic conductor.

b) Shield-type Mineralization Timmins Area, Ontario Figure 36

One of the most important ore bodies discovered in Canada in recent years occurs near Timmins, Ontario. The ore zone was located by airborne and ground electromagnetic methods. In the years since the discovery of the

GEOPHYSICAL DATA AND DRILLING RESULTS FROM SHIELD TYPE MINERALIZATION NORANDA AREA, QUEBEC

MOBRUN EXTENSION LINE-24E

FREQUENCIES - 0·31/5 HZ

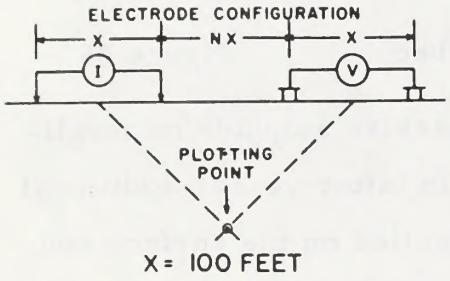

X = 100 FEET

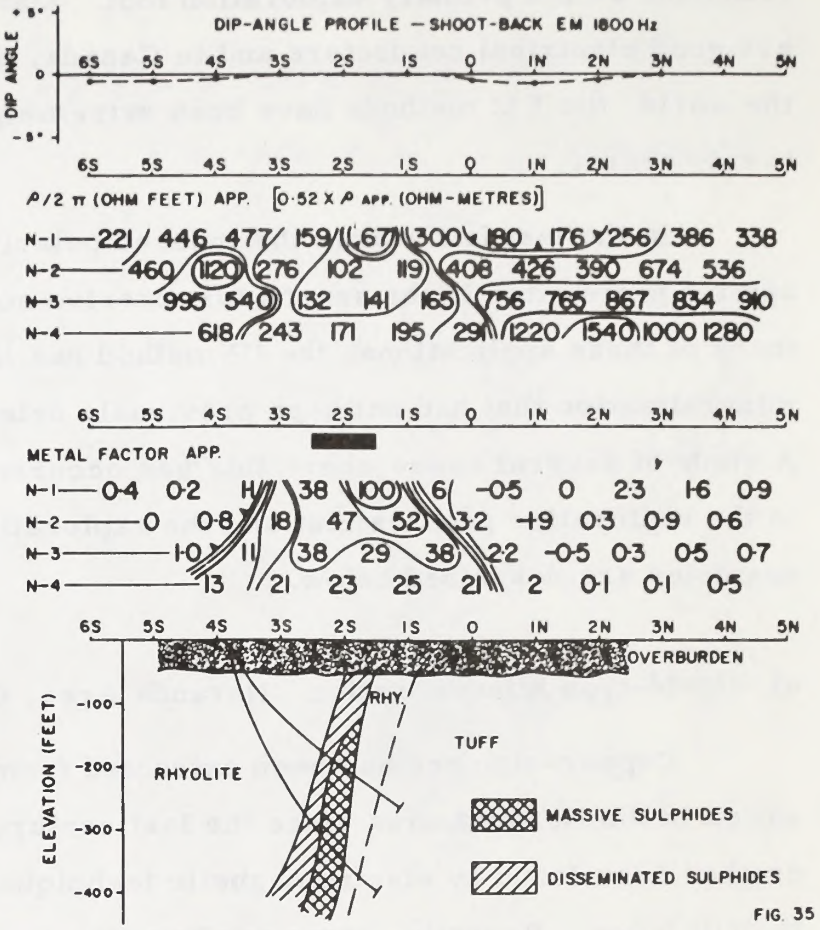

FIG. 35

GEOPHYSICAL DATA AND DRILLING RESULTS FROM SHIELD TYPE MINERALIZATION TIMMINS AREA, ONTARIO

LINE-12S

FREQUENCIES - 0·31/2·5 HZ

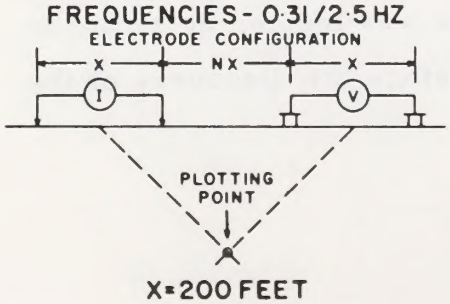

X = 200 FEET

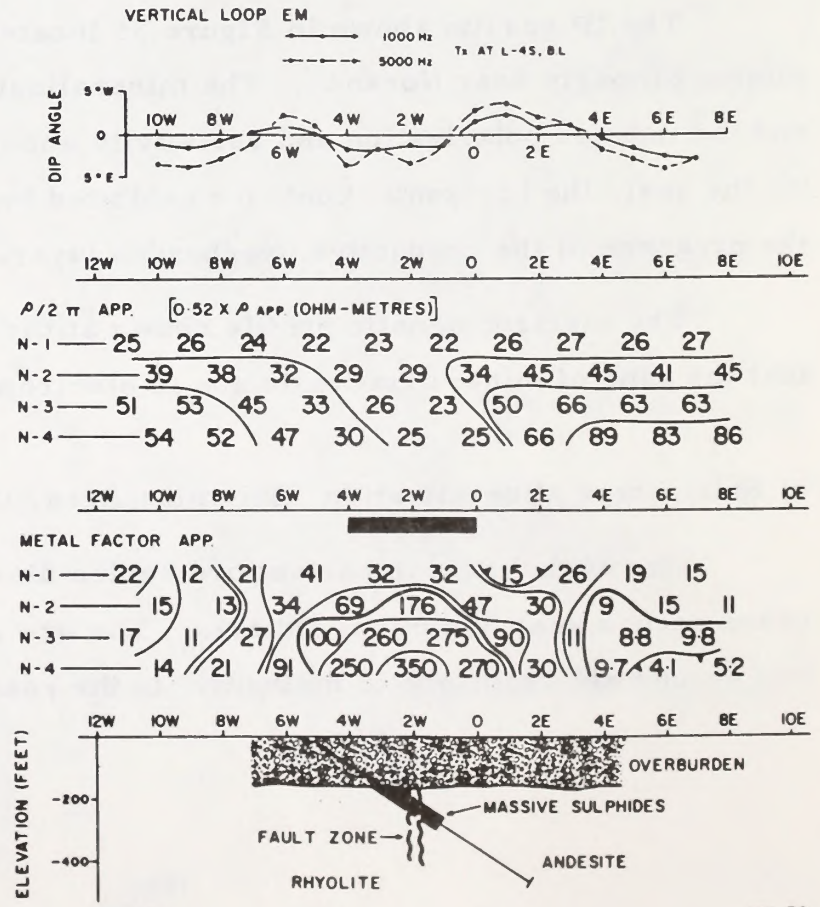

FIG. 36

Kidd Creek orebody, a great deal of exploration has been completed in that area of Ontario. Some massive mineralization has been found that cannot be detected using electromagnetic methods.

The IP data shown in Figure 36 located a large zone of massive sulphide mineralization beneath 180' of glacial overburden. Later tests using the vertical loop (dip angle) electromagnetic method did not detect an anomaly. In the profiles shown, the transmitter-receiver separation was 800'.

The apparent resistivity data clearly show the presence of the conductive overburden layer. At depth (measurements for n = 4), the data show a higher resistivity value for the andesites to the east than for the rhyolites to the west. The mineralization does not show a low for the n = 1 measurements, but there is a low for the n = 4 measurements.

c) Shield-type Mineralization Flin Flon Area, Manitoba Figure 37

The ore zones being mined at Flin Flon, Manitoba, are contained within

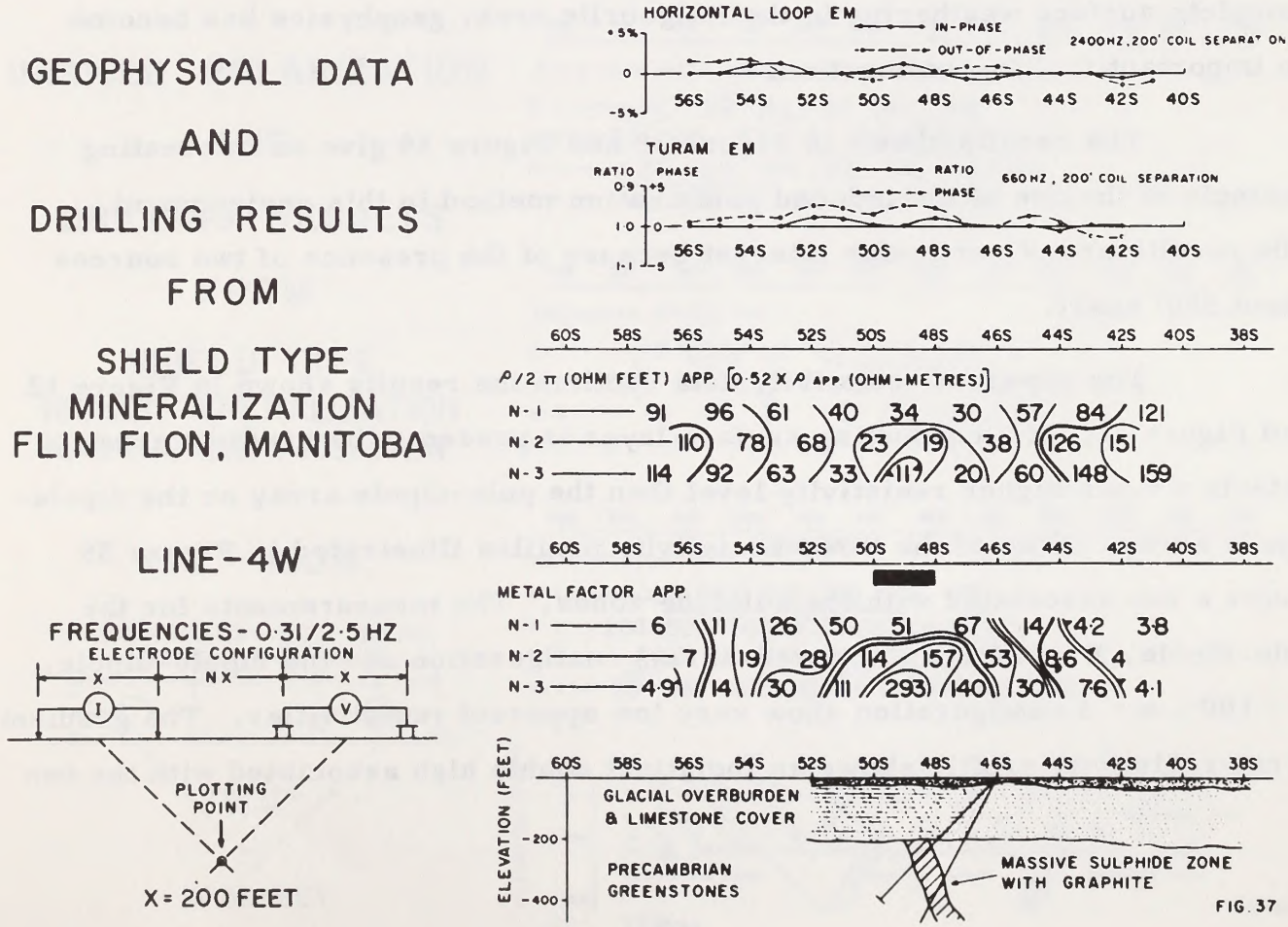

FIG. 37

the Precambrian Shield rocks. In the surrounding areas, the Paleozoic limestones lie on top of the Shield rocks. The sulphide zone shown in Figure 37 was located by IP using the dipole-dipole electrode configuration and X = 200', n = 1,2,3. The anomalous pattern suggests a relatively narrow source at considerable depth. Later drilling intersected the massive source beneath 220' of glacial overburden and limestone.

This zone of mineralization has a strike length of more than one-quarter mile. It was located by the IP technique in an area in which electromagnetic methods had already been applied with no anomalous results. The horizontal loop EM data and the Turam EM data shown on the upper portion of Figure 37 are from surveys previously completed on the same grid.

d) Shield-type Mineralization Kalgoorlie Area, West Australia

Figure 38 and Figure 39

Recently, intense exploration has been centred in the regions of ultrabasic rocks within the West Australian Precambrian Shield. This work has resulted in the discovery of several major nickel deposits. Due to the deep, complete surface weathering in the Kalgoorlie area, geophysics has become an important tool for exploration.

The results shown in Figure 38 and Figure 39 give an interesting example of the use of the induced polarization method in this environment. The results are of particular interest because of the presence of two sources about 300' apart.

The apparent resistivity data confirm the results shown in Figure 12 and Figure 16. If a conducting surface layer is present, the gradient array detects a much higher resistivity level than the pole-dipole array or the dipole-dipole array. None of the three resistivity profiles illustrated in Figure 38 shows a low associated with the sulphide zones. The measurements for the pole-dipole, X = 200', n = 1 (three-array) configuration and the dipole-dipole, X = 100', n = 3 configuration show very low apparent resistivities. The gradient array resistivity profile shows an indistinct double high associated with the two

INDUCED POLARIZATION AND DRILLING RESULTS FROM SHIELD TYPE NICKEL MINERALIZATION KALGOORLIE AREA, W.A.

LINE - 180 N

DIPOLE-DIPOLE ARRAY, X = 100 Ft., N = 3

POLE - DIPOLE ARRAY, X = 200 Ft., N = 1 (REMOTE ELECTRODE - WEST)

GRADIENT ARRAY, a = 100 Ft.

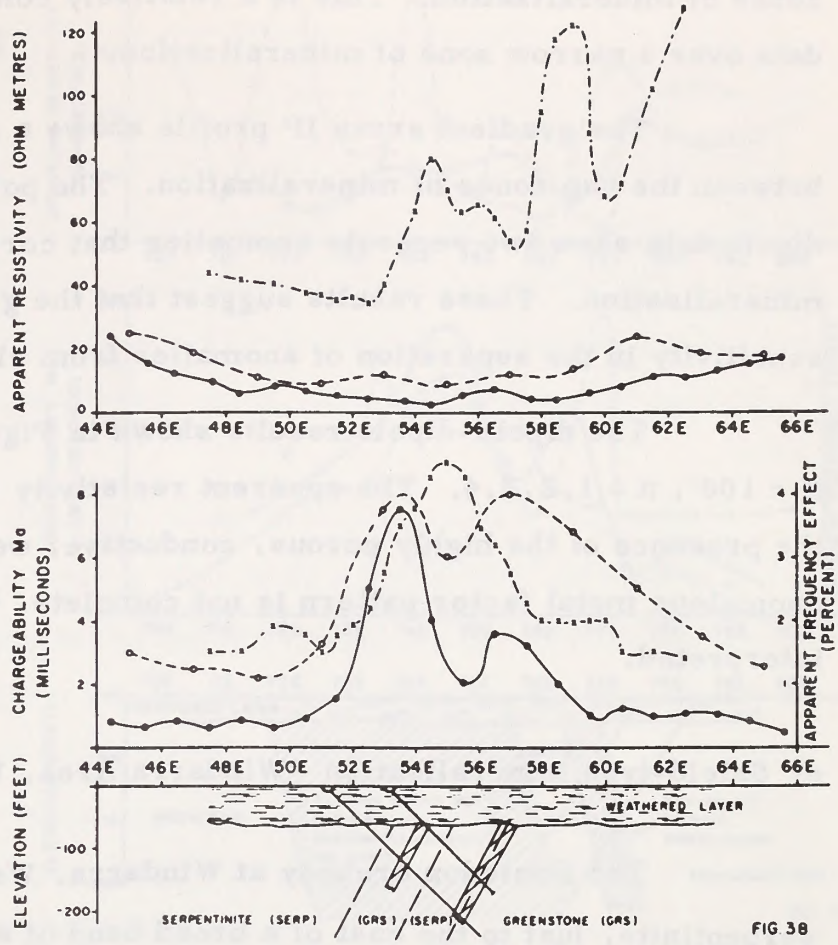

FIG. 38

INDUCED POLARIZATION AND DRILLING RESULTS FROM SHIELD TYPE NICKEL MINERALIZATION KALGOORLIE AREA, W.A.

LINE - 180 N

FREQUENCIES - 0.31 / 2.5 HZ.

ELECTRODE CONFIGURATION

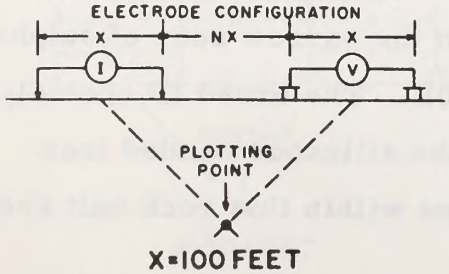

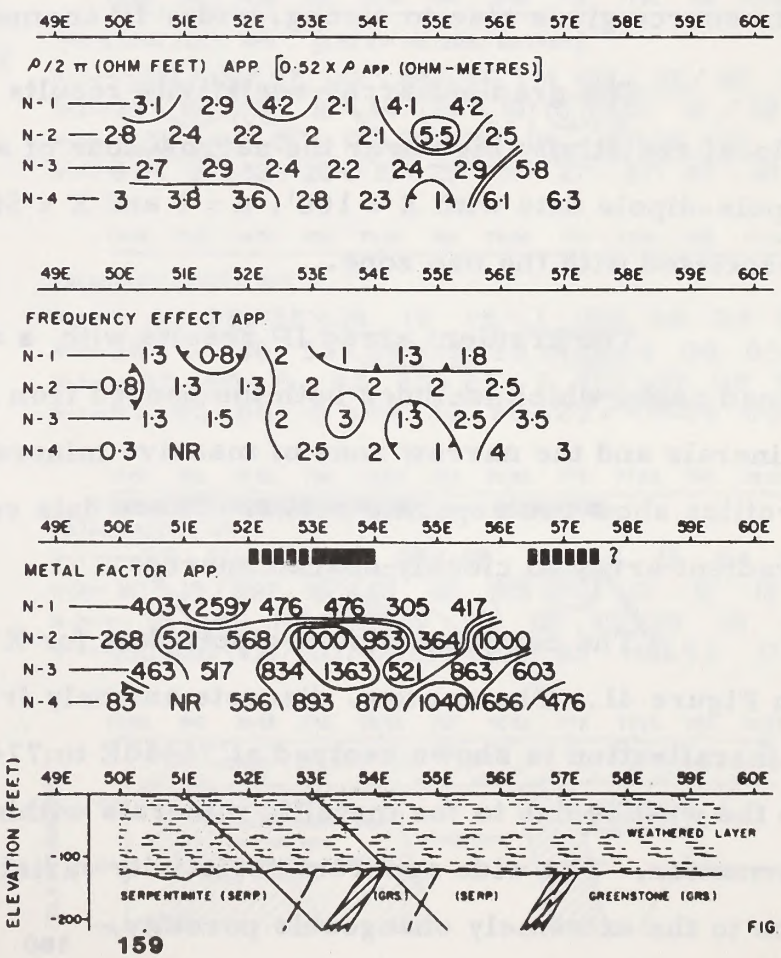

FIG. 39

zones of mineralization. This is a relatively common result for gradient array data over a narrow zone of mineralization.

The gradient array IP profile shows a single anomalous peak centred between the two zones of mineralization. The pole-dipole data and the dipole-dipole data show two separate anomalies that correlate with the two zones of mineralization. These results suggest that the gradient array has the least sensitivity in the separation of anomalies from closely-spaced sources.

The dipole-dipole results shown in Figure 39 were measured using X = 100', n = 1,2,3,4. The apparent resistivity level is very low, reflecting the presence of the highly porous, conductive, weathered surface layer. The anomalous metal factor pattern is not complete, but the double anomaly can be interpreted.

e) Shield-type Mineralization Windarra Area, West Australia

Figure 40 and Figure 41

The Posiedon orebody at Windarra, West Australia, is located within serpentinite, just to the east of a broad band of siliceous banded iron formation. The iron formation contains pyrite and metallic magnetite; this source gives rise to strong, wide, IP anomalies.

The gradient array resistivity results give irregular values, with a local resistivity high over the narrow zone of sulphide mineralization. The dipole-dipole data with X = 100', n = 1 and X = 50', n = 2 show a modest low associated with the ore zone.

The gradient array IP results with a = 100' show only a single, broad peak, which includes both the banded iron formation containing metallic minerals and the narrow zone of massive mineralization. The dipole-dipole profiles show two separate peaks. These data confirm the insensitivity of the gradient array to closely-spaced sources.

The complete dipole-dipole data for X = 50', n = 1,2,3,4 are shown on Figure 41. The narrow, discrete anomaly from the narrow zone of sulphide mineralization is shown centred at 76+50E to 77+00E. The broad IP anomaly to the west is due to the metallic minerals within the siliceous banded iron formation. The wide apparent resistivity variations within this rock unit are due to the extremely changeable porosity.

INDUCED POLARIZATION AND DRILLING RESULTS FROM SHIELD TYPE NICKEL MINERALIZATION WINDARRA AREA, W.A.

LINE - IN

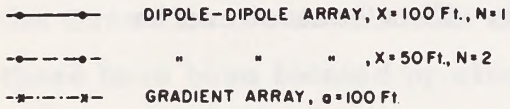

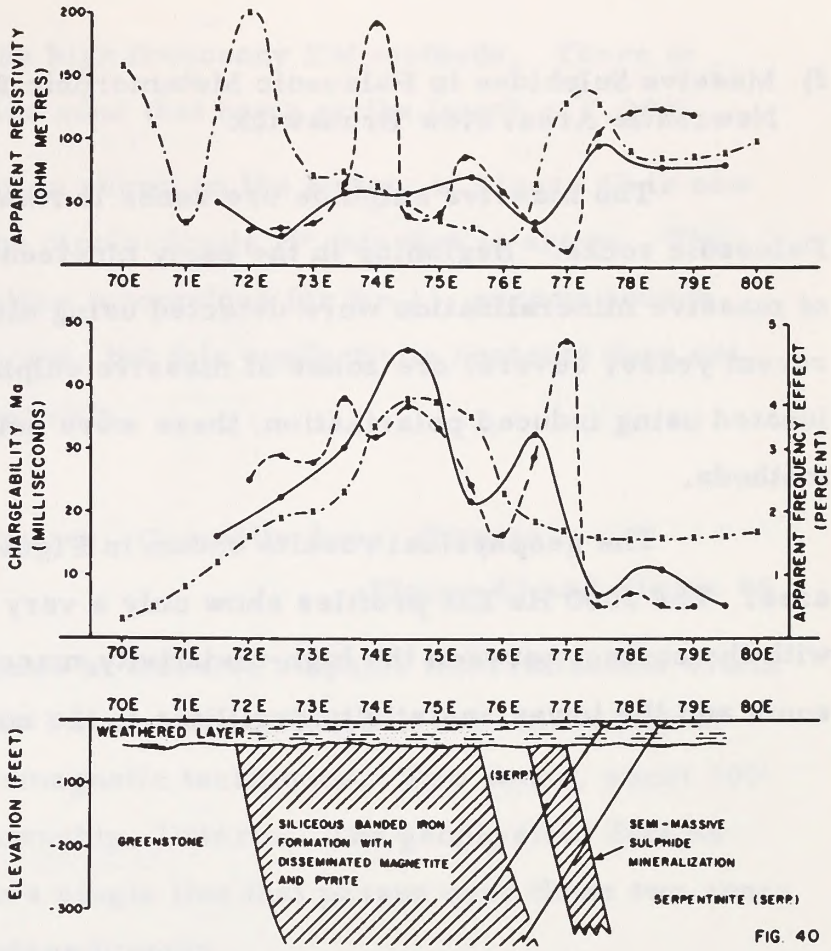

FIG. 40

INDUCED POLARIZATION AND DRILLING RESULTS FROM SHIELD TYPE MINERALIZATION WINDARRA AREA, W.A.

LINE - IN

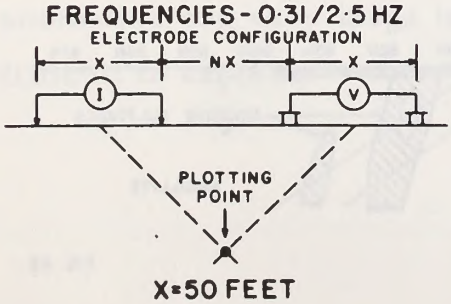

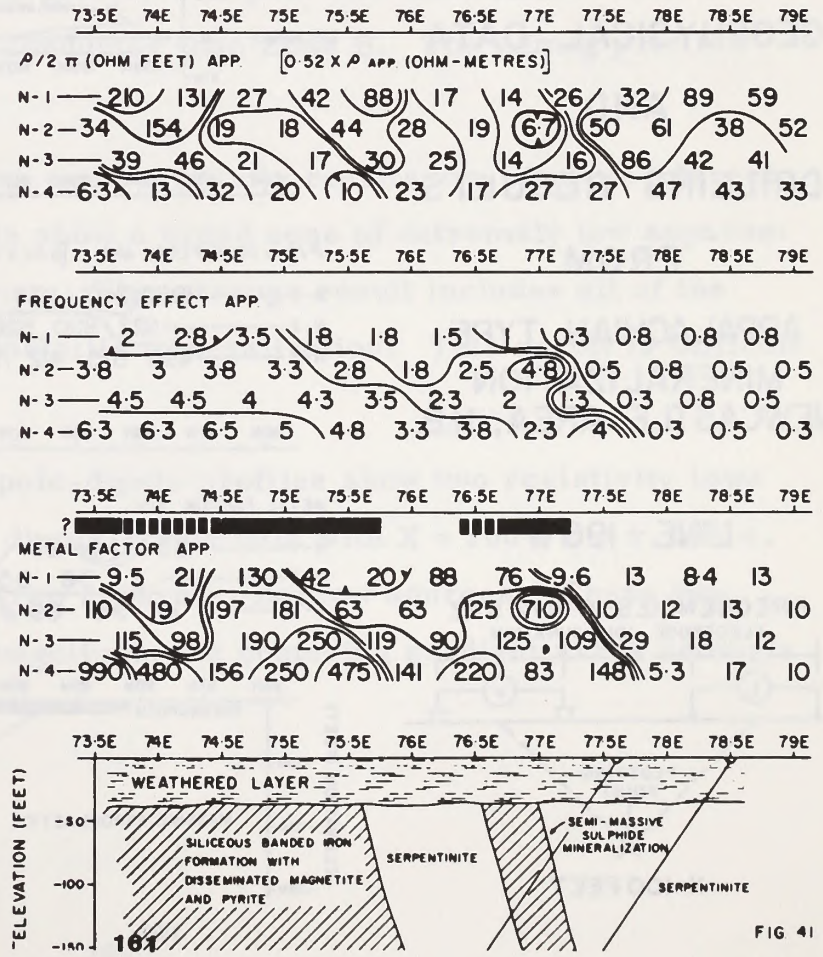

FIG 41

f) Massive Sulphides in Paleozoic Metamorphic Rocks
Newcastle Area, New Brunswick Figure 42

The massive sulphide ore zones in New Brunswick are contained within Paleozoic rocks. Beginning in the early nineteen fifties, many of these zones of massive mineralization were detected using electromagnetic methods. In recent years, several ore zones of massive sulphide mineralization have been located using induced polarization; these were not previously detected by EM methods.

The geophysical results shown in Figure 42 are from the Newcastle area. The 5000 Hz EM profiles show only a very weak anomaly that correlates with the contact between the high-resistivity, massive, pyroclastic rocks to the south and the lower resistivity argillites to the north. This contact can be

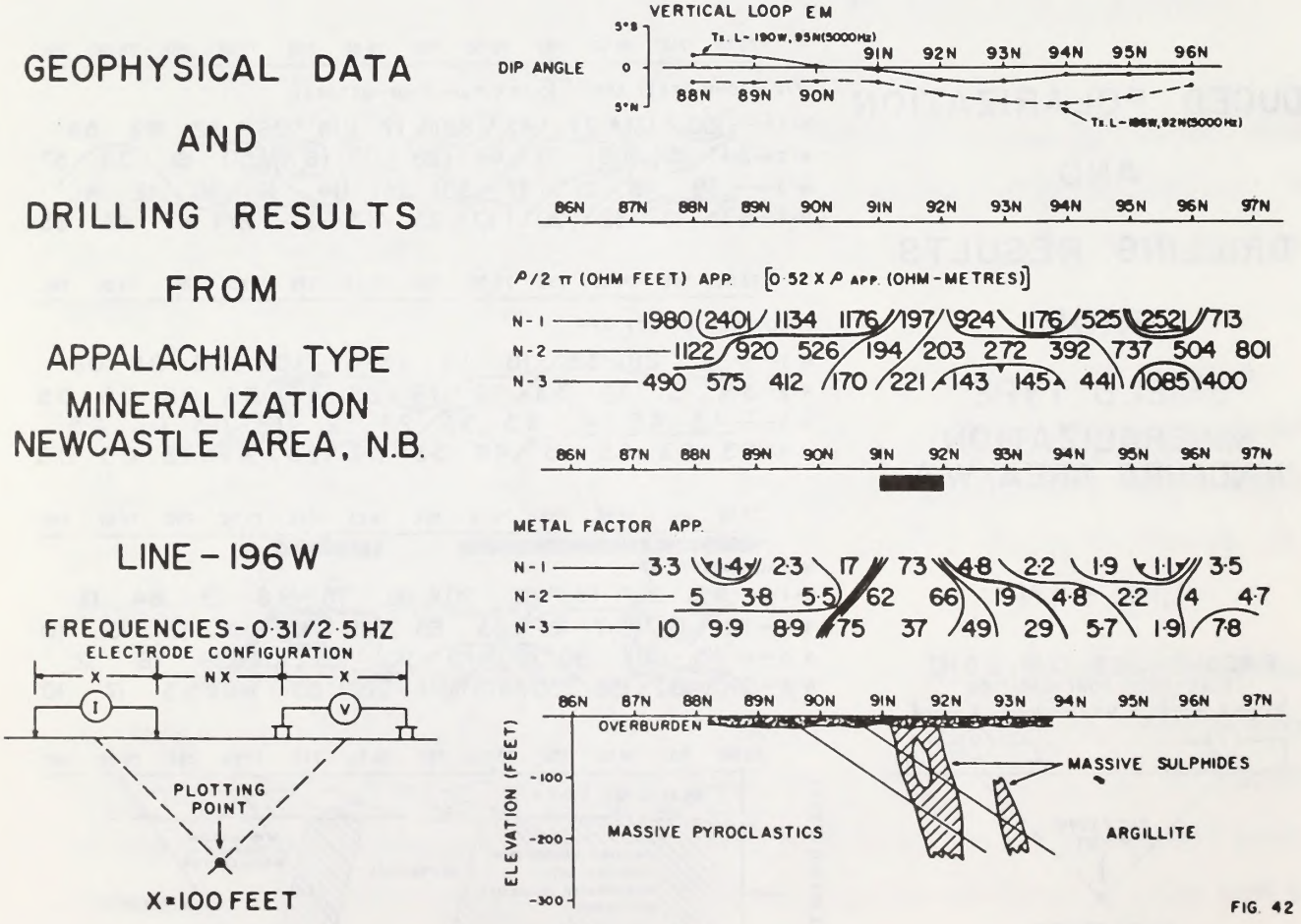

FIG. 42

traced for several miles with these high frequency EM methods. There is no evidence of the massive sulphide zone that has a strike length of 2,000'.

The zone of mineralization shown on the bottom of Figure 42 is now being mined. It was located by the dipole-dipole IP data that is shown. The anomalous pattern suggests a shallow (anomalous for n = 1), narrow source. There is a correlating resistivity low, but this conductivity contrast does not give rise to an electromagnetic anomaly.

g) Massive Sulphides in Metasediments Grenville Area, Ontario

Figure 43 and Figure 44

There are numerous zones of massive sulphide mineralization within the Grenville metasediments of the Precambrian Shield in Canada. Many of these have been located by electromagnetic techniques. Two zones, about 500' apart, are known in Cavendish Township, Ontario. The geophysical data on Figure 43 and Figure 44 are from a single line that passes over these two zones of mineralization within limey metasediments.

Both Zone A and Zone B give rise to poor EM anomalies. Zone A appears to be a somewhat better conductor than Zone B. The Afmag profiles also show two conductors.

The induced polarization and resistivity results are of great interest. The gradient array measurements show a broad zone of extremely low apparent resistivities and negative IP effects. This strange result includes all of the region between the two zones of metallic mineralization. This result is difficult to explain!

The pole-dipole and dipole-dipole profiles show two resistivity lows and frequency effect highs. The dipole-dipole data with X = 100', n = 1,2,3,4, shown in Figure 44, confirm the two separate, narrow sources. These two IP anomalies are very large in magnitude; the confusing gradient array anomaly is difficult to explain.

GEOPHYSICAL DATA AND GEOLOGIC SECTION FROM GRENVILLE TYPE MINERALIZATION

CAVENDISH TWP., ONTARIO LINE- D

DIPOLE-DIPOLE ARRAY, X = 50 Ft., N-2

POLE - DIPOLE ARRAY, X = 50 Ft., N-2 (REMOTE ELECTRODE - EAST)

GRADIENT ARRAY, o = 50 Ft.

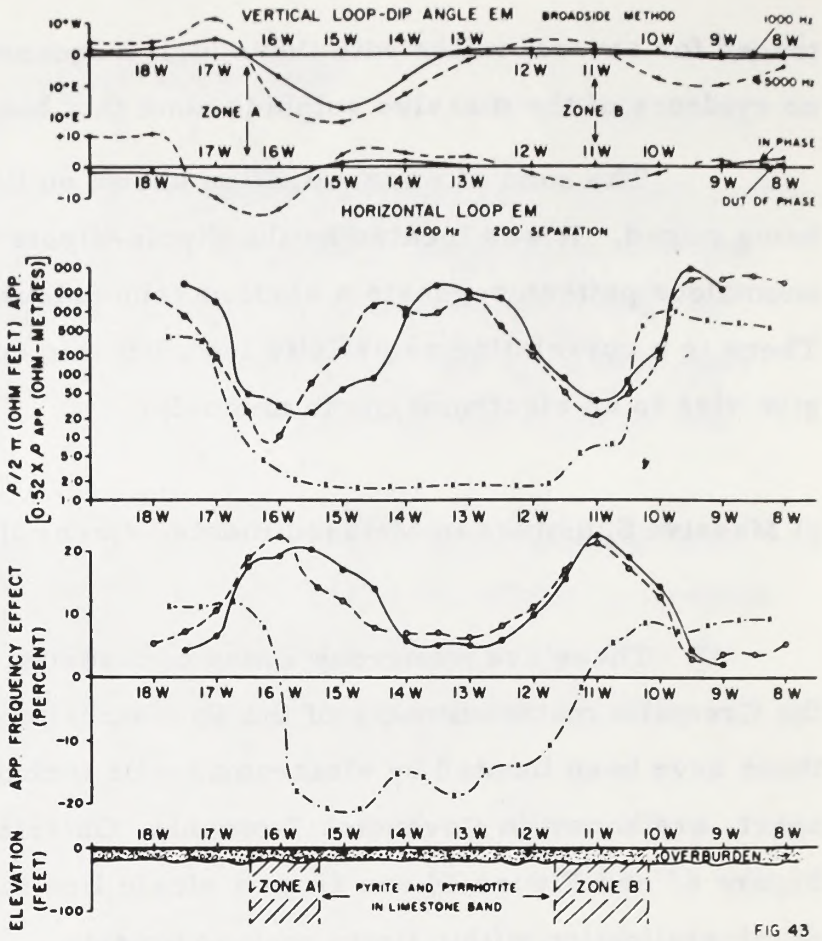

FIG 43

GEOPHYSICAL DATA AND DRILLING RESULTS FROM GRENVILLE TYPE MINERALIZATION

CAVENDISH TWP., ONTARIO LINE- D

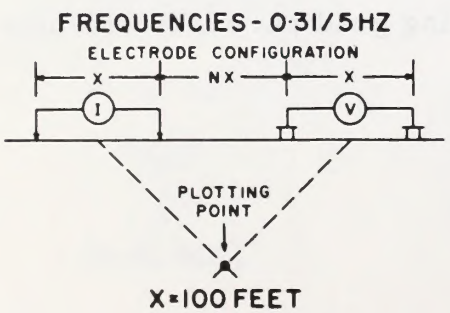

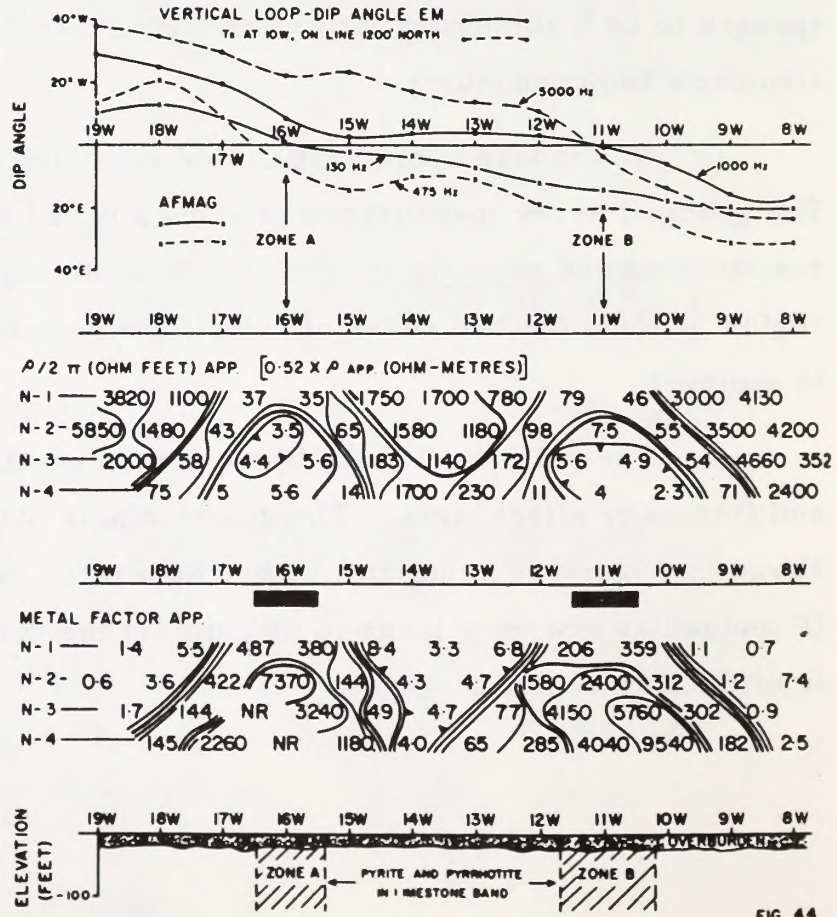

FIG. 44

Conclusions

The induced polarization method can be of great use in many exploration problems. The various methods of measurement of the IP effect are mathematically equivalent; the electrode interval and the electrode configuration used for a particular survey are of greater importance than the method of measurement.

For broad, shallow zones of mineralization all electrode configurations give much the same shape and magnitude anomaly. However, for smaller sources, sources at some depth, sources under conductive overburden and multiple sources,some electrode configurations are less useful than others.

The IP method has obvious usefulness in the search for exploration for disseminated sulphide mineralization. In this type of exploration,other geophysical techniques have found little application. However, the IP method has also been found to be of use in exploration for zones of mineralization that are not disseminated.

A better understanding of the induced polarization method and a knowledge of its usefulness will be helpful to persons involved in mineral exploration.

Acknowledgements

The data that have been presented in this technical paper has been made available by the several mining companies involved. Some of the data have previously been published, but most have not been released before. To all of these mining companies we owe our thanks for permission to publish the data.

American Metal Climax Inc.

Anaconda Copper Company

Brenda Mines Ltd.

Cominco Ltd.

El Paso Natural Gas Co.

Heath Steele Mines Ltd.

Lornex Mining Corp. Ltd.

Metals Exploration, N.L.

Noranda Mines Ltd.

Pine Point Mines Ltd.

Posiedon Ltd.

Pyramid Mining Co. Ltd.

Texas Gulf Sulphur Company

United Nations Special Fund

Wisconsin Mining Company Limited

References

Hallof, P.G. 1967 — An Appraisal of the Variable Frequency IP Method After Twelve Years of Application.

Presented at the University of California at Berkeley Symposium on Induced Polarization.

Madden, T.R. and Cantwell, T. 1967 — Induced Polarization, A Review Society of Exploration Geophysicists "Mining Geophysics"

Vol. II page 373-400.

Seigel, H.O. 1967 — The Induced Polarization Method Mining and Groundwater Geophysics 1967.

Proceedings of the Canadian Centennial Conference on Mining and Groundwater Geophysics held at Niagara Falls, Ontario, Canada.

Wait, J.R. (editor) 1959 — Overvoltage Research and Geophysical Application. Pergamon Press.

THE USE OF THE PHOENIX IPV-2 PHASE IP RECEIVER FOR DISCRIMINATION BETWEEN SULPHIDES AND GRAPHITE

BY

P.G. Hallof, P.A. Cartwright, W.H. Pelton

Prepared for Presentation
Society of Exploration Geophysicists
Annual Meeting
New Orleans, Louisiana,
November 4-8, 1979

- - - - - - - - - - - - - - - - - - - -

ABSTRACT

Previous work has demonstrated that four parameters can be used to completely describe the induced polarization-resistivity phenomena: the d.c. resistivity, the exponent of the frequency term in the transfer function, the IP effect reported as the chargeability, and the time constant of the transfer function. All of these parameters can be expected to vary from source to source, but it has been shown that the time constant can be directly related to the grain-size of the metallic particles creating the IP effect. In all laboratory and field work to date, the time constant for graphite sources has been 10^{+4} to 10^{+5} times greater than for massive sulphide sources.

In the general field application of the spectral IP method, the following steps are necessary:

1) measure broad spectrum IP phase data for each electrode site
2) remove inductive coupling effects by computer inversion of field data
3) correct for effect of dilution to convert apparent spectrum into true spectrum within the source.
4) use computer inversion to obtain true values of the parameters that describe the source.

However, for shallow sources, measurements with short electrode intervals and a limited frequency spectrum will greatly reduce, or eliminate, the distortions due to inductive coupling and dilution. In this situation, measurements with the IPV-2 frequencies (0.11 - 0.33 - 1.0 - 3.0 - 9.0 Hz) can be used to give some estimates of the maximum value and peak frequency on the phase vs. frequency curve.

This information can be used to give an approximate estimate for the time constant for the source of the effects measured. In some environments, at least, this parameter can be used to relate the source to massive sulphides or graphite.

Theoretical Development and Experimental Measurements on Correlation Between Grain-Size and Time-Constant

In previous publications, Pelton (1977) and Pelton, et al (1978) have demonstrated the effective use of the equation governing a Cole-Cole dispersion to describe the induced polarization phenomenon. The equation and curves shown on Figure 1 illustrate the four parameters that can be used to completely describe the induced polarization phenomenon we measure in exploration.

The four parameters are:

- R_o the d.c. resistivity
- m the induced polarization effect, reported as the dimensionless parameter, chargeability.
- c the exponent of the frequency dependent term.
- τ the time-constant of the dispersion

The curves in Figure 1 show how the phase and amplitude curves are altered by a change in the magnitude of the chargeability, (m) . It is easily seen that a ten-fold change in the time-constant (τ) will shift the curves one decade along the frequency axis.

The curves in Figure 2 demonstrate the effects of varying the exponent (c) while holding the other three parameters constant. The exponent (c) is the asymptotic slope of the log-log plots for low and high frequencies; as the parameter value is decreased, the curves become much "flatter". Even though the IP effect (m) is held constant, the maximum phase-shift measured is reduced as the value of the exponent is reduced.

Recently, two researchers, J. Wong (1979) and G.W. DeWitt (1978), have used entirely different approaches and assumptions to develop mathematical expressions to describe the IP phenomenon. As shown in Figure 3 (from DeWitt) and in Figure 4 (from Wong), both developments result in the same relationship between the phase-shift curve expected and the grain-size of the metallic particles that are the source of the IP effects. As the grain-size of the metallic particle is increased, while the total concentration of metallic mineral is held constant, the frequency at which the maximum phase-shift is measured i.e. the critical frequency, (f_c) moves to lower and lower frequencies.

A comparison between the curves in Figure 3 and Figure 4 and the Cole-Cole equation curve will convince one that for both mathematical developments it can be said that an increase in the grain-size of the metallic particles causing the IP effect, will give rise to a larger time-constant (τ) for the dispersion.

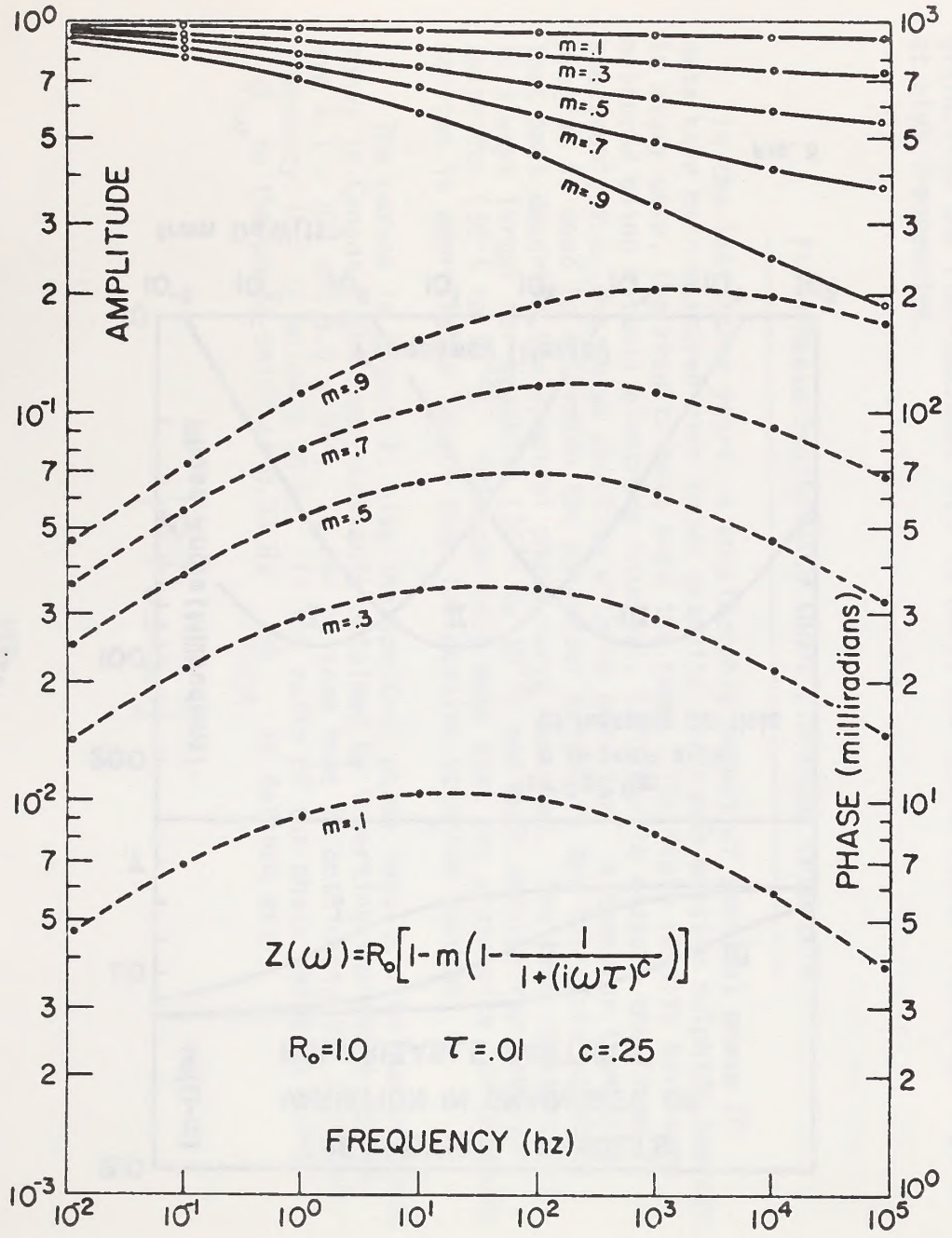
AMPLITUDE
PHASE (milliradians)
m=.1
m=.3
m=.5
m=.7
m=.9
$Z(\omega)=R_o\left[1-m\left(1-\frac{1}{1+(i\omega\tau)^c}\right)\right]$
R_o=1.0 τ=.01 c=.25
FREQUENCY (hz)

FIG. 1

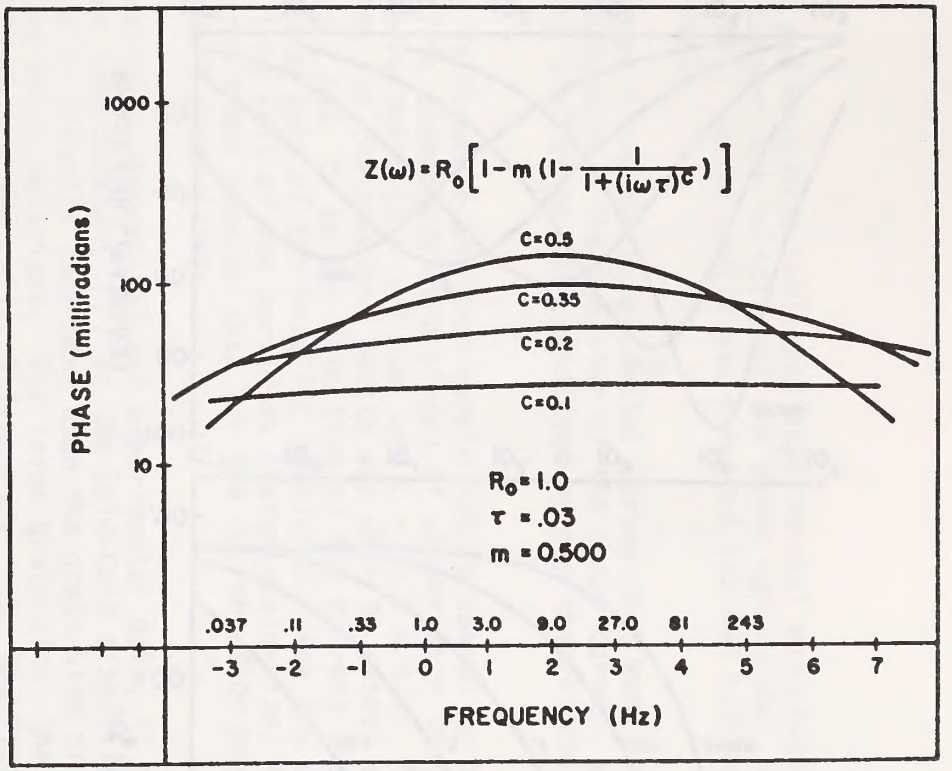
PHASE (milliradians)
$Z(\omega)=R_o\left[1-m\left(1-\frac{1}{1+(i\omega\tau)^c}\right)\right]$
C=0.5
C=0.35
C=0.2
C=0.1
R_o=1.0
τ=.03
m=0.500
.037 .11 .33 1.0 3.0 9.0 27.0 81 243
FREQUENCY (Hz)

FIG. 2

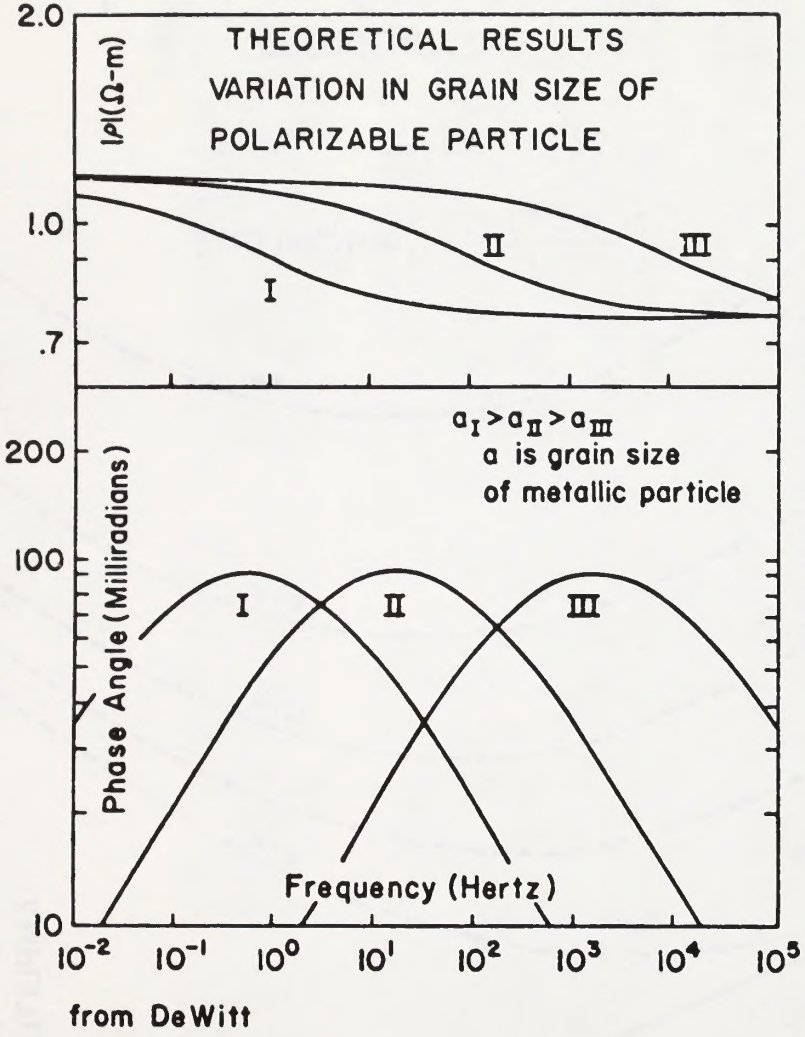

from DeWitt

FIG. 3

THEORETICAL RESULTS FOR VARIATION IN
GRAIN SIZE OF POLARIZABLE PARTICLE

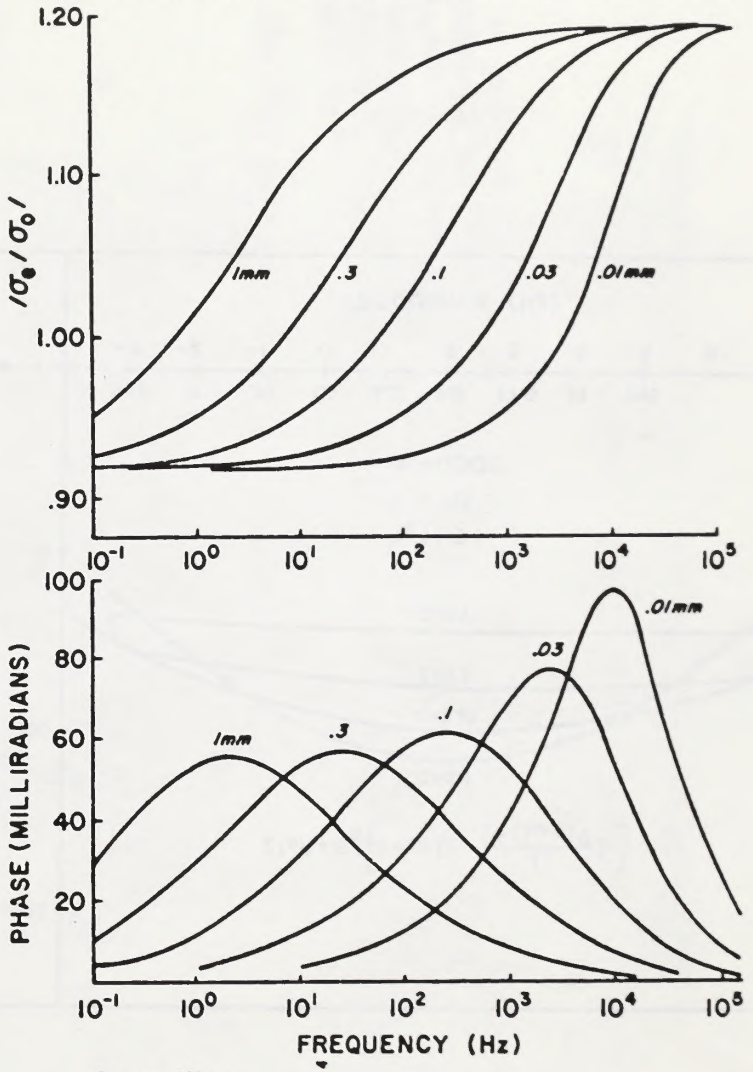

from Wong

FIG. 4

Both DeWitt and Wong have published experimental measurements on synthetic rock samples to support the validity of the above conclusion. Wong used data from Grisseman (1971), while DeWitt has prepared his own synthetic samples and made the measurements.

Shown in Figure 5 are the experimental curves that Wong has derived from Grissemann's measurements. The behavior of the phase curves, as the grain-size is varied, is very similar to that predicted by his theoretical development (Figure 4).

The results in Figure 6 are from sample S10, prepared by DeWitt. In these samples the metallic components were pieces of copper wire that were ten times as long as they were thick (d = 1.0 m.m. and L = 10.0 m.m.). As shown by the idealized sketches for the samples, DeWitt was able to detect a change in the parameters m, c, and τ as the direction of the current flow was varied, relative to the long axis of the metallic particles. For the current flow parallel to the long axis of the particles (large grain-size) the time-constant (τ) is one hundred times greater than for the current flow perpendicular to the long axis (small grain-size).

From the available theoretical and experimental data, it seems safe to conclude that the time-constant (τ) of the Cole-Cole dispersion that describes the IP phenomenon is directly dependent upon the grain-size of the metallic particles that are being polarized. For large grain-size, the time-constant is large in magnitude and the critical frequency i.e. the frequency (f_c) at which the maximum phase-shift is measured is at low frequencies. For small grain-size the time-constant (τ) is small and the critical frequency (f_c) is at high frequencies.

Field Measurements with Short Electrode Intervals

In the last three years, a considerable amount of spectral phase IP data have been measured over known graphite and known massive sulphide sources. In every case, the results have been the same. The field results have been measured using a small electrode interval, in order to measure the "true IP spectrum", i.e. the phase spectrum with no dilution. A computer inversion program is used to determine the parameter values in the Cole-Cole equation that best describe the spectral phase curve measured. The time-constant (τ) is always larger for graphite (10^{+2} to 10^{+3}) and much smaller for massive sulphides (10^{-1} to 10^{-2}). This can only mean that the grain-size for graphite sources is appreciable larger than for massive sulphide sources.

The curves in Figure 7, give the spectral phase results from two graphite zones in Canada. The time-constants obtained by inverting the phase curves are 4.1×10^3 and 5.0×10^2. It can be seen that in both cases the critical frequency (f_c) is below 0.10 Hz. If the ratio of the phase shift at 3.0 Hz $\phi_{3.0}$ to the phase-shift at 0.33 Hz $\phi_{0.33}$ is defined as:

$$\left[R\phi_{0.3-3.0}\right]$$

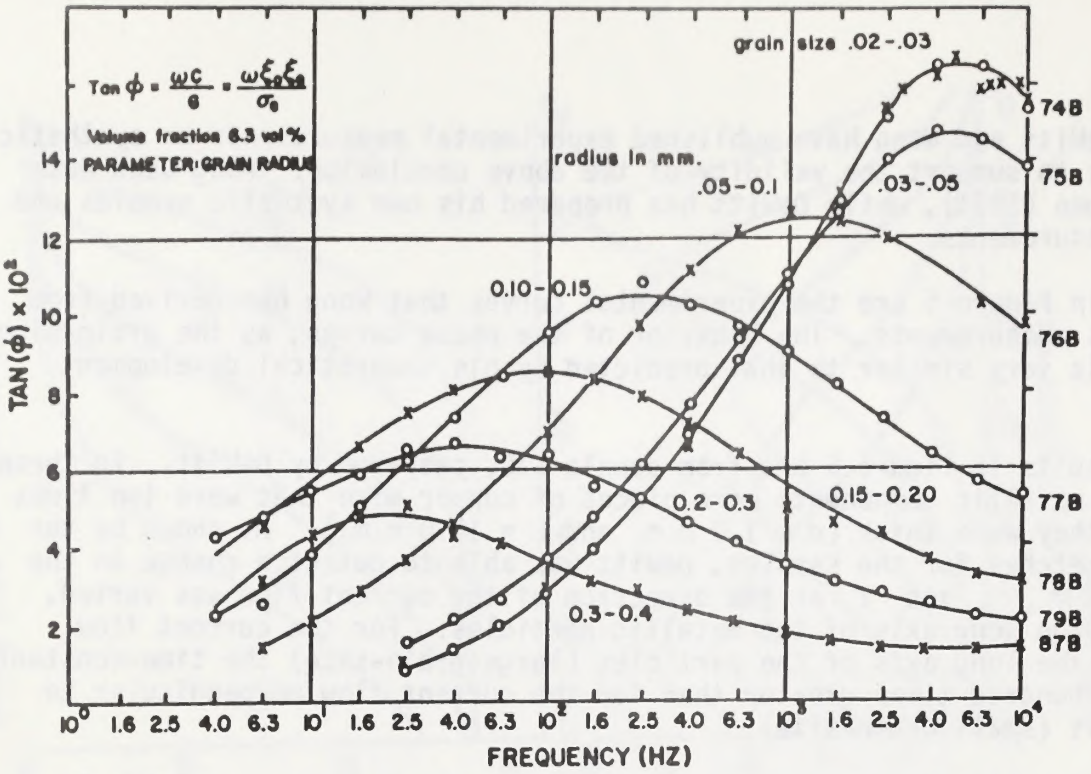

from Wong
data by Grissemann

FIG. 5

EFFECT OF GRAIN SIZE ON PHASE-SHIFT CURVE [τ and c]

Data from D.W. DeWitt

Artificial Sample S10 contains copper wire [r=1.0mm , l = 10mm]

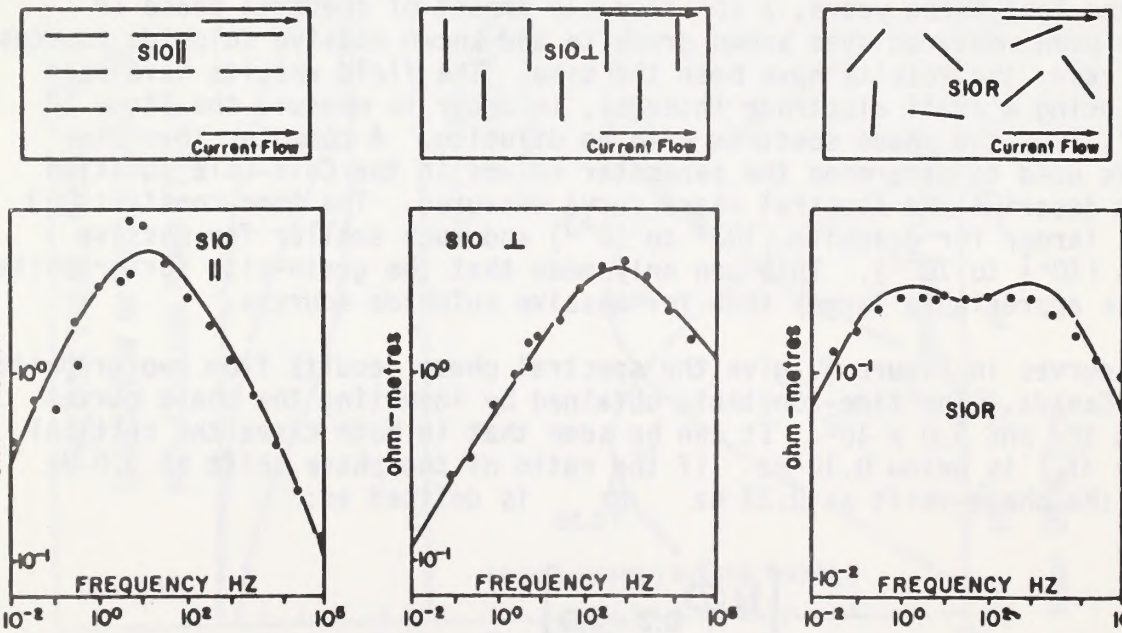

Cole – Cole parameters after inversion of phase curves

S10 ||	S10 ⊥	S10R
m = 0.971	m = 0.469	m = 0.858
c = 0.470	c = 0.402	c = 0.294
τ = 1.28 × 10⁻²	τ = 2.5 × 10⁻⁴	τ = multiple

FIG. 6

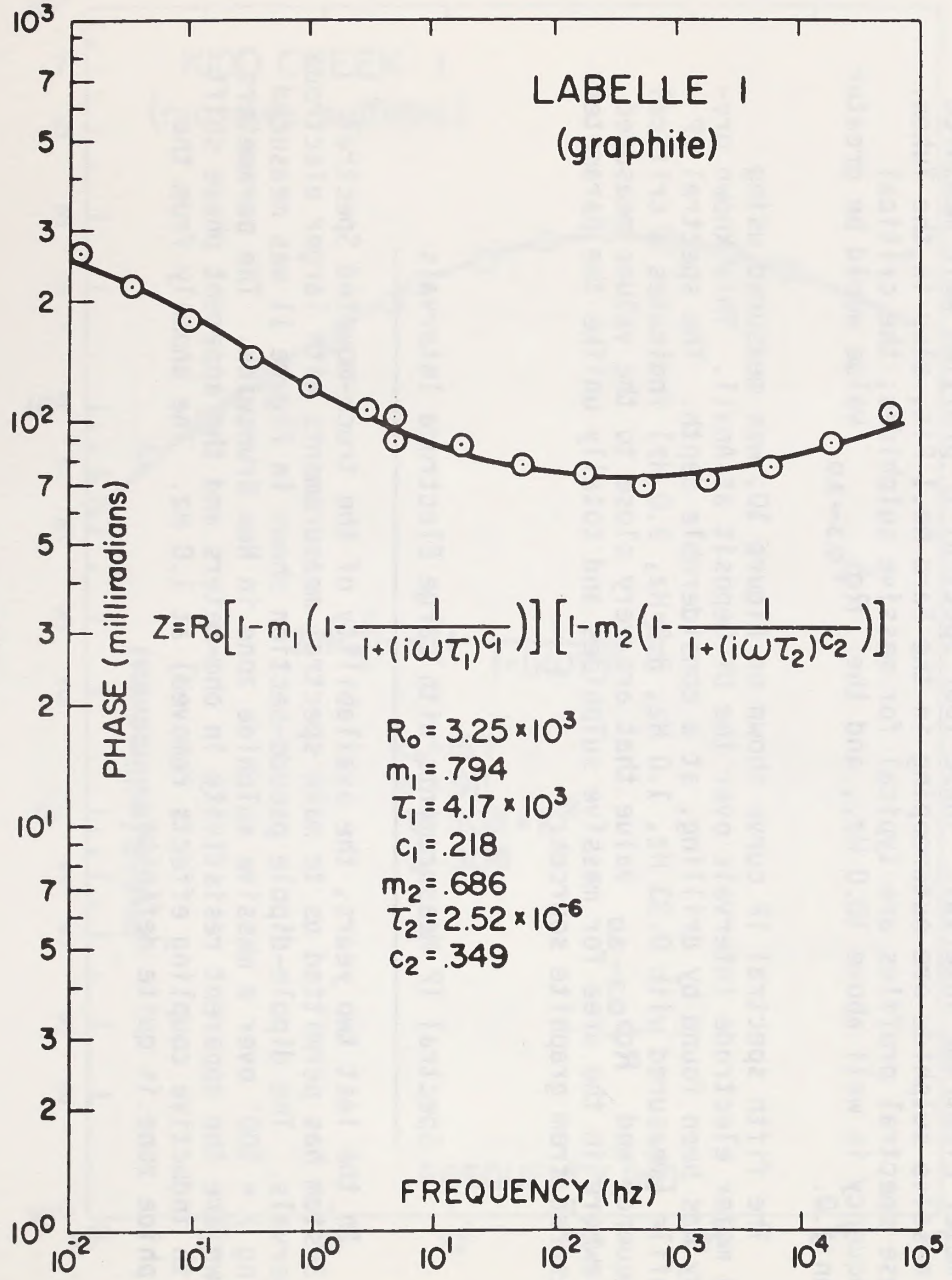
LABELLE 1
(graphite)
PHASE (milliradians)
FREQUENCY (hz)
$Z=R_o\left[1-m_1\left(1-\frac{1}{1+(i\omega\tau_1)^{c_1}}\right)\right]\left[1-m_2\left(1-\frac{1}{1+(i\omega\tau_2)^{c_2}}\right)\right]$
$R_o = 3.25\times10^3$
$m_1 = .794$
$\tau_1 = 4.17\times10^3$
$c_1 = .218$
$m_2 = .686$
$\tau_2 = 2.52\times10^{-6}$
$c_2 = .349$

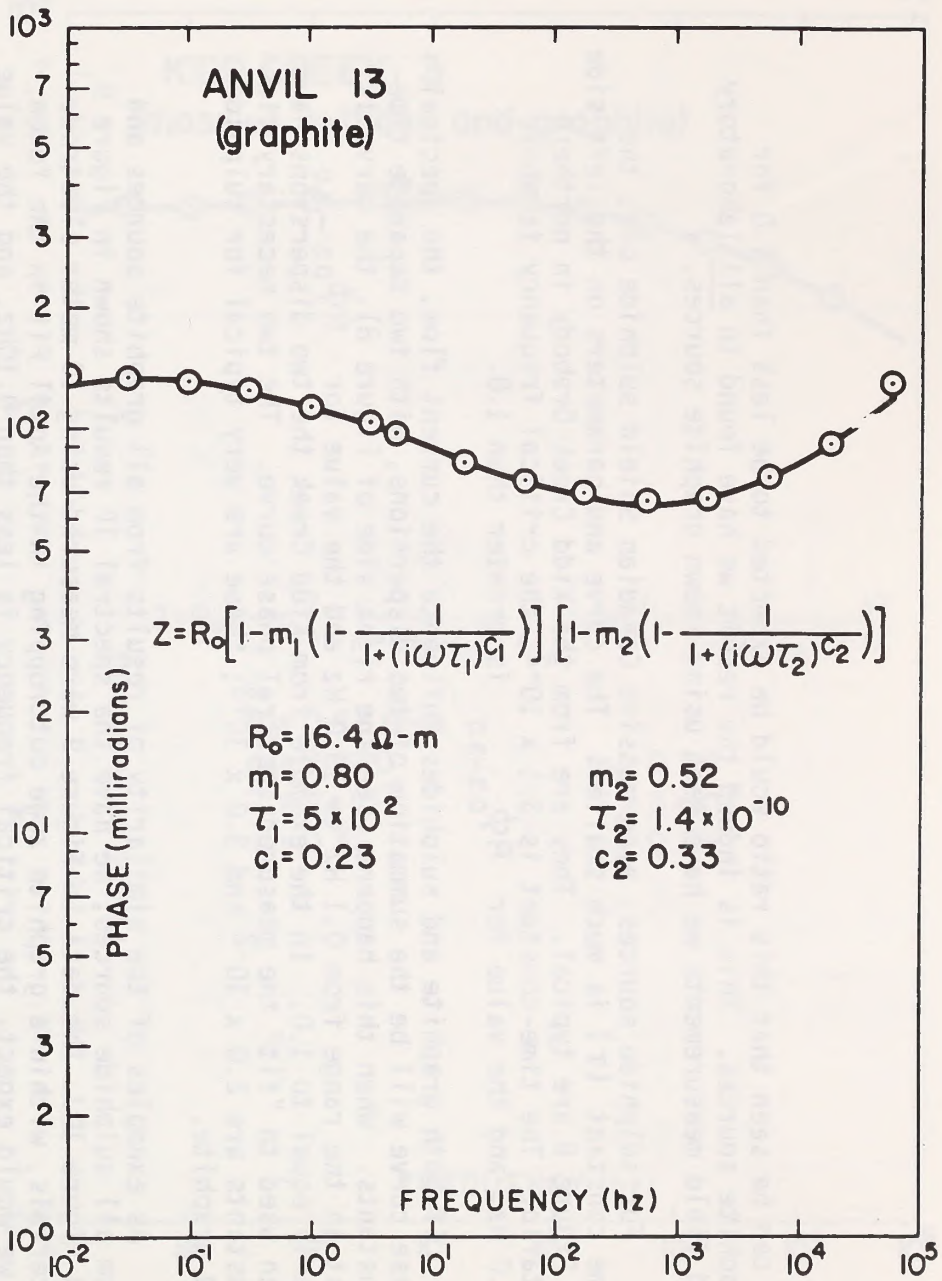
ANVIL 13
(graphite)
PHASE (milliradians)
FREQUENCY (hz)
$Z=R_o\left[1-m_1\left(1-\frac{1}{1+(i\omega\tau_1)^{c_1}}\right)\right]\left[1-m_2\left(1-\frac{1}{1+(i\omega\tau_2)^{c_2}}\right)\right]$
$R_o = 16.4\ \Omega\text{-m}$
$m_1 = 0.80$
$\tau_1 = 5\times10^2$
$c_1 = 0.23$
$m_2 = 0.52$
$\tau_2 = 1.4\times10^{-10}$
$c_2 = 0.33$

FIG. 7

It can be seen that this ratio would be expected to be less than 1.0 for graphite sources. This is indeed the result we have found in all laboratory and field measurements we have made using known graphite sources.

For sulphide sources, even massive Canadian Shield sulphide ore, the time constant (τ) is much smaller. The curve and parameters on the left side of Figure 8 are typical. They are from the Kidd Creek Orebody in northern Ontario. The time-constant is 3.1×10^{-2}, the critical frequency is above 10.0 Hz, and the value for $R\phi_{0.3\text{-}3.0}$ is greater than 1.0.

If both graphite and sulphides influence the current flow, the spectral phase curve will be the summation of two dispersions, with two separate time-constants. When this happens (see the right side of Figure 8), the curve is flat in the range from 0.1 Hz to 10.0 Hz and the value for $R\phi_{0.3-3.0}$ is nearly equal to 1.0. In the example from Kidd Creek the two dispersions have been used to "fit" the measured spectral phase curve. The two necessary time-constants are 2.0×10^{-2} and $3.0 \times 10^{+3}$; these are very typical for sulphide and graphite.

As examples of the similarity of results from all graphite sources and from all sulphide sources, we have the spectral IP results shown in Figure 9 and Figure 10. The data in Figure 9 were measured using 10 meter electrode intervals, within a graphite zone outcropping in the Anvil Pit in the Yukon. As we would expect, the critical frequency is less than 0.10Hz, and the value of $R\phi_{0.3-3.0}$ would be less than 1.0.

Most of the results shown in Figure 10 were also measured using a 10 meter electrode interval. These four spectral IP profiles were measured on massive sulphide ore outcropping in the Faro No.1 Pit, also in the Yukon. These spectral profiles are typical for massive sulphides; the critical frequency is well above 10.0 Hz., and the $R\phi_{0.3-3.0}$ value would be greater than 1.0.

The fifth spectral IP curve shown on Figure 10, was measured using 350 meter electrode intervals over the DY Deposit at Anvil. This known ore-body has been found by drilling, at a considerable depth. The spectral IP profile (measured with 0.33 Hz, 1.0 Hz, 3.0 Hz, 9.0 Hz) indicates a critical frequency and $R\phi_{0.3-3.0}$ value that are very close to the values measured elsewhere in the area for massive sulphides and totally unlike the parameters measured from graphite sources.

Spectral IP Measurements with Large Electrode Intervals

In the last two years, the availability of the truck-mounted Spectral IP System has permitted us to make spectral measurements with larger electrode intervals. The dipole-dipole pseudo-section shown in Figure 11 was measured using X = 100' over a massive sulphide zone in New Brunswick. The parameters shown are the apparent resistivity in ohm-meters and the apparent phase shift (with inductive coupling effects removed) at 1.0 Hz. The anomaly from the sulphide zone is quite definite.

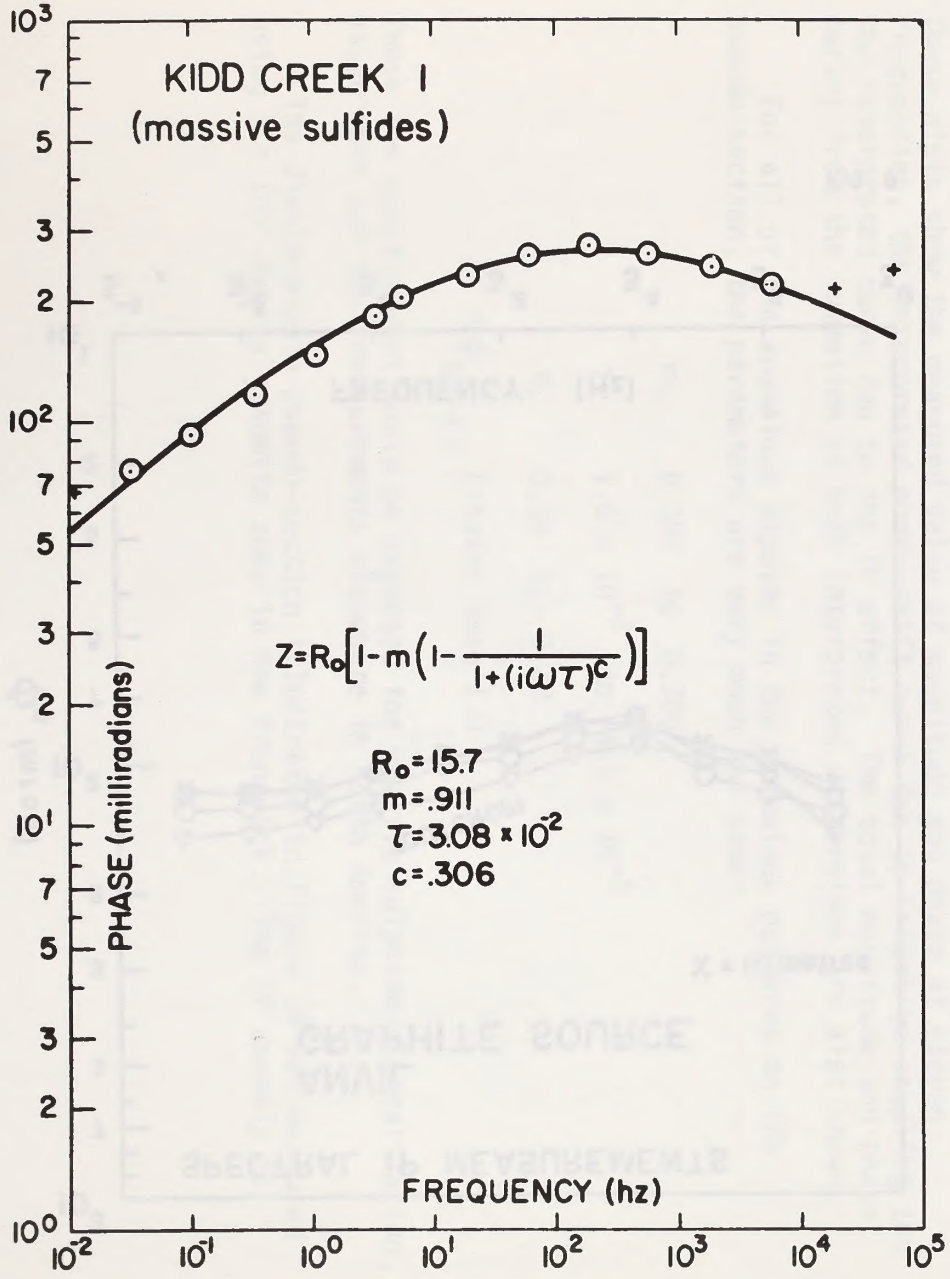
KIDD CREEK 1
(massive sulfides)
$Z=R_o\left[1-m\left(1-\frac{1}{1+(i\omega\tau)^c}\right)\right]$
R_o= 15.7
m=.911
τ=3.08 x 10^{-2}
c=.306
PHASE (milliradians)
FREQUENCY (hz)

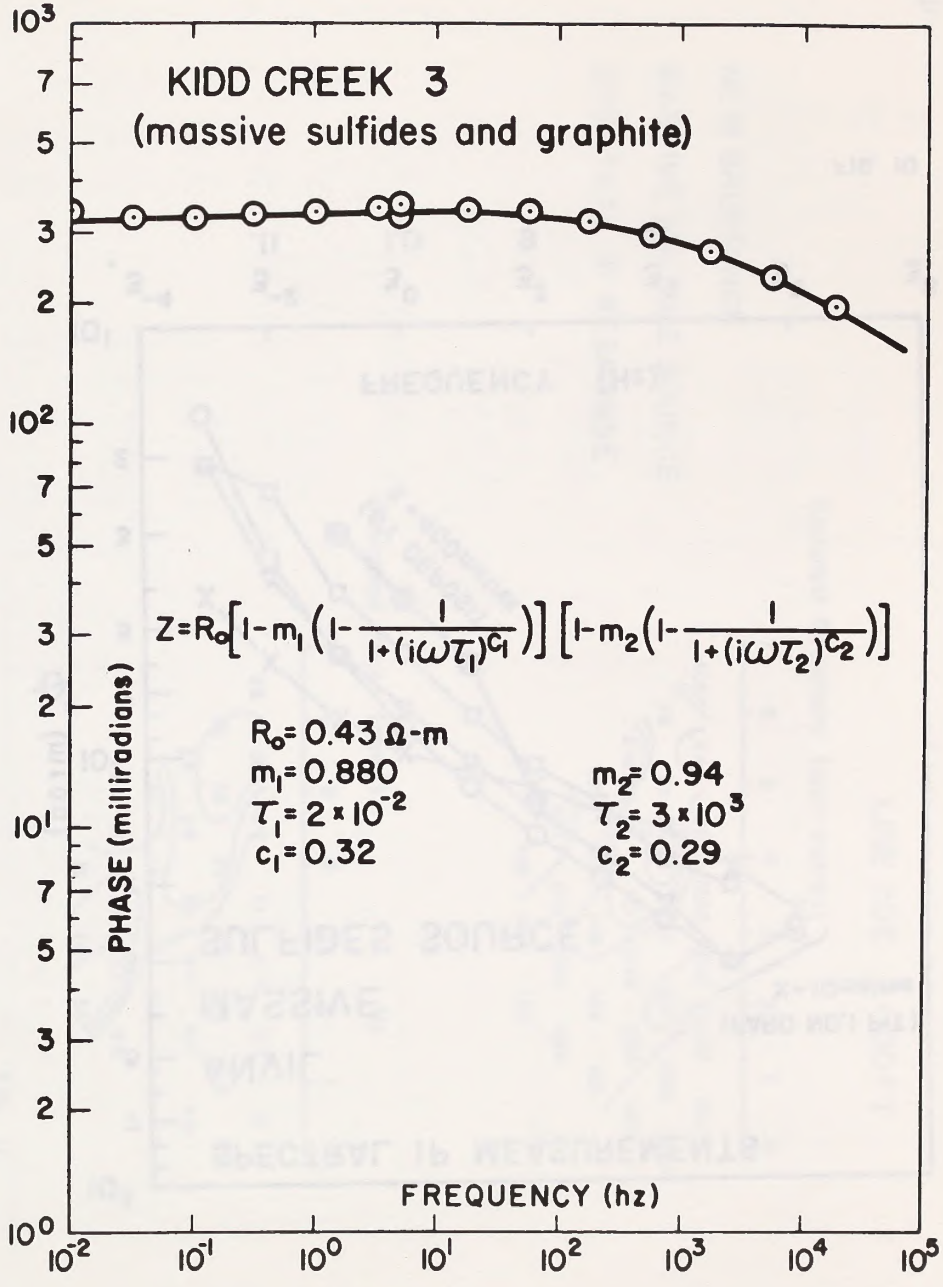
KIDD CREEK 3
(massive sulfides and graphite)
$Z=R_o\left[1-m_1\left(1-\frac{1}{1+(i\omega\tau_1)^{c_1}}\right)\right]\left[1-m_2\left(1-\frac{1}{1+(i\omega\tau_2)^{c_2}}\right)\right]$
R_o= 0.43 Ω-m
m_1= 0.880
τ_1= 2 x 10^{-2}
c_1= 0.32
m_2= 0.94
τ_2= 3 x 10^3
c_2= 0.29
PHASE (milliradians)
FREQUENCY (hz)

FIG. 8

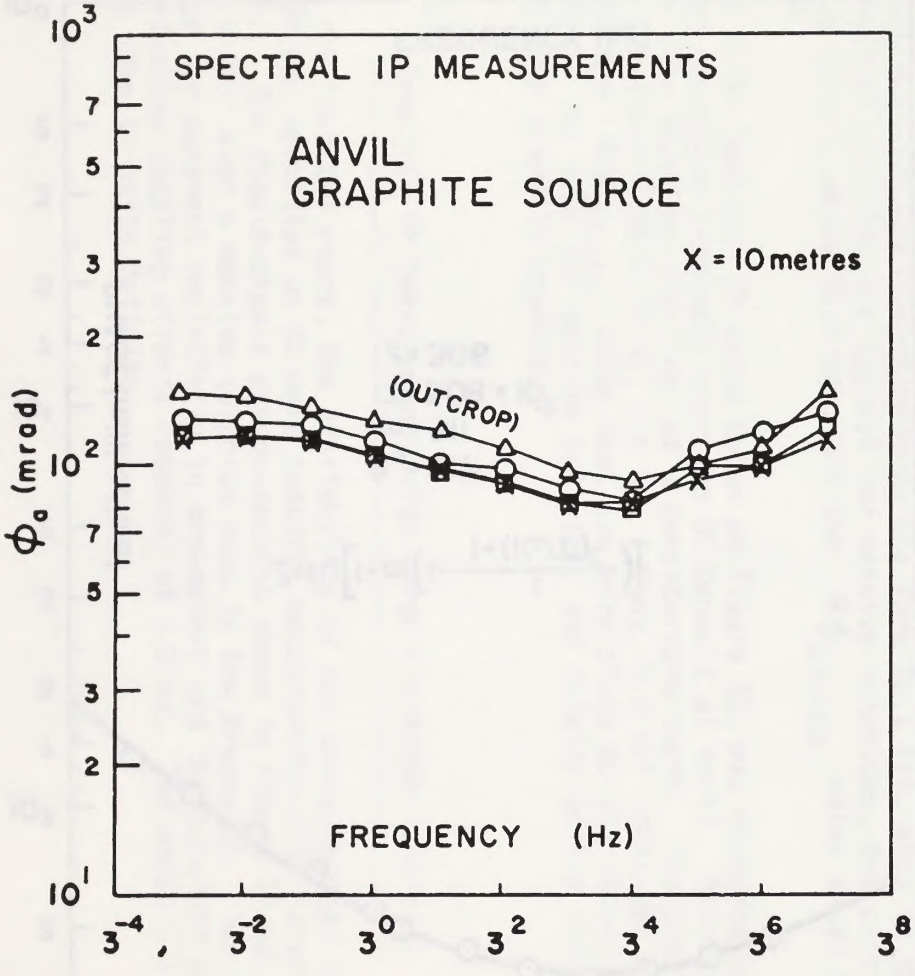
SPECTRAL IP MEASUREMENTS
ANVIL
GRAPHITE SOURCE
X = 10 metres
(OUTCROP)
ϕ_a (mrad)
FREQUENCY (Hz)
10^3
7
5
3
2
10^2
7
5
3
2
10^1
3^{-4}
3^{-2}
3^0
3^2
3^4
3^6
3^8

FIG. 9

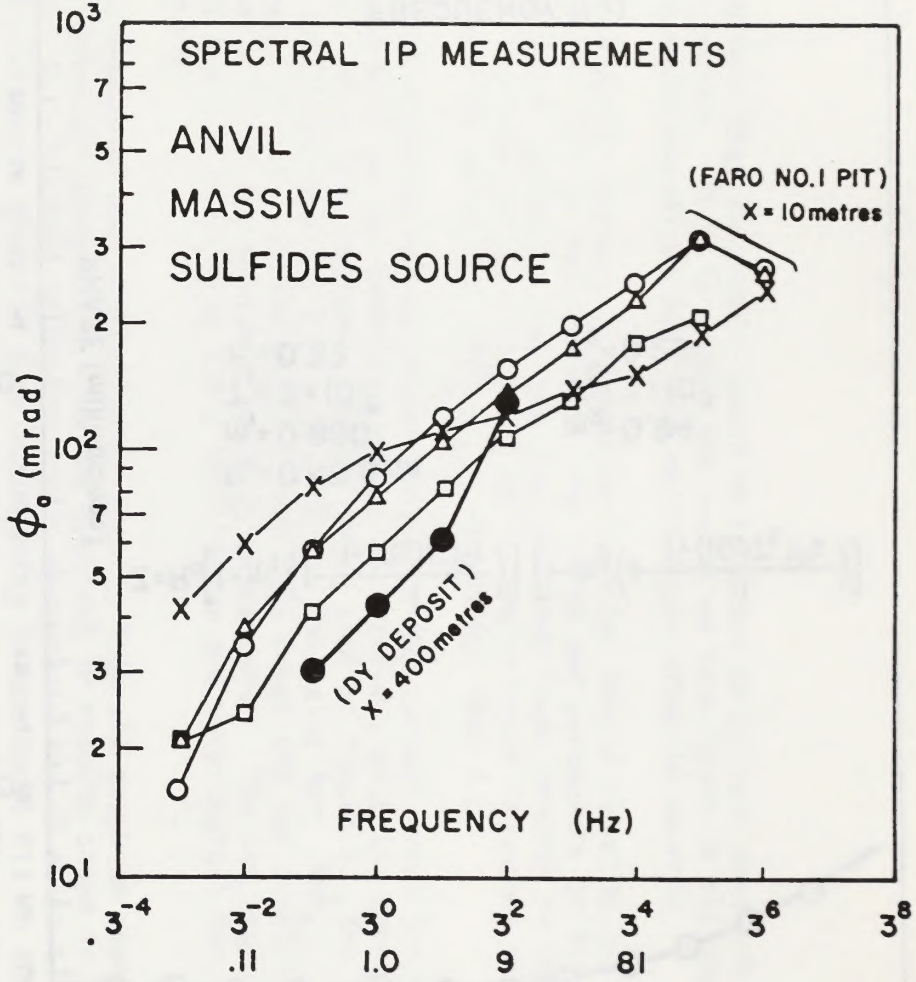
SPECTRAL IP MEASUREMENTS
ANVIL
MASSIVE
SULFIDES SOURCE
(FARO NO.1 PIT)
X = 10 metres
(DY DEPOSIT)
X = 400 metres
ϕ_a (mrad)
FREQUENCY (Hz)
10^3
7
5
3
2
10^2
7
5
3
2
10^1
3^{-4}
3^{-2}
3^0
3^2
3^4
3^6
3^8
.11
1.0
9
81

FIG. 10

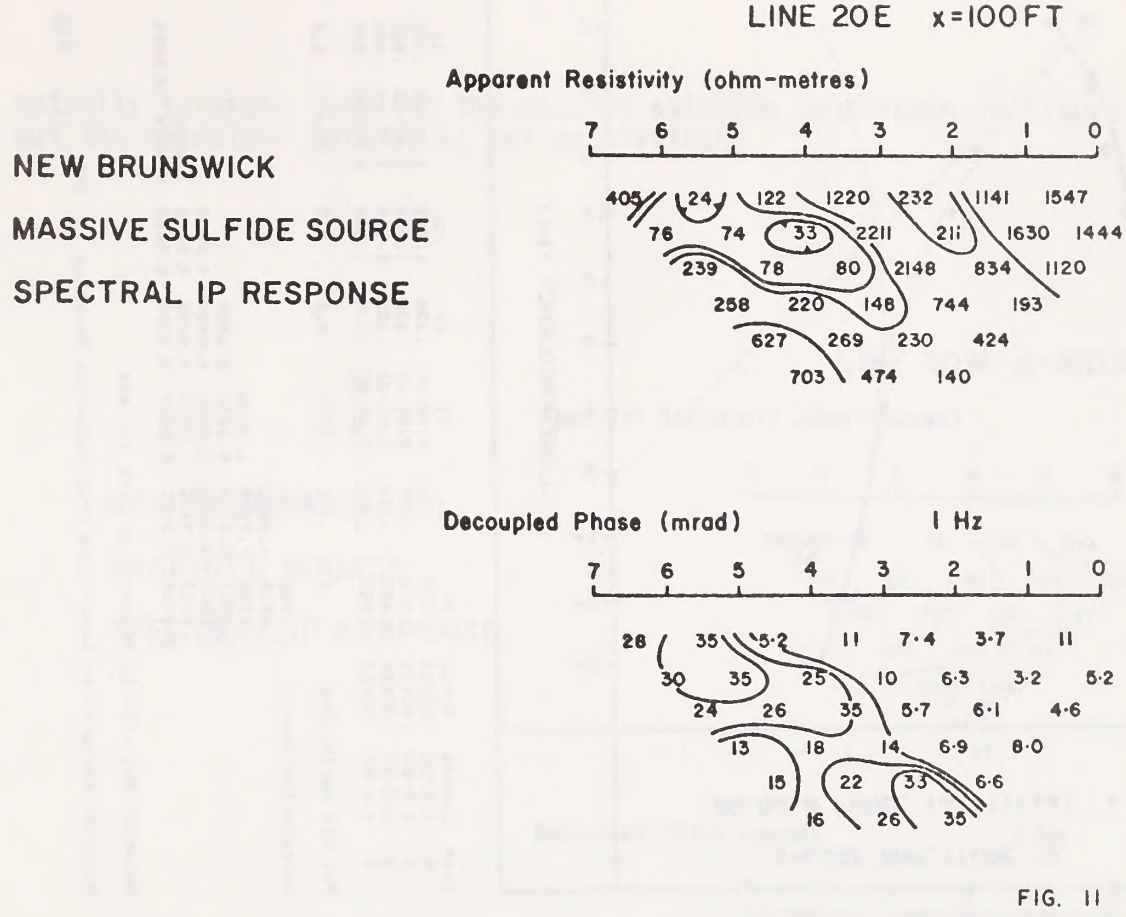

FIG. 11

In Figure 12 and Figure 13 are reproduced copies of the computer "print-out" from the spectral analysis of the data from two dipole pairs. These plots show the measured value of magnitude and phase at eleven frequencies, the interpreted phase-shift curve due to inductive coupling and the interpreted curve due to the IP effect. The total magnitude and phase curves from the summation of both interpreted dispersions are also shown.

For all of the anomalous dipoles in the anomalous patterns on the pseudo-section, the parameters are very much the same:

m_1 0.150 to 0.300

τ_1 1.5×10^{-2} to 4.5×10^{-2}

c_1 0.35 to 0.38

$R\phi_{0.3-3.0}$ greater than 1.0

These are exactly what would be expected for massive sulphide mineralization, based upon our test measurements elsewhere in North America.

The dipole-dipole pseudo-section illustrated in Figure 14 was measured using X = 100' over a graphite zone in New Brunswick. The IP anomaly is

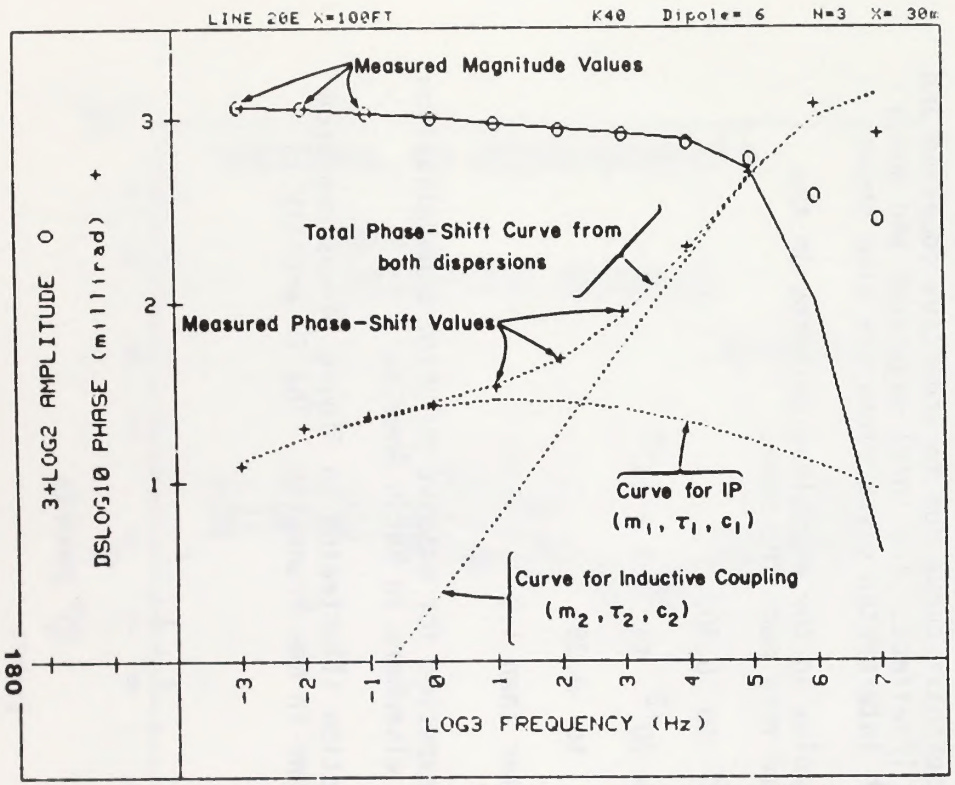

				IP EFFECT			INDUCTIVE COUPLING EFFECT		
Iter	Lambda	Rchsq	P0	M1	T1	C1	M2	T2	C2
0	1.E-02	.03408	1.089	.221	4.0E-02	.329	1.000	1.1E-04	1.000
1	1.E-02	.00168	1.063	.196	2.5E-02	.373	1.000	3.6E-04	1.000
2	1.E-03	.00058	1.072	.186	3.1E-02	.355	1.000	3.3E-04	1.000
3	1.E-04	.00067	1.071	.174	4.3E-02	.373	1.000	3.4E-04	1.000
4	1.E-05	.00066	1.071	.172	4.4E-02	.376	1.000	3.4E-04	1.000
Pct Std Deviations			.8	16.4	84.2	13.5	0.0	5.5	0.0

Correlation Matrix

1.0000							
.5173	1.0000						
-.4289	-.9715	1.0000					
-.5302	-.9438	.8971	1.0000				
0.0000	0.0000	0.0000	0.0000	0.0000			
-.2093	-.6596	.6657	.5340	0.0000	1.0000		
0.0000	0.0000	0.0000	0.0000	0.0000	0.0000	0.0000	

Apparent Resistivity Measured at 1 Hz is 78

Apparent Resistivity Calculated from Inductive Coupling is 10

FIG. 12

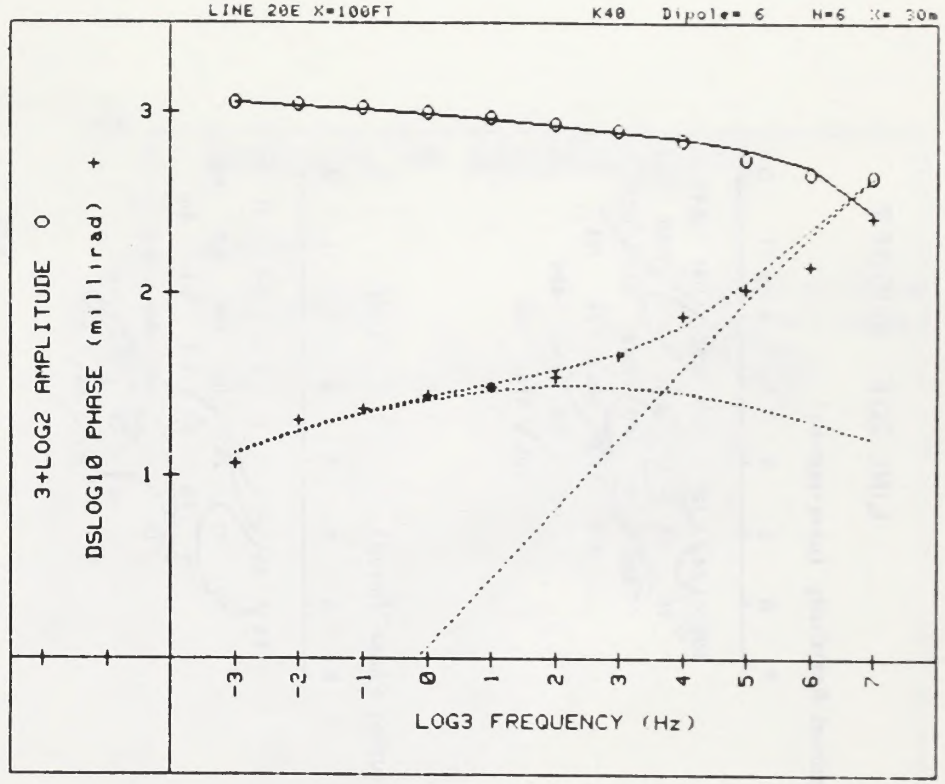

Iter	Lambda	Rchsq	P0	M1	T1	C1	M2	T2	C2
0	1.E-02	.02363	1.070	.160	4.0E-02	.330	1.000	1.2E-05	.800
1	1.E-02	.00134	1.064	.207	2.2E-02	.330	1.000	3.4E-05	.800
2	1.E-03	.00124	1.065	.210	1.6E-02	.330	1.000	3.6E-05	.800
3	1.E-04	.00124	1.065	.211	1.6E-02	.330	1.000	3.6E-05	.800
Pct Std Deviations			.9	7.1	50.1	0.0	0.0	15.4	0.0

Correlation Matrix

1.0000							
.0539	1.0000						
.1205	-.8760	1.0000					
0.0000	0.0000	0.0000	0.0000				
0.0000	0.0000	0.0000	0.0000	0.0000			
.0103	-.7222	.6609	0.0000	0.0000	1.0000		
0.0000	0.0000	0.0000	0.0000	0.0000	0.0000	0.0000	

Apparent Resistivity Measured at 1 Hz is 474

Apparent Resistivity Calculated from Inductive Coupling is 145

FIG. 13

actually stronger than for the massive sulphide zone shown in Figure 11, but the anomalous pattern is not as distinct.

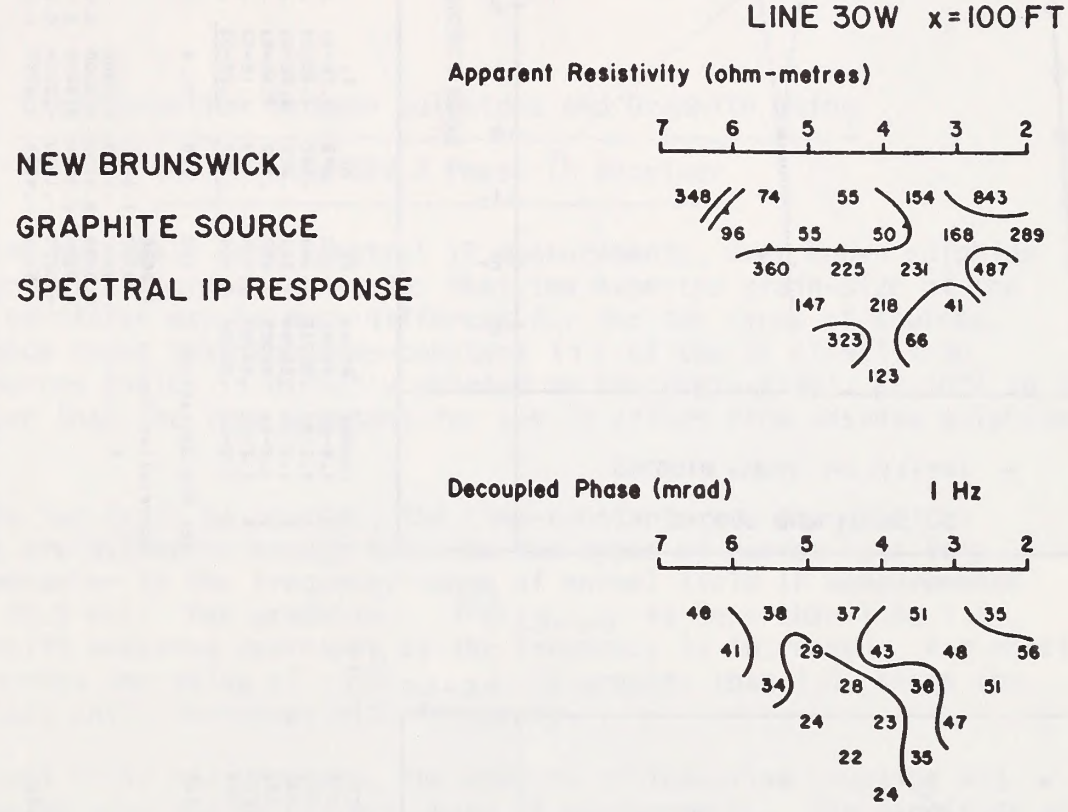

FIG. 14

The computer "print-out" for two dipole pairs are shown on Figure 15 and Figure 16. As is usually the case, the results of the inversion are very similar for all of the anomalous dipole pairs. In this case the values were:

m_1 0.350 to 0.550

τ_1 $1.0 \times 10^{+2}$ to $6.0 \times 10^{+2}$

c_1 0.180 fixed

$R\phi_{0.3-3.0}$ less than 1.0

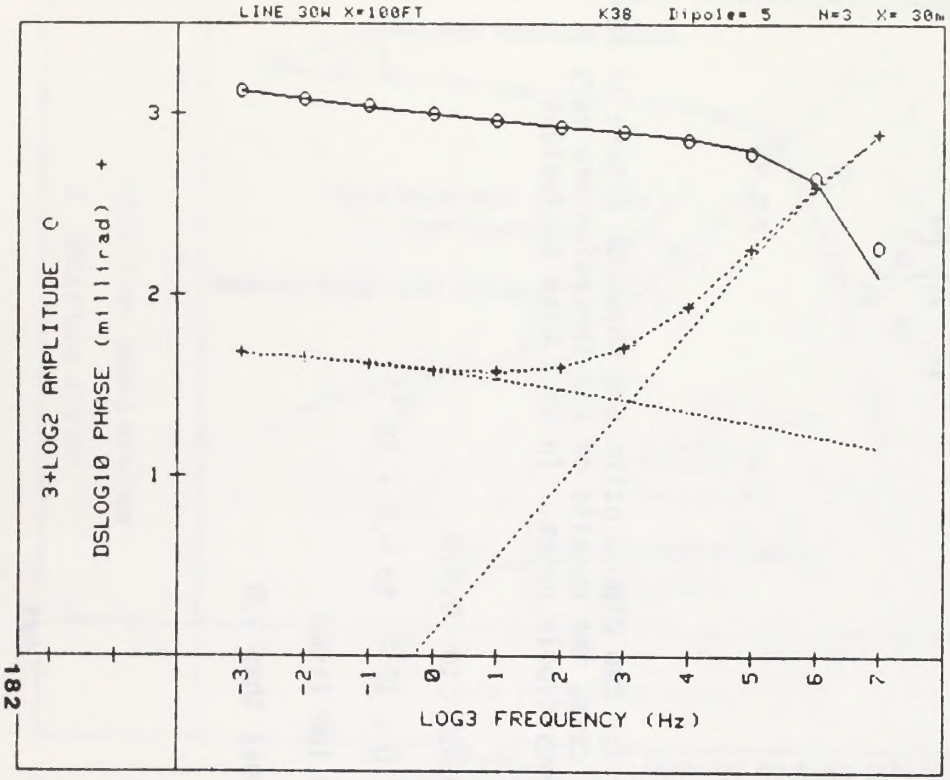

182

Iter	Lambda	Rchsq	R0	M1	T1	C1	M2	T2	C2
0	1.E-02	.01496	1.776	.571	1.2E+02	.100	1.000	1.5E-04	.970
1	1.E-02	.00083	1.569	.483	1.3E+02	.100	1.000	9.3E-05	.083
2	1.E-03	.00008	1.616	.487	1.9E+02	.100	1.000	8.8E-05	.891
3	1.E-04	.00006	1.677	.502	4.0E+02	.100	1.000	0.7E-05	.082
4	1.E-05	.00005	1.704	.508	5.3E+02	.100	1.000	0.7E-05	.879
5	1.E-06	.00005	1.707	.509	5.4E+02	.100	1.000	0.7E-05	.079

Pct Std Deviations	2.4	2.0	53.1	0.0	0.0	2.0	1.0

Correlation Matrix

	1.0000						
	.9916	1.0000					
	.9885	.9710	1.0000				
	0.0000	0.0000	0.0000	0.0000			
	0.0000	0.0000	0.0000	0.0000	0.0000		
	-.1166	-.0989	-.1282	0.0000	0.0000	1.0000	
	-.4909	-.4260	-.5273	0.0000	0.0000	.7128	1.0000

Apparent Resistivity Measured at 1 Hz is 231

Apparent Resistivity Calculated from Inductive Coupling is 26

FIG. 15

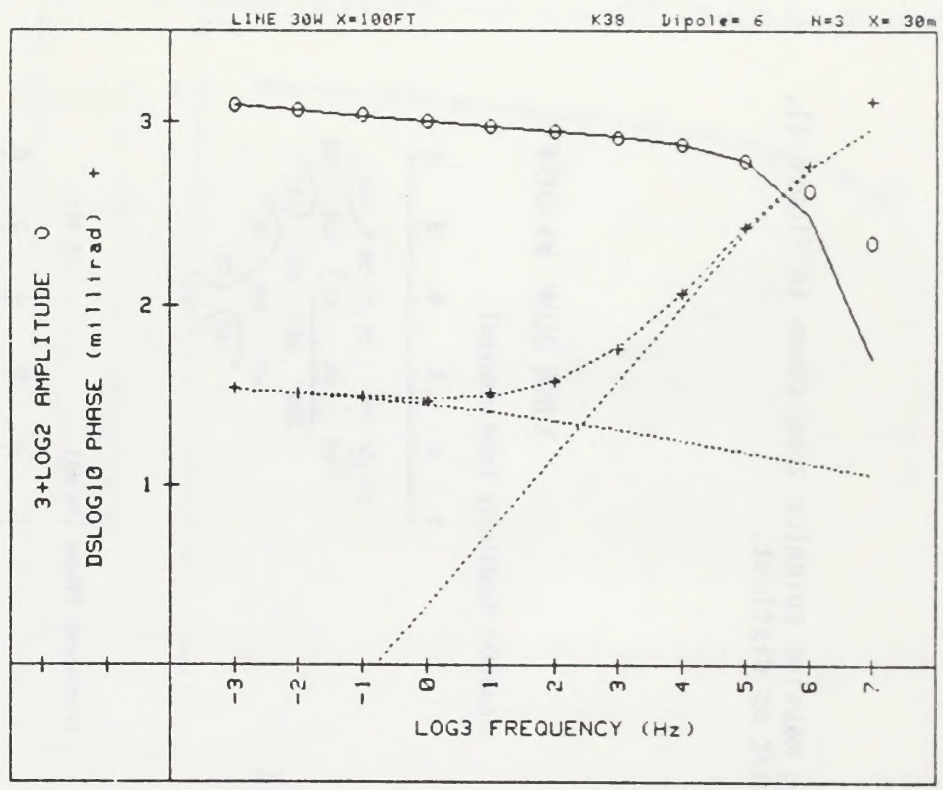

Iter	Lambda	Rchsq	R0	M1	T1	C1	M2	T2	C2
0	1.E-02	.00041	1.353	.370	1.7E+01	.100	1.000	1.4E-04	.927
1	1.E-02	.00012	1.345	.367	1.0E+01	.100	1.000	1.5E-04	.903
2	1.E-03	.00009	1.361	.371	2.8E+01	.100	1.000	1.5E-04	.899
3	1.E-04	.00005	1.402	.382	7.6E+01	.100	1.000	1.5E-04	.881
4	1.E-05	.00004	1.424	.389	1.1E+02	.100	1.000	1.5E-04	.876
5	1.E-06	.00004	1.426	.390	1.2E+02	.100	1.000	1.5E-04	.875

Pct Std Deviations	1.5	1.8	51.4	0.0	0.0	2.4	1.2

Correlation Matrix

	1.0000						
	.9787	1.0000					
	.9837	.9479	1.0000				
	0.0000	0.0000	0.0000	0.0000			
	0.0000	0.0000	0.0000	0.0000	0.0000		
	-.2625	-.1920	-.2824	0.0000	0.0000	1.0000	
	-.5785	-.4708	-.6207	0.0000	0.0000	.8060	1.0000

Apparent Resistivity Measured at 1 Hz is 225

Apparent Resistivity Calculated from Inductive Coupling is 15

FIG. 16

These parameters are also similar to those we have measured elsewhere in North America, over graphite sources.

Measurements in North America and Australia, over numerous sulphide and graphite sources, have shown for many hundreds of dipole pairs, that the time-constant of the IP spectral IP effect measured from graphite is 10^{+3} to 10^{+4} times greater than that from massive sulphides.

Discrimination Between Sulphides and Graphite Using the Phoenix IPV-2 Phase IP Receiver

The data available from spectral IP measurements, over known sulphide and known graphite sources, indicates that the expected grain-size of the polarizing particles may be much different for the two types of sources. Our experience shows that the time-constant (τ) of the IP effect from graphite sources (which is directly related to the grain-size), is 10^{+3} to 10^{+4} times greater than the time constant for the IP effect from massive sulphide sources.

For the two types of sources, the time-constants and the critical frequencies are different enough that the two types of curves have very different behavior in the frequency range of normal field IP measurements (0.1 Hz to 10.0 Hz). For graphite, $R\Phi_{0.3-3.0}$ is less than 1.0; i.e., the phase-shift measured decreases as the frequency is increased. For massive sulphide sources the value of $R\Phi_{0.3-3.0}$ is greater than 1.0, since the measured phase shift increases with frequency.

In normal field measurements, the effects of inductive coupling and dilution can be expected to distort phase IP measurements. The magnitude of the distortions will depend upon the parameters of the earth, the parameters of the source, the electrode interval and the frequencies used. However, for shallow sources, short electrode intervals and low frequencies, these effects will be small, or negligible. In this situation, phase IP measurements with even two frequencies may give some information about the time constant of the IP effect measured.

The Phoenix Prospecting Phase IP Receiver (Figure 17 and Figure 18) is a two voltage channel system, that was designed to be used at a single frequency to do reconnaissance and detailed surveys. The five frequencies (0.11 Hz, 0.33 Hz, 1.0 Hz, 3.0 Hz, 9.0 Hz) were included to give the geophysicist a choice of frequencies. The survey progresses faster at the higher frequencies, and depending upon the conditions and parameters encountered, a choice of frequencies is desirable.

However, once the IP anomalies are located, and evaluated by detailed measurements, it is usually possible to use the IPV-2 to gather some data regarding the time constants of the sources.

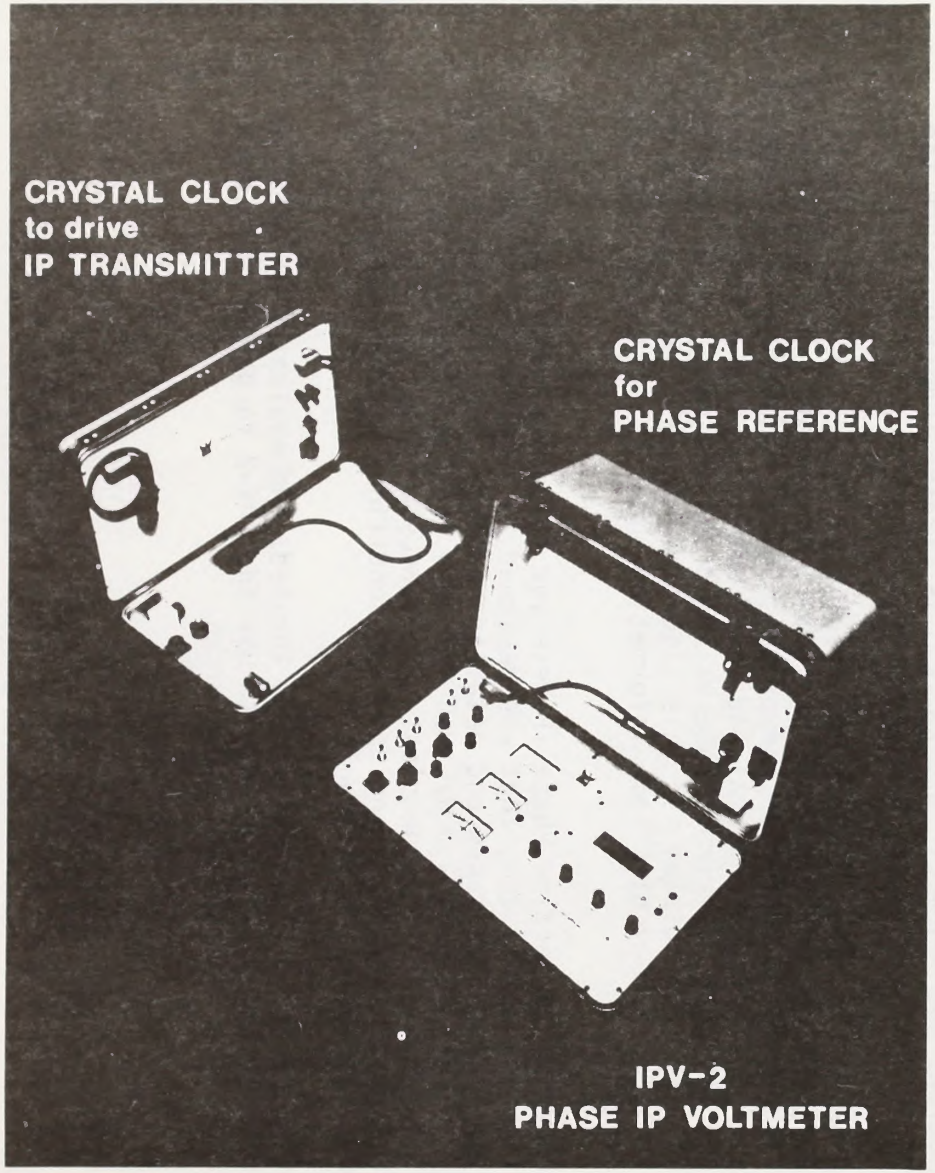
CRYSTAL CLOCK
to drive
IP TRANSMITTER
CRYSTAL CLOCK
for
PHASE REFERENCE
IPV-2
PHASE IP VOLTMETER

FIG. 17

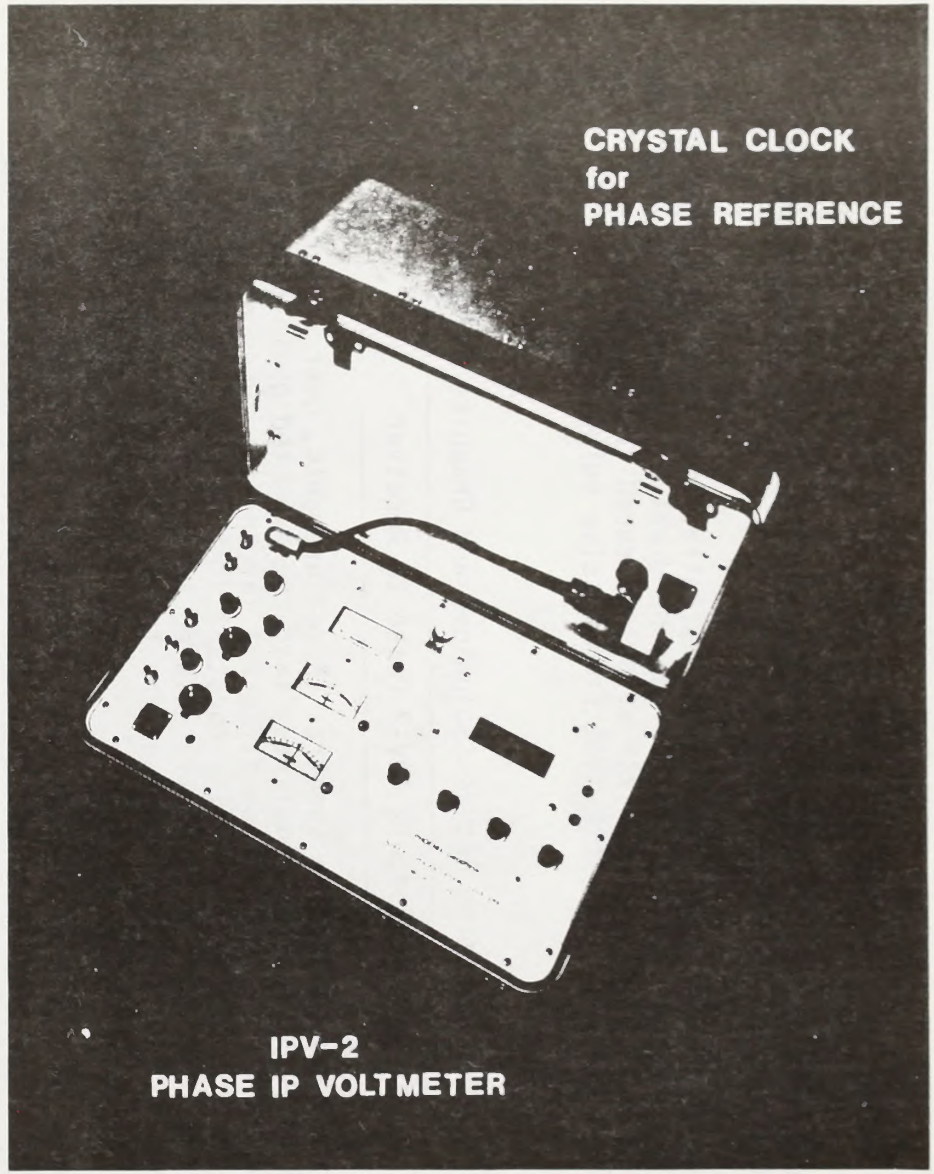
CRYSTAL CLOCK
for
PHASE REFERENCE
IPV-2
PHASE IP VOLTMETER

FIG. 18

In Figure 19 and Figure 20 are detailed IP and resistivity data measured using X = 100' over two different sources on a property in the Sturgeon Lake Area of Ontario. On the basis of the original IP data, both sources were tested by drilling. The anomaly at Line 18E, 53+50S was due to massive sulphides; the anomaly at Line 15E, 79+00S was due to graphite, with some pyrite present.

The induced polarization and phase IP anomalies are very similar; it would be expected that the sources would have similar true resistivity and true IP values. If the dipole-dipole pseudo-section anomalies are interpreted using a computer inversion program, assuming a two-dimensional source (Pelton, et al, June 1978), the results are indeed very similar.

The results of the computer inversions of the two sets of data are shown on Figure 21 and Figure 22. The source on Line 18E is at somewhat less depth, and the true IP effect in the source is interpreted to be lower in magnitude. Other than that, the sources are very much the same. Based upon simply the magnitude of the IP and resistivity anomaly alone, the two sources are indistinguishable.

The phase results shown on the pseudo-sections were measured using 0.33 Hz. The anomalous measurements identified by the symbols on the data plots were repeated using 3.0 Hz. The results, identified by the symbols, are plotted on Figure 23 and Figure 24. The results are plotted on a log-log plot, as was the case with the spectral phase data.

For the sources on Line 18E (the sulphide source), it can be seen that the critical frequency (f_c) is indicated to be above 3.0 Hz and the value $R\phi_{0.3-3.0}$ would be greater than 1.0. For the graphite (with pyrite) source the critical frequency is below 0.33 Hz and the value of $R\Phi_{0.3-3.0}$ would be less than 1.0.

CONCLUSIONS

In the last two years we have had available, increasing amounts of spectral IP data from known sources. In addition, we now have available theoretical experience and laboratory measurements on synthetic rock samples in which the metallic, polarizable particles have been controlled. From this work, several definite, and/or tentative conclusions can be made regarding the effect of mineral type, mineral texture and grain-size upon the critical frequency, time constant (τ) and frequency term exponent (c) of the Cole-Cole dispersion equations. This equation, using four parameters has been found to satisfactorily describe the IP effects measured from metallic mineralization.

$$Z(\omega) = R_o\left[1 - m\left(1 - \frac{1}{1+(i\omega\tau)^c}\right)\right]$$

PRICE COMPANY BLOCK NO.8 PROPERTY

IPV-2 PHASE IP TEST

LINE-18E

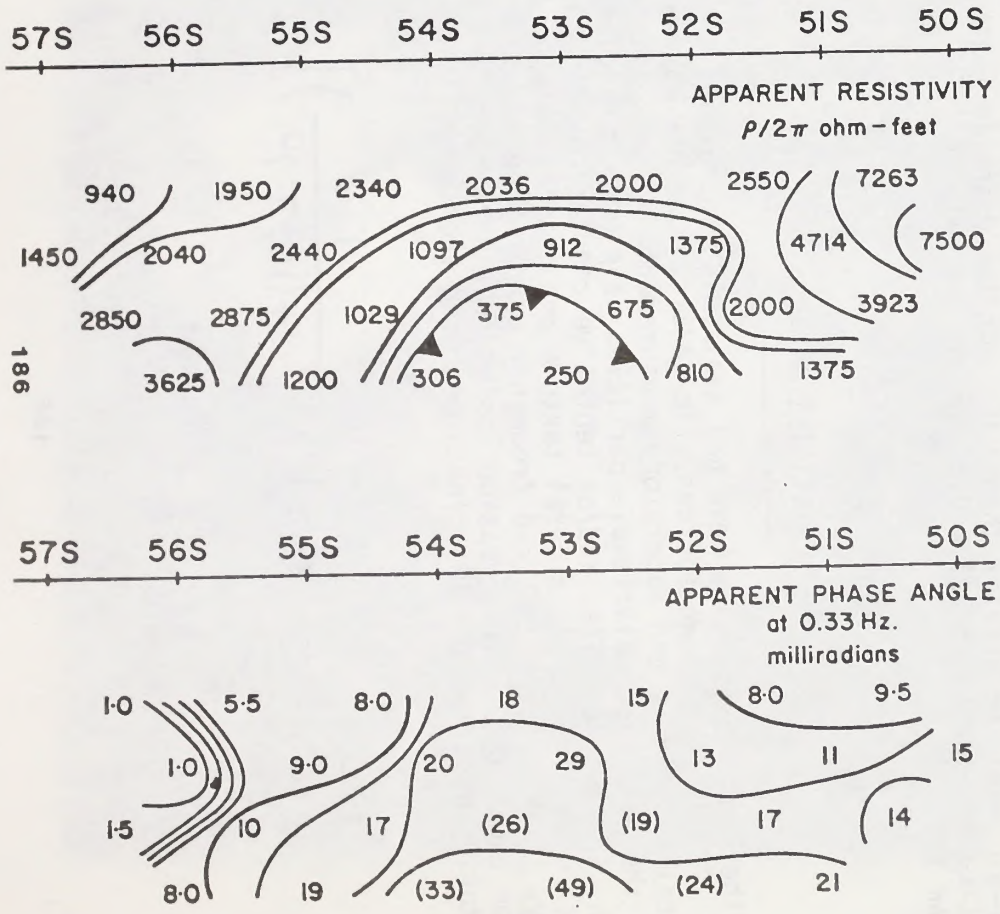

FIG. 19

PRICE COMPANY BLOCK NO.8 PROPERTY

IPV-2 PHASE IP TEST

LINE-15E

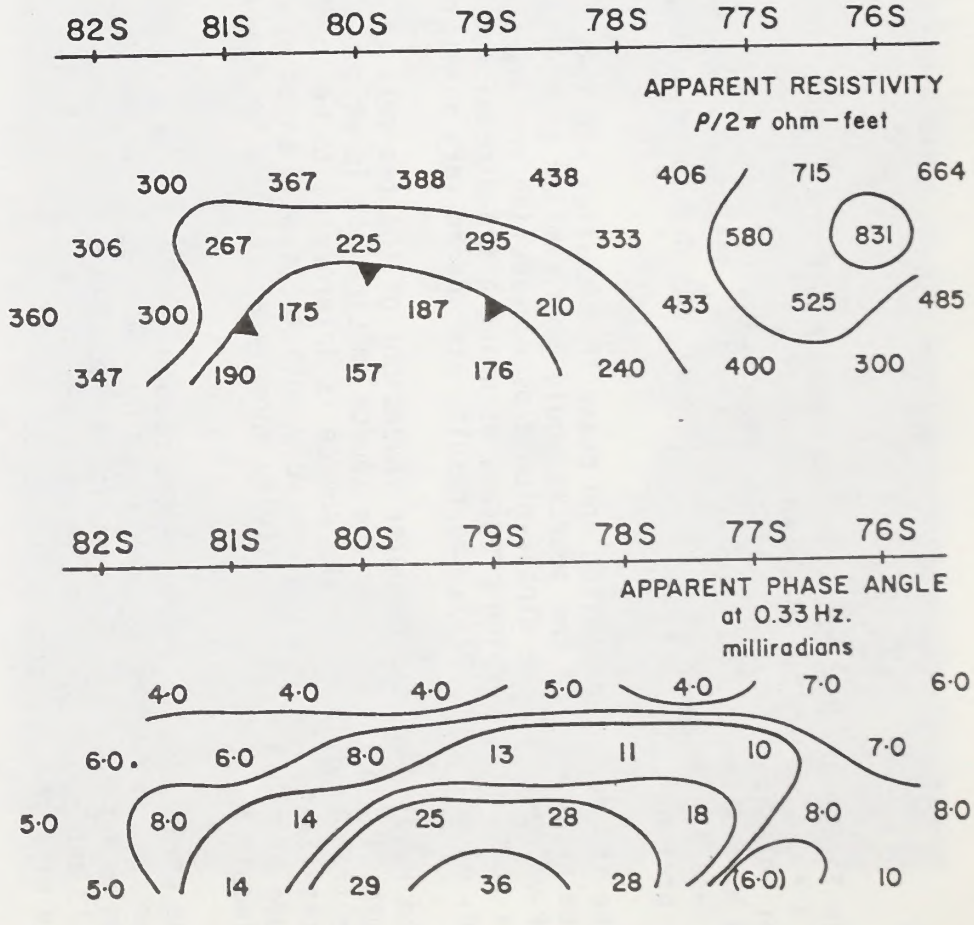

FIG. 20

LINE-18E

FINAL MODEL FOR DATA SET 1

OBSERVED DATA

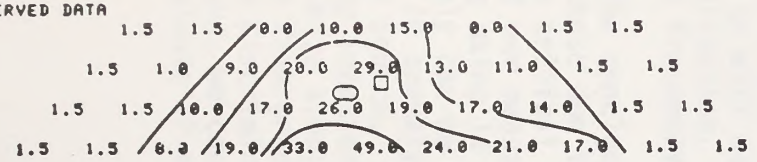

100•DIAGONAL OF INFORMATION DENSITY MATRIX

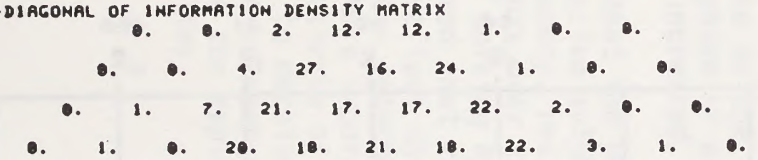

CALCULATED DATA

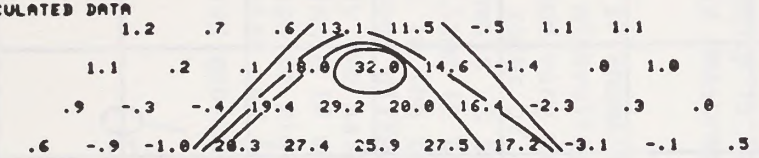

187

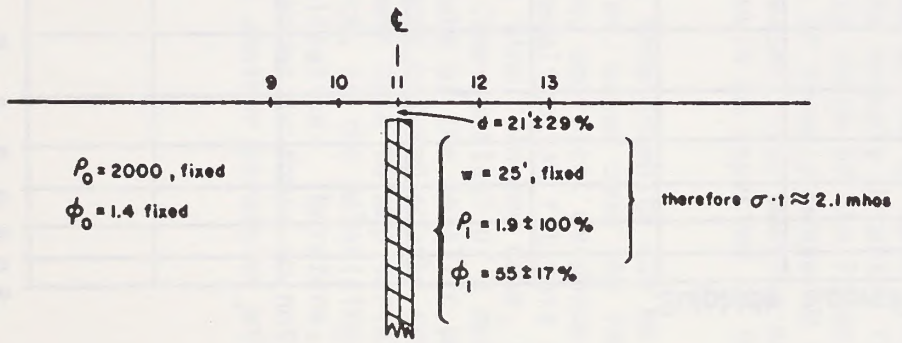

FIG. 21

LINE-15E

graphite source, with some pyrite

LINE-15E

phase at 0.3 Hz.

FINAL MODEL FOR DATA SET 1

OBSERVED DATA

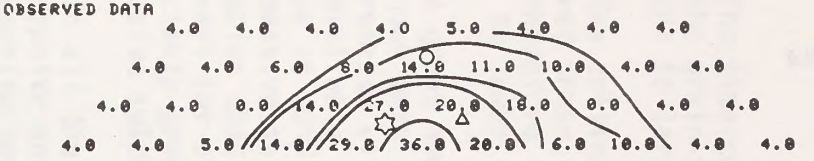

100•DIAGONAL OF INFORMATION DENSITY MATRIX

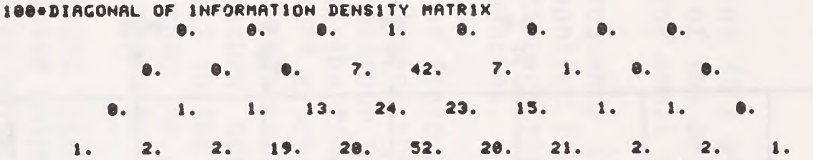

CALCULATED DATA

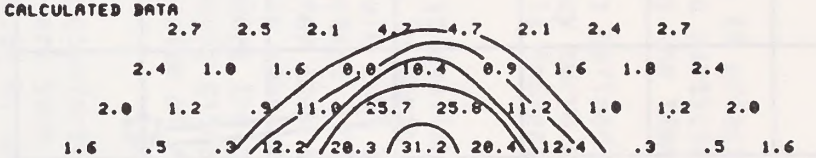

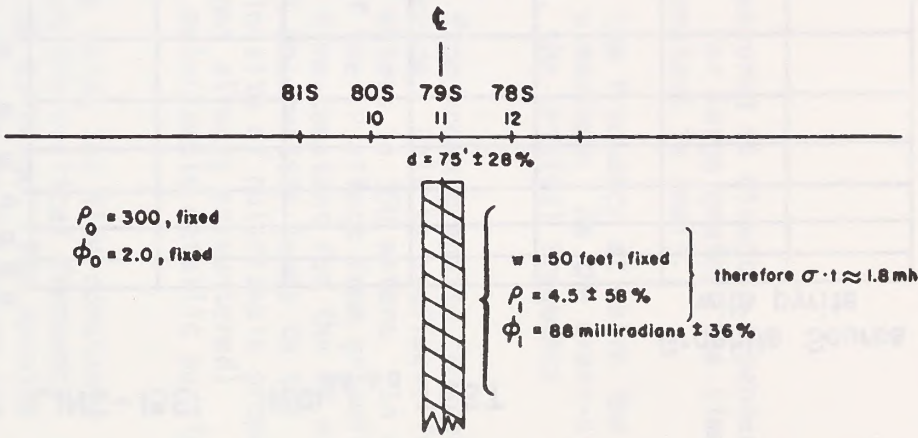

FIG. 22

LINE-18E $R\Phi_{0.3-3.0}$ TEST

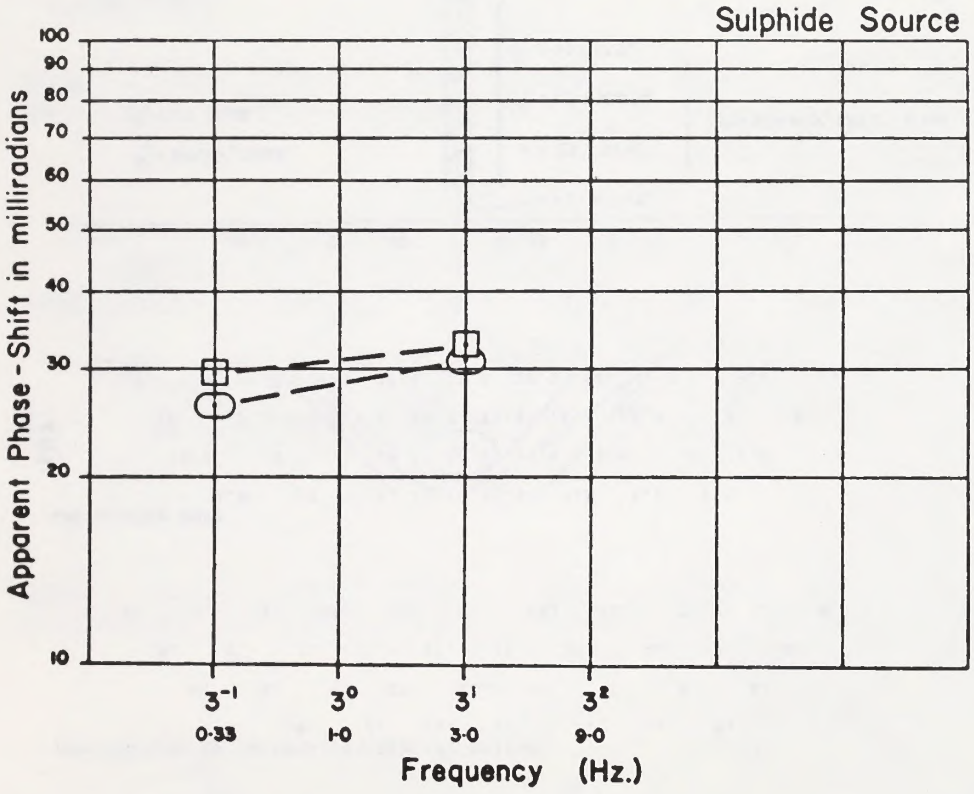

188

FIG. 23

LINE-15E $R\Phi_{0.3-3.0}$ TEST

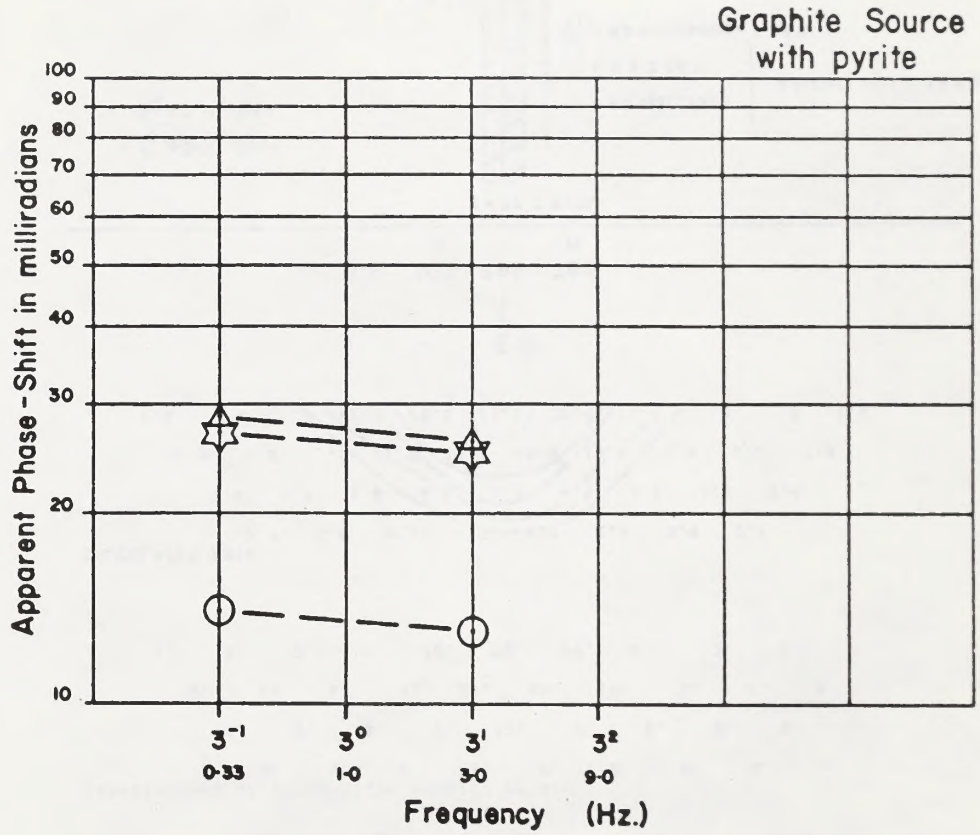

FIG. 24

i) The time-constant (τ) of the IP effect measured is directly dependent upon the grain-size of the metallic particles. For large grains, the time-constant is large; for small grains the time-constant is small.

ii) The critical frequency (f_c) is defined as the frequency at which the measured phase vs. applied frequency curve has a maximum. As the grain-size (and therefore the time-constant) is increased, the critical frequency moves to lower frequencies.

iii) A great amount of field data is available from known graphite sources and known massive sulphide sources in North America. Data is available from measurements with electrode intervals from 3.0 meters to 350 meters. In all data available to us, the time-constant (τ) of the IP effect from graphite sources is 10^{+3} to 10^{+4} times greater than the time-constant for the IP effect from massive sulphide sources. This consistent observation leads to the conclusion that in natural occurrences the grain-size of polarizable graphite is always (or at least in the geologic situations already encountered) appreciably greater than the grain-size of the polarizable metallic particles in massive sulphide deposits.

iv) In all the geologic locales encountered to date, the time-constants for graphite and massive sulphides are such that the critical frequency for graphite zones lies below the 0.10 Hz to 0.30 Hz range. For massive sulphide mineralization, the critical frequency appears to lie above the 1.0 Hz to 3.0 Hz range.

v) The result of all of the above is that if the effects of inductive coupling and dilution can be reduced, or eliminated, in a phase IP measurement, there is some hope that measurements at two or more frequencies can be used to indicate whether the source of the anomaly detected is graphite or massive sulphides. In the operating frequency range of the Phoenix IPV-2 Phase IP receiver (0.11 Hz to 9.0 Hz) the phase IP anomaly measured from graphite will decrease as the frequency is increased. For massive sulphide mineralization, the phase IP anomaly measured would be expected to increase as the frequency is increased.

vi) The conclusion that the phase IP anomalies from graphite can be separated from those due to massive sulphide mineralization, based upon the location of the critical frequency, rests upon very strong empirical evidence. Since all of our measurements over known zones of mineralization fit this concept, we are using it as a working hypothesis at this time. In any case, it probably can be assumed that variations in the time-constant of a measured phase IP anomaly do reflect changes in the texture of the metallic particles in the source. We have detected these differences between nearby sources in many locations. More importantly, we have been able to map variations in grain-size along the strike of a single IP source, as the polarizing minerals change from graphite to massive sulphide mineralization. Therefore, even if the discrimination between graphite and sulphides is found to not be rigorous, we can give the exploration geologist another parameter with which to evaluate IP anomalies.

REFERENCES

DeWitt, G.W., 1978, Parametric studies of induced polarization spectra: M.S. Thesis, University of Utah, Salt Lake City, Utah.

Grissemann, C., 1971, Examination of the frequency-dependent conductivity of ore-containing rock on artificial models. Scien. rep. no. 2, Electr. Lab., Univ. of Innsbruck, Austria.

Pelton, W.H., 1977, Interpretation of induced polarization and resistivity data: Ph.D. thesis, Univ. of Utah, Salt Lake City, Utah.

Pelton, W.H., Ward, S.H., Hallof, P.G., Sill, W.R., and Nelson, P.H. 1978, Mineral discrimination and removal of inductive coupling with multifrequency IP: Geophysics, v. 43, p. 588-609.

Pelton, W.H., Rijo, L., and Swift, C.J. Jr., 1978, Inversion of two-dimensional resistivity and induced polarization data: Geophysics, v. 43, p. 788-803.

Wong, J., 1979, An electrical model of the induced polarization phenomenon in disseminated sulphide ores: Geophysics, vol. 44, p. 1245 - 1265.

Toronto Office: 200 Yorkland Blvd., Willowdale, Ont. M2J 1R5
Vancouver Office: 310 - 885 Dunsmuir St., British Columbia, V6C 1N5
Denver Office: 4690 Ironton St., Colorado, 80239, U.S.A.

APPENDIX VIII

Magnetometers

(Breiner, S:1973): Applications Manual for Portable Magnetometers; EG & G Geometrics, Sunnyvale, California, p. 11-32. [Reprinted by permission of the author and EG & G Geometrics.]

Table of Contents

IV.

FIELD PROCEDURES AND DATA REDUCTION

Magnetic Cleanliness and Sensor Positions

Most of the applications for portable magnetometers require that *the operator be relatively free of magnetic materials on his person.* The importance of checking oneself cannot be over-estimated if measurements on the order of 1 gamma are desired. In field surveys, the usual magnetic material one may have may include, of course, the obvious such as a rock pick, Brunton compass, pocket knife, or instrument console and the not-so-obvious effects of the pivot in eyeglasses, the pants clip at the top of men's trousers, the light meter in a camera, the magnet in the speaker of a tape recorder, metal in a clipboard, some mechanical pencils, some keychains, and the steel shank in one's shoes or boots. Of course, some of these items cannot be altered or left behind and some are not significant in any event. The sensor itself should be kept clean to avoid possible contamination by magnetite-bearing dirt on the sensor surface. In order to check the 'heading effect', i.e., the effect of orientation on the observed field intensity during a field survey, the operator can take readings at each of the four cardinal directions while pivoting about the position of the sensor and note the changes. If the maximum change is typically less than 10 gammas, the average readings on a line will probably not be affected by more than 5 gammas and individual readings by less than this inasmuch as readings along the profile are more-or-less along a given heading ± perhaps 30° about one orientation. If a sensitivity of 1 gamma is desired, the heading error should be less than several, preferably 2 gammas or less and depending upon the desired sensitivity, the operator should make some effort to face in the same direction, if possible, for all readings on a given traverse.

The sensor for a proton magnetometer may be carried on a 8-foot (2.2 meter) staff, on a backpack, on an extended staff to 12 feet (4 meters) or more as necessary, or by a second person as represented in *Figure 8.* The sensor on an 8-foot staff is by far the most common means for field measurements removing the sensor sufficiently far from the console and from the operator so as not to be much affected by normal items of clothing, etc. The purpose of mounting a sensor on an extended 12 foot or longer staff is to remove the sensor from the locally disturbing effects of highly magnetic surface materials, such as surface laterite, glacial till, or highly magnetic outcropping rocks. The sensor may also be raised in the case of very high magnetic gradients which would otherwise ruin the magnetometer signal and prevent any reading whatsoever (see following sections). An additional reason for an extended staff will be described in Chapter VIII in reference to vertical gradient measurements. There are also occasional reasons for a second person carrying the sensor while the first person carries the console together, perhaps, with magnetic or other materials that must necessarily be on his person such as pick, tape recorder, another instrument or rock samples.

The sensor may be carried in a backpack pouch for more convenient field operation where 5 or 10 gamma sensitivity is all that is desired, but care should be taken to check the effects of the batteries and console (particularly the very magnetic alkaline batteries). The backpack pouch frees the hands for taking notes, pushing aside the underbrush and, in general, balances the load of the console and decreases fatigue.

Operational Considerations

Valid Readings Vs. Noise

It is important to establish that, in fact, the magnetometer is providing valid readings. The simplest means of confirming that what is being observed is a magnetic field reading and not random, meaningless instrument readings (i.e., noise) is to take several readings in succession in one location without moving anything, and note the repeatability. Successive readings should be within ± 1 gamma, ± 0.25 gamma or ± 1 count for whatever the sensitivity setting. Valid readings should not, under any naturally-occurring circumstances including magnetic storms, vary by as much as ± 10 or ± 100 gammas in a few seconds; if such is observed, the readings represent either noise or a degradation of the signal-to-noise ratio with the observed corresponding loss in terms of sensitivity. Under certain circumstances even successive readings repeating to within several gammas may still represent noise. To confirm that these readings are indeed magnetic field, simply 'kill' the signal by placing,

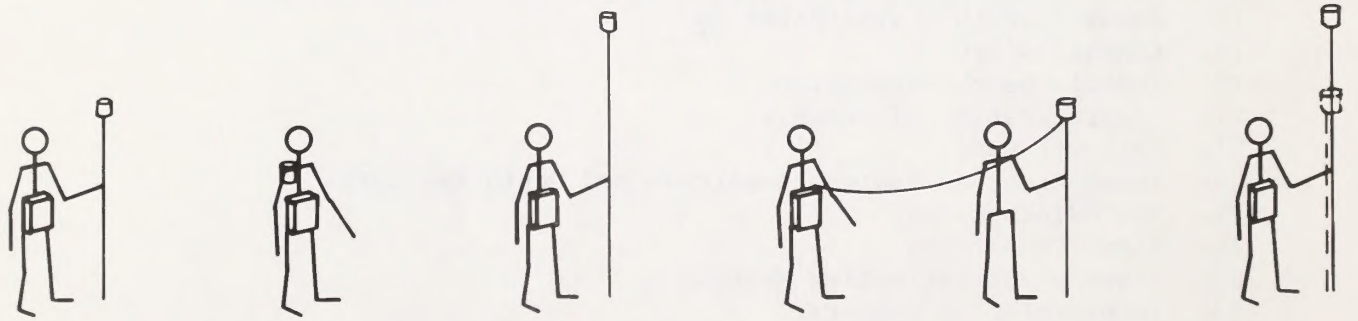

Figure 8. Sensor Carrying Positions

momentarily during the reading, something magnetic adjacent to the sensor such as one's shoe, watch, certain rocks, etc. Random readings varying by 10 or 100 gammas or more would then be observed in addition to their deviating considerably from the readings without the object present. Another but less certain method is to take readings at intervals of increasing distance from an object or location known to produce a magnetic anomaly.

Typical reasons for a proton magnetometer not producing valid readings may be: electrical noise from AC power lines, transformers or other radiating sources; high magnetic gradients from underlying rocks, nearby visible or hidden iron objects, fence lines or improvised iron hardware improperly used near the sensor; improper orientation of the sensor (even when 'omni-directional'); expired batteries, incorrect range setting or instrument failures, broken or nearly broken sensor cable, and other malfunctions usually described in the instrument operating manual.

Valid but distorted readings may result from several other conditions including the above effects of high magnetic gradients, magnetic dirt or other magnetic contamination on the sensor and any magnetic bias on the operator. Time variations (Chapter III and following) and the effects of direct current in distant power lines and trains (Chapter IX) can also distort magnetic observations.

Sensor Orientation

According to the theory of operation of the proton magnetometer, the total intensity, measured as the *frequency* of precession, is independent of the orientation of the sensor. The *amplitude* of the signal, however, does vary (as $\sin^2\theta$) with the angle between the direction of the applied field within the sensor and the earth's field direction. Variation of signal amplitude does not normally affect the readings unless there is simply insufficient signal to be measured accurately, i.e., a minimum signal amplitude is required above which a variation in amplitude does not affect the readings.

Ideally, the applied field in the sensor should be at right angles to the earth's field direction. The direction of the applied field is governed by the configuration of the polarizing coils in the sensor which are commonly either solenoids (cylindrical) or toroids (ring or doughnut-shaped). The solenoid produces an applied field parallel to its axis, whereas the toroid produces a field which is ring-shaped about the axis of the toroid (consult the instrument operations manual to determine the direction of these axes with respect to the sensor housing). Solenoids are used because they produce somewhat higher signal than a toroid and are less perturbed by electrical noise, whereas a toroid is inherently omnidirectional. In the ideal case, a solenoid should be held horizontal and in any direction in a vertical field, and should be held vertical in a horizontal (equatorial) field for maximum signal amplitude. A toroidal sensor should be held with its axis vertical in a vertical field, and pointing north in an equatorial field to obtain maximum signal. A field which dips greater or less than 45°, should be treated as though it were a vertical or horizontal field respectively.

Instrument Readings

Measurements are normally made at regular intervals along a grid or otherwise selected path whose locations are noted for subsequent plotting. Simple pacing is usually adequate with readings every 6, 10, 50, 100, 500, or even 1,000 feet (2 to 300 meters), as anomalies, field, and either geological or search requirements dictate. Traverses may be selected along pathways or other accessible routes and occasional locations noted on an aerial photograph or map using paced distances in between. The density of readings along the traverse should be related to the wavelength of anomalies of interest such that several readings are obtained for any such anomaly. A single trial line with relatively dense stations is usually attempted first to determine the required station density. It is important never to hold the magnetometer sensor within one or two feet of the ground, if possible, in order to avoid effects of minor placer magnetite which usually collects on the surface of the ground, and also to avoid the effects of microtopography or outcropping rock surfaces.

Readings may be noted in a field notebook or, if desired, on a miniature tape recorder, but care must be taken to magnetically compensate the speaker magnet and motor following the theory given in Chapter VI if one is to use a recorder. The convenience of the recorder is that only one hand is needed and the data may be played back for fast, convenient plotting.

Correction for Time Variations

Some ground magnetic surveys require correction for diurnal and micropulsation time variations. Correction is required if the anomalies of interest are broad (thousands of feet) and typically less than 20 to 50 gammas, or if the profile lines are very long, or if the objective of the survey is a good magnetic contour map expressive of deep-seated anomaly sources. Also, if the survey is performed in the high magnetic latitudes in the auroral zone where typical micropulsations are 10 to 100 gammas, correction for such variations would be necessary. On the other hand, if one is merely interested in profile information of anomalies of several hundred gammas or if the anomalies are only 20 gammas but can be traversed completely in less than 5 minutes, no time variation correction is needed. Perhaps *most surveys* fit the latter criteria and *do not actually require any such correction for time variations.*

The simplest method of correcting for time variations involves repeated readings in the same orientation at the same station at different times during the survey. If a smooth curve is drawn through the readings plotted as a function of time (every hour or so), these values can be subtracted from all other readings provided that each reading also includes the time at which it was observed. To avoid an extremely long and repeated walk to a single reference station, it is also possible to 'double-back' to take a second or third reading on each given traverse to determine at least the time variations for that traverse. Still another technique is to emulate what is done on aeromagnetic surveys, namely, obtain rapidly acquired measurements on tie lines or lines which cross the principal traverse lines at each end and perhaps in the center. The stations common to each traverse and tie lines should be known and occupied while facing the same direction to avoid heading errors. The simplest method for using these tie lines is to make each intersection agree by linearly distributing the error on each traverse line and holding the tie line values fixed—provided the tie line data were acquired rapidly.

A local recording base station, i.e., diurnal station monitor, is the most ideal method and certainly the most accurate for removing time variations. The time variations can readily be removed from each reading, again assuming that the time is noted for each reading on the traverse to within a minute or so of the base station. The base station should not be further away than 100 miles from the area of the survey for agreement within a few gammas and should be positioned more than 200 feet away from local traffic and other disturbances (see Chapter VII). The diurnal base station, if left to continue recording during each evening, can indicate magnetic storms in progress and may be examined at the start of a survey day to determine if any useful measurements can actually be obtained during such conditions. During a magnetic storm, it is best not to obtain field data with the objective of removing the storm variations as the survey magnetometer and base station may not agree better than 5 or 10 gammas.

High Magnetic Gradients

In the case where an extremely high magnetic gradient destroys the signal as evidenced by successive non-repeating measurements, it may be necessary to raise the sensor up to 10 or 12, sometimes 15 feet in order to move the sensor to a region of lower gradient. This will only happen over outcropping or nearly outcropping large masses of perhaps altered ultrabasic rocks, magnetic iron ore deposits or ore bodies containing a large percent of pyrrhotite and in the near vicinity of buried iron objects in the applications for search. Such an event would only occur if the gradient exceeds several hundred gammas per foot. If the span of high gradient is not too wide, it may not actually be necessary to obtain measurements precisely at the highest gradient. Measurements on either side of the anomaly can be extrapolated or be used to at least indicate the contacts of such a highly magnetized formation. Furthermore, as the signal disappears and the readings diverge considerably from ± 1 or 2 counts, it may be worthwhile to note approximate indications of magnetic field gradient which on some instruments is displayed on the front panel as signal amplitude (which is a function of gradient). In areas of highly magnetic surface conditions, as noted in a previous section but where a signal is still obtained, another alternative in acquiring meaningful data other than that of using an extended staff would be to make 2 to 5 measurements per station, for example, at the points of a cross centered at the actual primary station location. The average of these readings would later be used to draw a profile. In this way, some of the surface noise is averaged out.

In the absence of anomalous surface conditions and for reasons more fully described in Chapter VIII, it may be useful for both geological and search applications to measure the vertical gradient of the total field. The vertical gradient is obtained by making 2 total field measurements, one over another, taking the difference in the readings and dividing by the distance between them.

Data Reduction

The profiles when plotted should be smoothly varying and expressive of the anomalies of interest. (NOTE: The nature of the disturbances or anomalies of interest, their width, character, signature, and amplitude are discussed in Chapter V, following.) Should there be an excessive amount of such geologic/magnetic noise, at a wavelength much shorter or much longer than is of interest, it is possible to apply simple filtering or smoothing techniques to facilitate interpretation of the profile. As a rule of thumb, *never remove or filter out anomalies whose wavelength is on the order of the depth to sources of interest.* A number of advanced techniques for data enhancement or filtering as employed in airborne surveys or well-gridded ground surveys will not be discussed within the scope of the Manual but are listed to acknowledge their existence: vertical derivatives, upward and downward continuation, reduction-to-the-pole, bandpass filtering, trend surface filtering, spectral analysis, trend enhancement, magnetization filtering, and others most of which are applied to two-dimensional data.

Profile Smoothing

Anomalies of very short wavelength (much shorter than the probable depths to sources of interest) may be present and caused by the magnetic effects of the magnetometer operator, or simply by surface magnetization contrasts in the surface or near-surface materials as mentioned earlier. In removing such effects, the eye itself tends to enhance what one is seeking. Another simple and obvious method is of course to pencil or trace through the noise. A more objective technique is to apply a running average or weighted running average to the data (see Figures 9 and 10). For a 3-point weighted

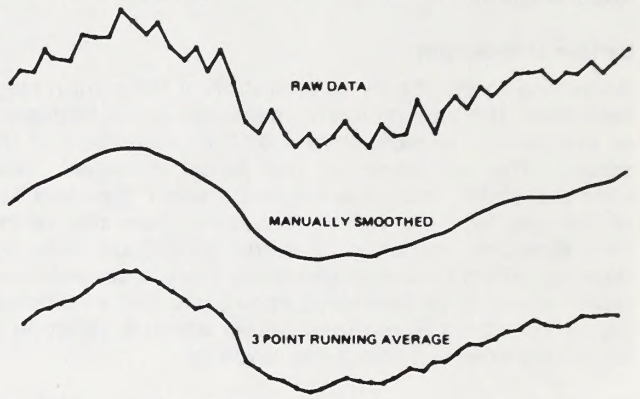

Figure 9. Profile Smoothing

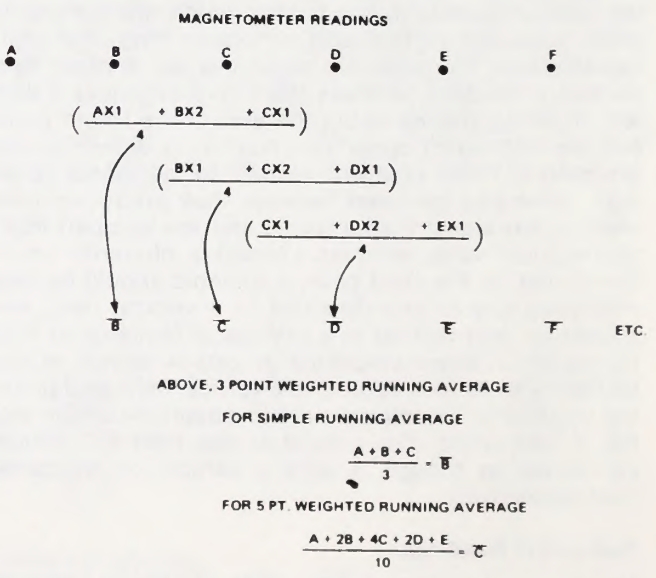

Figure 10. Running Averages

running average, for example, one would multiply the value at a given station by 2, add the values of the two adjacent stations, divide the sum by 4. This value is then set aside for that station for later recompilation of a new profile while advancing to the next station to perform the same procedure *(see Figure 10)*. A 5-point running average might utilize a weighting factor of 4 for the central point, 2 for each adjacent point, and 1 for the outside points while dividing by 10 to obtain the averaged value. More sophisticated techniques are also possible such as polynomial curve fitting, least squares, digital bandpass filtering, etc. The number of points or interval over which the averaging or filtering is to be performed for removal of such 'noise' should be much shorter (perhaps $\frac{1}{5}$ to $\frac{1}{10}$) than the anomalies of interest.

Removal of Regional Gradients

In most cases, the anomalies of interest usually appear superimposed on a much broader anomaly which is not of interest. This broader anomaly, or regional gradient, due to the main earth's field or very deep or distant sources, may appear simply as a component of slope in the curve and although it is subjectively determined, is often removed from the data in order to better examine the anomaly. This gradient is removed from a single profile as shown by *Figure 11* by drawing a straight line or broadly-curved line through the non-anomalous portions of the curve. The values are then subtracted at each station and replotted to present the 'residual' values, hopefully expressing only the anomalies of interest which in this case would be the anomalies occurring at the shallower depths. The vertical gradient, measured according to the methods prescribed in Chapter VIII, also serves to remove or largely reduce the regional gradient.

Contour Maps

Most survey traverses are not sufficiently close nor well-arranged in plan to allow the compilation of a contour map. Such is usually the case when only mineral exploration data are desired, in broad reconnaissance surveys, or when surveying in extremely rugged terrain where large areas are otherwise inaccessible. Profiles are, in fact, usually adequate particularly for anomaly sources with very long, horizontal dimensions. Contour maps are nevertheless useful in cases where little is known of the geology or magnetic sources, where the anomaly sources are either small or extremely large, or for ascertaining, on a more objective basis, the distribution of the anomalous masses or very subtle longer wavelength features. Many surveys for search also require broad coverage and perhaps contour map presentation. An alternative to the construction of contour maps for broad two-dimensional coverage is the presentation of 'offset profiles' or profiles plotted on abscissae which also serve to show the location of the traverse lines drawn on a map.

Constructing a contour map requires that large effects from diurnal variations or the heading effects, if any, be removed; that is, that there be a single datum level for all traverses or readings. The process of removing the regional gradients, as described above, frequently serves to remove these other sources of errors as well and is satisfactory as long as one is not interested in the longer wavelength anomalies removed as part of the gradient.

The following guide should be useful to one not familiar with the techniques of constructing a magnetic contour map, or plan view of the anomalous total intensity. A contour or iso-intensity map is analogous to a topographic map and is a map on which are drawn lines (contours) of equal intensity, at convenient and regular intensity intervals, as would be observed were a magnetometer used to occupy every point on the surface of the ground. The contoured values are at best extrapolations and interpolations across areas where measurements are not actually taken. Such a map is drawn with the knowledge that the magnetic field is smoothly

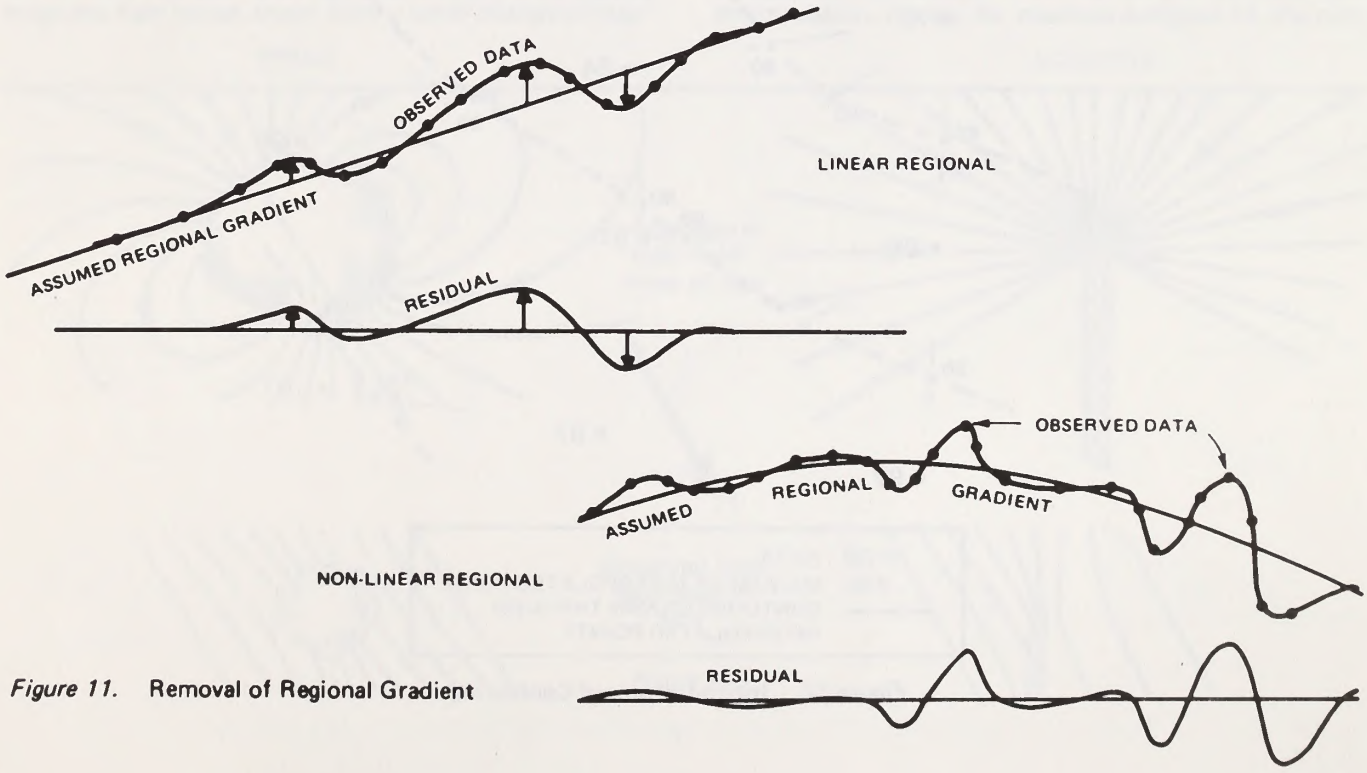

Figure 11. Removal of Regional Gradient

varying and on the assumption that one is interested only in broad features expressed by such a map. Features much smaller than the spacing between adjacent traverses should be examined on a profile basis only and should not be sought nor included on a map presentation.

Construction of a Contour Map

Given a set of readings obtained on a traverse, the time variations, if significant, should be removed, perhaps the regional gradient removed and the profiles smoothed. Values are then selected from these smoothed profiles at widely-spaced intervals not less than, say, ½ or ¼ the spacing between adjacent traverses or at similarly spaced but significant points on the profile, namely, maxima, minima, inflection points, etc. In other words, the values to be contoured should be more-or-less equally distributed in plan view. Anomalous features which 'obviously' extend across several traverses might be included also. The total intensity values thus selected and representative of the principal features are posted at their proper locations on a base map made of material which will support numerous erasing of penciled lines and including references to location.

Examine the dynamic range of the values and select 5 or 10 intensity levels through this range at convenient values such as every 20, 100, or 1000 gammas. Draw these contours according to the instructions below and then fill in the intermediate contour lines, i.e., every 10, 50, or 500 gamma contours, depending upon which coarse valuse above were originally selected, until contours appear in all segments of the map. Magnetic intensity values and contours should, in theory, be smoothly varying and should thus be smoothed at the later stages of contouring by removing sharp bends or corners. After such smoothing, other contour lines as needed to cover the map adequately are carefully drawn between the fair-drawn contours and appropriate labels applied. In areas of steep gradients, only a few coarse contour lines are drawn to avoid numerous and insignificant fine details. Since closed contours (closures) appear the same for maxima and minima, they are differentiated by applying hashure marks or other indications on the inside of the minima.

The position of the various contours is selected by manually (eye and mental calculation or by using proportional dividers, although not really necessary) interpolating linearly between all the neighboring values as shown in *Figure 12*. In this case, it was decided to draw contours at 10 gamma intervals. The contour line near data point value 91 would subsequently be smoothed to pass through this data point following the guidelines given above.

Contour lines should never cross nor pass between pairs of data points which are both higher or both lower than the value of the contour. Also in some regions of zero or near zero gradient such as at a saddle point (region between two adjacent maxima or minima), there exists an ambiguity in the direction of the lines. However, it does not matter under such conditions which of the two possible sets of contours are drawn.

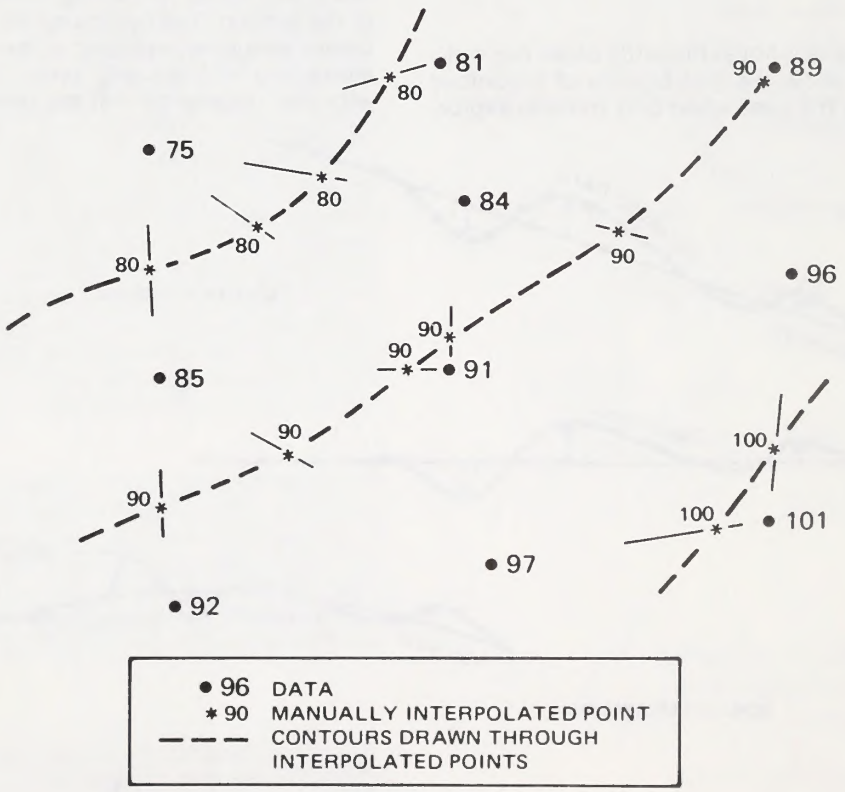

Figure 12. Interpolation and Contouring

V.

INTERPRETATION

Introduction

Total magnetic intensity disturbances or anomalies are highly variable in shape and amplitude; they are almost always asymmetrical, sometimes appear complex even from simple sources, and usually portray the combined magnetic effects of several sources. Furthermore, there are an infinite number of possible sources which can produce a given anomaly. The apparent complexity of such anomalies is a consequence of the net effect of several independent but relatively simple functions of magnetic dipole behavior. With an understanding of these individually simple functions however, and given some reasonable assumptions regarding the geology, buried object or whatever other source one is seeking to understand, a qualitative but satisfactory interpretation can usually be obtained for most anomaly sources.

The interpretation, explanation and guide presented here is directed primarily towards a qualitative interpretation for both geological reasons as well as search applications, i.e., an understanding of what causes the anomaly, its approximate depth, configuration, perhaps magnetite content or mass, and other related factors. But even if qualitative information is derived from the data, it is important to have applied a reasonable amount of care in obtaining precise measurements. Quantitative interpretations are possible, but are applied more to airborne data, entail relatively complex methods for depth determination, and are the basis for a relatively large body of literature on the subject, references to which are given in the Manual.

An anomaly represents a local disturbance in the earth's magnetic field which *arises from a local change in magnetization, or magnetization contrast* as it is termed. A profile, for example over a very broad uniformly magnetic surface, although magnetic itself, will not exhibit a magnetic anomaly as there is no local change in magnetization. A local increase or even decrease on the other hand would constitute such a change and produce a locally positive or negative anomaly.

The observed anomaly expresses only the net effect of the induced and remanent magnetizations which usually have different directions and intensities of magnetization. Since the remanent magnetization is so variable and measurements of its properties seldom made, *anomalies are all interpreted* in practice as though *induced magnetization were the total source of the anomalous effects.*

Asymmetry

The asymmetrical nature of total field anomalies is primarily a consequence of the directions of the field lines of the locally created magnet or source and the earth's-field-component nature of a total field magnetometer in the usually-inclined direction of the earth's magnetic field. Recall that a total field magnetometer measures only the component of any local perturbation which is in the direction of the earth's magnetic field at that point. Anomalies in the earth's field, whether created by induced or permanent magnetization, exist as arrangements of magnetic dipoles, monopoles (effectively), lines of dipoles and monopoles and sheet-like distributions of such poles. It is important therefore to understand the nature of the dipole or monopole field as it will be shown that a summation of such elementary forms will explain the most complex characteristics of anomalies and facilitate their interpretation. Notice, for example in *Figure 13,* the con-

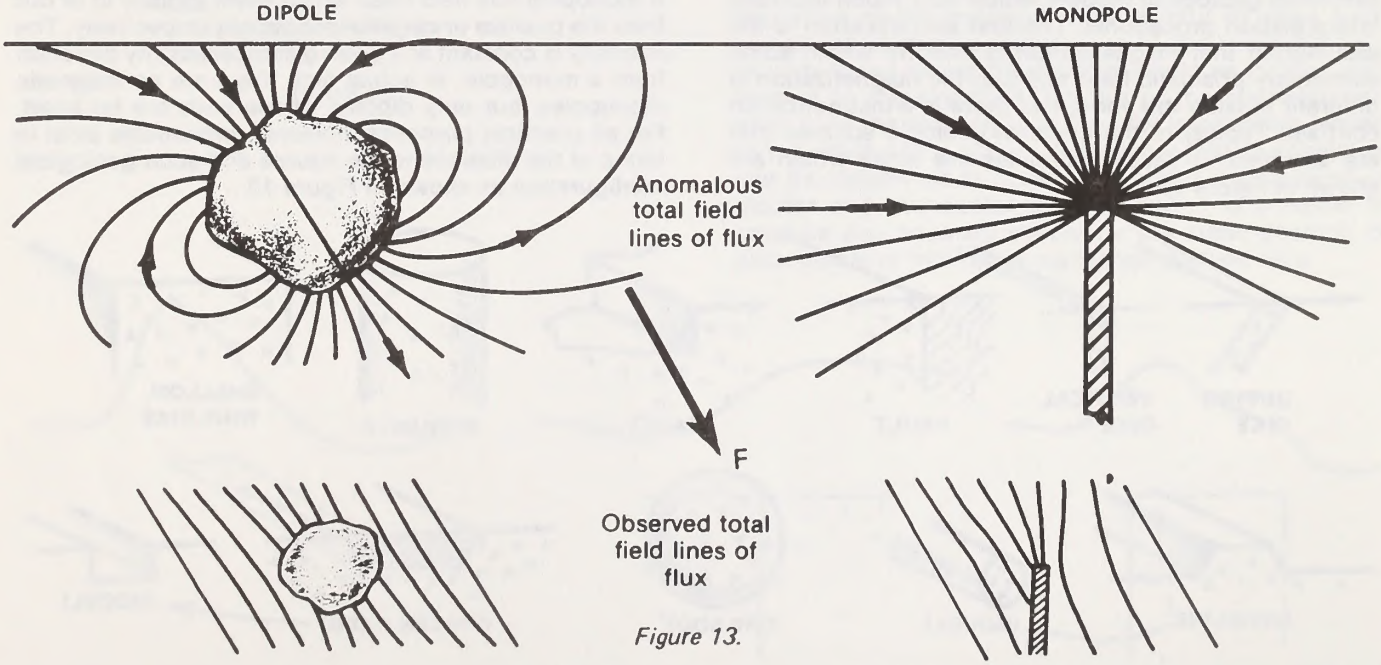

Figure 13.

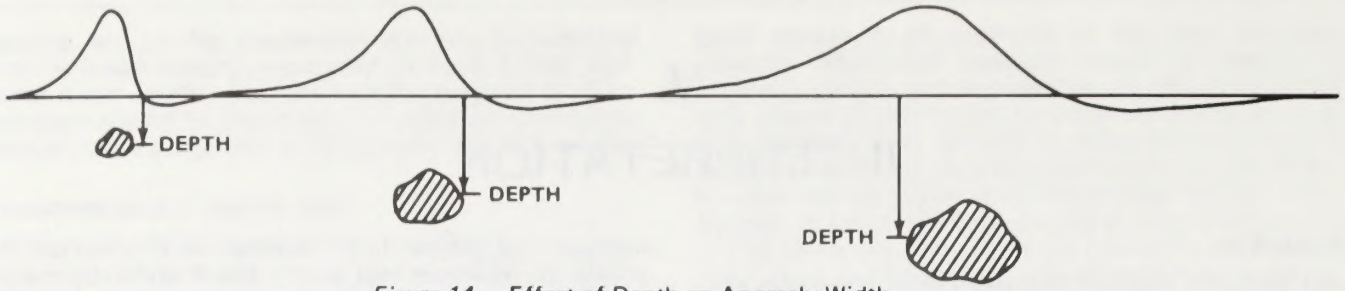

Figure 14. Effect of Depth on Anomaly Width

figuration for such fields as they would appear if one were to measure the direction of the anomalous field.

Depth Dependence

Another significant characteristic of a magnetic anomaly is its variation with the depth between the magnetometer and source, the deeper the source, the broader the anomaly as expressed in *Figure 14*. It is this property which enables one to determine the approximate depth to the source independent of any other information concerning the source. *If one familiarizes himself with only one subject in this discussion on interpretation, it should be the general characteristics of anomaly wavelength, or width, as a function of depth.* A knowledge of this subject allows rapid and easy interpretation of anomalies of interest when numerous anomalies arising from various depths appear in the observed total intensity profile.

Other Anomaly Shape Factors

Other factors which affect the anomaly shape and amplitude are the relative amounts of permanent and induced magnetization, the direction of the former, and the amount of magnetite present in the source compared to the adjacent rocks. The actual configuration of the source, that is, whether it is narrow, broad or long in one dimension and its direction in the earth's field, also control the anomaly signature.

Geological Models

Geological anomalies are interpreted in terms of much simplified geological models which very much facilitate interpretation procedures. The first simplification is the assumption that magnetization is uniform within some elementary prismatic form and that the magnetization is different outside this form, i.e., there is a magnetization contrast. Typical of the kinds of geologic sources that are assumed to cause anomalies are those which are shown in *Figure 15*.

As was stated, in any potential field method the given magnetic signature can be produced by an infinite combination of sources so that there is no unique interpretation. For example, the same anomaly could be produced by the peculiar distribution of magnetite (unrealistic geologically), and a uniform distribution of magnetite within the prismatic form (realistic), both of which are shown in *Figure 16*. It must be emphasized that not only are simplifications required, but a reasonable geologic framework must be used as a guide when considering the various possible sources. A typical set of anomaly signatures of various sources might appear as in *Figure 17*.

Elementary Dipoles and Monopoles

Since anomalies are explained herein in term of various arrays of dipoles and monopoles, it is important to examine their geometry and intensity characteristics. A magnetic dipole produces a field with imaginary lines of flux. as shown in *Figure 18*. The intensity of the field, which is proportional to the density of the flux lines is drawn as lines of equal intensity to express this relationship. From *Figure 18*, notice that 1) the intensity of the dipole is twice as large off the ends of the dipole as it is at the same distance off the side of the dipole. This explains, for example, why the earth's magnetic field is approximately 30,000 gammas at the magnetic equator and 60,000 gammas at its poles; 2) the direction of the field off the side of the dipole is parallel to the dipole itself, but opposite in sense; 3) the direction of the tangent of the field lines of a dipole are parallel along any radial line from the dipole.

A monopole has field lines which point radially in or out from the positive or negative monopole respectively. The intensity is constant at a given distance and any direction from a monopole. In actual fact, there are no magnetic monopoles, but only dipoles whose ends are far apart. For all practical purposes, however, monopoles exist in terms of the distance to the source and such geological configuration as shown in *Figure 13*.

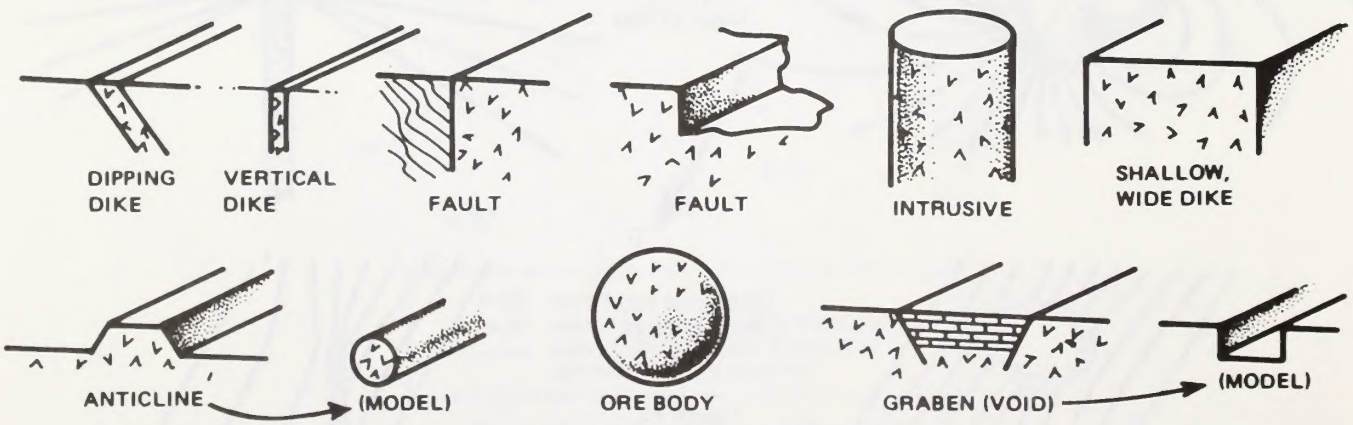

Figure 15. Geological Model Representations of Common Magnetic Anomaly Sources

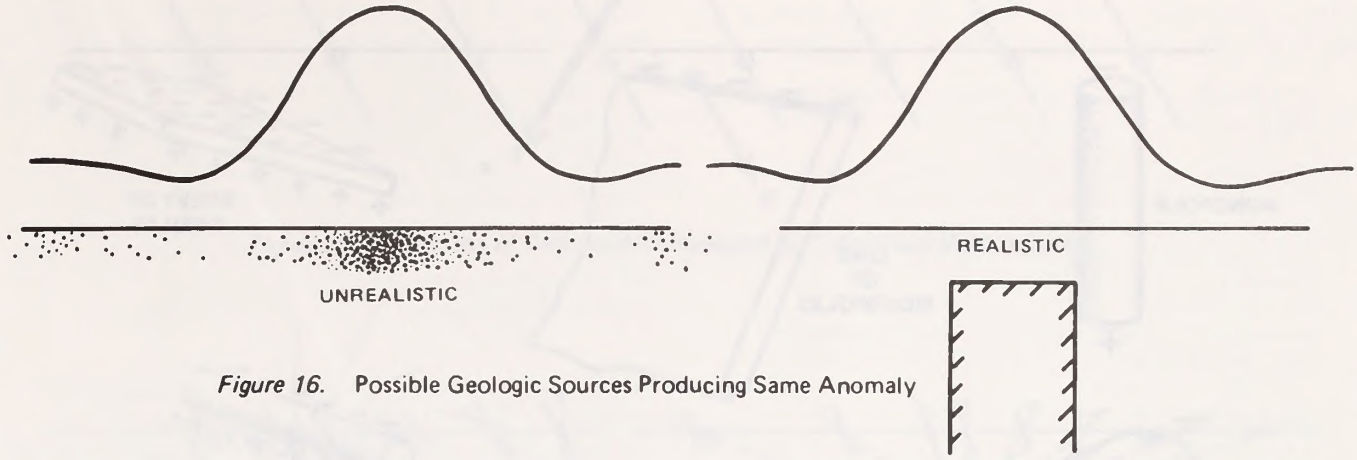

Figure 16. Possible Geologic Sources Producing Same Anomaly

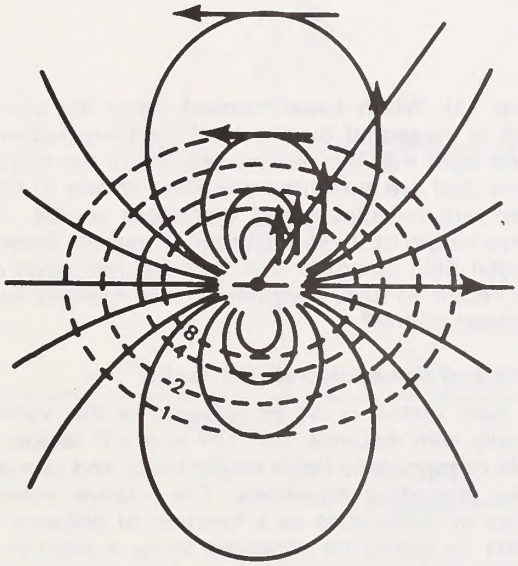

LINES OF FLUX (——)
AND
LINES OF EQUAL INTENSITY (— —)
FOR A DIPOLE

Figure 18.

Having outlined the qualitative geometry of the intensity T from a dipole, the quantitative aspects can be considered as follows:

The intensity, T, from a dipole can be expressed as

$T = \frac{2M}{r^3}$ along the axis, i.e., off the end of the dipole,

and $T = \frac{M}{r^3}$ along a line at right angles to the dipole,i.e., off the side of the dipole,

and for a monopole

$T = \frac{M}{r^2}$ in any direction from a monopole, where

M = magnetic moment and r is the distance to the pole. A more detailed mathematical formulation for the intensity due to a dipole is given subsequently in this Chapter.

Simplified Method for Total Field Signature

From the above description of a dipole and monopole and with the knowledge of the earth's-field-component-nature of the total field magnetometer, it is possible to sketch the signature of an anomaly for any given orientation of the dipole (orientation caused by field direction, the direction of remanent magnetization, or by the configuration of the geology). It is helpful to draw such signatures at various inclinations of the magnetic field to understand where the sources would be located with respect to the signature, the dip of the magnetization producing the anomaly, and even for information related to the depth of the source. Remember that all anomalies can be considered as caused by various distributions of dipolar and monopolar sources and it is possible to produce any anomaly simply by the super-position of such dipole or monopole signatures derived here.

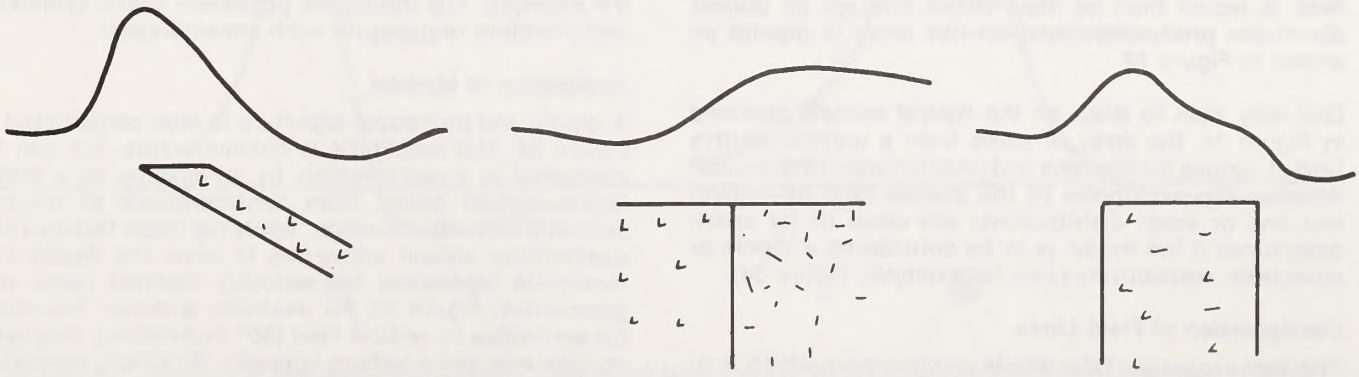

Figure 17. Typical Anomalies for Simple Geologic Models

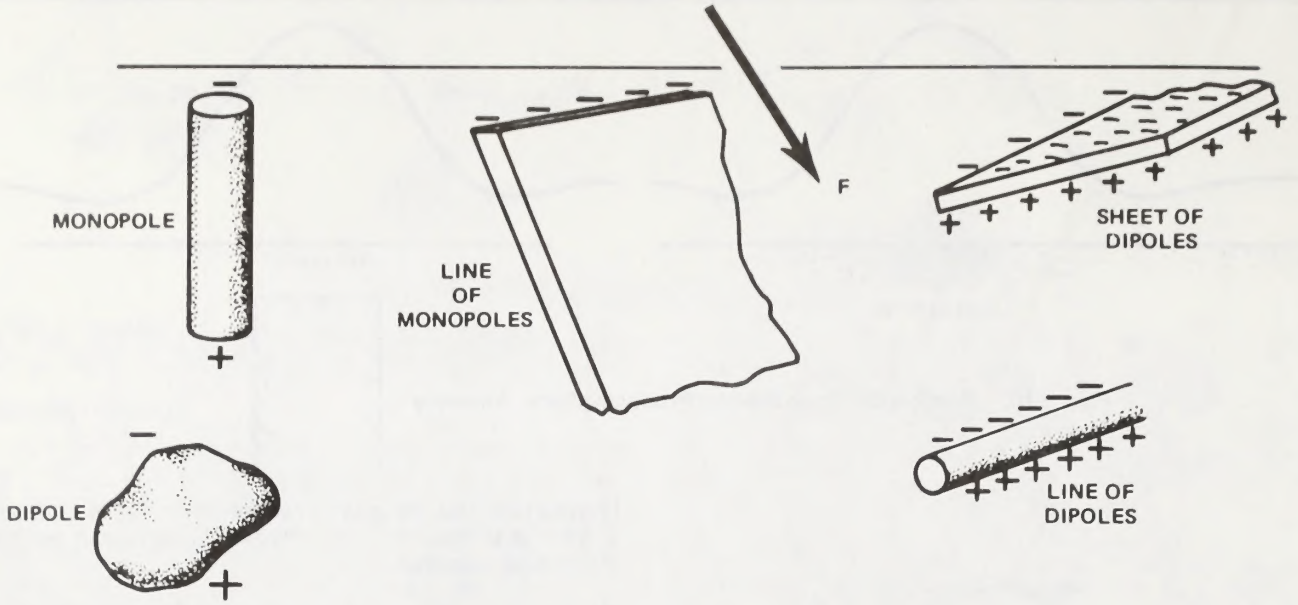

Figure 19.

Earth's Field Component Behavior

This method of predicting or drawing the anomaly signature depends upon one property of the field, namely, inclination, and three properties peculiar to the dipole or monopole source, whichever is assumed. The dip of the earth's field is first considered because this is the direction, the only direction, of the components of any local magnetic anomalies which are measured by a total field magnetometer. (If one is using a vertical component magnetometer, this guide still applies except that instead of using the earth's field as the direction of measurement, simply use the vertical.) In other words, the magnetometer will only measure the component of a local perturbation in this direction, i.e., as projected into this direction. See *Figure 20.*

Dipoles vs. Monopoles vs. Arrays of Poles

The decision to use dipoles, monopoles, or other configurations as the model is based upon the manner in which the earth's field induces a local field and this in turn depends upon the configuration of the geologic body which exhibits the magnetization contrast and the direction of the field. For example, a long body which nearly parallels the earth's field will tend to be magnetized along its long dimension. Furthermore, if the body is sufficiently long with one end near the magnetometer, the anomaly will appear as a monopole seeing only the upper pole with the lower pole removed effectively to infinity. If the same long, thin body were normal to the field, it would then be magnetized through its thinest dimension producing the sheet-like array of dipoles as shown in *Figure 19.*

One may wish to draw on the typical models depicted in *Figure 15,* the array of poles from a uniform earth's field at various inclinations and orientations of the source. Whether the monopoles or the dipoles (and its equivalent line or sheet distributions) are close or far apart, determines if the model is to be considered a dipole or monopole, respectively *(see, for example, Figure 34).*

Configuration of Field Lines

The first property of the dipole or monopole which is to be considered is the configuration of the field lines *(see Figure 13).* When superimposed upon the component which is measured by the total field magnetometer, it can be seen that the relative lengths of the disturbance vectors that are measured are those shown in *Figure 21* for an induced dipole and monopole source. It is the relative length of these disturbance vectors drawn along the total field direction that is measured, each disturbance vector, in turn, weighted by the intensity functions described below.

Dipole and Monopole Fall-Off Factor

The next factor to be considered is the variation of intensity with distance, i.e., $1/r^3$ and $1/r^2$ factors for the dipole or monopole fields respectively and as expressed in the preceding equations. The relative intensity for dipoles or monopoles as a function of distance to their centers as would be observed along a traverse is presented in *Figure 22* and described mathematically under "Anomaly Amplitude" below. This factor multiplies the length of net vectors in *Figure 21.*

Dipole Factor-of-Two

The last consideration really only applies to the dipole and that is a factor of 2 when one is off the end of the dipole compared to a position off the side. In other words, at a given distance, the intensity varies by a factor of 2 as a function of the angle between the radial line to the dipole and the dipole axis. This function is shown approximately in *Figure 23* for the dipole used in the example. The monopole possesses radial symmetry and therefore requires no such consideration.

Application of Method

A dipole and monopole signature is thus constructed in *Figure 24.* The amplitude is dimensionless, but can be compared to a real anomaly by multiplying by a single factor derived below from considerations of volume, susceptibility, etc. However, applying these factors even qualitatively should allow one to draw the dipole and monopole signatures for variously inclined fields and geometries. *Figure 25,* for example, is drawn free-hand for anomalies in vertical field (90° inclination), magnetic equator and mid-southern latitudes. By simply sketching in the earth's field direction and the dipole's field lines

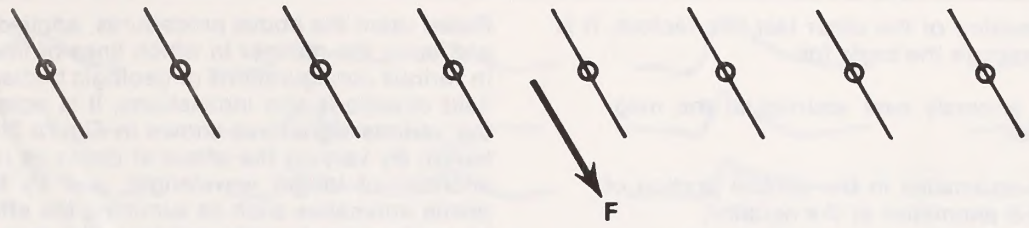

Figure 20. Direction of Components Measured by Total Field Magnetometer

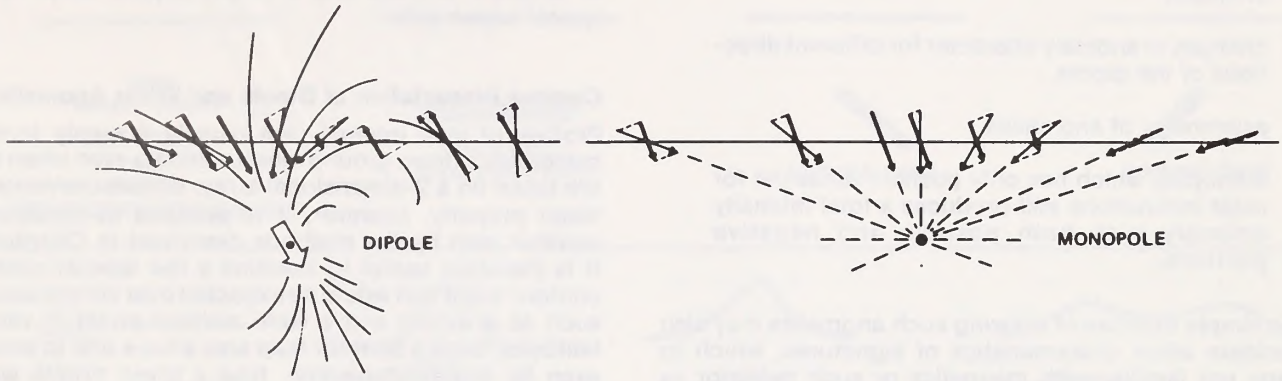

Figure 21. Total Field Components of Tangent to Field Lines of Dipole and Monopole

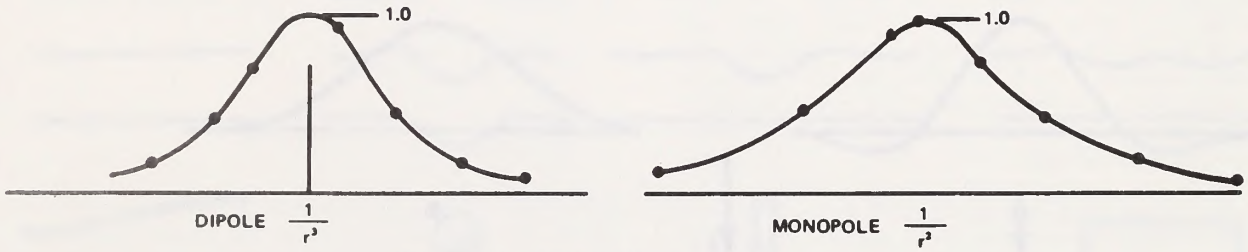

Figure 22. Fall-off Rate
(Relative intensity or length of vectors in Figure 21)

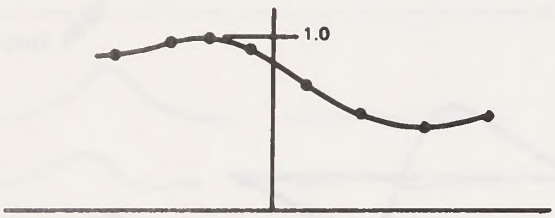

Figure 23. Aspect Factor
(Relative Intensity of Dipole of Figure 21 with Respect to Angle from Axis at Various Points Along Profile)

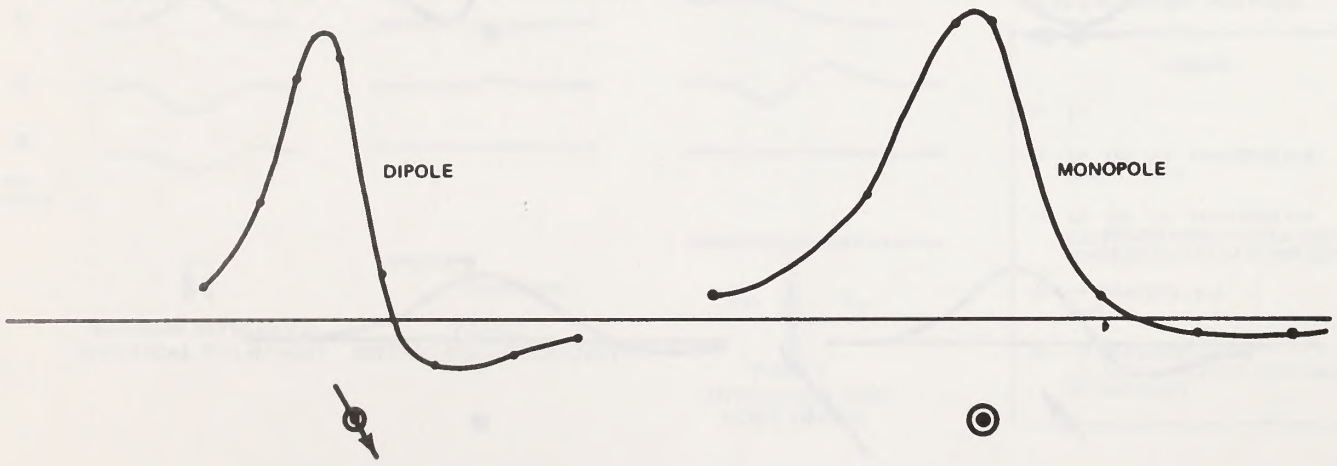

Figure 24. Dipole and Monopole Signatures (Constructed from Figures 20-23 according to methods described in text.)

without consideration of the other last two factors, it is possible to appreciate the basis for:

a negative anomaly over sources at the magnetic equator,

absence of anomalies in the central portion of elongate N-S anomalies at the equator,

both positive and negative fields for almost any anomaly,

changes in anomaly character for different directions of the dipole,

asymmetry of anomalies,

monopole which has only positive sense yet for most inclinations still produces a total intensity anomaly with both positive and negative portions.

The simple exercise of drawing such anomalies may also elucidate other characteristics of signatures, which to many not familiar with magnetics or such behavior as shown here, appear to be complex and difficult to comprehend.

Based upon the above procedures, applied qualitatively, and upon the manner in which lines of flux are induced in various configurations of geologic bodies and ambient field directions and inclinations, it is possible to derive the various signatures shown in *Figure 26* (drawn freehand). By varying the effect of depth as it produces an anomaly of longer wavelength, and by building composite anomalies such as summing the effect of 2 faults to create a single wide, shallow dike, it is also possible to generate a composite curve demonstrating the effect of different sources and different depths which is the typical observation.

Contour Presentation of Dipole and Prism Anomalies

Profiles of total intensity are usually the only form of presentation from ground measurements even when data are taken on a 2-dimensional array. If measurements are taken properly, however, it is possible to construct a contour map by the methods described in Chapter IV. It is therefore useful to examine a few special cases of contour maps that would be expected over simple sources such as a dipole and a wide, vertical prism in various latitudes. Such a contour map also allows one to extract, even by simple inspection, how a given profile would appear at various positions over such simple-shaped forms which is useful information both in search and in

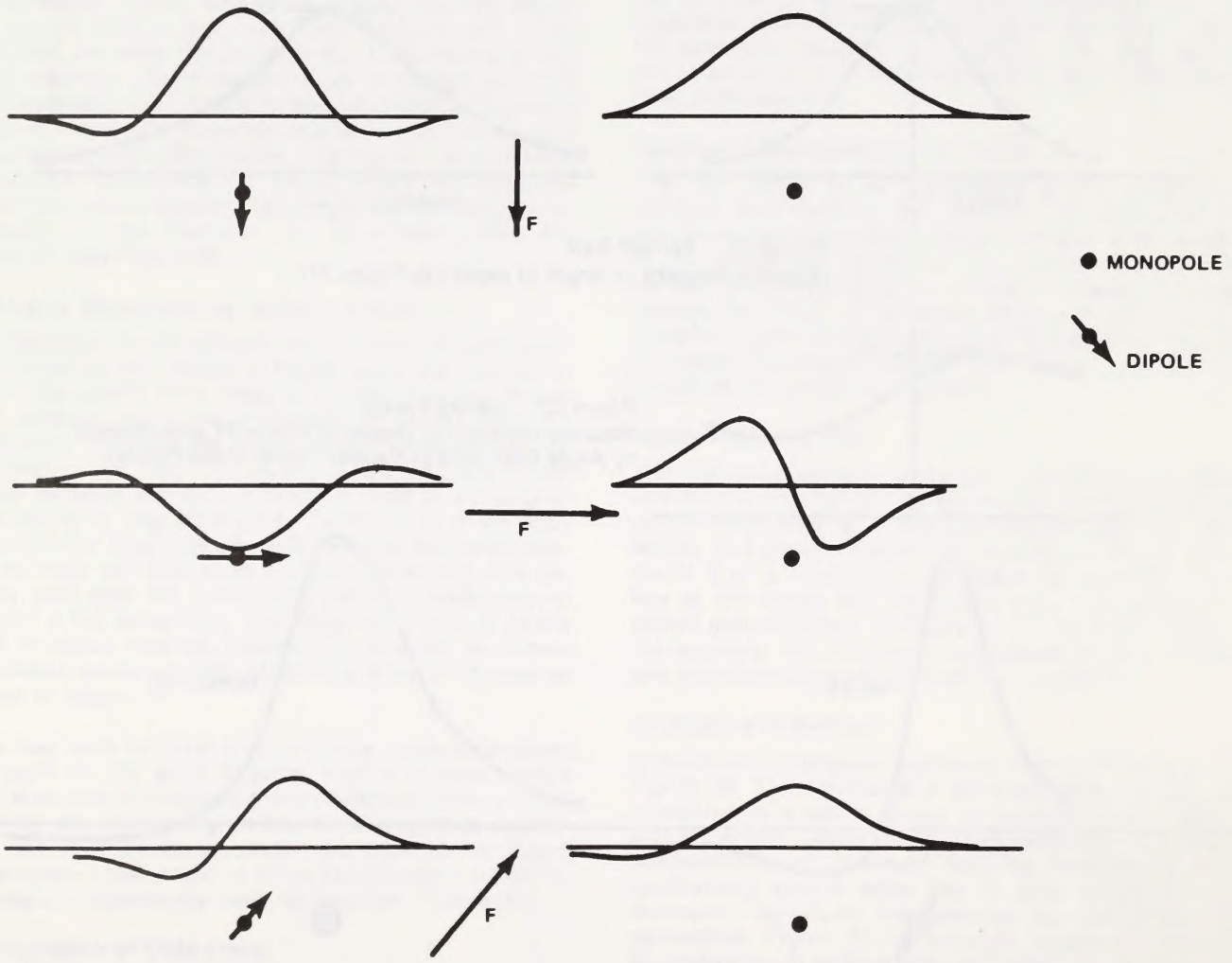

Figure 25. Free Hand Sketch of Dipole and Monopole for Various Inclinations

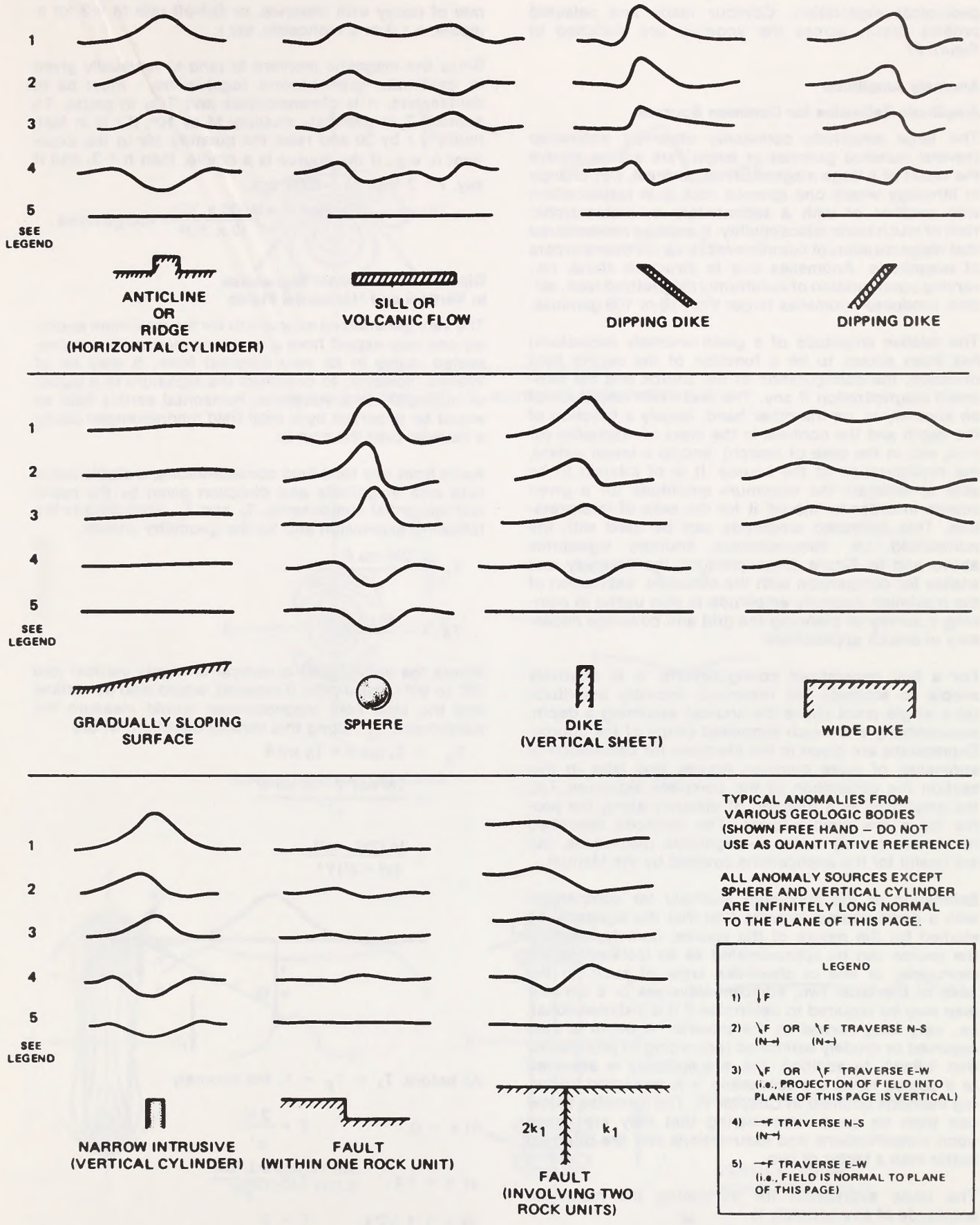

Figure 26. Anomalies for Geologic Bodies at Various Orientations and Different Inclinations of the Field

geological exploration. Contour maps and selected profiles drawn across the anomaly are sketched in *Figure 27*.

Anomaly Amplitude

Amplitude Estimates for Common Sources

The large amplitude commonly observed anomalies (several hundred gammas or larger) are almost always the result of a large magnetization contrast, i.e., change in lithology where one igneous rock is in juxtaposition with another or with a sedimentary or metamorphic rock of much lower susceptibility. It must be remembered that magnetization of common rocks varies over 6 orders of magnitude. Anomalies due to structure alone, i.e., varying configuration of a uniformly magnetized rock, seldom produces anomalies larger than 10 or 100 gammas.

The relative amplitude of a given anomaly (signature) has been shown to be a function of the earth's field direction, the configuration of the source and the remanent magnetization if any. The *maximum* amplitude of an anomaly is, on the other hand, largely a function of the depth and the contrast in the mass of magnetite (or iron, etc. in the case of search), and to a lesser extent, the configuration of the source. It is of interest to be able to estimate the maximum amplitude for a given source in order to 'model' it for the sake of interpretation. This estimated amplitude can be used with the normalized, i.e., dimensionless, anomaly signatures above and in *Figure 26* to produce the anomaly one wishes for comparison with the observed. Estimation of the maximum anomaly amplitude is also useful in planning a survey or planning the grid and coverage necessary in search applications.

For a few generalized configurations, it is relatively simple to estimate the maximum anomaly amplitude (at a single point above the source) assuming a depth, susceptibility and much simplified shape of the source. Expressions are given in the literature for calculation of anomalies of more complex figures and later in this section the calculation of the complete signature, i.e., the amplitude as a function of distance along the profile for a few simple forms. The methods described herein are merely order-of-magnitude techniques, but are useful for the applications covered by the Manual.

Estimation of the maximum anomaly for comparison with a given source requires first that the signature be studied for the nature of the source; namely, whether the source can be approximated as an isolated dipole, monopole, or line or sheet-like array of such. In the case of the latter two, adjacent traverses or a contour map may be required to determine if it is 2-dimensional, i.e., very long normal to the traverse. A depth is then assumed or crudely estimated (according to procedures that follow). In addition, the susceptibility is assumed or if source rocks are accessible, it is measured following methods outlined in Chapter VI. The formulae below can then be used remembering that they are based upon simplifications and assumptions and are often no better than a factor of two.

The basic expression for estimating the maximum amplitude of any anomaly is

$$T = \frac{M}{r^n}$$

where T is the anomaly, M the magnetic moment, r the distance (depth) to the source, and n a measure of the rate of decay with distance, or fall-off rate (n = 3 for a dipole, n = 2 or a monopole, etc.).

Since the magnetic moment M (and k) is usually given in centimeter-gram-second (cgs) units, r must be in centimeters, n is dimensionless and T is in gauss. To express T in gammas, multiply M by 10^5; if r is in feet, multiply r by 30 and raise the quantity 30r to the exponent n, e.g., if the source is a dipole, then n = 3, and if say, r = 2 feet, M = 1000 cgs,

$$\text{then } T = \frac{1000 \times 10^5}{(2 \times 30)^3} = 460 \text{ gammas}.$$

Dipole and Monopole Signatures in Vertical and Horizontal Fields

The very generalized expression for the maximum anomaly one may expect from a dipole or monopole was presented above in its very simplest form. It may be of interest, however, to construct the signature of a dipole or monopole in a vertical or horizontal earth's field as would be observed by a total field magnetometer along a traverse over the source.

Apart from any total field considerations, a dipole has a field with magnitude and direction given by the radial and tangential components, T_r and T_θ, according to the following expression and for the geometry shown.

$$T_r = \frac{2M \cos\theta}{r^3}$$

$$T_\theta = -\frac{M \sin\theta}{r^3}$$

Where the earth's field is vertical or nearly vertical (dip 70° to 90°), the dipole, if induced, would also be vertical and the total field magnetometer would measure the component, T_z, along this vertical direction, where

$$T_z = T_r \cos\theta + T_\theta \sin\theta$$

$$= \frac{2M \cos^2\theta - M \sin^2\theta}{r^3}$$

$$= \frac{M(2z^2 - x^2)}{(x^2 + z^2)^{5/2}}$$

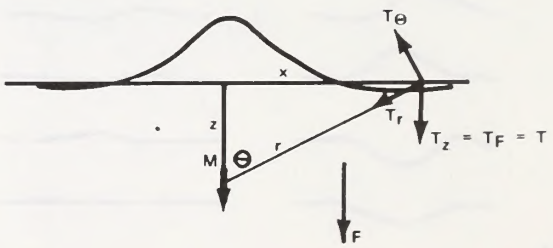

As before, $T_z = T_F = T$, the anomaly.

At x = 0, $T = \frac{2M}{z^3}$

at x = ± z, $T = \frac{0.175M}{z^3}$

at x = ± √2 z, $T = 0$

at x = ± 2z $T = \frac{-0.04M}{z^3}$

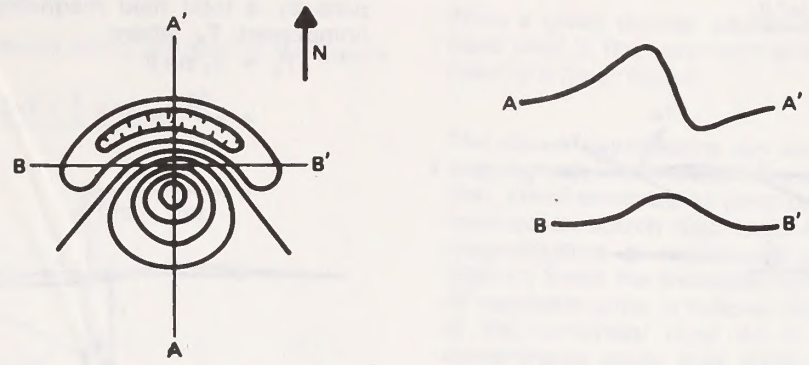

DIPOLE, INCLINATION OF F, 60°
(FOR INCLINATION –60°, I.E., SOUTHERN HEMISPHERE, N IS ↓)

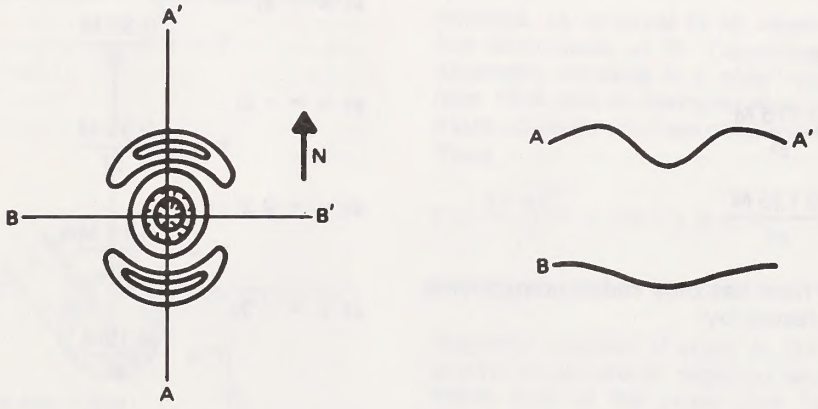

DIPOLE, HORIZONTAL FIELD

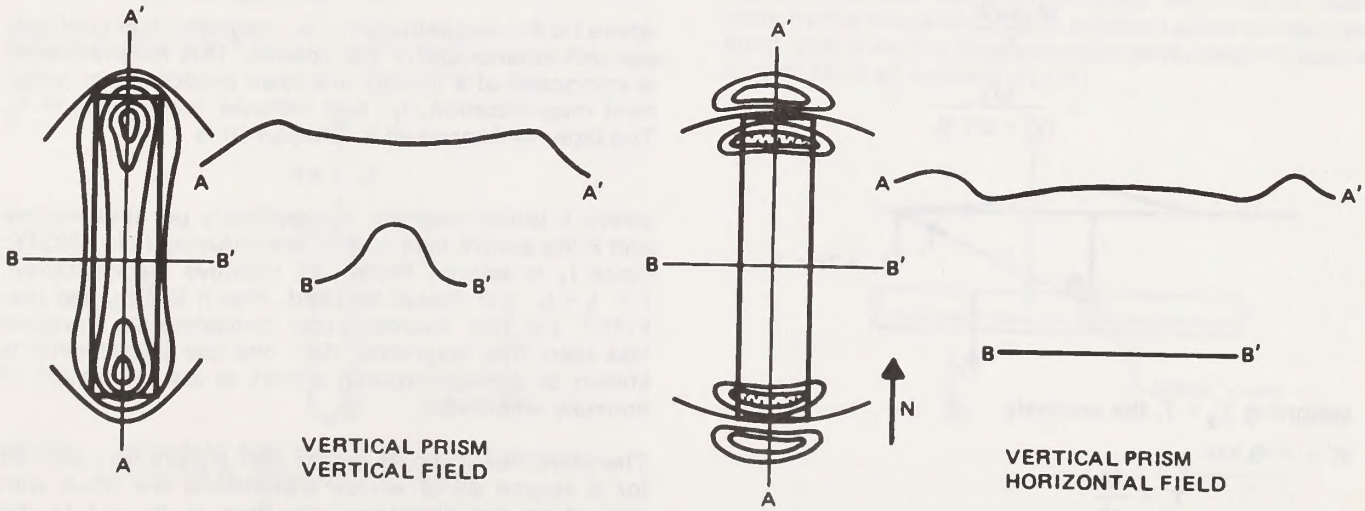

VERTICAL PRISM
VERTICAL FIELD

VERTICAL PRISM
HORIZONTAL FIELD

Figure 27. Contour Maps of Total Intensity

For magnetic equatorial fields, the induced anomaly is horizontal and the total field magnetometer would measure the components shown and expressed by

$$T_x = T_r \cos\theta + T_\theta \sin\theta$$

$$= \frac{2M\cos^2\theta - M\sin^2\theta}{r^3}$$

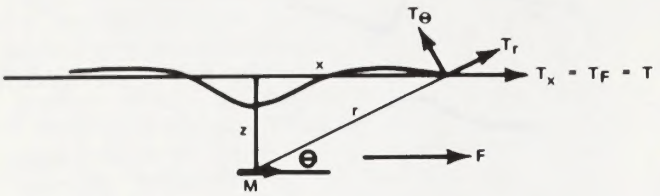

$$= \frac{M(2x^2 - z^2)}{(x^2 + z^2)^{5/2}}$$

as before, $T_x = T_F = T$ the total field anomaly, where,

at $x = 0$,

$$T = -\frac{M}{z^3}$$

at $x = \pm\frac{z}{\sqrt{2}}$,

$$T = 0$$

at $x = \pm z$,

$$T = \frac{0.175\,M}{z^3}$$

at $x = \pm 2z$,

$$T = \frac{0.125\,M}{z^3}$$

The monopole shown here has only radial components whose intensity is expressed by

$$T_r = \frac{M}{r^2}$$

The monopole anomaly in a vertical field as measured by a total field magnetometer would be the component in the z direction (vertical) or

$$T_z = T_r \cos\theta$$

$$= \frac{M\cos\theta}{r^2}$$

$$= \frac{Mz}{(x^2 + z^2)^{3/2}}$$

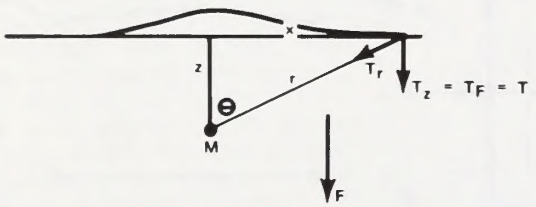

assigning $T_z = T$, the anomaly

at $x = 0$,

$$T = \frac{M}{z^2}$$

at $x = \pm z$,

$$T = \frac{0.35\,M}{z^2}$$

at $x = \pm 2z$,

$$T = \frac{0.09\,M}{z^2}$$

The monopole field in a horizontal field would be measured by a total field magnetometer as the horizontal component, T_x where

$$T_x = T_r \sin\theta$$

$$= -\frac{M}{r^2}\sin\theta$$

$$= -\frac{Mx}{(x^2 + z^2)^{3/2}}$$

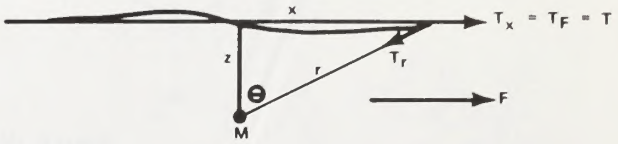

Again, $T_x = T_F = T$, the anomaly, where

at $x = 0$,

$$T = 0$$

at $x = z$,

$$T = -\frac{0.35\,M}{z^2}$$

at $x = -z$,

$$T = \frac{0.35\,M}{z^2}$$

at $x = 2z$,

$$T = -\frac{0.18\,M}{z^2}$$

at $x = -2z$,

$$T = \frac{0.18M}{z^2}$$

Maximum Amplitude Given Magnetization and Generalized Form

The magnetic moment M is more usefully expressed as

$$M = IV$$

where I is the magnetization (i.e., magnetization contrast) per unit volume and V the volume. This magnetization is composed of a usually unknown proportion of remanent magnetization, I_r, and induced magnetization I_i. The latter as expressed in Chapter III is

$$I_i = kF$$

where k is the magnetic susceptibility per unit volume and F the earth's field or ambient inducing field. (NOTE: Since I_r is seldom known, an effective magnetization, $I = I_i + I_r$, will always be used. Also it is assumed that $k < 10^{-2}$, i.e., the source under consideration contains less than 10% magnetite; then one can ignore what is known as demagnetization effects in the calculation of anomaly amplitude).

Therefore, for a dipole which can always be assumed for a source all of whose dimensions are small with respect to the distance (less than $\frac{1}{5}$ or $\frac{1}{10}$) to the magnetometer,

$$T = \frac{M}{r^3} = \frac{IV}{r^3} = \frac{kFV}{r^3}$$

If the source is approximately spherical, then

$$T = \frac{kF\left(\frac{4}{3}\pi R^3\right)}{r^3}$$

where R is the radius of the source as in *Figure 28*

If the measurement is made along the axis of the dipole (see *Figure 29*), then

$$T = \frac{2kF\left(\frac{4}{3}\pi R^3\right)}{r^3}$$

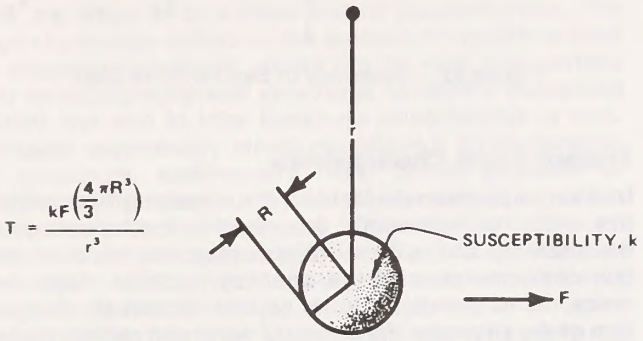

Figure 28. Anomaly of Sphere in Horizontal Field

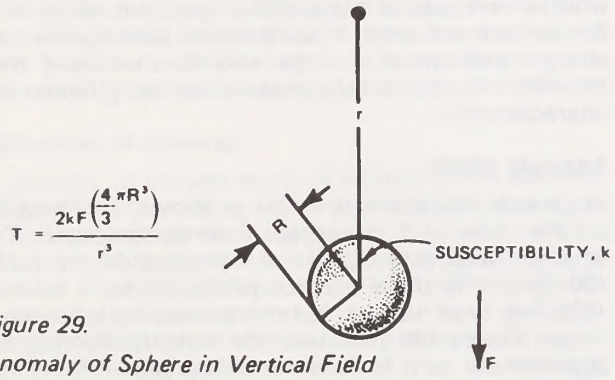

Figure 29.
Anomaly of Sphere in Vertical Field

As an example, consider an ore body 100 feet wide (R = 50), 500 feet deep comprised of 10% magnetite (k = 0.3), in a steeply dipping field (60° to 90° latitude) in a field of 60,000 gammas:

$$T = 2\,(0.10 \times 0.3) \times 6 \times 10^4 \left(\frac{4\pi}{3}\right)\left(\frac{50}{500}\right)^3 = 14.4 \text{ gammas}$$

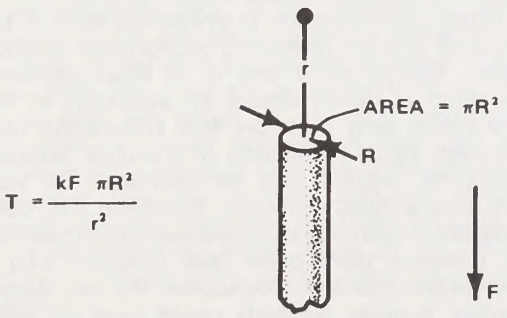

(NOTE: ALSO VALID FOR END OF N-S HORIZONTAL CYLINDER IN HORIZONTAL FIELD)

For the same ore body in an equatorial field where F = 30,000 gammas and the induced dipole is now observed at a point on a line normal to the axis (no factor of 2)

T = - 3.6 gammas

Thus a given dipolar source in an equatorial field will have only ¼ the maximum anomaly amplitude it would have in a polar region.

The above expressions are usually valid only for such sources as a small distant ore body (containing magnetite), small structure in deep basement, or most objects involved in search applications (see Chapter VII). The magnetization is expressed in gauss or gammas as desired. Since the anomalies are also expressed in terms of magnetic units, it follows that the units of dimension in the numerator must be of the same order as the denominator since they must cancel. Therefore, for a dipole whose anomaly varies as $\frac{1}{r^3}$ (said to have a fall-off of $\frac{1}{r^3}$), the volume, V, has dimensions of R^3. In the case of a monopole, which varies as $\frac{1}{r^2}$, the magnetic moment, M, is equal to IA where A is surface area and has dimensions of R^2. Consider for example, a vertical basement intrusive in a polar region with an upper surface 1000 feet in diameter at a depth of 5000 feet, with a susceptibility contrast of 10^{-2} in a field of 60,000 gammas. Thus,

$$T = \frac{kF\pi R^2}{r^2} = 10^{-2} \times 6 \times 10^4 \times \pi\left(\frac{50}{500}\right)^2 = 18 \text{ gammas.}$$

Horizontal prisms or cylinders also vary as $\frac{1}{r^2}$, with magnetic moment M equal to 2IA (IA for E-W horizontal prisms in equatorial regions) where A is the cross-sectional area of the prism *(see Figure 30)*. (NOTE: The long horizontal prism varies as $\frac{1}{R^2}$ not because it appears to be comprised of a monopole, but because it is a line of dipoles (in steeply dipping fields) and the effect of adjacent dipoles along an infinitely long line is 'seen' more by the magnetometer at a distant point of measurement than if all the magnetization were concentrated at a point as in an isolated dipole).

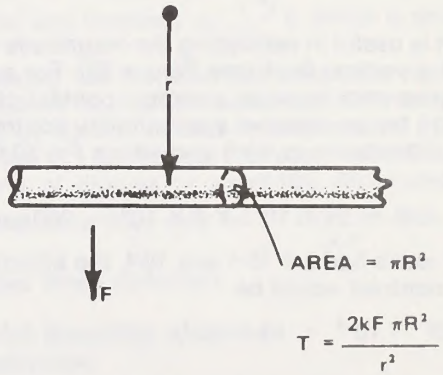

(NOTE: ALSO VALID FOR E-W HORIZONTAL CYLINDER IN HORIZONTAL FIELD)

Figure 30. Anomaly of Vertical and Horizontal Cylinders

A narrow, vertical dike in steep field or the edge of a horizontal sheet in a horizontal field can be considered as a line of monopoles varying as 1/r which is a lower rate of fall-off than a single monopole for the same reasons given above for a horizontal cylinder *(see Figure 31)*. The magnetic moment M = It where t = width of dike. Since the anomaly varies as 1/r, the dimensions of t are simply length. As an example, a vertical dike might be 100 feet wide, at a depth of 500 feet, with $k = 10^{-3}$ in a field of 50,000 gammas, or

$$T = \frac{kFt}{r} = \frac{10^{-1} \times 5 \times 10^{4} \times 10^{2}}{5 \times 10^{2}} = 10 \text{ gammas}$$

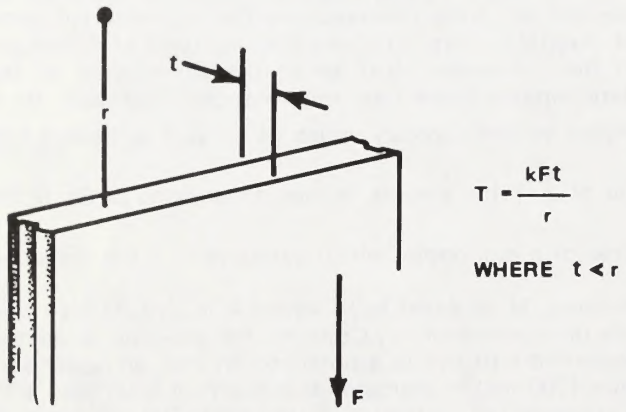

Figure 31. Anomaly of Narrow Vertical Dike

A common point of ambiguity arises with such simplified schemes as these in the case of a dike which is nearly as wide as it is deep. In this case, the anomaly is approximated as something between a line of monopoles as above and a sheet of monopoles as shown in the following. Moreover, as the dike is even wider than its depth, it can be approximated simply by 2 faulted contacts with 'no anomaly' in between.

For a semi-infinite slab of material such as a rock surface of great thickness and breadth in a non-horizontal field, the flux lines do not vary in direction or density above the slab, therefore the field does not vary at all with distance to its surface (similar to the limit of the spherical dipole above where R = r) so that

$$T = \frac{M}{r^{0}} = \frac{2\pi I}{1}, \text{ or } T = 2\pi kF$$

which is useful in estimating the magnitude of the anomaly at a vertical fault *(see Figure 32)*. For example, consider two rock types at a vertical contact of $k = 10^{-3}$ and $k = 10^{-5}$ for an effective susceptibility contrast of $k = 10^{-3}$ ($10^{-5} \approx 0$ relative to 10^{-3}) and where F = 50,000 gammas. Thus

$$T = 2\pi \times 10^{-3} \times 5 \times 10^{4} = 300 \text{ gammas}$$

If the rocks had $k = 10^{-4}$ and 10^{-3}, the effective susceptibility contrast would be

$$10^{-3} - 10^{-4} = 10 \times 10^{-4} - 10^{-4} = 9 \times 10^{-4} \text{ and}$$

$$T = 2\pi \times 9 \times 10^{-4} \times 5 \times 10^{4} = 270 \text{ gammas}$$

This simple example of two adjacent rock types is probably applicable in more instances in interpretation than any of the other geometries discussed above.

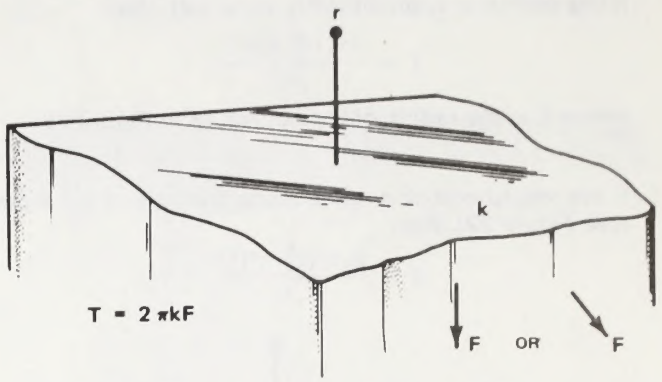

Figure 32. Anomaly of Semi-infinite Slab

Anomaly Depth Characteristics

In a very approximate fashion, the wavelength, or, effective width (or 'half-width' described in the following) of the anomaly and, with more accuracy, the width of certain characteristics of the anomaly such as slope, are measures of the depth to its source. However, recognition of the anomaly, the anomaly 'zero' and certain slopes would not only appear as different values as determined by different interpreters, but they also depend upon what is removed as the regional gradient. More objective criteria are used in some cases such as the nearly straight portions of a slope, and distances and angles between inflection points, peak values and other anomaly characteristics.

Anomaly Width

In general, the anomaly width as shown in *Figure 33* is on the order of 1 to perhaps 3 times the depth. Thus, when an anomaly appears to have a width as such of 100 feet, it is definitely not produced by a source at 1000 feet or at 10 feet, but more likely by a source between 30 and 100 feet deep (or distant). Such criteria, approximate as it is, is nevertheless useful for cursory interpretation of profiles and maps.

Anomaly Depth Estimation

Much is written on the variety and relative merit of methods for estimating the depth to the source of anomalies. Since the magnetometer is primarily a tool for subsurface mapping and detection, it follows that determination of the depth as well as edges of bodies is important in its application to geological exploration and search. The basis for depth determination is presented here in brief which, together with the foregoing background on anomaly behavior, should allow one to at least appreciate how a variation in depth affects an anomaly. In most cases, one needs only to apply this knowledge qualitatively through visual inspection of a profile. Whatever the requirement, depths may be estimated by visual inspection, several rules of thumb, modeling (i.e., calculation of assumed source and comparison with observed), measured gradient techniques (see Chapter VIII), or various computer-oriented procedures. As was demonstrated earlier, a given anomaly could have an infinite number of possible sources and source depths, but the realistic models that are assumed usually produce maximum depth estimates.

Knowledge of the depth of a particular formation or source may have considerable geological significance as it determines the nature or configuration of a forma-

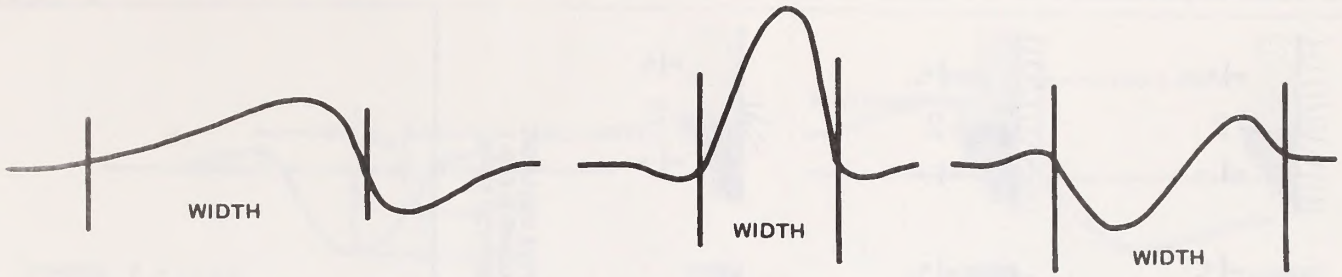

Figure 33. Anomaly 'Width'

tion, the slope of its surface and its discontinuities. The depth to various points on the surface of crystalline rock or magnetic basement allows one to map that surface and its topography and structures to depths exceeding 30,000 feet and to infer thickness of sediments or conformable sedimentary structures above it for exploration of petroleum, sedimentary ores, placer deposits or groundwater. Areas underlain by pediment or other sedimentary deposits may be ruled economic or non-economic according to depth. The depth to ore deposits associated with pyrrhotite, magnetite or ilmenite may be estimated as an aid to a drilling program or even for estimation of total tonnage of magnetic iron ore deposits. Black sand deposits of rutile, zircon, monazite, diamonds, gold, platinum, etc. are often associated with other high density, very resistant yet magnetic minerals, namely, magnetite or ilmenite. The depth to objects of search whether buried iron or man-made structures is invaluable in guiding the subsequent excavation efforts.

Identification of Anomaly

The anomaly of interest must be identified and discriminated against the obscuring effects of others. Recognition of the anomaly itself is usually the most difficult aspect of depth determination because of the composite effects of multiple sources, sources at various depths and at various distances in any direction from the magnetometer. Only the net effect of all anomalies are measured by the magnetometer since it has no inherent discrimination ability at the disposal of the operator. The anomaly should be inspected to ascertain the probable source and, if complex, the possible combination of sources. For example, a wide, shallow dike will appear as two anomalies which may or may not coalesce depending upon the relative width and depth. A very broad anomaly or regional gradient (described in Chapter IV). is usually caused by anomalies which are extremely deep or distant or by the normal variation in the earth's magnetic field. If one wishes to remove this gradient, it can be done either by drawing a straight line through the non-anomalous portions of the profile (away from the anomaly of interest) or by drawing a very smooth but broad wavelength curve through the data of much longer wavelength than any anomalies of interest. This regional gradient or background is then subtracted from the anomaly and the remaining, or residual anomaly, replotted. It is this anomaly which is then interpreted for either depth or for amplitude or general configuration of sources as described in Chapter IV.

Fall-Off Rate

The variation of anomaly amplitude with distance, or fall-off rate, is important in the interpretation of anomalies for it relates the anomaly to depth, it describes in a general way the configuration of the source, and it assists in determining susceptibility and mass of the causative magnetite. Recall that the anomaly from a dipole varies as $\frac{1}{r^3}$ and that of a monopole as $\frac{1}{r^2}$. The fall-off rate, in actual practice, does not involve precisely such factors or exponents but, in fact, is typically $\frac{1}{r^{2.5}}, \frac{1}{r^{0.6}}$, etc., or even $\frac{1}{r^0}$ as described above. In other words, various configurations of dipoles, monopoles, lines and sheet-like distributions of these poles constitute a continuous series of fall-off rates even in the vicinity of a single anomaly as one is much closer or further away from the source.

Representing various geologic sources as simple prismatic bodies, one may assume the following fall-off rates: a dipole will be produced by a source all of whose dimensions are small (less than $1/10$ compared to the distance between the source and magnetometer). Such a body is rarely seen in nature except as a very confined, usually magnetite-rich ore body. A monopole varying as $\frac{1}{r^2}$ will be produced by a long, thin, vertical prism, such as a narrow vertical intrusive in steeply dipping fields or a horizontal cylinder striking N-S in equatorial fields (e.g., a N-S anticlinal structure on the basement, one end of which is near the magnetometer). A line of dipoles is produced by a long, horizontal cylinder magnetized through its short dimension as in steeply dipping latitudes or striking E-W in equatorial regions. Such a cylinder will also vary as $\frac{1}{r^2}$. A line of monopoles would effectively be observed near one edge of a dike dipping in the direction of the field and would vary approximately as $\frac{1}{r}$. At a point above a horizontal semi-infinite sheet, the field would vary inversely as $\frac{1}{r^0} = 1$, which is another way of expressing the fact that the field does not vary at all with distance from a horizontal semi-infinite sheet of monopoles or dipoles. A wide vertical dike in a steep field or the edge of a fault might represent combinations between a line of dipoles or sheet-like distribution of monopoles and may thus vary as $\frac{1}{r^2}$, or $\frac{1}{r^{0.5}}$ or less. *Figure 34* indicates these variations.

Assumptions on Maximum Amplitude and Depth Estimates

Unless the remanent magnetization is actually measured, it is generally disregarded, and only the induced magnetization and susceptibility are utilized in these expressions. The magnetic anomaly calculated from these

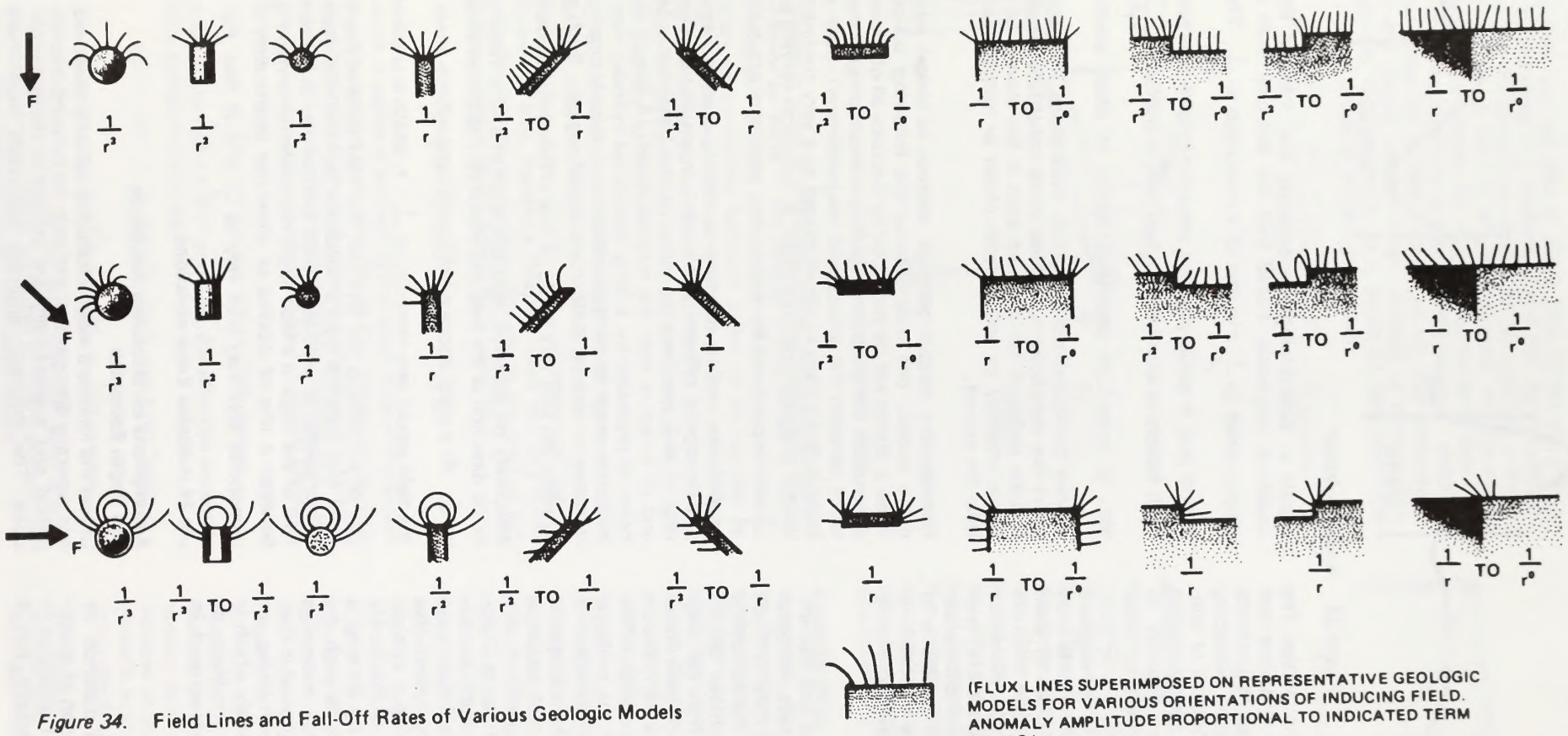

Figure 34. Field Lines and Fall-Off Rates of Various Geologic Models

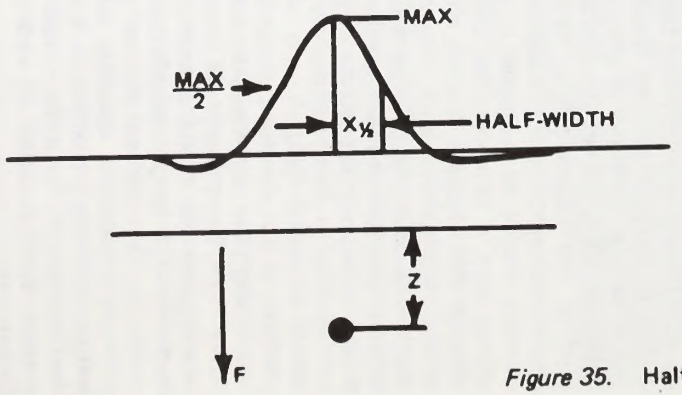

SPHERE (DIPOLE)	$Z = 2X_{½}$
VERTICAL CYLINDER (MONOPOLE)	$Z = 1.3X_{½}$
EDGE OF NARROW DIKE (LINE OF MONOPOLES)	$Z = X_{½}$
HORIZONTAL CYLINDER (LINE OF DIPOLES)	$Z = 2X_{½}$

Figure 35. Half-width Rules – Vertical Field

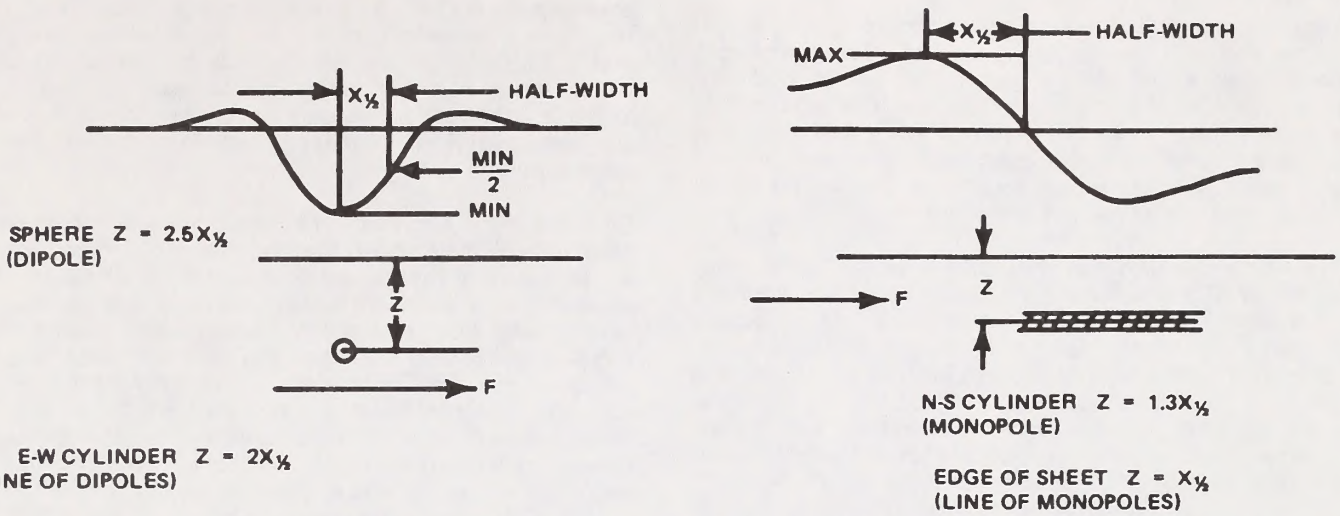

Figure 36. Half-width Rules – Horizontal Field (Equatorial)

highly simplified expressions represents the maximum amplitude from the local zero, non-anomalous field to the positive peak value in the northern and sourthern latitudes and to the minimum negative value in equatorial regions. It does not represent the peak-to-peak value which includes both positive and negative portions of the anomaly signature. The depth estimates derived from any of the techniques described are seldom more accurate than 10% of the actual depth and sometimes as poor as 50%. By theory most of the estimates are maximum estimates so that the actual source will actually be at a shallower depth. Moreover, the 'poles' or source described frequently throughout their chapter are within the geologic body or object of search and not simply on the surface; therefore, such depths are again maximum depths.

Half-Width Rules

In vertical or horizontal fields, it can be shown, from the previous expressions for dipoles and monopoles, that for simple forms of anomaly sources, the depth to their centers is related to the half-width of the anomaly. The half-width is the horizontal distance between the principal maximum (or minimum) of the anomaly (assumed to be over the center of the source) and the point where the value is exactly one-half the maximum value *(see Figure 35)*. This rule is only valid for simple-shaped forms such as a sphere (dipole), vertical cylinder (monopole), and the edge of a narrow, nearly vertical dike (line of monopoles) in the polar regions. At the magnetic equator, the half-width rules are somewhat different with the sphere remaining unchanged, an E-W horizontal cylinder being a line of dipoles, a N-S cylinder being a monopole, and the edge of an E-W striking horizontal sheet representing a line of monopoles. The rules presented in *Figure 36* apply according to the corresponding array of poles and in the case of the latter two, the half width being the horizontal distance between the point of maximum (or minimum) and zero anomaly. The half width rules are derived from formulae given above in "Dipole and Monopole Signatures in Vertical and Horizontal Fields".

Slope Techniques

Perhaps the most commonly used set of methods for estimating depth are those which utilize criteria involving the measurement of the horizontal gradient or slope at the inflection points of the anomaly. Based upon empirical observations utilizing computed models, these slopes are measured according to the horizontal extent of the 'straight' portion of the slope *(see Figure 37)* or the horizontal extent determined by different combinations of the tangent or slope at the inflection point, maximum of the anomaly and half slopes, etc. Each of these horizontal distance measurements when multiplied by an empirically-determined factor equals the depth to the top of the anomaly source. (The straight-slope, for example, is multiplied by a factor between 0.5 and 1.5). Detailed explanations of these methods are available in the references cited.

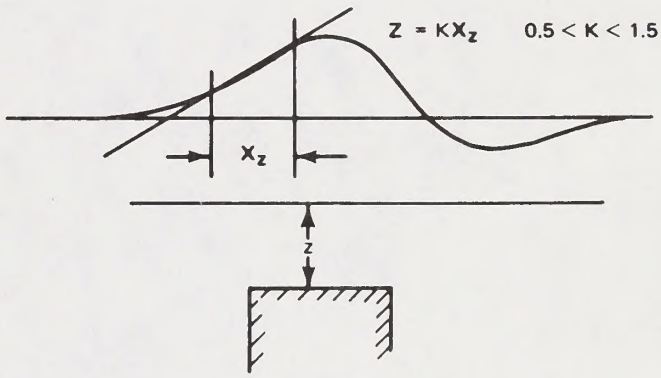

Figure 37.

Other Depth Estimating Methods

Modeling techniques require that one examine the observed anomaly for its likely source configuration. A model is assumed, the anomaly calculated, compared with the observed and repeatedly altered until a satisfactory fit to the observed data is finally achieved, with such work usually performed on a computer. Other computer-oriented depth estimating methods include programs utilizing Fourier and Hilbert transforms, convolution and other semi-automated programs which are usually applied to large volumes of data. Gradiometer measurements made with sensors at two points usually vertically arranged can also be used for depth estimates (see Chapter VIII).

Interpretation Summary

Interpretation is facilitated if one can thoroughly familiarize himself with how and why a given source produces an anomaly in the earth's field, the nature of total field measurements and the general behavior of an anomaly signature with increasing depth. What at first may have appeared complex in the interpretation of field profiles and maps is more readily understood when the above phenomena are examined one at a time.

The first procedure that should be followed in the interpretation of a given profile is to focus on the anomaly width and shape and attempt to construct at least a mental image of the source in realistic geologic terms (or object in the case of search) and its depth. Use the eye to discriminate against noise and the regional gradient or filter by one of the suggested techniques. Anomalous horizontal gradients should then be used, for lack of any other specific criteria, as an indicator of the edge of subsurface structures producing a magnetization contrast. Most anomalies on any given profile or map represent a simple contrast in magnetization or lithology, i.e., the edge of a body. Attempt to correlate such features on adjacent lines or interpret them as contacts on a total intensity contour map. The cessation, displacement or interruption of otherwise long or continuous features may also represent significant geologic structural information. However, one must realize also that a magnetic survey is only able to map a contact where there is a magnetization contrast so that, for example, different lithologies on either side of a long continuous fault will be mapped only in segments where such contrasts occur.

Changes in the character of the short wavelength anomalies (noise) may also represent mappable information if one is careful to evaluate their typical depth so as not to be mapping irrelevant soil anomalies. Negative anomalies arising from features of locally lower magnetization are as important geologically as the more common positive anomalies. Furthermore, the *most geologically significant anomalies on a given map are probably the more subtle ones and not necessarily the largest, most prominent anomalies.* Lastly, the total intensity profiles and maps are not an end in themselves, but are rendered usable only when expressed in terms of geology (or objects of a search). The more geological information one has (or size, magnetic or depth information for an object of search) the more valuable the total intensity data becomes and vice-versa.

APPENDIX IX

Down-hole Pulse Electromagnetic (PEM) System

(Woods, D.V., and Crone, J.D.:1980): Scale Model Study of a Pulse Electromagnetic System; The Canadian Mining and Metallurgical Bulletin, May, p. 96-104 [reprinted by permission of The Canadian Institute of Mining and Metallurgy].

Table of Contents

MINERAL EXPLORATION TECHNIQUES

Scale model study of a borehole pulse electromagnetic system

DENNIS V. WOODS
Department of Geological Sciences
Queen's University
Kingston, Ontario
J. DUNCAN CRONE
Crone Geophysics Limited
Mississauga, Ontario

ABSTRACT

In order to determine its capabilities and to aid in the interpretation of field results, a scale model study and field tests were carried out on the Crone borehole pulse electromagnetic (PEM) system. The model results indicate that if a borehole passes in the vicinity of a tabular conductive body, the system will not only detect the presence of the body, but will also return information as to its conductivity-thickness product, size, attitude and position.

The effect of variation of these electromagnetic and geometric factors on the shape of the response curve from a borehole PEM survey is displayed by a number of suites of scale-model response curves. These model curves can be used directly as type curves in the interpretation of field results. Field tests of a prototype PEM system provide a check on the scale-model results and also summarize the procedure of interpreting field data using the model type curves.

The borehole pulse EM system can be effectively used as a follow-up geophysical instrument for locating and delineating known conductive bodies. It can also be profitably utilized as a primary geophysical exploration tool in areas of deep mineralization below the depth limit of conventional airborne and ground geophysical systems. The probed area of a diamond drill hole in these cases is increased from a 1-inch drill core to a zone extending hundreds of feet from the hole.

D.V. Woods

Dennis Woods obtained a B.Sc. (Eng.) degree in 1973 and an M.Sc. (Eng.) degree in 1975 from Queen's University, where he studies applied geophysics, particularly the electromagnetic methods. He then attended the Australian National University in Canberra, Australia, where he carried out a large-scale, geomagnetic induction project in central Australia, obtaining a Ph.D. for this research in April of this year. He joined the staff of Queen's University in September 1979 and is currently teaching applied geophysics to graduate and undergraduate students as well as continuing his research in the electromagnetic methods as applied to resource exploration and the investigation of the state of the earth's interior.

J.D. Crone

J. Duncan Crone graduated from the University of Toronto in 1951, receiving a B.A. degree in mathematics and physics. He then joined Newmont Exploration Company for the period 1951-1953, and was engaged in mining exploration in the southwestern United States utilizing the induced polarization method pioneered by this company. Returning to Canada, he was employed by Radar Exploration Company and was in charge of gravity surveys in both the mining and petroleum exploration fields. From 1956 to 1962, he was engaged by Noranda Mines Ltd. as senior geophysicist, supervising geophysical field operations and research.

In 1962 Mr. Crone formed Crone Geophysics Ltd. in Toronto. He is a member of the CIM, SEG and EAEG.

Keywords: Mineral exploration, Exploration techniques, Borehole surveys, Electromagnetic systems, PEM systems, Geophysical exploration, Scale modelling, Drilling.

Manuscript submitted October 23, 1979; revised version received March 25, 1980.

Introduction

Most ground electromagnetic systems now used in geophysical exploration are of the frequency-domain type, employing a sinusoidally varying electromagnetic field. A fundamentally different EM system which operates in the time domain was first developed by Wait (1956) at Newmont Mining Corporation. In this system, an electromagnetic field is produced from a current transient or instantaneous turn-on or turn-off of current in a long wire transmitter. An adaptation of this method using the same square current waveform and a single, large horizontal transmitter/receiver loop was later produced in the Soviet Union (described by Veliken and Bulgakov, 1967) and more recently improved in Australia by Buselli and O'Neill (1977)

A group of workers at Newmont (Dolan, *et al.*, 1966) revised Wait's original transient EM system by designing a system specifically to detect the response from deeply buried, highly conductive orebodies in a conductive host rock or blanketed by conductive overburden. Instead of the instantaneous turn-off of current used by Wait, they produced a pulse of elec-

tromagnetic field by terminating the current in a transmitter loop at a linear rate. This ramp-function current waveform has intrinsic advantages over the square waveform, and also the half-sine waveform used in an airborne time-domain EM system (Barringer, 1962), for detecting highly conductive orebodies in conductive terrains (Dolan, 1967)

Crone Geophysics Limited developed a pulse electromagnetic (PEM) system in cooperation with Newmont in 1973. The receiver unit of the PEM system is synchronized to the transmitter by radio or connecting cable and measures the secondary field in 8 preselected sample windows after the primary pulse (further details of the PEM system are discussed in Crone, 1979). A borehole PEM system built by Crone Geophysics Limited uses the same instrumentation as the ground unit, except for the addition of a downhole receiver probe with connecting cable and reel.

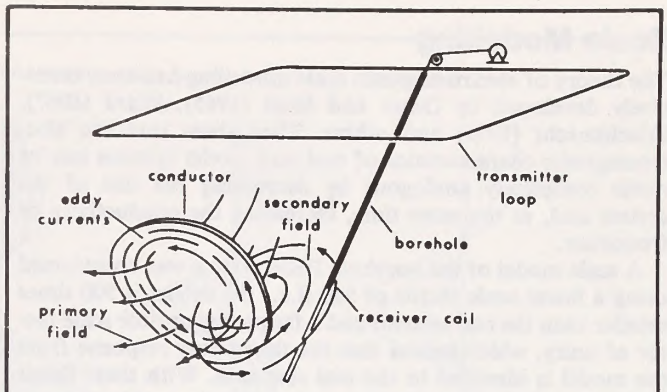

FIGURE 1. Schematic diagram of the Crone borehole PEM system.

Borehole EM Systems

An electromagnetic induction system for use in a borehole was first developed for petroleum exploration by Doll (1949). His induction log was designed to measure the resistivity of formations in petroleum exploration boreholes and consists of closely spaced, coaxial transmitter and receiver coils lowered down the hole. An adaption of the induction log using the same geometric configuration, but with the coil spacing increased to 100 feet, was later developed by Elliot (1961) for use in mineral exploration. An improved version of this system, with coil spacings of up to 300 feet for a greater detection range, was studied by Drinkrow and Duffin (1978).

An earlier borehole EM system specifically designed for mineral exploration by Ward and Harvey (1954) utilizes a fairly large transmitter loop upright over the collar of a diamond drill hole. The plane of the transmitter loop is aligned parallel to the axis of the borehole and a coaxial receiver coil is lowered down the hole. In this minimum coupling configuration, only secondary voltages are induced in the receiver coil, but if the system is misaligned or the borehole curves, anomalous readings will result.

A frequency-domain borehole EM system employing a large Turam-type transmitter loop laid out on the ground about the collar of a diamond drill hole was first studied by Noakes (1951) and later tested in 1962 by Crone Geophysics Limited on an orebody in the Noranda area of Quebec (subsequently reported by Salt, 1966). In this system, a coaxial receiver coil is lowered down the hole and the phase and amplitude of its signal is compared to a standard signal from a small reference coil on surface.

The large, horizontal-loop borehole system has the greatest depth of penetration from the surface and the largest range of detection from the borehole of any of the other borehole EM systems because of its extremely large primary field. In addition, the large loop system tends to increase the effect of larger, more remote conductive bodies, whereas the induction log method will give good responses to small, near-hole conductors. However, the frequency-domain, horizontal-loop system has disadvantages due to measuring the secondary field in the presence of a strong primary field. The amplitude of the received signal has to be corrected according to the primary field geometry, and curving boreholes will give anomalous readings.

The Crone Borehole Pulse EM system, as shown schematically in Figure 1, eliminates the problem caused by curving boreholes because it is a time-domain system and the secondary field is measured in the absence of any primary field. In order to determine the capabilities of this system and to facilitate the interpretation of field results, a scale model of the borehole PEM system was built and studied by Woods (1975), the results of which are presented here. Results from field tests of the borehole PEM system are also presented in this paper for comparison with the model results and to demonstrate the interpretation procedures using the model results.

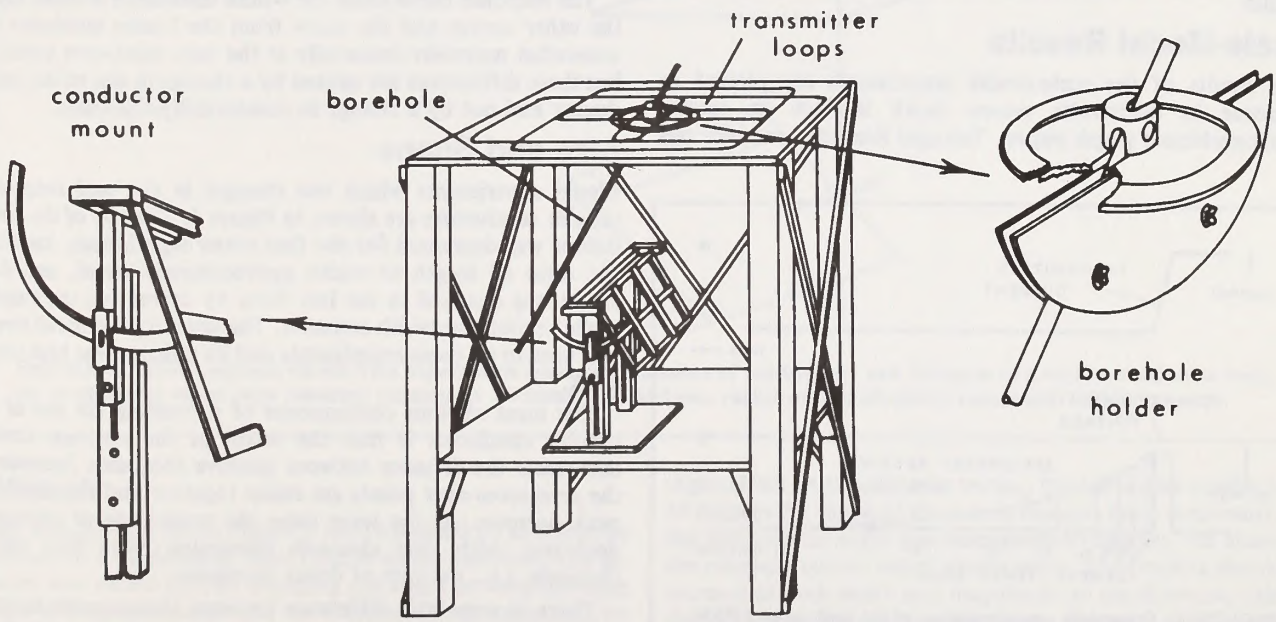

FIGURE 2. Sketch of the borehole PEM scale model, with detail on the borehole holder and the conductor mount.

Scale Modelling

The theory of electromagnetic scale modelling has been extensively developed by Grant and West (1965), Ward (1967), Frischknecht (1971) and others. They show that the electromagnetic characteristics of real and model systems can be made completely analogous by decreasing the size of the system and, at the same time, increasing the conductivity or frequency.

A scale model of the borehole PEM system was constructed using a linear scale factor of 500 (i.e., the model is 500 times smaller than the real system) and a frequency or time scale factor of unity, which means that the time decay response from the model is identical to the real response. With these linear and time scale factors, theory requires that the conductivity of the test bodies be increased 250,000 times. Therefore, orebodies ranging in conductivity between 5 and 200 mhos/metre can be simulated by metals such as stainless steel, brass, aluminum and copper with conductivities of from 1.5×10^6 to 5×10^7 mhos/metre. Displacement currents are neglected in the EM model theory and permeability is taken to be that of free-space by considering only non-ferromagnetic materials. The scale model is a free-air type, so the effect of conducting rock surrounding the conductive orebody has also been neglected.

A schematic diagram of the model is shown in Figure 2. The top level represents the ground surface with four separate transmitter loops, each measuring 2 by 3 feet (1000 by 1500 feet scaled). Different transmitter loops were used to test the effect of changing the transmitter loop position, however the results are not presented in this paper. Rectangular metal sheets and plates, used to simulate tabular conductive bodies, are held on a conductor mount, which allows the sheet to be placed in any spatial attitude as well as any vertical or lateral position. A small receiver coil is connected by means of a coaxial cable to the receiver, where the secondary signal is amplified and then displayed on the screen of an oscilloscope.

A total of 140 experiments were completed using this model to test the effect on the borehole PEM response of the variation of conductivity, thickness, size, shape, attitude and position of the tabular conductive bodies. The attitude and position of the borehole and conductor were kept constant when various types and sizes of conductors were tested and the same metal sheet was used in all of the attitude and position experiments. Additional tests were carried out with other metal sheets in various attitudes and positions to cross-correlate the results.

Scale-Model Results

The results of the scale-model experiments are plotted as response in microvolts versus depth in feet on special semilogarithmic graph paper. Voltages from the receiver coil are plotted on a linear basis for the first 10 microvolts (both positive and negative) and on a logarithmic basis thereafter. This lowers the extremely high values while keeping the small responses recognizable. The sign of the secondary signal is defined as positive if it has the same sense as the primary pulse directly beneath the transmitter loop.

For each experiment, there are eight response-versus-depth curves corresponding to the eight sampling times shown in Figure 3. These samples are not exactly the same as for the present borehole PEM system, however they do cover approximately the same range and therefore produce approximately the same response-versus-depth curves.

The absolute magnitudes of the receiver voltages are only applicable to the scale model, as they depend on the electrical characteristics of the model system: size, number of turns and current of the transmitter loop; and size, number of turns and type of core of the receiver coil. However, the primary pulse of the model system has an absolute magnitude of about one millivolt at a depth of about 2000 feet, so that the units of the secondary response may be thought of as parts per thousand of the primary pulse instead of microvolts. Because this approximation is not precise and because the model units are not exactly the same as field units, absolute magnitude is not used in this study and only relative magnitudes are discussed in the following sections.

The response curves have been arranged according to physical parameters of the conductor and are shown in Figures 4 to 9. On the basis of form, they can be categorized into two groups: those with a large, central negative peak and two positive shoulders obtained when the borehole passes by the outside edge of the conductor; and those with a single, broad positive response when the borehole passes through the interior of the conductor. Response curves obtained from a borehole passing through the conductor near one edge have characteristics of both groups.

Conductivity and Thickness

The collection of response curves in Figure 4 shows the effect of varying a) conductivity and b) thickness of a tabular conductive body; all other parameters are held constant. All of the response curves are somewhat similar, the major difference between them being a change in the magnitude of response. As the conductivity or thickness increases, the relative magnitude of response of the late channels increases; i.e., the rate of decay of the transient response decreases.

The response curve from the 4-mho conductor is wider than the other curves and the curve from the 1-mho conductor is somewhat narrower (especially at the zero cross-over points), but these differences are caused by a change in size of the conductor and not by a change in conductivity-thickness.

Size and Shape

Model experiments which test changes in size and shape of tabular conductors are shown in Figure 5. The size of the conductor was decreased for the first seven experiments, keeping the ratio of length to width approximately equal, and the shape was changed in the last three by decreasing the length while keeping the width constant. The same type of metal sheet was used in all these experiments and its attitude was kept constant.

The most obvious consequence of decreasing the size of a tabular conductor is that the width of the response curve decreases: the distance between positive shoulders decreases, the zero cross-over points get closer together and the negative peak narrows. At the same time, the magnitude of response decreases, with later channels decreasing more than early channels, i.e., the rate of decay increases.

There is very little difference between the response curves where the width of the conductor is constant and only the length varies. This indicates that for large sheets the smallest dimension determines the shape of the response curves.

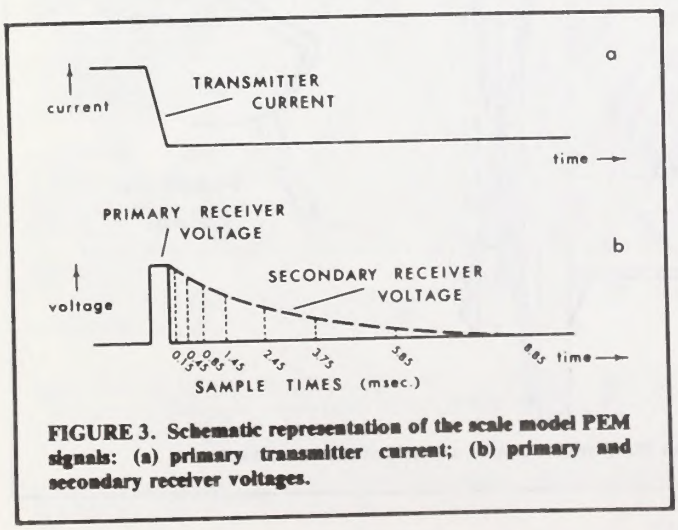

FIGURE 3. Schematic representation of the scale model PEM signals: (a) primary transmitter current; (b) primary and secondary receiver voltages.

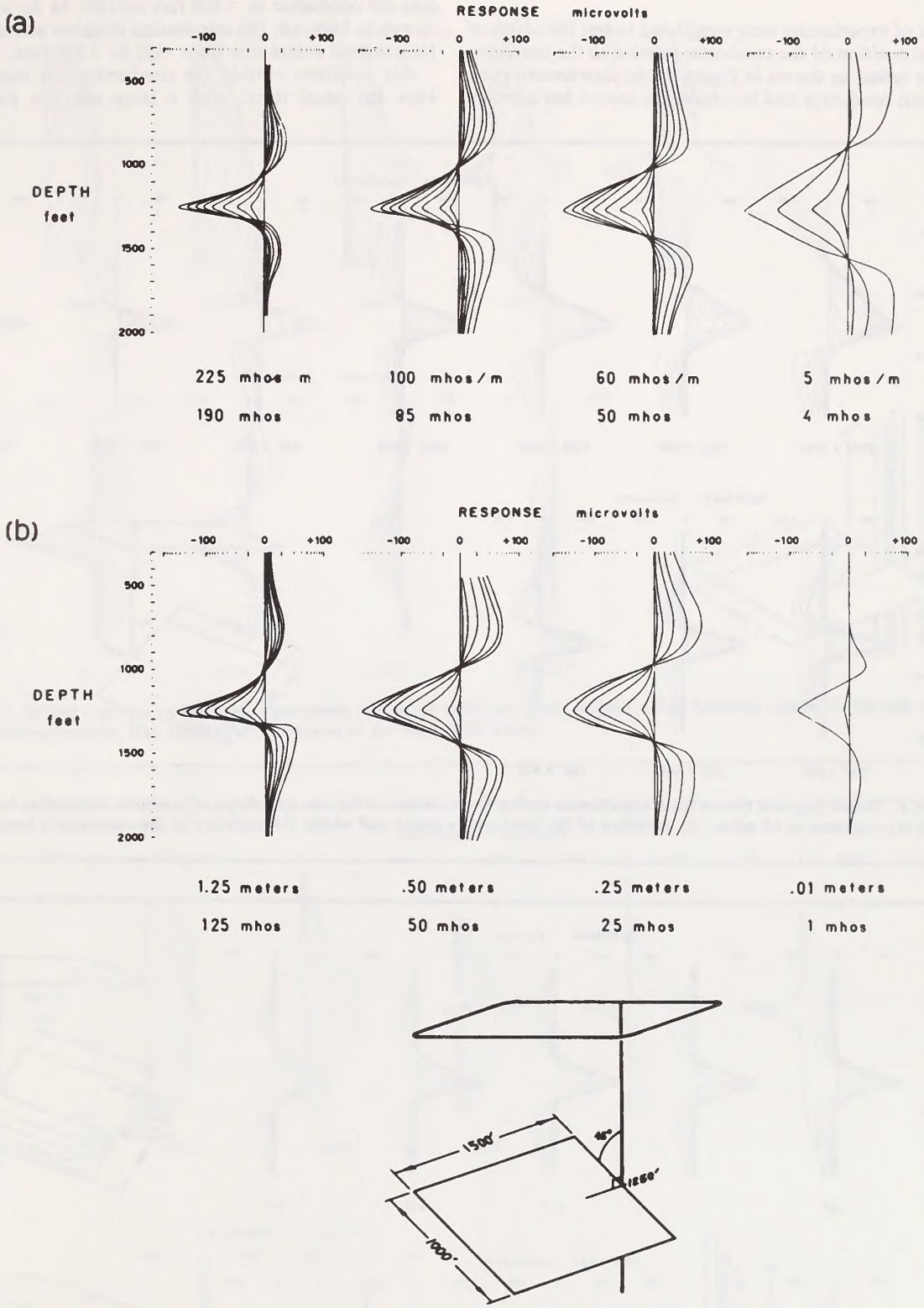

FIGURE 4. Model response curves from experiments testing the variation of conductivity and thickness of a tabular conductive body: (a) conductivity varied with thickness constant at .85 metre; (b) thickness varied with conductivity constant at 100 mhos/metre.

Attitude

The response curves in Figure 6 were obtained by altering the attitude of a single metal sheet relative to the borehole. The attitude was varied first by changing the angle between the near edge of the conductor and the borehole and, secondly, by changing the intersection angle between the borehole and the plane of the conductor.

Decreasing the edge angle from 90 to 45 degrees has only a slight effect on the response curves, but for angles smaller than 45 degrees the shape of the curves changes more noticeably. As the intersection angle decreases from 90 degrees, the shape of the response curves varies significantly. The positive shoulders increase in both width and magnitude on the down-dip side of the conductor and correspondingly decrease on the up-dip side. At the same time, the shape of the negative peak becomes progressively more asymmetric: the up-dip side becomes much steeper and the down-dip zero cross-over points shift upward.

Position

Two series of experiments were completed to test the effect of varying the position of the conductor relative to the borehole. In the first series, as shown in Figure 7, the intersection position between conductor and borehole was moved horizontally along the centre line of the rectangular plate from -500 feet inside the conductor to +500 feet outside. In the second series, shown in Figure 8, the intersection position was moved up the longitudinal centre line from -500 to +100 feet.

For positions outside the conductor, the response curves have the usual form, with a large negative peak and two

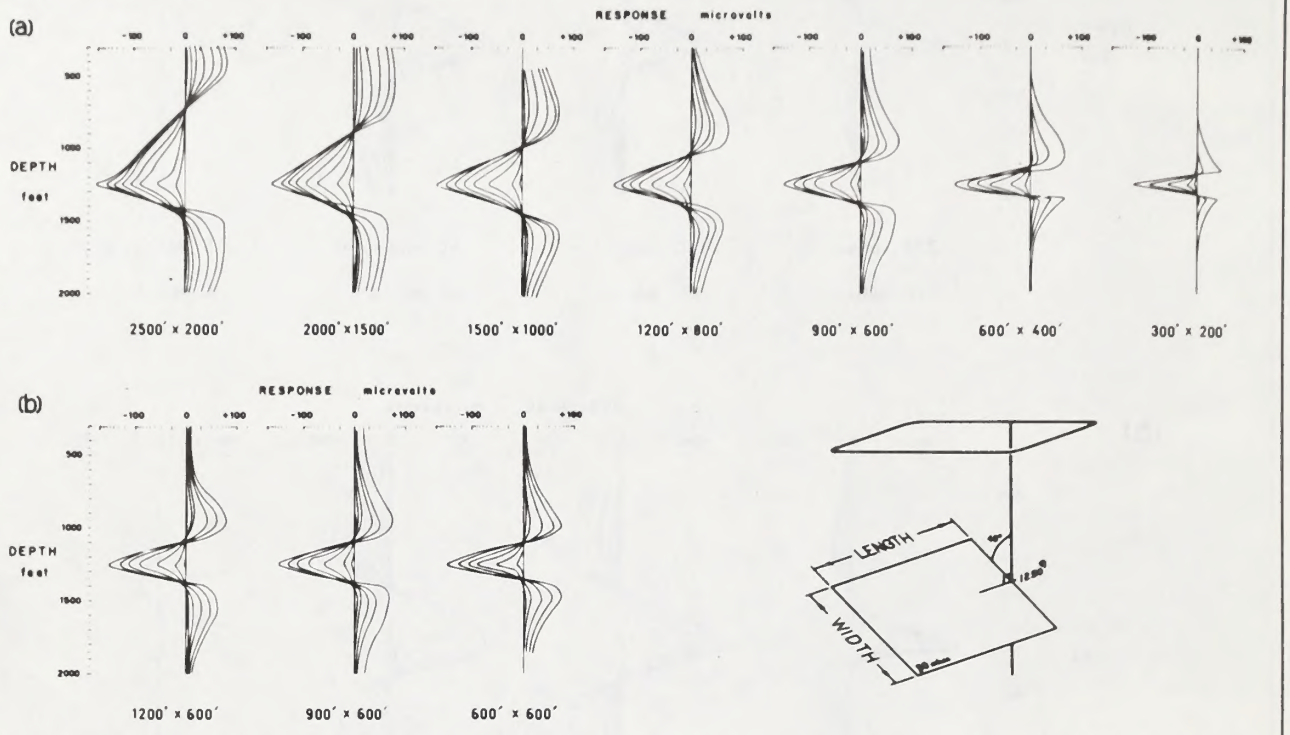

FIGURE 5. Model response curves from experiments testing the variation of the size and shape of a tabular conductive body with a conductivity-thickness of 50 mhos: (a) variation of the conductor's length and width; (b) variation of the conductor's length only.

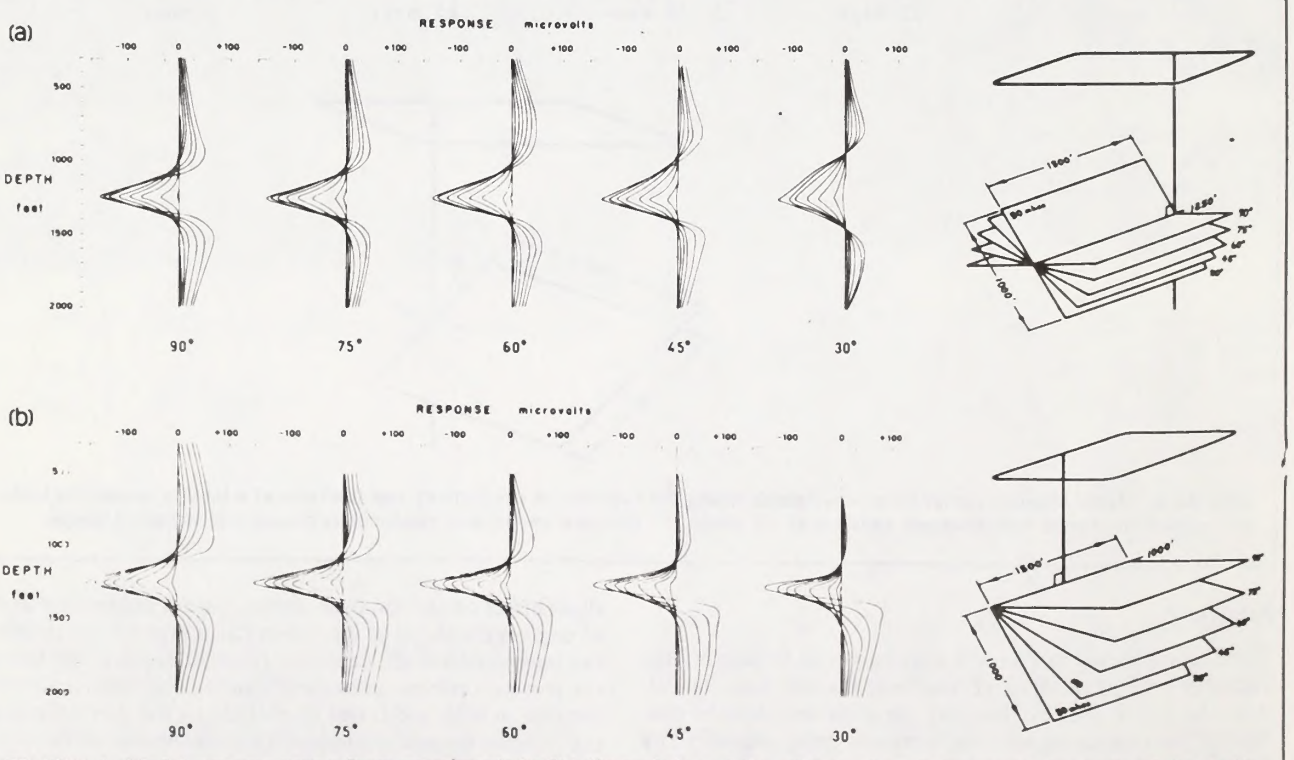

FIGURE 6. Model response curves from experiments testing the variation of the attitude of a tabular conductive body relative to the borehole. The conductivity-thickness of the body is 50 mhos: (a) variation of the edge angle; (b) variation of the intersection angle.

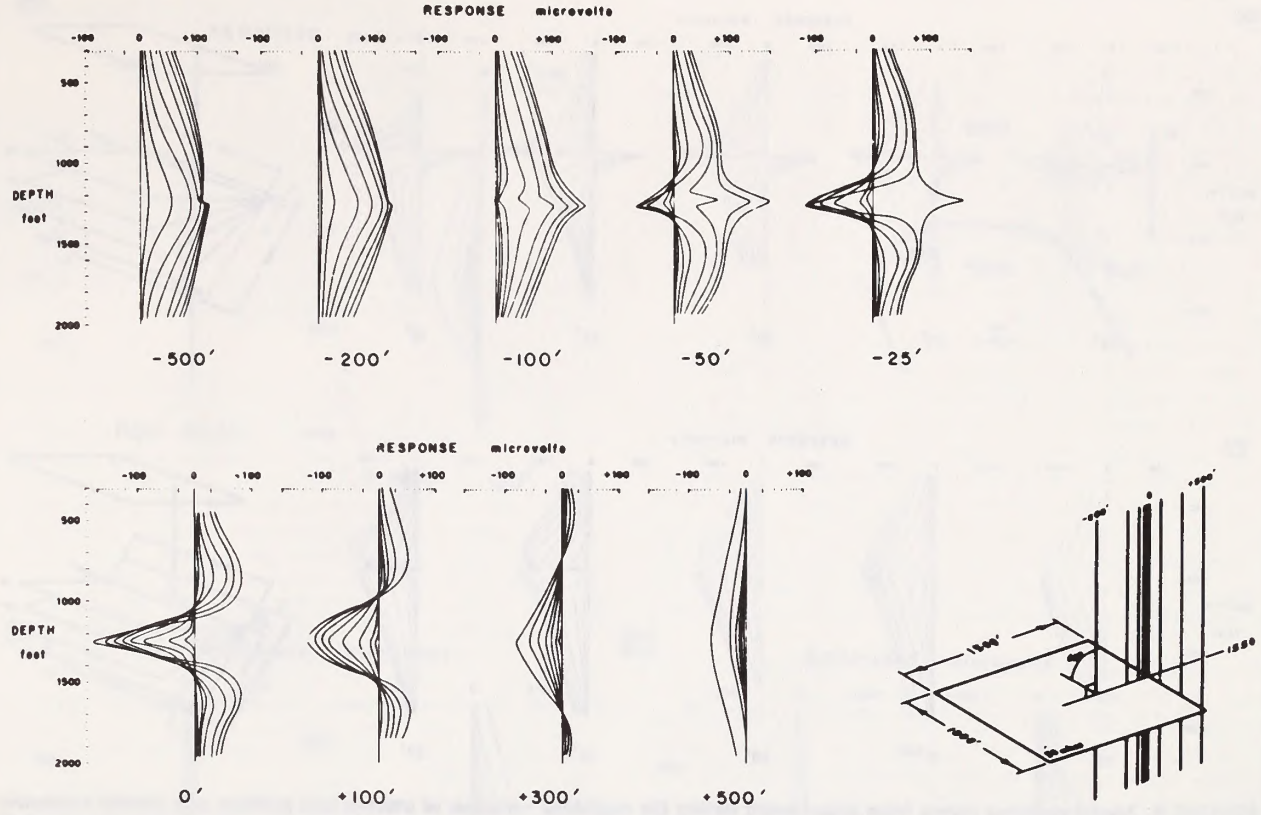

FIGURE 7. Model response curves from experiments testing the variation of the position of the borehole relative to the side edge of a tabular conductive body. The conductivity-thickness of the body is 50 mhos.

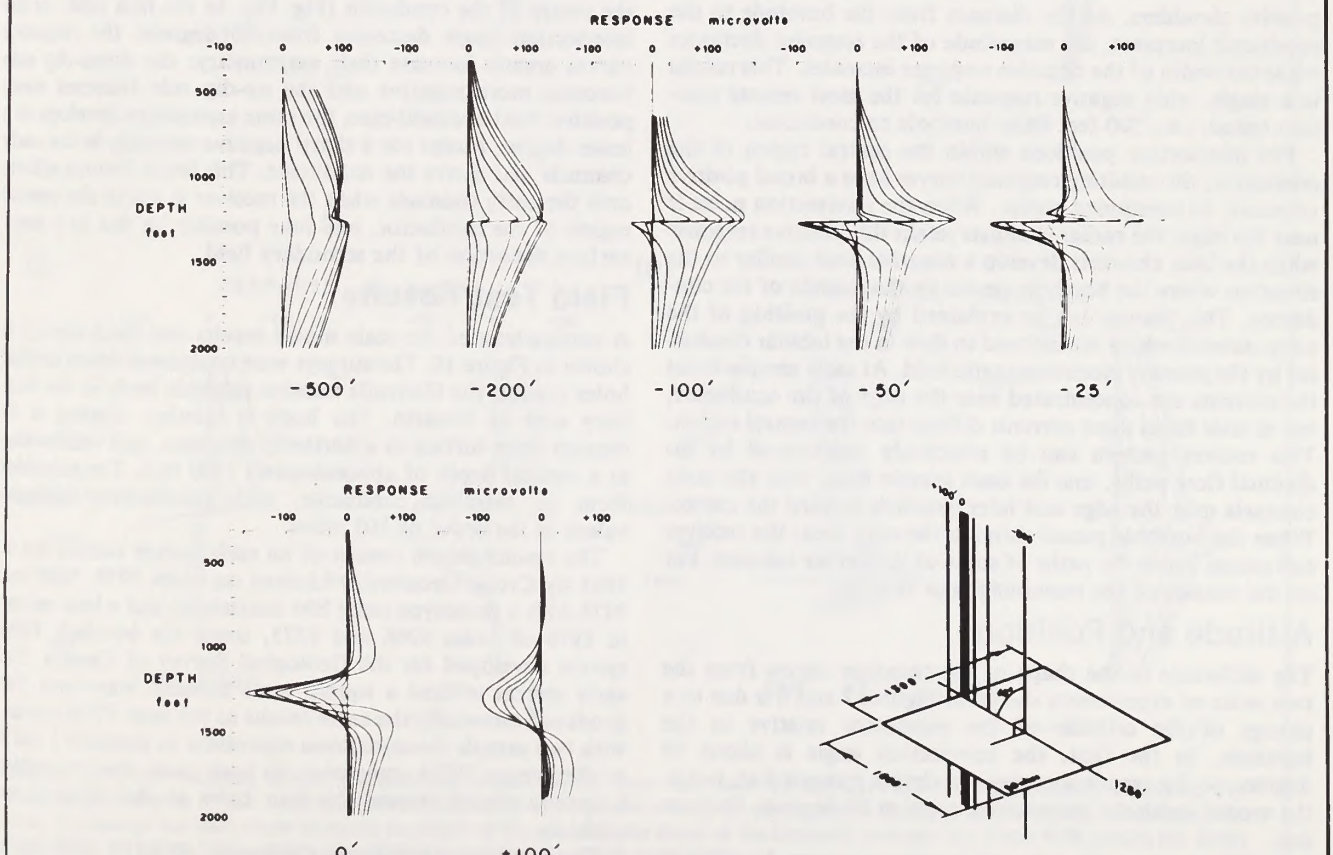

FIGURE 8. Model response curves from experiments testing the variation of the position of a borehole relative to the top edge of a tabular conductive body. The conductivity-thickness of the body is 50 mhos.

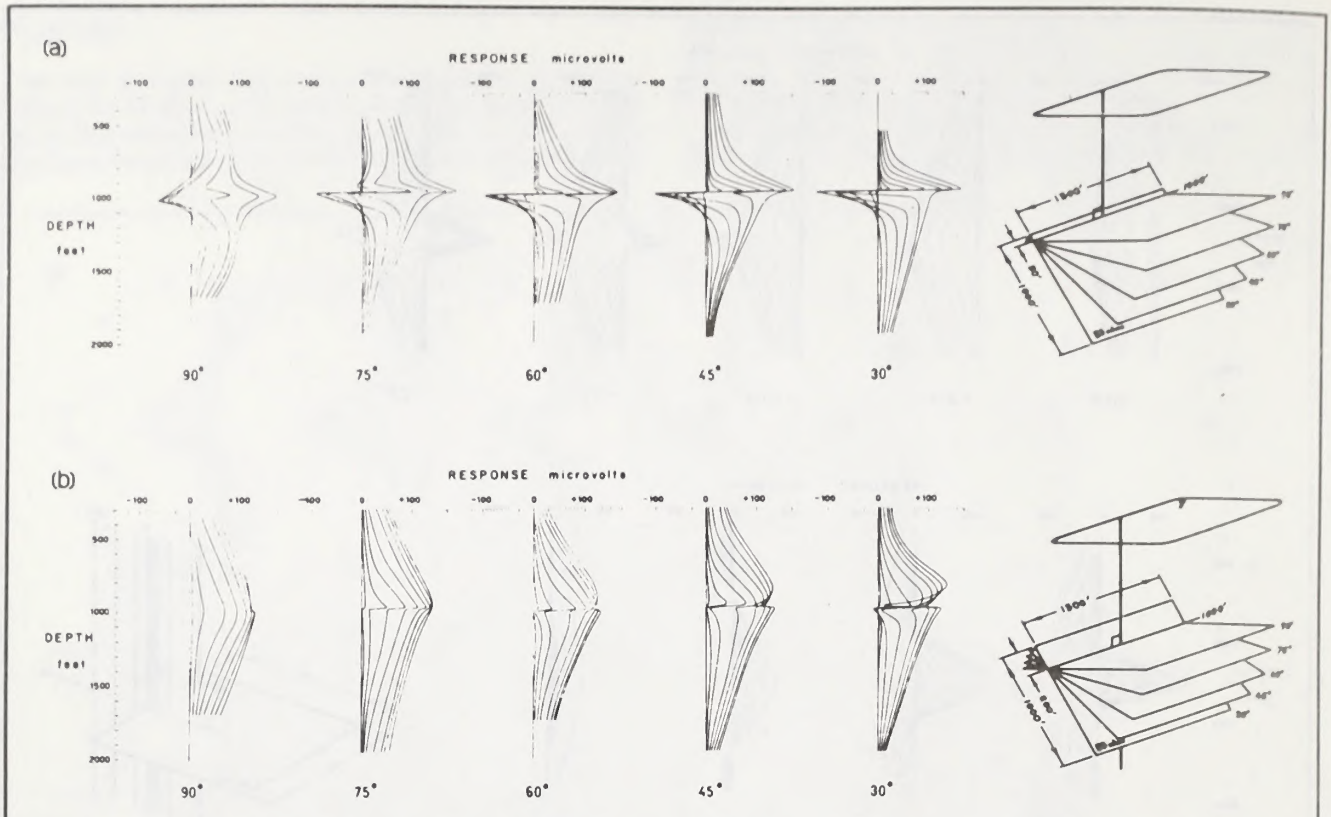

FIGURE 9. Model response curves from experiments testing the combined variation of attitude and position of a tabular conductive body with a conductivity-thickness of 50 mhos: (a) variation of the intersection angle with the borehole intersecting the edge area of the conductor (50 feet from the top edge); (b) variation of the intersection angle with the borehole toward the centre of the conductor (200 feet from the top edge).

positive shoulders. As the distance from the borehole to the conductor increases, the magnitude of the response decreases while the width of the negative response increases. This results in a single, wide negative response for the most remote position tested; i.e., 500 feet from borehole to conductor.

For intersection positions within the central region of the conductor, the resulting response curves have a broad positive response, as mentioned earlier. When the intersection point is near the edge, the earlier channels retain this positive response while the later channels develop a negative peak similar to the situation where the borehole passes by the outside of the conductor. This feature can be explained by the position of the eddy currents which are induced to flow in the tabular conductor by the primary electromagnetic field. At early sample times the currents are concentrated near the edge of the conductor, but at later times these currents diffuse into the central region. This current pattern can be effectively represented by individual flow paths, one for each sample time, with the early channels near the edge and later channels toward the centre. When the borehole passes through the edge area, the receiver coil passes inside the paths of some of the earlier samples, but on the outside of the remaining later samples.

Attitude and Position

The difference in the shape of the response curves from the two series of experiments shown in Figures 7 and 8 is due to a change in the attitude of the conductor relative to the borehole. In the first, the intersection angle is about 90 degrees, so the response curves are almost symmetrical, but in the second, with the intersection angle at 60 degrees, they are not.

In Figure 9, two series of response curves have been generated by varying the intersection angle between the borehole and conductor, with the borehole intersecting first the edge area of the conductor (Fig. 9a) and, secondly, toward the centre of the conductor (Fig. 9b). In the first case, as the intersection angle decreases from 90 degrees, the response curves greatly increase their assymmetry: the down-dip side becomes more negative and the up-dip side becomes more positive. In the second case, the same asymmetry develops to a lesser degree, except for a sharp negative anomaly in the early channels just above the conductor. This latter feature affects only the early channels when the receiver is above the central region of the conductor, and may possibly be due to a near-surface distortion of the secondary field.

Field Test Results

A comparison of the scale model results and field surveys is shown in Figure 10. The surveys were completed down vertical holes around the Gertrude massive sulphide body in the Sudbury area of Ontario. The body is tabular, dipping at 45 degrees from surface in a northerly direction, and terminating at a vertical depth of approximately 1300 feet. The sulphides form an excellent conductor, with conductivity-thickness values in the order of 160 mhos.

The results shown consist of an early survey carried out in 1963 by Crone Geophysics Limited on holes 9279, 9266 and 9276 with a prototype pulse EM instrument and a later survey in 1976 of holes 9266 and 9273, using the borehole PEM system developed for the Geological Survey of Canada. The early system utilized a square wave transmit waveform that produced essentially the same results as the later PEM system, with two sample measurements equivalent to channels 2 and 4 of the present PEM equipment. In both cases, the transmitter loop was placed around the four holes to the north of the orebody.

The response curve from the survey of DDH 9279 has a broad negative shape similar to the scale-model response curves where the borehole passes a considerable distance outside the conductor. The closest matching model curve is from

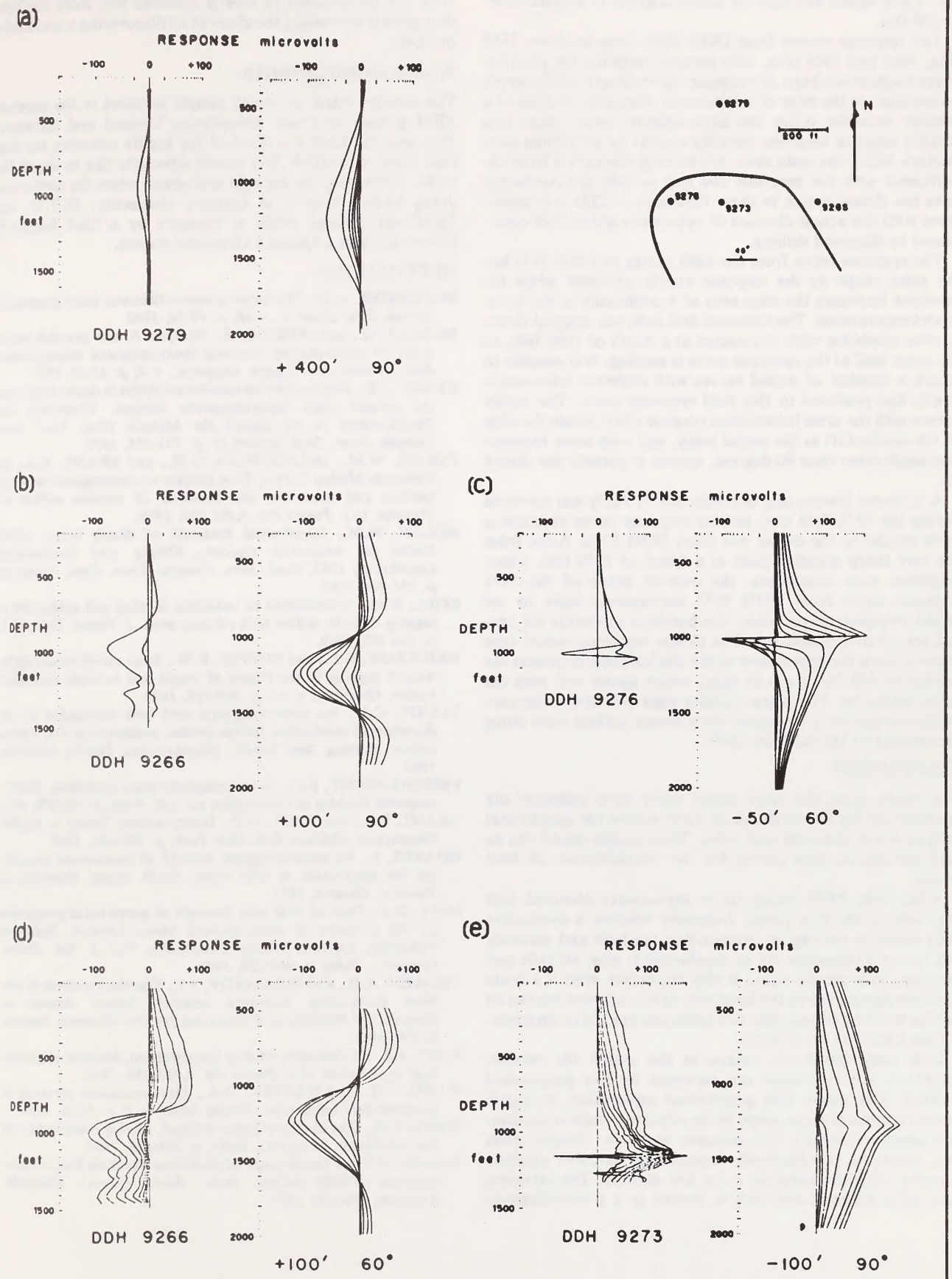

FIGURE 10. Field response curves and matching model curves from field tests on the Gertrude orebody, Sudbury, Ontario. The conductivity-thickness of the Gertrude orebody varies from 20 to 160 mhos; the conductivity-thickness of the model conductors is 50 mhos. No attempt has been made to match the depth of the model to the depth of the Gertrude orebody. (a) DDH 9279 (1963); (b) DDH 9266 (1963); (c) DDH 9276 (1963); (d) DDH 9266 (1976); (e) DDH 9273 (1976).

the experiment where the borehole is 400 feet from the conductor, which agrees well with the actual distance of approximately 350 feet.

The response curves from DDH 9266 from both the 1963 (Fig. 10b) and 1976 (Fig. 10d) systems resemble the positive-negative-positive shape of response curves where the borehole passes close to the edge of a conductor. However, instead of a positive shoulder below the large negative peak, there is a smaller negative response possibly caused by additional conductors below the main zone. Model response curves from experiments with the borehole 100 feet outside the conductor have the closest match to these field curves. This is in agreement with the actual distance of approximately 60 feet determined by diamond drilling.

The response curve from the 1963 survey of DDH 9276 has the same shape as the response curves obtained when the borehole intersects the edge area of a conductor in the scale-model experiments. The diamond drill hole was stopped shortly after sulphides were intersected at a depth of 1040 feet, so the lower half of the response curve is missing. It is possible to match a number of model curves with different intersection angles and positions to this field response curve. The model curves with the same intersection position (50 ft inside the edge of the conductor) as the actual body, and with some intersection angle other than 90 degrees, appear to provide the closest fit.

A different intersecting borehole (DDH 9273) was surveyed during the 1976 field test, but the response curve obtained is quite similar to the earlier one from DDH 9276. Aside from the very sharp negative peak at a depth of 1150 feet, where sulphides were intersected, the over-all shape of the 1976 response curve from DDH 9273 corresponds more to the model response curves where the borehole intersects the central region of a conductor. The closest matching model type curve is from the experiment where the borehole intersects the conductor 100 feet from its edge, which agrees well with the actual situation. The sharp negative peak just above the conductor surface may be caused by a strong surface field along the contact of the sulphide body.

Conclusion

The results from the scale model study have indicated the capability of the Crone Borehole PEM system for geophysical exploration in diamond drill holes. These model results can be used directly as type curves for the interpretation of field results.

A borehole PEM survey of an exploratory diamond drill hole will, in the first place, determine whether a conductive body exists in the region surrounding the hole and secondly will return information on its conductance, size, attitude and position. This second point is also important even if a body has been intersected by the borehole, as the information can be used in spotting subsequent drill holes and can aid in determining the extent of an orebody.

Most deep boreholes, drilled in the search for massive sulphides, are at present not surveyed by any geophysical method. This means that geophysical exploration, in highly potential mineral areas, stops at the relatively shallow penetration depth of surface and airborne methods. Deeper zones can, however, be effectively explored for massive sulphide deposits using the borehole pulse EM method. The sampling zone of a diamond drill hole is limited to a 1-inch-diameter drill core; through the use of pulse EM borehole surveys this zone can be extended to several hundred feet from the hole, thus greatly increasing the chances of discovering a conductive orebody.

Acknowledgments

The authors thank the many people involved in the borehole PEM project at Crone Geophysics Limited and elsewhere. Inco and the GSC are thanked for kindly releasing the field tests. One of us (D.V.W.) would especially like to thank Dr. M.M. Fitzpatrick for his help and advice when the author was doing M.Sc. research at Queen's University. D.V.W. was financially assisted while at Queen's by a Carl Reinhardt Fellowship and a Queen's Graduate Award.

REFERENCES

BARRINGER, A.R., The input airborne electrical pulse prospecting system. *Min. Cong. J., v.48, p. 49-54, 1962.*

BUSELLI, G., and O'NEILL, B., Sirotem: A new portable instrument for multi-channel transient electromagnetic measurements. *Bull. Austral. Soc. Explor. Geophys., v. 8, p. 82-87, 1977.*

CRONE, J.D., Exploration for massive sulphides in desert areas using the ground pulse electromagnetic method. *Geophysics and Geochemistry in the Search for Metallic Ores, Geol. Surv. Canada, Econ. Geol. Report 31, p. 745-755, 1979.*

DOLAN, W.M., McLAUGHLIN, G.H., and BRANT, A.A., (to Newmont Mining Corp.), Time domain electromagnetic induction method and apparatus for detection of massive sulfide ore deposits. *U.S. Patent No. 3,263,160, 1966.*

DOLAN, W.M., Geophysical detection of deeply buried sulfide bodies in weathered regions, *Mining and Groundwater Geophysics, 1967, Geol. Surv. Canada, Econ. Geol. Report 26, p. 336-344, 1967.*

DOLL, H.G., Introduction to induction logging and application to logging of wells drilled with oil base mud. *J. Petrol. Tech., v. 1, p. 148-162, 1949.*

DRINKROW, R.L., and DUFFIN, R.W., Scale model results for inductive logging in the region of single and multiple conductive bodies. *Geophys., v. 43, p. 804-818, 1978.*

ELLIOT, C.L., An electromagnetic drill hole instrument for the detection of conductive sulfide bodies; *presented at 31st Annual Intern. Meeting, Soc. Explor. Geophysicists, Denver, Colorado, 1961.*

FRISCHKNECHT, F.C., Electromagnetic scale modelling, *Electromagnetic Probing in Geophysics,* ed. J.R. Wait, *p. 266-270, 1971.*

GRANT, F.S., and WEST, G.F., Interpretation Theory in Applied Geophysics, *McGraw-Hill, New York, p. 479-482, 1965.*

NOAKES, J., An electromagnetic method of geophysical prospecting for application to drill holes, *Ph.D. thesis, University of Toronto, Ontario, 1951.*

SALT, D.J., Tests of drill hole methods of geophysical prospecting on the property of Lake Dufault Mines Limited, Dufresnoy Township, Quebec, *Mining Geophysics, Vol. I, Soc. Explor. Geophys., Tulsa, p. 206-226, 1966.*

VELIKEN, A.B., and BULGAKOV, J.I., Transient method of electrical prospecting (one-loop version). *Intern. Seminar on Geophysical Methods of Prospecting for Ore Minerals, Moscow, USSR, 1967.*

WAIT, J.R. (to Newmont Mining Corporation), Method of geophysical exploration. *U.S. Patent No. 2,735,980, 1956.*

WARD, S.H., and HARVEY, H.A., Electromagnetic surveying of diamond drill holes. *Can. Mining Man., v. 1, p. 19-24, 1954.*

WARD, S.H., The electromagnetic method, *Mining Geophysics, v.II Soc. of Explor. Geophys., Tulsa, p. 308-315, 1967.*

WOODS, D.V., A model study of the Crone Borehole Pulse Electromagnetic (PEM) system, *M.Sc. thesis, Queen's University, Kingston, Ontario, 1975.*

APPENDIX X

Additional Interpretation Aids for VLF, IP, and DIGHEM II Data

(Fraser, D.C.:1981a): A Review of Some Useful Algorithms in Geophysics; The Canadian Mining and Metallurgical Bulletin, Vol. 74, No. 828, p. 76-83. [Reprinted by permission of The Canadian Institute of Mining and Metallurgy.]

Table of Contents

A review of some useful algorithms in geophysics

DOUGLAS C. FRASER
Fraser Consultants Inc.,
Mississauga, Ontario

ABSTRACT

Geophysical data are often presented on maps, sections or profiles with minimal data processing. A common example is magnetic data, in which the diurnal-free raw readings are merely contoured on a map. Other examples include profile presentation of VLF-EM data, IP pseudo-sections and airborne EM anomalies which may be shown on a map with only the measured amplitudes indicated.

In recent years, efforts have been directed to the portraying of data in more useful forms. A number of algorithms (i.e., manipulative procedures and equations) have proven to contribute significantly to the usefulness of geophysical data. Some can be applied manually; others are sufficiently complicated to require a computer. Some merely alter the data to a more useful geometric form without altering the units. Others yield quantitative estimates of source body parameters such as conductivity and shape. Several examples follow:

1. A simple algorithm is in common use which transforms noisy non-contourable VLF-EM data into less noisy contourable data. The input is the dip angle in degrees or per cent and the output is also in these same units.

2. A simple algorithm has recently been developed which allows multi-level dipole-dipole IP data to be contoured on a map. Again, the units are not altered.

3. A relatively complicated algorithm is in common use which transforms non-contourable height-sensitive helicopter EM data into contourable resistivity data.

4. An algorithm has been recently developed which transforms non-contourable height-sensitive EM data into contourable weight per cent magnetite.

The purpose of all the above techniques is to present the data in a simplified form. This, in turn, allows an easier assimilation by the user of much of the information content of the data.

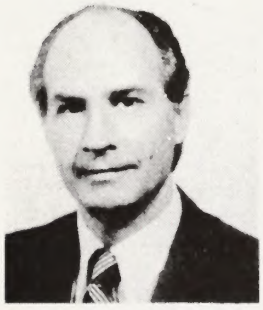

D.C. Fraser

Douglas C. Fraser obtained a Bachelor's and Master's degree in geology at the University of New Brunswick and, in 1966, a Ph.D. degree in geophysics at the University of California at Berkeley. He has published papers on copper geochemistry, electromagnetics, VLF-EM, induced polarization, ground and airborne resistivity, digital filtering and correlation techniques, and on the design of new interpretation methods. He has been responsible for the design and development of the DIGHEM airborne electromagnetic system.

Dr. Fraser has been employed in geological mapping and geophysical exploration in both the mining and petroleum industries, and in geochemical prospecting for base metals. He is president of Dighem Limited and Fraser Consultants Inc., and is a member of the CIM, the Association of Professional Engineers of Ontario, the Society of Exploration Geophysicists and the European Association of Exploration Geophysicists, and is a member and past president of the Canadian Exploration Geophysical Society.

Keywords: Exploration, Geophysical exploration, Algorithms, Data processing, Electromagnetic methods, Induced polarization, Resistivity, Magnetometers, Magusi River deposits.

Introduction

Geophysics over the decades has advanced primarily through the development of instrumentation. Many of the techniques in use today were designed in the last 15 years or so. For example, Vanio Ronka was giving personal demonstrations of his VLF-EM receiver in 1966, and these receivers are now used worldwide. Other advances made during this period include improvements to horizontal-loop EM equipment which allow a substantial increase in depth of exploration, development of sophisticated IP equipment which may allow sulphides to be distinguished from graphite and new airborne EM systems which yield multiple parameters through the use of multiple frequencies or multiple coil orientations.

During this period, new emphasis also was given to the manipulation of data. Data processing developments now may be close in importance to hardware developments. Innovations in processing tend to follow developments in hardware, as, for example, in the transformation of VLF-EM data to a contourable form. However, data processing techniques may actually precede hardware developments. The airborne electromagnetic DIGHEM[II] system is an example, where the subtraction of geologic noise was conceived as a processing development. The concept led to the design and construction of hardware for the specific purpose of providing data in which geologic noise could be eliminated through processing.

This paper will discuss several algorithms which contribute to the geologic usefulness of data. Some are geometric algorithms, so-called because they merely rearrange the geometric form of the data without changing the units. Others are quantitative algorithms, so-called because they yield quantitative estimates of geologic parameters.

VLF-EM

Simple lowpass filtering, or smoothing of data, is an example of a geometric algorithm. Another example is the algorithm used to phase shift VLF-EM data spatially to permit contouring on a map.

The VLF-EM algorithm is shown in the upper left corner of Figure 1. It is a running four-point weighted average using weights of -1 -1 +1 +1. This simple digital filter operator passes over the dip angle profiles which are shown on the upper half of the figure. Its output is then contoured as shown on the lower half. The filtering procedure is quite useful because it simplifies the form of the data, and this aids geologic interpretation. The technique is applicable to inphase dip angles and is described in Fraser (1969, 1971). It is generally not applicable to quadrature dip angles because the sense of quadrature anomalies is often reversed, and this can cause considerable confusion in the contour patterns if the data are filtered.

The filtering procedure is quite useful because it provides a means of displaying complicated waveforms in a manner which aids geologic interpretation. In a qualitative sense, it does not matter whether or not VLF-EM theory is understood. There is an analogy to magnetics: a magnetic contour map can be interpreted qualitatively without knowing magnetic theory in detail. It is nevertheless obvious that interpretation improves with an understanding of theory, and so a brief review of VLF-EM follows.

VLF-EM anomalies are not EM anomalies in the conventional sense. Conventional EM anomalies primarily reflect eddy currents flowing in conductors which have been energized inductively by the primary field. In contrast, VLF-EM anomalies primarily reflect current channeling, which is a non-inductive phenomenon. The primary field generates currents which flow weakly in rock and overburden, and these tend to be channeled by low-resistivity zones. Such zones may be due to massive sulphides, shears, river valleys and even unconformities.

VLF-EM dip angle data in profile form are often difficult to interpret. This is because anomalies in a given area can arise from the overburden as well as from both stratiform and cross-cutting geologic features. This problem gave rise to the filtering technique mentioned above. The VLF-EM contour presentation can help considerably in the interpretation of the various conductors in a survey area.

VLF-EM data commonly are collected at 100- or 200-foot station intervals. Such spacings are too coarse if the collected data give the impression that the source feature is deeper than it really is. The majority of VLF-EM currents flow in the upper 50 to 100 feet. The bedrock target may be buried deeper than this, but currents in the overburden will exist and will produce anomalies. A means of separating overburden conductors from bedrock conductors is to use a sufficiently tight station spacing to allow the depth of the various current flows to be estimated. This usually requires a station spacing of about 50 feet. A saving feature of VLF-EM is that the flanks of a dip-angle anomaly from a single conductor are broad and fairly featureless. Consequently, a 50-foot station spacing needs to be used only in the vicinity of crossovers or inflections.

A variant on the usual contour map presentation of filtered VLF-EM data is a sectional presentation which can provide information in the third dimension. A VLF-EM computer program has been constructed which provides filtered VLF-EM data at six depth levels in the manner described below. Contouring these levels in section along each traverse line provides a pictorial view of the depths of the various current concentrations (e.g., Fig. 2).

In Figure 2, the values of level 1 may be thought of as reflecting the current flow at a nominal depth equal to the station spacing (i.e., 50 feet in this example). The VLF-EM digital filter operates on all the dip-angle data shown in Figure 2 to produce the filtered data for level 1 (see insert of Fig. 2 for the filter operator). It then operates on every second dip-angle value to produce the filtered data for level 2 (see insert) and so on for the deeper levels. Level 1 is useful even if only a few stations were recorded at a station spacing of 50 feet*, because resolution is greatest on level 1. In Figure 2, only the positive

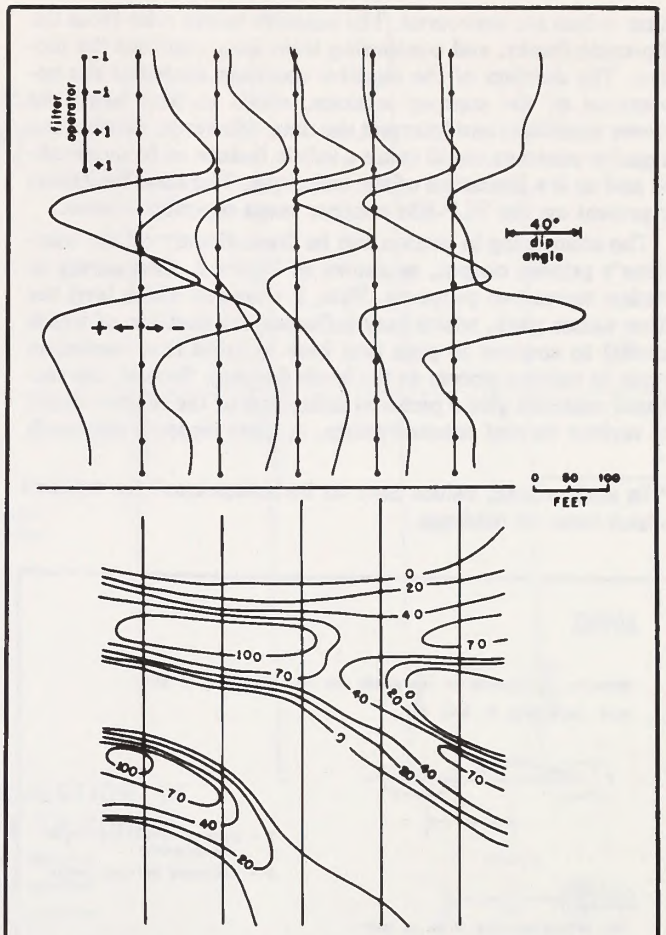

FIGURE 1. Example of VLF-EM filtering. The profiles show the raw dip-angle data and the contours represent the filtered data in units of degrees.

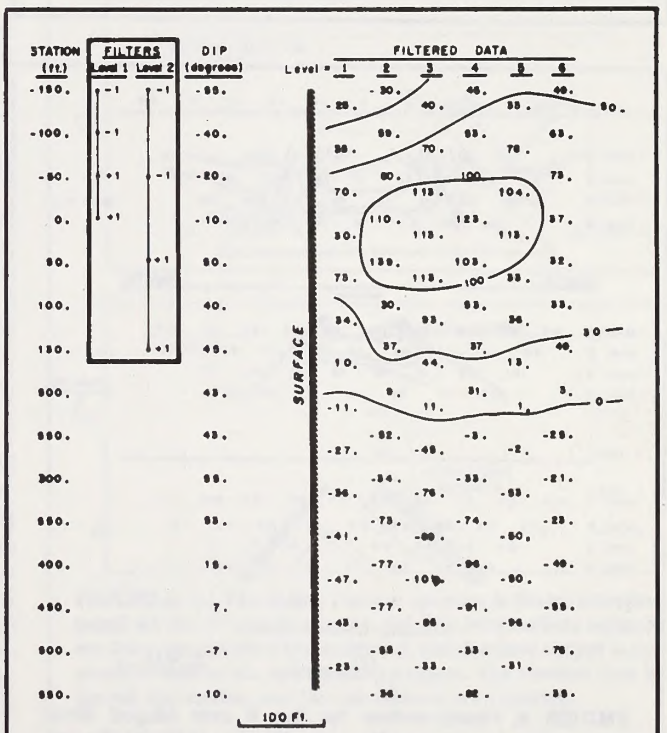

FIGURE 2. Sectional presentation of filtered VLF-EM data resulting from variable-spacing operators. The filter operators for the first two levels are shown in the insert (upper left).

filter values are contoured. The negative values arise from the dip-angle flanks, and contouring these only confuses the picture. The deletion of the negative contours simplifies the appearance of the contour sections, which in turn helps the viewer assimilate and interpret the data. However, deleting the negative contours could cause a subtle feature to be overlooked and so is a limitation of the technique. The same limitation is present on the VLF-EM contour maps described above.

The contouring in section can be done directly on the computer's printed output, as shown in Figure 2. Contouring in section serves two purposes. First, it shows at which level the filter values peak, which may influence the decision of which level(s) to contour in plan (but bear in mind that resolution tends to become poorer as the levels deepen). Second, the sectional contours give a pictorial indication of the relative depth of various current concentrations. A more rigorous approach is described by Karous and Hjelt (1977) using a more involved algorithm.

The computer program also provides a crude interpretation assuming that the VLF-EM responses can be modelled by simple current flow lines. Figure 3 shows the input and output of this quantitative algorithm. The input is the peak-to-peak anomaly amplitude P (in degrees) and the distance D between the peaks. The output is (a) the depth to the current flow and (b) the quality of the conductor as indicated by the amount of current it carries per unit of primary field.

The quality factor of the conductor is expressed mathematically as

$$I/(2\pi H)$$

where I is the current flow and H is the primary field strength. The quality factor increases with conductivity and size of the conductor, but is also affected by the conductivity of the host rock. The quality factor is expressed in units of distance, because I is in units of amperes and H is expressed in units of amp/metre or amp/foot. As an example, the equations of Figure 3 yield a depth estimate of 63 ft and a quality factor of 295 amperes per amp/ft for the dip-angle data of Figure 2. In a given area, it may be found that quality factors of VLF-EM conductors can be of some use in the sorting of anomalies.

The equations of Figure 3 show that the interpreted depth and quality are both directly proportional to D, where D is the distance between the positive and negative dip-angle peaks. Consequently, the validity of the interpretation bears a close relationship to the accuracy of defining the peaks. This accuracy suffers as station spacing increases. This fundamentally is why it is important to take fill-in readings in the vicinity of dip-angle crossovers. Expressed geophysically, a station spacing which is too large generates aliasing, which causes shallow sources to appear deeper.

The depth and quality estimates must be viewed with caution. A swamp can produce an anomaly with a large separation between the dip-angle peaks. The resulting large value of D produces erroneously large values of depth and quality.

* In such a case, values have to be interpolated for stations which have no readings.

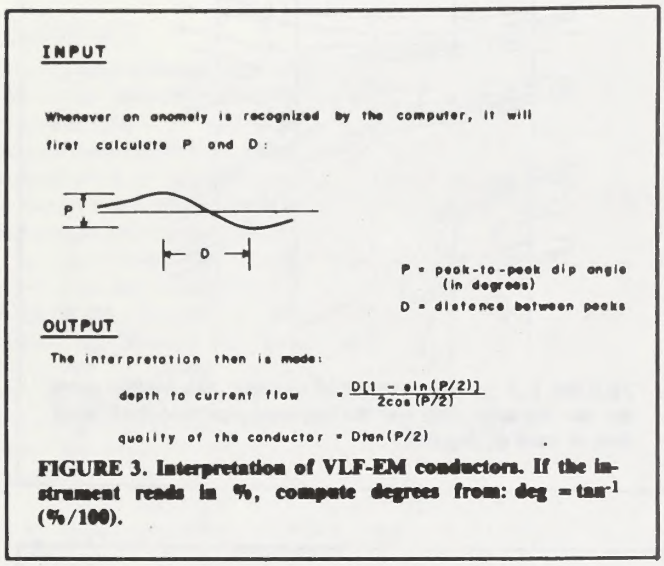

FIGURE 3. Interpretation of VLF-EM conductors. If the instrument reads in %, compute degrees from: deg = $\tan^{-1}$ (%/100).

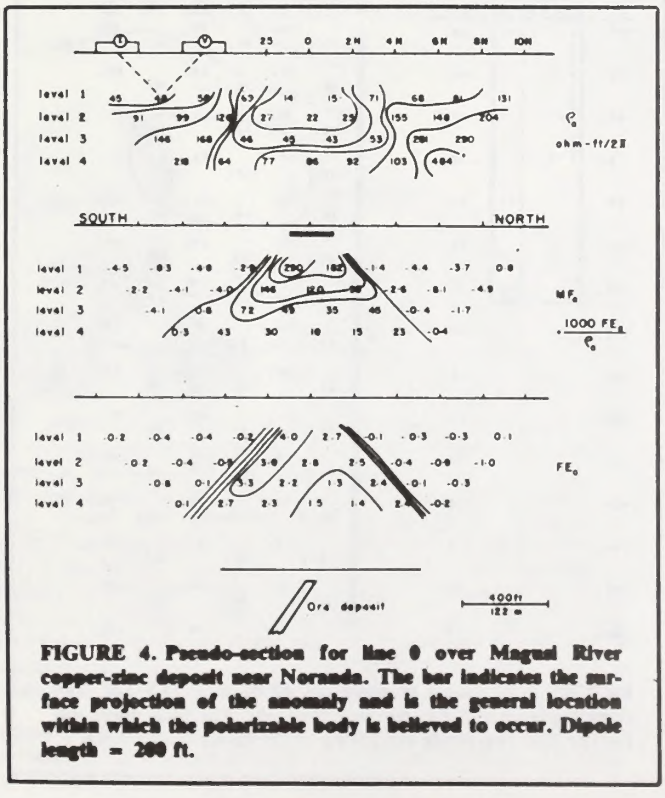

FIGURE 4. Pseudo-section for line 0 over Magusi River copper-zinc deposit near Noranda. The bar indicates the surface projection of the anomaly and is the general location within which the polarizable body is believed to occur. Dipole length = 200 ft.

Induced Polarization

Dipole-dipole IP data (i.e., apparent resistivity ρ_a, metal factor MF_a and frequency effect FE_a) typically are displayed as so-called pseudo-sections, with the interpreted locations of polarizable bodies indicated by bars (e.g., Fig. 4). IP maps constructed from pseudo-sections typically consist only of the bars (e.g., Fig. 5). This type of map presentation does not provide the viewer with any feeling for the strength of the anomalies relative to background. Various levels may be contoured on a plan map, e.g., level 3 of Figure 4. This usually is unsatisfactory because the most anomalous values generally do not overlie the body.

A technique has been developed recently for the quantitative presentation of dipole-dipole IP data in map form (Fraser, 1981). It is a geometric algorithm which employs simple averaging filters. These can be used manually if desired. The method yields a single number per station which reflects data from all levels of the pseudo-section. The most anomalous values overlie the body when using this method.

Figure 6(a) illustrates the filtering technique. A simple averaging filter is first applied to each level. The average of two adjacent values is taken for the second level, three for the third level, etc. The first level is unaltered. Figure 6(b) shows the results of this averaging, where the average values are termed the intermediate outputs. The final output is the average of the intermediate outputs. If some stations within the window have no values, the intermediate filter output for a level reflects the average of a fewer number of values. This approach is also used at the ends of lines, where data typically are absent on the deeper levels (e.g., Fig. 4). The filtering therefore yields an output value for every input value on level 1 of the pseudo-section. The plot point relative to the electrode

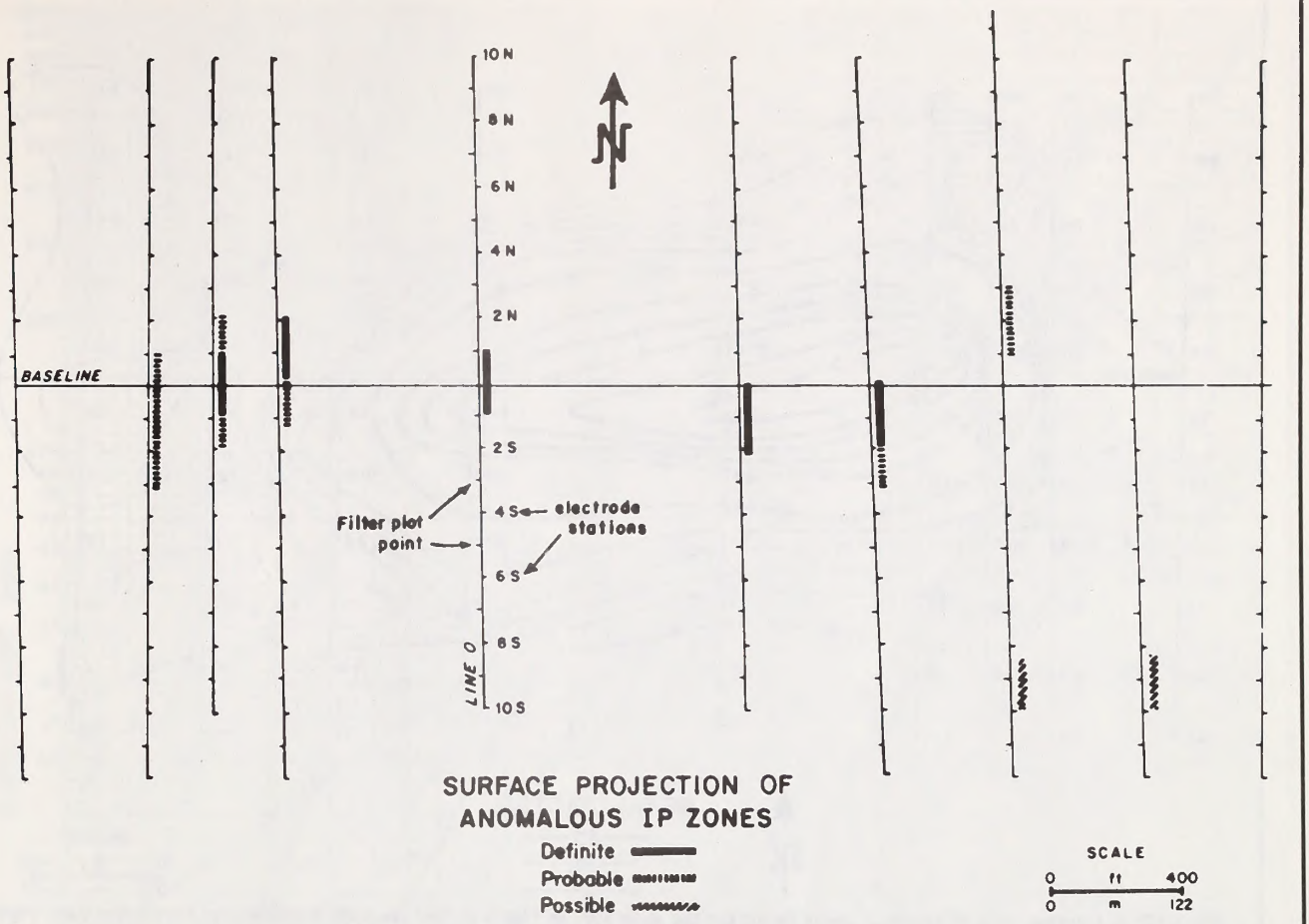

FIGURE 5. The bars represent the surface projections of anomalous IP zones. The interpretation was made from pseudo-sections by the contracting geophysical company which performed the survey.

stations is indicated in Figure 5. The filtered output then is contoured on a base map.

The filter method is used for each of frequency effect, metal factor and resistivity. Contour maps are constructed for each of these parameters (e.g., Fig. 7). A comparison of Figures 5 and 7 illustrates the advantage of the contour map, which provides a quantitative presentation of IP data (Fig. 7) vs a qualitative one (Fig. 5). The viewer obtains a sense of the strength of anomalies relative to background variations.

As for VLF-EM contour maps, the IP contour presentation does not in itself facilitate the interpretation of conductivity, size, depth, etc. These quantitative interpretations must be made from the basic data. The contour map merely yields a geometric presentation of the data (analogous to a magnetic contour map), which itself can provide a better comprehension of the geologic significance of the data in a qualitative sense.

Airborne EM/Resistivity

The interpretation of earth resistivity from DIGHEM[II] EM data has proved to be extremely useful in conductive environments. The quantitative algorithm used to interpret the airborne data is shown pictorially in Figure 8. This algorithm and the DIGHEM[II] system itself are described in detail by Fraser (1978, 1979). The inputs to the resistivity algorithm are the inphase and quadrature components of the vertical coaxial or horizontal coplanar coil-pair, and the outputs are the resistivity of the conductive half space and the height of the EM bird above the conductive material. Figure 9 is an example of the airborne data and the channels are identified in Table 1.

Airborne EM data are extremely sensitive to variations in flying height as well as variations in resistivity. Figure 9 shows how the recorded EM signal levels (channels 22-25) of the

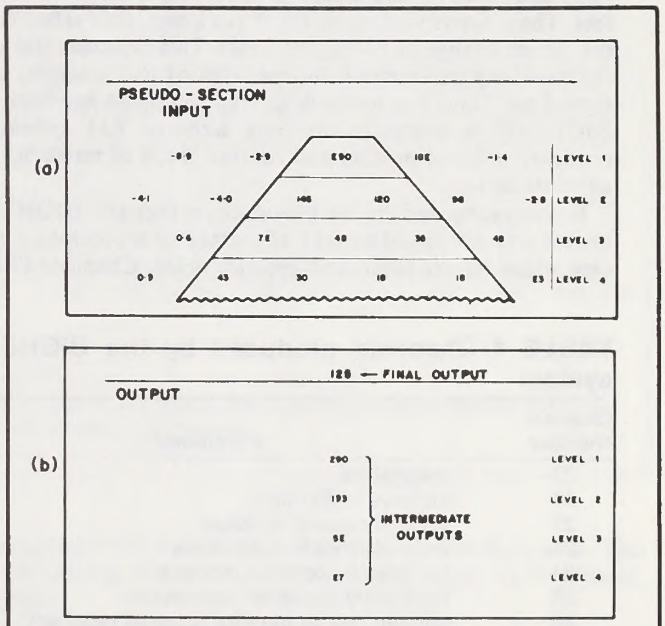

FIGURE 6. (a) The sliding window operator is shown superimposed on the IP pseudo-section. (b) The intermediate outputs are the average values for each level, and the final output is the average value of the intermediate outputs. The window then is moved one station and the calculations are repeated.

DIGHEM[II] system drop as flying height (channel 21) increases. At point A, the EM signals have decreased substan-

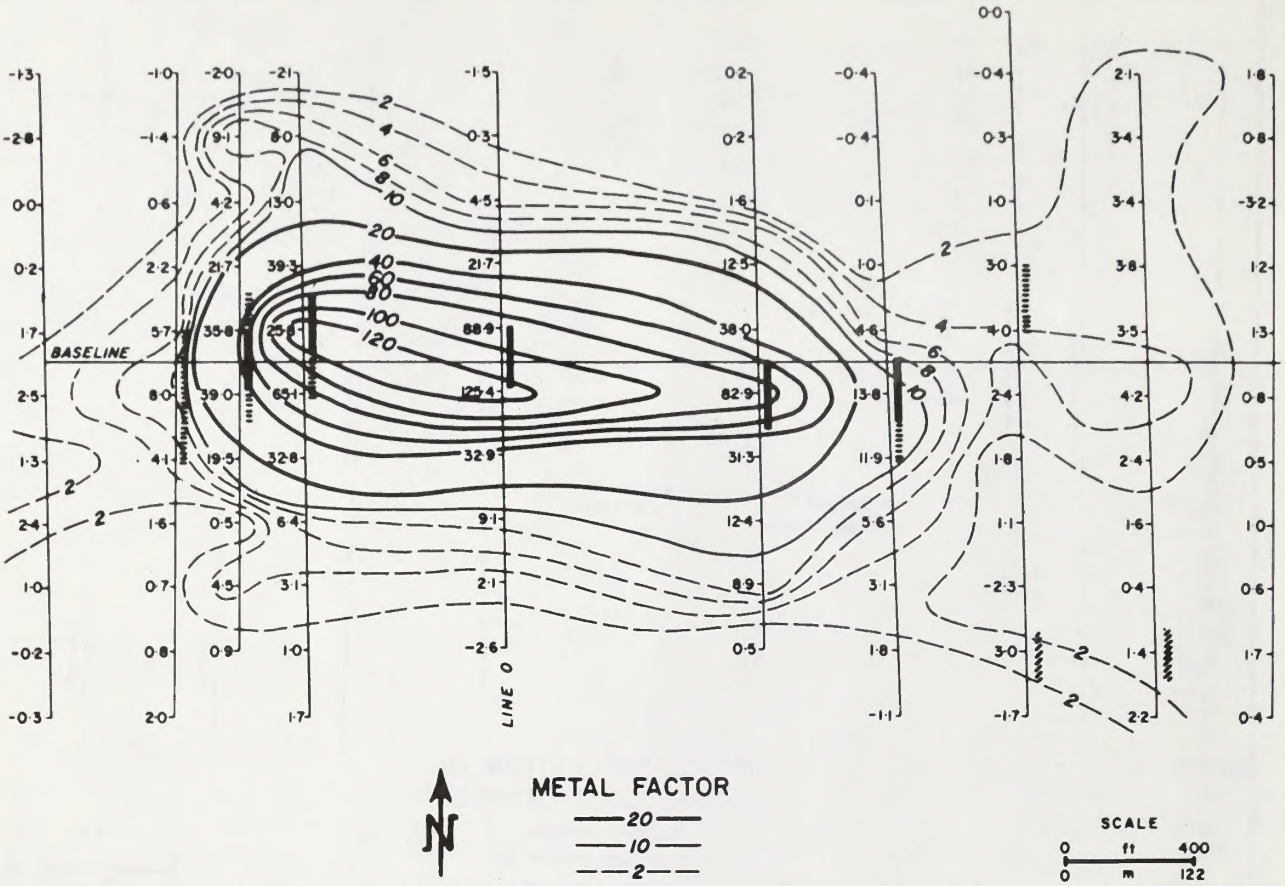

FIGURE 7. Contour map of apparent metal factor for the same area as Figure 5. The anomaly location bars were taken from Figure 5 for ease of comparison.

tially as a result of an increase in flying height from 100 to 200 feet. The resistivity (channel 40) shows a negligible effect from this severe change in EM signal levels. This demonstrates that the resistivity parameter is independent of flying height, as it should be. Thus, it is useful in geologic mapping applications. DIGHEM[II] is currently the only airborne EM system to routinely produce profiles and contour maps of resistivity for all of its surveys.

It was mentioned in the introduction that the DIGHEM[II] system was developed to take advantage of a processing concept which largely eliminates geologic noise. Channels 33 and 34 of Figure 9 are the inphase and quadrature *difference* components, which are the output of a very simple geometric algorithm. These channels are fairly free of the response of conductive overburden. It is conductive overburden which produced the high degree of activity on the recorded EM channels 22 to 25. This relative freedom of the difference channels 33 and 34 from geologic noise has been of significant help in identifying bedrock conductors in conductive environments (e.g., Fig. 10).

TABLE 1. Channels produced by the DIGHEM[II] system

Channel Number	Parameter
20	magnetics
21	altitude of EM bird
22	vertical coaxial inphase
23	vertical coaxial quadrature
24	horizontal coplanar inphase
25	horizontal coplanar quadrature
28	ambient noise monitor (coaxial receiver)*
29	ambient noise monitor (coplanar receiver)*
31	sums function, inphase*
32	sums function, quadrature*
33	differences function, inphase
34	differences function, quadrature
35	first anomaly recognition function*
36	second anomaly recognition function*
37	conductance
40	log resistivity

* Not shown in all of Figures 9 to 11

Airborne Magnetite Mapping

The information content of data from an inphase-quadrature electromagnetic system consists of a combination of conductive eddy current response and magnetic polarization response. The secondary field resulting from conductive eddy current flow is frequency-dependent and consists of both inphase and quadrature components. Conversely, the field resulting from magnetic polarization is frequency-independent and consists of only an inphase component. Both types of responses appear on the DIGHEM[II] record of Figure 11. The magnetic polarization responses are hachured in this figure.

The (negative) inphase component from magnetic polarization is opposite in sign to the (positive) inphase component from conductive eddy currents. When magnetic polarization manifests itself by decreasing the measured amount of positive inphase, its presence may be difficult to recognize. However, when it manifests itself by yielding a negative inphase anomaly (e.g., Fig. 11), its presence is assured. In this latter case, the negative component can be used to estimate the per cent magnetite content.

A magnetite mapping algorithm was developed for the coplanar coil-pair of the DIGHEM[II] system. The technique yields contours of apparent weight per cent magnetite accor-

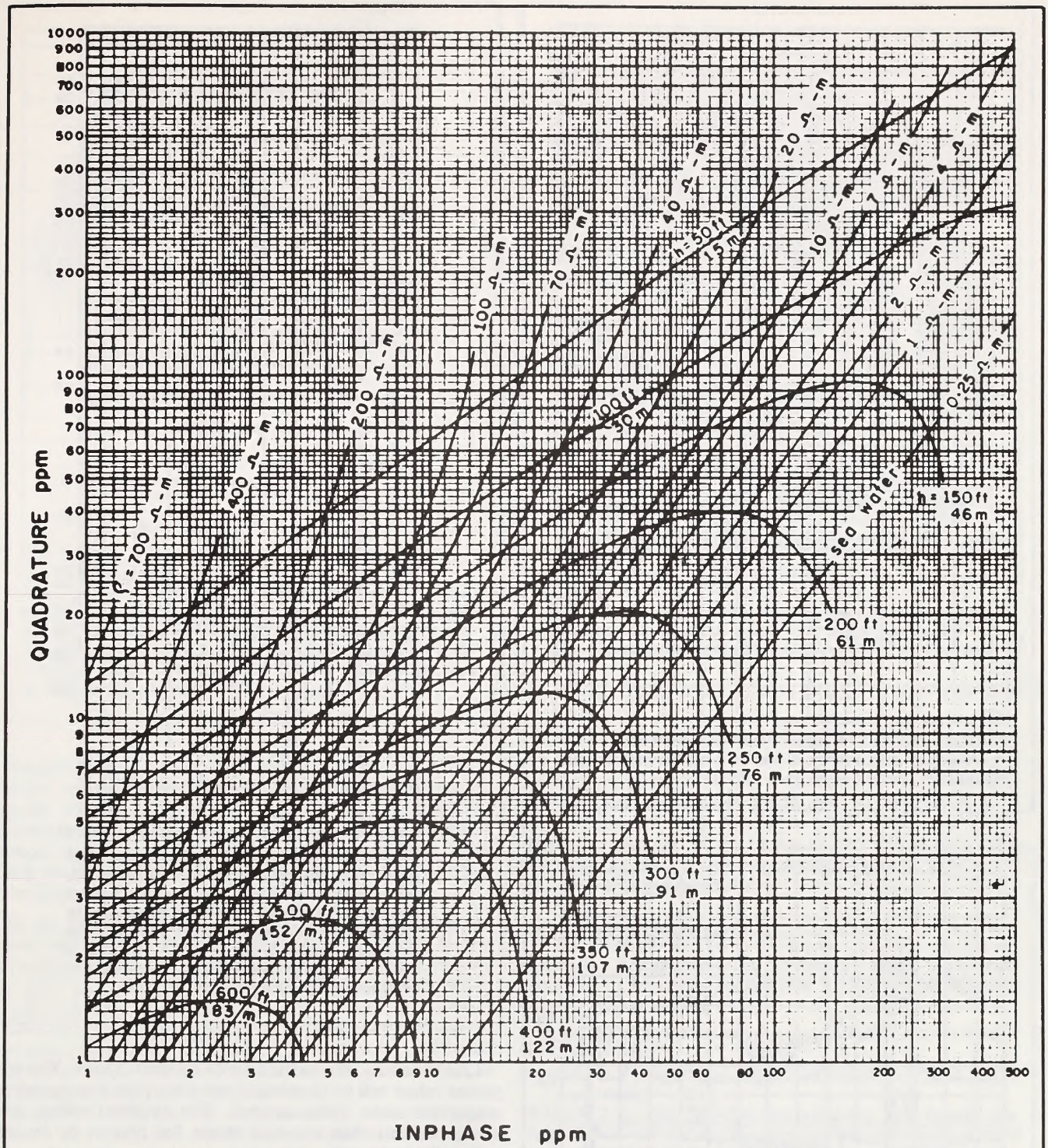

FIGURE 8. Graphical representation of the DIGHEM[II] resistivity algorithm for both vertical coaxial and horizontal coplanar coil-pairs at 900 Hz. For the coplanar data, divide inphase and quadrature by 2 before using the diagram.

ding to a homogeneous half-space model. The method can be complementary to magnetometer mapping in certain cases. Figure 12 presents an example of a per cent magnetite contour map and Figure 13 shows the magnetometer map for comparison. Compared to magnetometry, EM magnetite mapping is far less sensitive, but is more able to resolve closely spaced magnetite zones. The method is sensitive to ¼% magnetite by weight when the sensor is at a height of 100 ft above a magnetitic half space. It can individually resolve steeply dipping magnetite-rich bands which are separated by 200 ft.

The EM magnetite algorithm is basically quite simple because a linear relationship exists between volume per cent magnetite V and the negative inphase response R_o in ppm. This relationship has been determined empirically to be (Fraser, 1980)

$$V = -R_o/25$$

This linear relationship is true for a fixed survey altitude of 100 ft when demagnetization effects are disregarded and when a fixed susceptibility-volume per cent relationship is assumed. The technique, in practise, involves (1) correction of the actual EM response R for variations in flying altitude to yield R_o and (2) computation of the volume per cent magnetite. The conversion from volume per cent to weight per cent is relatively trivial.

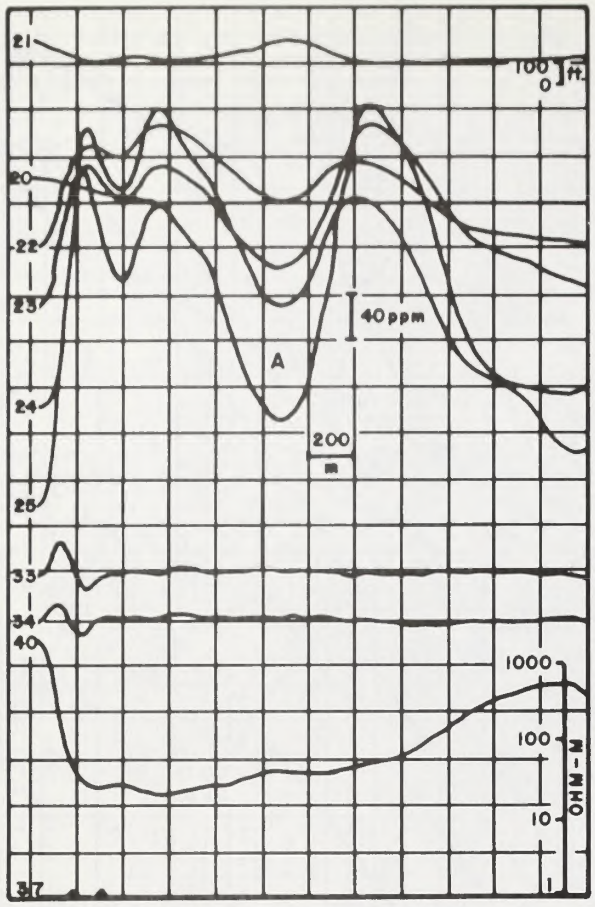

FIGURE 9. DIGHEM[II] digital record over conductive terrain. The resistivity channel 40 was derived from the coplanar EM channels 24 and 25. Frequency = 3600 Hz.

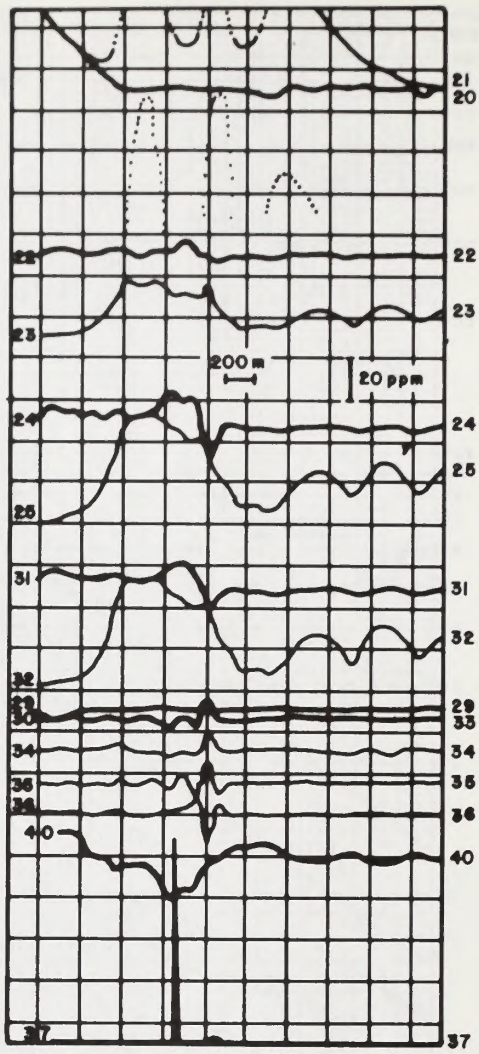

FIGURE 10. The encircled inphase and quadrature *difference* anomalies (channels 33, 34) identify a conductor, the recorded inphase response (channels 22, 24) of which is hidden in geologic noise caused by magnetite, with the recorded quadrature response (23, 25) largely hidden in geologic noise caused by conductive overburden. Frequency = 900 Hz.

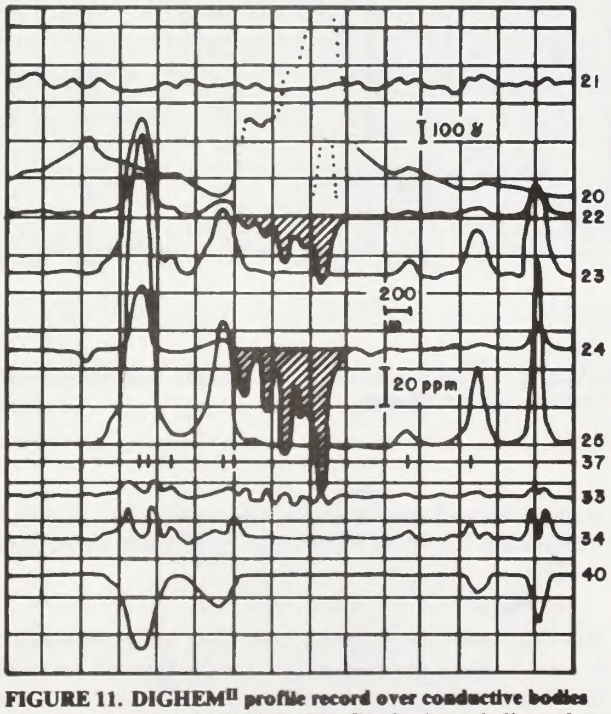

FIGURE 11. DIGHEM[II] profile record over conductive bodies and magnetically polarizable bodies. The hachures indicate the negative inphase response caused by magnetic polarization. The positive anomalies identify conductors. Frequency = 900 Hz.

Like resistivity, the method yields *apparent* values. The apparent values will be identical to true values for homogeneous magnetitic rocks which outcrop. The apparent values will always be less than the true values for narrow or buried magnetitic bodies.

Unlike magnetometry, the EM magnetite method is not influenced by remanent magnetism or magnetic latitude. The method has been used to differentiate between various rock types and to define rock contacts more closely than was possible from magnetometer data alone.

Summary

Advances in geophysical hardware have resulted in large amounts of data being produced during surveys. This in turn has encouraged automated means of treating the data. Because the quantity of data is substantial, a common goal is *simplification*. A geologic body of given conductivity and size, for example, can yield many channels of data from an EM system having various frequencies and coil orientations. If the data can be used to produce information on conductivity and size, then many EM parameters can be reduced to yield two very useful geologic parameters.

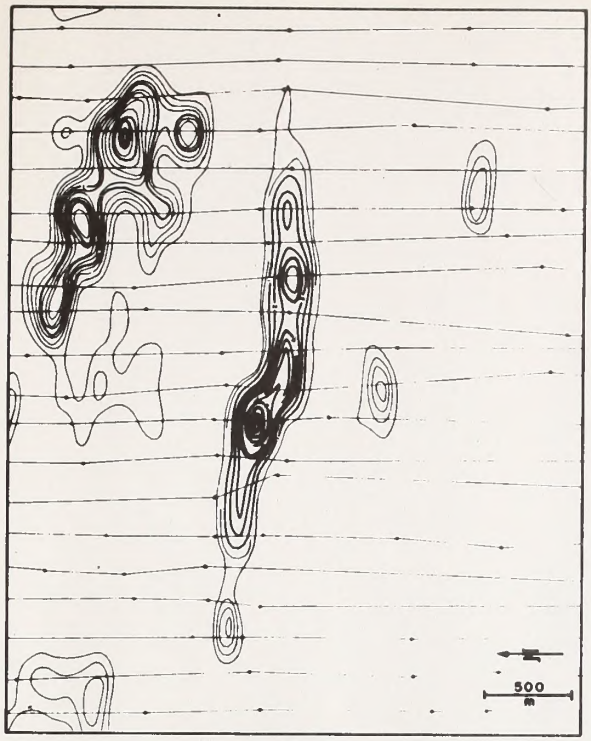

FIGURE 12. EM magnetite map from a survey over iron formation, gabbro and volcanic rocks in the Canadian Precambian Shield. The EM bird was approximately 100 feet above the magnetic rocks. The contour interval is ¼ per cent by weight.

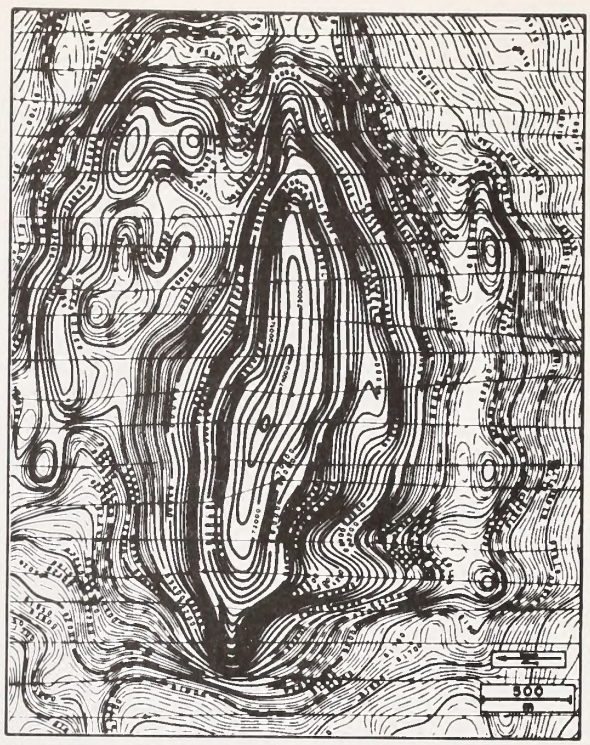

FIGURE 13. Magnetometer map of the same area as Figure 12, where the magnetic sensor was approximately 150 feet above the magnetic rocks. The contour interval is 25 gammas.

Simplification, therefore, is one criterion for judging whether or not various data handling techniques are useful. Another criterion is that of *interpretability*; i.e., the simplified parameters should improve the understanding of the data in a geologic context. Several techniques are described above, all of which simplify recorded geophysical data and improve interpretability.

In the case of VLF-EM, the data handling technique involves transforming noisy non-contourable profile data into less noisy contourable data. The process simplifies the form of the data in a manner which aids geologic interpretation. Another technique accomplishes similar results for induced polarization data. The IP transform method allows the data of pseudo-sections to be displayed on contour maps. The most anomalous values occur over the polarizable body, which is not the case for pseudo-section data.

Both the VLF-EM and IP data processing methods may be referred to as geometric algorithms because they merely rearrange the geometric form of the data without altering the units. In contrast, data processing methods which yield quantitative estimates of geologic parameters (such as conductivity, size, etc.) may be referred to as quantitative algorithms. An example is the algorithm which transforms non-contourable height-sensitive EM data, from the helicopter-borne DIGHEM[II] electromagnetic system, into contourable resistivity data. Another example is the technique used to estimate weight per cent magnetite when magnetic polarization response is evident on the EM channels of the DIGHEM[II] system.

It is using conventional wisdom to state that the interpretation of geophysical data should be performed by people experienced in geophysics. The techniques mentioned above, however, yield parameters which *can* be interpreted in a geologic context with but little geophysical knowledge. Therein lies their charm. Of course, therein also lie the pitfalls which may be present whenever the limitations of a technique are poorly comprehended.

Acknowledgments

This paper was presented at the KEGS Mining Geophysics Symposium, American Geophysical Union Spring Meeting, Toronto, Ontario, May 1980.

REFERENCES

FRASER, D.C., 1969, Contouring of VLF-EM data: *Geophysics, v. 34, p. 958-967.*

FRASER, D.C., 1971, VLF-EM data processing: *CIM Bulletin, Jan.*

FRASER, D.C., 1978, Resistivity mapping with an airborne multicoil electromagnetic system: *Geophysics, v. 43, p. 144-172.*

FRASER, D.C., 1979, The multicoil II airborne electromagnetic system: *Geophysics, v. 44, p. 1367-1394.*

FRASER, D.C., 1980, Magnetite mapping with a multicoil airborne electromagnetic system: *presented at the International Geological Congress, Paris, July 1980, and submitted for publication.*

FRASER, D.C., 1981, Contour map presentation of dipole-dipole induced polarization data: *acepted for publication by Geophysical Prospecting.*

KAROUS, M., and HJELT, S.E., 1977, Determination of apparent current density from VLF measurements: *Dept. of Geophysics, Univ. of Oulu, Finland, Contrib. no. 89.*

☆ U.S. GOVERNMENT PRINTING OFFICE: 1986 676-003/40632

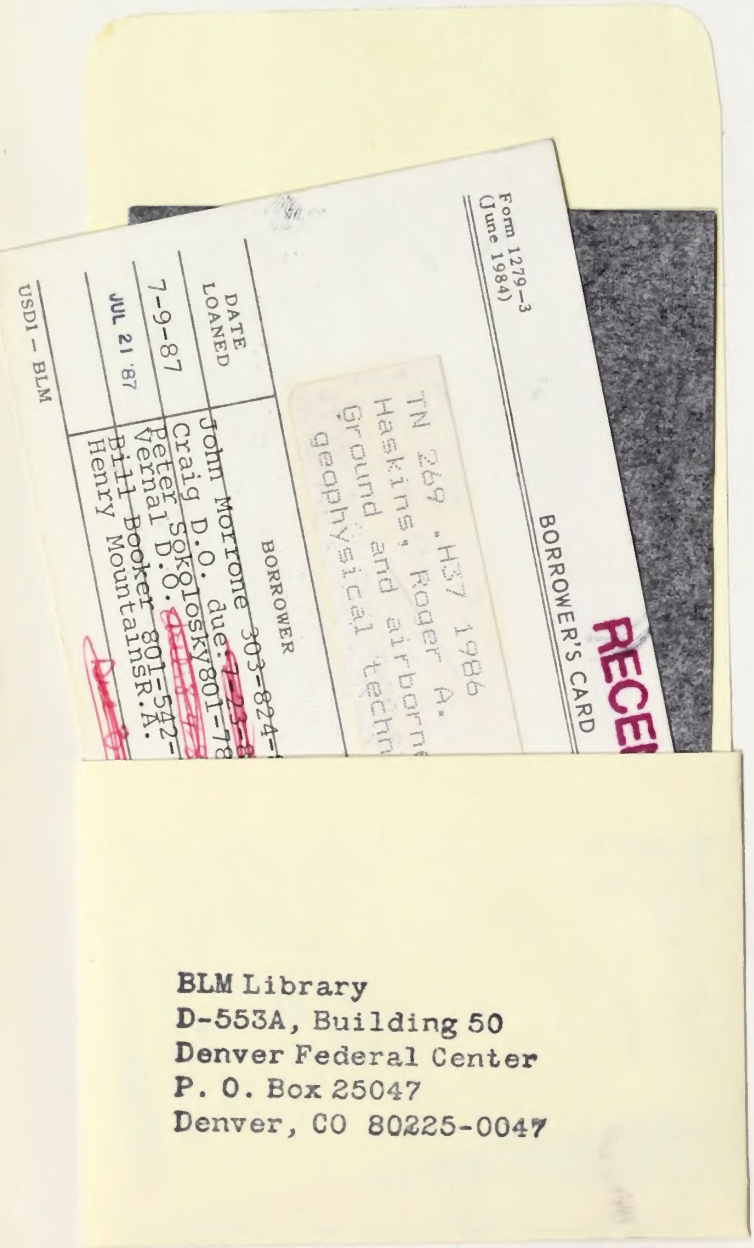

BLM Library
D-553A, Building 50
Denver Federal Center
P. O. Box 25047
Denver, CO 80225-0047